UNIVERSITY OF CALIFORNIA, SAN DIEGO

The Seismic Response of Precast Segmental Bridge Superstructures with Bonded Tendons

A Dissertation submitted in partial satisfaction of the requirements for the degree

Doctor of Philosophy
in
Structural Engineering

by
Marc John Veletzos

Committee in Charge:

Professor José I. Restrepo, Chair
Professor Yehuda Bock
Professor Joel P. Conte
Professor Frieder Seible
Professor Peter Shearer

The Dissertation of Marc John Veletzos is approved and it is acceptable in quality and form for publication on microfilm:

_____

_____

_____

_____

_____

Chair

University of California, San Diego

2007

For my daughter Fiona Mairead.

As a reminder that it is never too late
to tickle the brain with advanced studies,
formal or otherwise.

TABLE OF CONTENTS

LIST OF SYMBOLS

+2CS	Pre-earthquake stress-state based on stresses at end of construction plus two times creep and shrinkage losses
+CS	Pre-earthquake stress-state base on end of construction plus creep and shrinkage losses
a_0	Mass proportionality coefficient
a_1	Stiffness proportionality coefficient
AASHTO	American Association of State Highway and Transportation Officials
ASBI	American Segmental Bridge Institute
c	Damping matrix
Caltrans	California Department of Transportation
COV	Coefficient of variation
CQC	Complete quadratic combination modal combination technique
-CS	Pre-earthquake stress-state based on end of construction minus creep and shrinkage losses
D	Colum Depth
D1	1st segment joint down-station of the pier (300 foot span model)
D2	2nd segment joint down-station of the pier (300 foot span model)
D3	3rd segment joint down-station of the pier (300 foot span model)
D13	13th segment joint down-station of the pier and two away from midspan (300 foot span model)
D14	14th segment joint down-station of the pier and one away from midspan (300 foot span model)
d_b	Diameter of pre-stressing strands
d_{bl}	Diameter of the column longitudinal reinforcement
DL	Dead Load
E1	1st segment joint down-station of the pier (525 foot span model)
E2	2nd segment joint down-station of the pier (525 foot span model)
E3	3rd segment joint down-station of the pier (525 foot span model)
E8	8th segment joint down-station of the pier and two away from midspan (525 foot span model)

E9	9^{th} segment joint down-station of the pier and one away from midspan (525 foot span model)
EOC	Pre-earthquake stress-state at the end of construction
f'_c	Unconfined compressive strength of concrete
f_{pe}	Effective stress in pre-stressing strands (ksi)
f_{ps}	Full design strength of pre-stressing strands (ksi)
f_{pt}	Stress in the post-tensioning tendons (ksi)
f_u	Ultimate stress of pre-stressing strands (ksi)
f_y	Yield strength of the mild reinforcement
k	Stiffness matrix
L	Column shear span length
L_{end}	End span length from the first segment joint near the pier to the abutment bearing centerline
L_b	Flexural bond length of pre-stressing strands
LCA	Longitudinal construction staging analysis
L_{int}	Clear interior span length between the first segment joints near the piers
L_t	Transfer length of pre-tensioned strands
L_u	Unbonded length for modeling of post-tensioning tendons
L_w	Withdraw length of pre-tensioned strands
m	Mass matrix
$m(x)$	Unit mass at location x along the bridge
MDOF	Multi-degree of freedom
$M^+_{Mid-end}$	Ultimate positive bending capacity of the middle segment joint of end spans
$M^+_{Midspan}$	Ultimate positive bending capacity of the midspan segment joint of interior spans
M_n	Modal mass coefficient of the n^{th} mode
M^-_{Pier}	Ultimate negative bending capacity of the segment joint adjacent to the pier
PT	Post tensioning
$q_i(x)$	Sinusoidal equivalent static load of the i^{th} mode
$q_{tot}(x)$	Total sinusoidal equivalent static load
SDC	Caltrans Seismic Design Criteria
SDOF	Single degree of freedom

SFOBB	San Francisco-Oakland Bay Bridge
S_{av_i}	Vertical spectral acceleration of the ith mode
$S_{c_{end}}$	Capacity of the end span collapse mechanism in terms of vertical earthquake accelerations
$S_{c_{\text{int}}}$	Capacity of the interior span collapse mechanism in terms of vertical earthquake accelerations
S_p	Plastic Section Modulus
u	Displacement vector
$\dot{u}$	Velocity vector
$\ddot{u}$	Acceleration vector
$\ddot{u}_g$	Ground acceleration vector
U1	1st segment joint up-station of the pier (300 foot span model)
U2	2nd segment joint up-station of the pier (300 foot span model)
U3	3rd segment joint up-station of the pier (300 foot span model)
U13	13th segment joint up-station of the pier and two away from midspan (300 foot span model)
U14	14th segment joint up-station of the pier and one away from midspan (300 foot span model)
UBC	Uniform Building Code
W1	1st segment joint up-station of the pier (525 foot span model)
W2	2nd segment joint up-station of the pier (525 foot span model)
W3	3rd segment joint up-station of the pier (525 foot span model)
W8	8th segment joint up-station of the pier and two away from midspan (525 foot span model)
W9	9th segment joint up-station of the pier and one away from midspan (525 foot span model)
w_{end}	Uniform distributed load that will develop an end span collapse mechanisms
W_{end}	Total weight of the end span segments
w_{int}	Uniform distributed load that will develop an interior span collapse mechanisms
W_{int}	Total weight of the interior span segments

ω_n	Circular frequency of the n^{th} mode
Φ_i	Mode shape of the i^{th} mode
Γ_i	Participation factor of the i^{th} mode
ξ_n	Percentage of critical damping of the n^{th} mode

LIST OF FIGURES

LIST OF TABLES

ACKNOWLEDGMENTS

I would like to express my sincere gratitude to a number of people who have assisted me, both personally and professionally, over the years. As my entire dissertation is based on non-linear time history analyses, I must begin with the author of the finite element program I used, Dr. Athol Carr at the University of Canterbury, New Zealand. Without his modeling expertise and guidance I'm quite sure I would still be struggling with numerical instabilities.

I must acknowledge a number of practicing engineers for their assistance with this dissertation. Thank you to Ben Soule of International Bridge Technologies who was extremely forthcoming with construction drawings, design calculations, construction photos, and drawings for the Otay River Bridge and was always quick to respond to my questions and requests on his time. Your confidence and competence as an engineer is admirable. On a similar vein, Charly Sikorsky was instrumental in obtaining design calculations and construction drawings of the San Francisco-Oakland Bay Bridge (SFOBB) as well as authorization for the Otay calculations. I would like to acknowledge Dr Sajid Abbas of TY Lin International

for his assistance with design details of the SFOBB and for his personal tour of the construction site. Thank you to Sami Megally for helping me understand the results of your research and to Cliff Freyermuth of the American Segmental Bridge Institute (ASBI) for supporting my trip to Taiwan to present results of my research and for inviting me to speak at the 19th Annual ASBI Convention.

There are two excellent engineers in academia who have made a great impression on me in recent years. One is my advisor Prof. José Restrepo, who has challenged me in my research, encouraged my teaching endeavors and showed me that teaching a course is not just about the subject matter, but that an important part of teaching is to challenge the students to strive for excellence. The second is Professor/Dean Frieder Seible who not only funded me and my research for a portion of my time here at UCSD, but was instrumental in by career from the beginning. While I credit Professor Gill Hegemier for introducing me to structural engineering with his Statics class back in 1990, I credit Professor Seible with setting me down the bridge engineering path. He helped me obtain my first industry position with Buckland & Taylor and after being a student in three of his classes in the 1990s, it was a great privilege to be on the teaching side with him in 2006. Professor Seible

has an incredible way of making complex concepts seem obvious and of turning every challenge into a learning opportunity. Thank you both for your assistance, your support, and for your inspiration.

I would like to thank my friends in the department (Yohsuke Kawamata, Andreas Stavridis, Matt Schoettler, Matt Tobolski, Marios Panagiotou, Babak Moaveni, Kelly Burnell, Azadeh Bozorgzadeh, Andre Barbosa, Mike Oesterle, Mike Gebman, Mike Fraser, Devon Lumbard, Anna Lang, Kendra Oliver, Janet Crumrine, and Jay Harris) for your camaraderie, conversations, competitive dart games and spirited soccer matches.

I would like to thank all my friends and family, of which there are too many to mention by name, for their support and understanding over the past four years. With special thanks to Beth Simon for her help in understanding and getting through "The Process".

I would like to acknowledge my parents, Guy and Thelma Veletzos, who have taught me, by example, that hard work, patience, and perseverance can overcome any obstacle in life.

And last but certainly not least, I would like to thank my wife, Maria Boyle, whose love, support and encouragement made this document possible.

VITA

1994	B.S., Structural Engineering, University of California at San Diego
1997	M.S., Structural Engineering, University of California at San Diego
1999	Registered Professional Civil Engineer, California
2007	Ph.D., Structural Engineering, University of California at San Diego

Experience

1992-1994	Engineering Aid, *Charles Lee Powell Structural Systems Laboratories*, La Jolla, CA
1994-1996	Research Assistant, Department of Applied Mechanics and Engineering Sciences, University of California at San Diego
1996-2001	Bridge Engineer/Resident Engineer, *Buckland & Taylor, Ltd.*, Walnut Creek, CA
2002-2003	Bridge Engineer, *Parsons*, San Francisco, CA
2003-2007	Graduate Student Researcher, Department of Structural Engineering, University of California at San Diego
2004	Bridge Engineer, *International Bridge Technologies*, San Diego, CA
2004-2006	Senior Teaching Assistant, Department of Structural Engineering, University of California at San Diego
2006-2007	Part-Time Faculty, Department of Civil and Environmental Engineering, San Diego State University

Publications

Veletzos, M.J., Van Den Einde, Y., Restrepo, J.I., Sahs, S., "Post Seismic Inspection and Capacity Assessment of Reinforced Concrete Bridge Columns", *1st US-Italy Seismic Bridge Workshop*, University of Pavia, Pavia, Italy, April, 2007.

Veletzos, M.J., Restrepo, J.I., Seible, F., "Seismic Response of Precast Segmental Bridge Superstructures", *Structural Systems Research Project, SSRP 06/18*, University of California at San Diego, La Jolla, CA, December 2006.

Veletzos, M.J., Restrepo, J.I., "Improved Seismic Performance of Precast Segmental Bridges Using Jointed Column Connections and Unbonded Tendons", *2nd US-Taiwan Workshop on Self-Centering Structural Systems*, Taipei, Taiwan, October 2006

Veletzos, M.J., Restrepo, J.I., "Seismic Response of Precast Segmental Bridge Superstructures with Bonded Tendons", *4th International Conference on Earthquake Engineering*, Taipei, Taiwan, October 2006

Veletzos, M.J., Restrepo, J.I., "Improved Seismic Performance of Precast Segmental Bridges Using Jointed Column Connections and Unbonded Tendons", *5th National Seismic Conference on Bridges and Highways*, San Francisco, CA, September 2006.

Veletzos, M.J., Panagiotou, M., Restrepo, J.I., Sahs, S., "Post Seismic Inspection and Capacity Assessment of Reinforced Concrete Bridge Columns", *5th National Seismic Conference on Bridges and Highways, San Francisco*, CA, September 2006.

Veletzos, M.J., Restrepo, J.I., "Seismic Response of Precast Segmental Bridge Superstructures with Bonded Tendons", *5th National Seismic Conference on Bridges and Highways, San Francisco*, CA, September 2006.

Veletzos, M.J., Panagiotou, M., Restrepo, J.I., "Post Seismic Inspection and Capacity Assessment of Reinforced Concrete Bridges", *Structural Systems Research Project, SSRP 06/19*, University of California at San Diego, La Jolla, CA, June 2006.

Veletzos, M.J., Restrepo, J.I., "Improved Seismic Performance of Precast Segmental Bridges Using Jointed Column Connections and Unbonded Tendons", *100th Anniversary Earthquake Conference*, San Francisco, CA, April 2006.

Veletzos, M.J., Priestley, M.J.N., Seible, F., "Seismic Isolation of Bridge Spans by Pendulum Suspension", *Structural Systems Research Project, SSRP 97/14*, University of California at San Diego, La Jolla, CA, November 1999.

Veletzos, M.J., "Seismic Isolation of Bridge Spans by Pendulum Suspension", *Masters Thesis,* Department of Structural Engineering, University of California at San Diego, La Jolla, CA, December 1997.

Veletzos, M.J., Priestley, M.J.N., "Seismic Isolation of Bridge Spans by Pendulum Suspension", *4th Caltrans Seismic Research Workshop*, Sacramento, CA, July 1996.

ABSTRACT OF THE DISSERTATION

The Seismic Response of Precast Segmental Bridge Superstructures

with Bonded Tendons

by

Marc John Veletzos

Doctor of Philosophy in Structural Engineering

University of California, San Diego, 2007

Professor José I. Restrepo, Chair

Precast segmental construction of bridges can accelerate construction and minimize the cost of bridges in highly congested urban environments, environmentally sensitive regions, difficult to access ravines, and wide river crossings where medium to long repetitive spans are needed. Despite their proven benefits, the use of precast segmental bridges in seismic regions of the United States remains very limited. A main obstacle to their use is concern regarding the seismic response of segment joints. Recent research has shown that segment joints can

undergo very large rotations that open up gaps in the superstructure, while maintaining its load carrying capacity, and with little, if any, damage.

This dissertation investigates the seismic response of precast segmental bridges using detailed 2D non-linear time-history analyses and focuses on the behavior of segment-to-segment joints constructed using the balanced cantilever method. The joint model was calibrated using results available from experimental work on large scale sub-assemblages. Analytical models of full scale precast segmental bridges with geometries and characteristics, similar to the Otay River Bridge and the San Francisco-Oakland Bay Bridge Skyway in California, were also used in this study.

A suite of twenty near field earthquake records was used to determine the median joint response as well as to quantify the effect of vertical motion on the joint response. The earthquake records were scaled using two different scaling methods and the effect on the structure response was studied. Four different pre-earthquake stress conditions were studied to determine if the effects of creep, shrinkage and temperature impact the seismic response of segment joints. In addition, a preliminary investigation into the possibility of removing a portion of the

superstructure longitudinal post-tensioning and allowing non-linear elastic response of the segment joints during a significant seismic event was performed.

Results indicated that vertical earthquake motions and the pre-earthquake stress-state can alter the response of segment joints. The results also showed that the method of record scaling does not significantly alter the median response, but may effect the variation in response. Furthermore, reducing the longitudinal post-tensioning near the piers may be possible provided that service load cases do not govern the design.

CHAPTER 1. INTRODUCTION

Precast segmental construction methods can ease bridge construction costs by reducing construction time while maintaining quality. In addition, the absence of falsework can minimize traffic congestion and environmental impact, adding to the benefits of this construction method. While the popularity of precast segmental bridge construction has increased throughout the world, its use in seismic regions of the United States has been hampered by a lack of research on the seismic response that would lead to reliability in its use. The California Department of Transportation (Caltrans) supported a research program to address this concern. This dissertation investigated the seismic response of precast segmental bridges with bonded tendons constructed with the balanced cantilever construction method, using detailed 2D non-linear time history analyses. A number of models were developed, including a validation model and two simulations of full scale balanced cantilever bridges. The primary difference between the two full-scale models was their span lengths (300 feet and 525 feet) and the use of continuity tendons. The 300 foot span bridge did not utilize continuity tendons, while the 525 foot span bridge did. The influence of

the pre-earthquake stress on the seismic response of segment joints was investigated and a preliminary study was conducted examining the possibility of reducing the longitudinal post-tensioning (PT) in the superstructure while allowing non-linear elastic segment joint response.

1.1. Benefits of Segmental Construction

The primary benefit of segmental bridges is that they can be constructed without temporary supports or falsework. Thus, segmental bridges are most effective for locations where falsework is expensive or impractical, such as deep ravines, wide water crossings, highly congested urban areas or environmentally sensitive regions.

The use of precasting technology can add to the general benefits of segmental bridge construction by improving quality control, reducing creep and shrinkage deformations, reducing weather dependence on production rates and improving construction speed.

1.2. Seismic Concerns

The primary seismic concerns regarding segmental construction are focused on the behavior of joints between segments as no mild reinforcement crosses such joints. The lack of reinforcement across segment joints allows for an increased rate of construction, yet creates inherent regions of weakness that act as crack initiators and can result in localized rotations. Thus, bridge owners, such as the California Department of Transportation (Caltrans), have questioned the response of segment joints during a seismic event in recent years. Do these joints open during an earthquake? Do they remain open after the earthquake? Does the joint opening affect shear transfer across the joints, thereby affecting dead load carrying capacity? Does joint opening alter the serviceability of the bridge? Do volumetric changes, such as creep and shrinkage, affect the joint response? These are the questions that have hampered the use of precast segmental bridges in seismic regions of the United States, namely California.

The seismic concerns for cast-in-place (CIP) segmental construction methods are no different than conventional CIP construction methods, since mild steel reinforcement crosses the segment joints, and will not be addressed in this study.

1.3. Gaps in Knowledge Identified and Covered in this Study.

Several knowledge gaps were identified in the literature and are addressed in this study. These knowledge gaps are as follows.

- Lack of studies on full bridge systems.
- Lack of studies on the impact of volumetric changes on the seismic response of superstructure segment joints.
- Influence of the vertical ground motion on the response of segment joints.
- Effect of the method of record scaling on the seismic response of segmental superstructures.

1.3.1. Full Bridge Systems

Recent research (Megally et al., 2002; Densley et al., 2003; Burnell et al., 2005) into the seismic performance of segmental bridge superstructures has advanced the general understanding of the characteristics of segmental bridge segment joints. However, all previous work has been conducted on joint or joint-column experiments. A study on the seismic response of full segmental bridge systems has never been performed.

1.3.2. Pre-Earthquake Stress-State

It is well known that volumetric changes can have a significant influence on the design for service load cases of prestressed concrete bridges. However, it is common practice to ignore these effects on bridges when considering seismic load cases. During a maximum credible earthquake, the bridge will be pushed to its ultimate capacity, which is generally insensitive to volumetric effects. In addition, standard practice is to capacity design the superstructure and foundations to force inelastic behavior to occur in the columns, thus the superstructure, which is the most sensitive to volumetric changes, will be significantly stronger than the piers, compounding the belief that volumetric effects are unimportant for seismic considerations. While this belief may be true for conventional cast-in-place bridges, the effect has never been studied for segmental bridges and may be important to the seismic response give the jointed nature of precast segmental bridge systems.

1.3.3. Vertical Earthquake Motion

Including the vertical component of earthquake ground motion is common practice for determining the seismic demands of 'Important' or 'Non-Standard' bridges in California. This is typically accomplished with time history analysis

based on three components of earthquake ground motion (T.Y. Lin International and Moffatt & Nichol Engineers, 2001). Seismic design codes however, provide little, if any, guidance with regard to a vertical design spectrum. Thus the large vertical accelerations in near field records at low periods may not be considered. In addition, segmental superstructures are designed to remain elastic, thus they are typically modeled with linear elements, without accurate modeling of the segment joints. A detailed investigation into the response of segmental bridge joints due to vertical earthquake motion has never been performed.

1.3.4. Record Scaling

A number of recent studies investigated the impact of different ground motion scaling option on structural response (Bazzurro and Luco, 2003; Bazzurro and Luco, 2006; Hancock et al., 2006; Watson-Lamprey and Abrahamson, 2006a). All of these studies compared amplitude scaled time history records with spectrum matched time history records. The amplitude scaled records were typically scaled for a best fit to the design spectrum over a period range. The researchers used these different ground motions on either non-linear single degree of freedom (SDOF) of multi-degree of freedom (MDOF) buildings. A study on the effect of different

amplitude scaling procedures, such as scaling to the natural period verses scaled for a best fit over a period range, has never been performed on detailed non-linear bridge structures.

1.4. Objectives

The large scale experiments on the seismic response of precast segmental bridge superstructures by Megally et al. (2002), Densley et al. (2003) and Burnell et al. (2005) achieved their objectives and determined the crack patterns, failure modes and ultimate behavior of precast segmental bridge superstructure joints. However a number of issues remain regarding the expected response of precast segment-to-segment joints during a significant seismic event and are outlined below.

1.4.1. Contribution of Vertical Earthquake Motions

Burnell et al. (2005) showed that precast segment joints open if the vertical ground motions accelerations of 0.75g are considered and the superstructure post tensioning is reduced by 25%, indicating that vertical motion contributes to joint opening (see Section 3.4.3). But this contribution was not decoupled from the effect

of reducing the longitudinal PT. The research presented in this study will quantify the impact of vertical earthquake motion on the segment joint response.

1.4.2. Joint Opening

Burnell et al. (2005) indicated that segment joints will likely open when vertical motion is considered and when the longitudinal post tensioning is reduced (see Section 3.4.3). But what about when the PT is not reduced? The research presented in this study will determine if segment joints are likely to open when full longitudinal post tensioning is considered along with vertical accelerations and will quantify the magnitude of the crack width if they do open.

1.4.3. Performance Limits States

Burnell et al. (2005) suggested that current seismic design procedures, based on capacity design principles, prevent residual joint opening and protect the longitudinal post tensioning tendons from yielding when vertical earthquake motion is not considered (see Section 3.4.3). Does this remain true when vertical earthquake motions are considered? The research presented in this study will compare the segment joint response to concrete and PT performance limit states, such as cracking,

crushing, and yielding, and assess the level of joint damage during a seismic event. In addition, residual crack widths will be quantified.

1.4.4. Pre-Earthquake Stress-State

The state of stress on the segment joints changes on a daily basis due to temperature and over the life of the bridge due to volumetric effects such as creep and shrinkage. The research presented in this study will assess the impact of the pre-earthquake stress-state on the response of segment joints.

1.4.5. Record Scaling

The Pacific Earthquake Engineering Research (PEER) Center approach to record scaling is to scale the lateral ground motions to match the design spectrum at the dominant natural period of the structure, and then use this scale factor on all components of the ground motion (Somerville and Collins, 2002). The approach outlined in the Uniform Building Code (UBC, 1997), however, is to scale the lateral earthquake record to match the design spectrum over a period range rather than a single period. The research presented in this study will assess the impact of these two different record scaling methods on the structure response.

1.4.6. Superstructure PT Sensitivity

The preferred seismic design practice is to ensure an elastic response in the superstructure by concentrating in-elastic behavior in the columns (Caltrans SDC, 2004). Is it possible to remove some of the longitudinal PT in the superstructure and allow non-linear elastic behavior in the superstructure and at the same time maintain an acceptable level of seismic safety and serviceability? The research presented in this study will investigate the sensitivity of the segment joint response due to reductions in the longitudinal superstructure PT.

1.5. Outline of the Dissertation

Chapter 1 discusses the motivation for this study and outlines the benefits and seismic concerns of segmental bridge construction methods. Chapter 2 is an overview of segmental bridge construction and discusses the history, describes typical design details as well as differences between various segmental construction methods. The chapter concludes with a discussion on current seismic design practices in California. A review of relevant literature is presented in Chapter 3. Chapter 4 discusses the validation of the joint model and summarizes the results of various sensitivity studies that were used to fully understand and optimize the

segment joint model. The earthquake records used for the time history analyses are described in Chapter 5. Chapter 6 documents the full bridge models and discusses the discretization and characteristics for both the 300 foot and the 525 foot span models. Chapter 7 presents the results of the two full bridge models. Chapter 8 documents the reduced PT models and presents the results of a preliminary study into the possibility of reducing the amount of superstructure longitudinal PT. The limitations of the models are outlined in Chapter 9. Chapters 10, 11, 12, and 13 present conclusions, design considerations, design recommendations and future research, respectively. Additional model results, parameter studies and photos of balanced cantilever segmental bridge construction are included in the Appendices.

CHAPTER 2. SEGMENTAL BRIDGES 101

This chapter reviews the basics of segmental bridge construction methods. The typical details of the various bridge components are described as well as a brief history of segmental bridge construction and a description of the different segmental construction methods. The chapter concludes with a summary of current seismic design practices in California.

2.1. Anatomy of Segmental Bridges

The components of a segmental bridge are for the most part the same as a typical prestressed concrete bridge. The bridge is divided into the superstructure and the substructure as shown in Figure 2-1. The superstructure is the portion of the bridge that supports the roadway/railway. The substructure is the portion of the bridge that supports the superstructure and consists of abutments and piers. The difference between a segmental bridge and a typical prestressed concrete bridge is in the details of these components. Typical details of the components of a segmental bridge are described below.

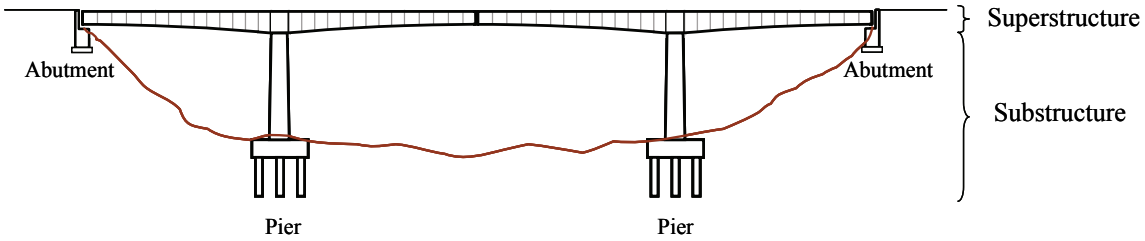

Figure 2-1 Anatomy of Segmental Bridges

2.1.1. Superstructure

In segmental bridge construction, the superstructure is divided into short pieces or segments that are constructed one at a time. Depending on the construction method, the superstructure segments may be cast-in-place (CIP), that is, in their final position on the bridge, or they may be precast, that is, constructed and stored at a fabrication facility off the bridge site and delivered as required (see Figure 2-2). Shear keys between segments may be required to ensure adequate load transfer (see Figure 2-3). The size of each segment will vary depending on the specific construction method and transportation means available for the bridge site. Match casting of precast segments, a process where the end of a previously constructed segment is used as a form for the adjacent segment, is common to ensure proper fit on site.

Figure 2-2 Precast Superstructure Segments for the San Francisco-Oakland Bay Bridge Skyway in the Stockton Casting Yard ready for Transport by Barge to the Bridge Site

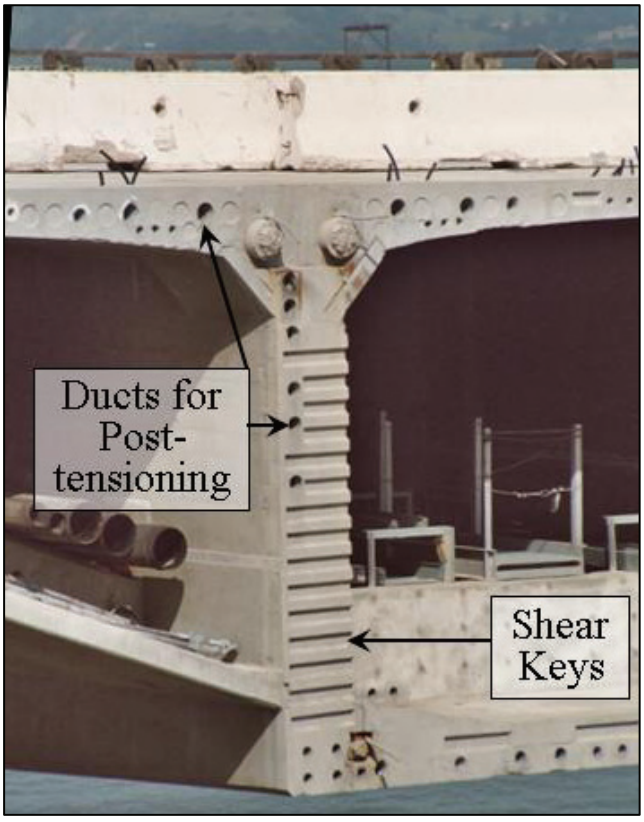

Figure 2-3 Details of Surface Between Segments

Expansions joints are discontinuity regions in the superstructure designed to allow the bridge to move freely due to temperature changes. Typically large beams are constructed inside the superstructure at the expansions joints to ensure moment and shear continuity while enabling axial movement.

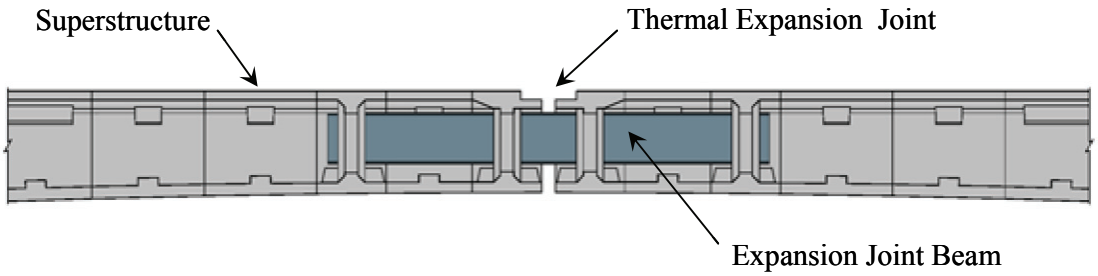

Figure 2-4 Superstructure Expansion Joint Beam (Courtesy of International Bridge Technologies)

2.1.1.1. Longitudinal Post-Tensioning Tendons

The post tensioning (PT) tendons in the superstructure may be either bonded or unbonded. Bonded PT tendons are threaded through ducts that are constructed inside the concrete portions of the superstructure (see Figure 2-3). These ducts are then grouted after the tendons are stressed, thereby bonding the tendons to the superstructure. Unbonded tendons are typically in ducts that are within the hollow center of the superstructure and only attached to the concrete superstructure at the ends of the tendons or at deviator block. Unbonded tendons are thus external to the concrete section, yet not necessarily visible from outside the bridge.

The PT tendons in segmental bridges are an essential part of the structural system and serve many functions throughout the construction and service life of the bridge. To simplify the construction process, it is common to label tendons that serve similar functions as a group. Common tendon groups include cantilever tendons, continuity tendons, harped tendons, top/bottom tendons, and deck tendons. Depending on the construction method and span length, the bridge will utilize some, but typically not all, of the tendon groups.

Cantilever tendons are used for the balanced cantilever or progressive cantilever construction methods to attach the new segment to the previously constructed portion of the bridge. Cantilever tendons are located in the top flange of the superstructure to counter act the negative bending moment generated by the dead load of the structure during construction (see Figure 2-5).

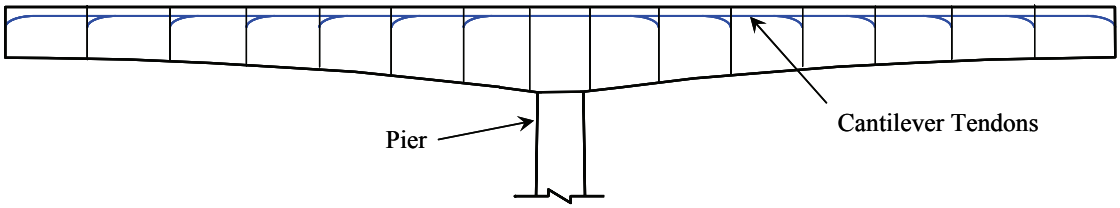

Figure 2-5 Schematic of Cantilever Tendons

Continuity tendons typically run the length of a frame and are used to counter act the live load on the structure and, as the name suggests, to ensure that the

structure acts as a continuous frame. Bonded continuity tendons are typically located within the web of the superstructure and are near the top flange over the piers and near the bottom flange at midspan (see Figure 2-6).

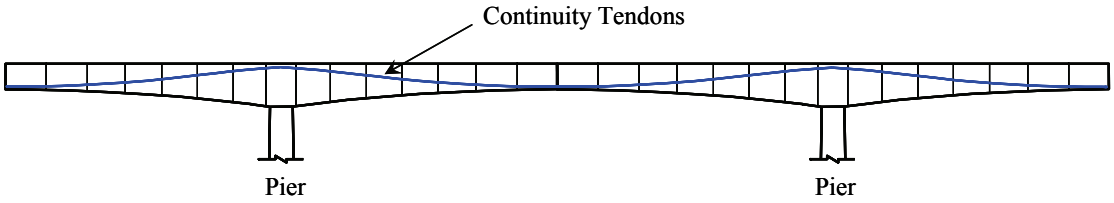

Figure 2-6 Schematic of Continuity Tendons

Harped tendons are used in span-by-span construction and are used to balance the positive moments during construction. Harped tendons are typically external and unbonded (see Figure 2-7).

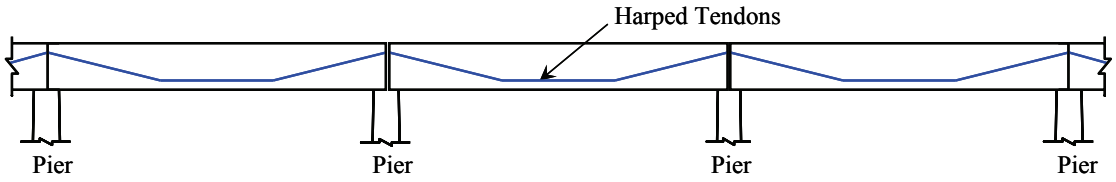

Figure 2-7 Schematic of Harped Tendons

Depending on the construction method and span length, additional tendons may be required at various locations in the top and bottom flanges to ensure that tensile stresses do not occur under any service load conditions (see Figure 2-8). Finally, low stressed tendons may be placed in the deck near the roadway surface to

ensure that the segment joints remain closed following a significant seismic event (see Figure 2-9).

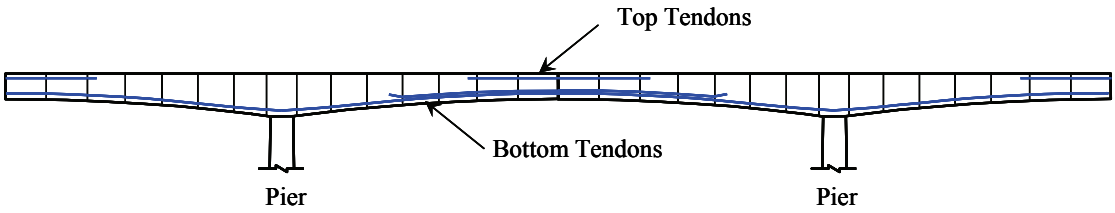

Figure 2-8 Schematic of Top and Bottom Tendons

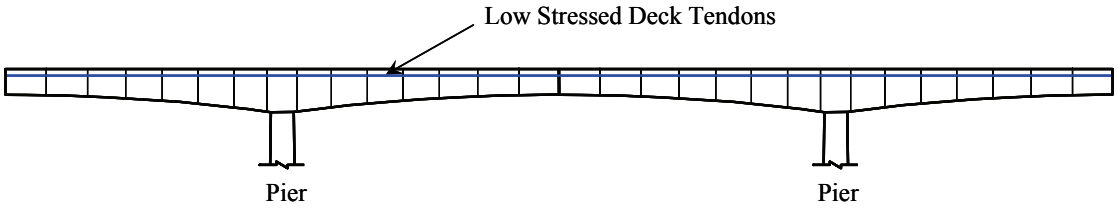

Figure 2-9 Schematic of Low Stressed Deck Tendons

2.1.2. Abutments

The abutments are the end supports of a bridge, and may be constructed with either a pile supported or a spread footing foundation, depending on the soil conditions of the site (see Figure 2-10). The abutments will typically restrain the superstructure from vertical and lateral translations as well as torsional rotations. Longitudinal motions are typically not restrained to allow for thermal expansion of the superstructure. An abutment for a segmental bridge is typically indistinguishable from an abutment for a conventional prestressed concrete bridge of comparable span length.

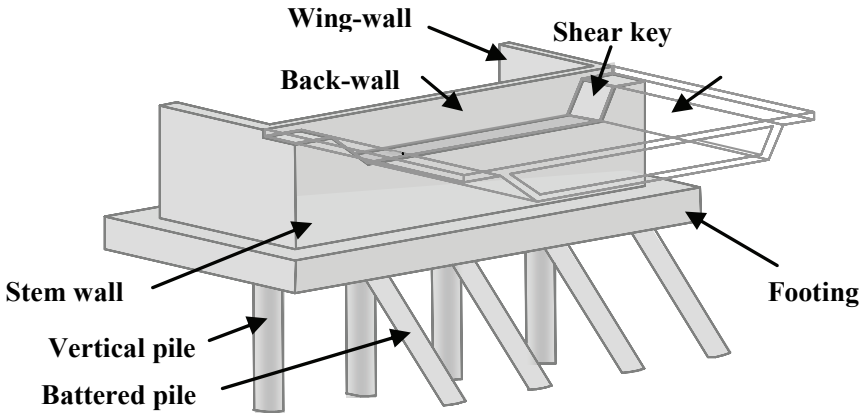

Figure 2-10 Elements of a Bridge Abutment (Megally et al., 2001)

2.1.3. Piers

The piers are intermediate supports of the superstructure and consist of a number of elements, as shown in Figure 2-11: the foundation, the column(s), and a pier table.

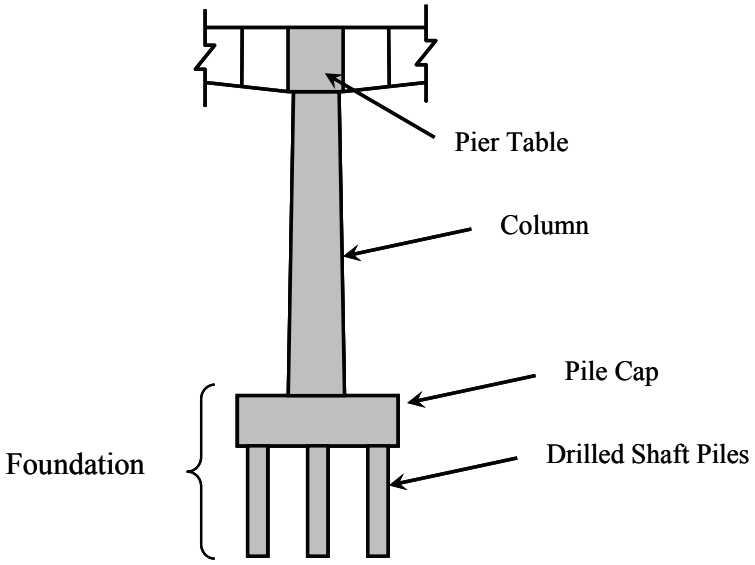

Figure 2-11 Elements of a Typical Segmental Bridge Pier

The pier table is the top portion of the column and can be considered part of the superstructure. The pier table is the starting point for the balanced cantilever construction operations. It is typically cast-in-place and may be either symmetric or asymmetric about the pier center-line. Asymmetric pier tables are used to maximize the unbalanced cantilever moment of each segment and allow for the largest possible segment size. This can minimize construction time by reducing the number of segment erection operations required to complete a span.

The columns transfer the weight of the superstructure down to the foundations. There may be more than one column in a pier depending on the requirements of the bridge. The column for long span segmental bridges will typically be hollow to improve the efficiency of the section. It is common practice to design the columns to develop a plastic hinge mechanism during a maximum credible earthquake. This design approach is intended to protect the superstructure and the foundation from in-elastic behavior

The foundation for a long span segmental bridge is typically very large and usually requires drilled shafts to support the forces coming in from the columns. It is common for these drilled shafts to be six feet in diameter or larger and to extend over

100 feet into the ground. A very large pile cap will be required to transfer the forces between the column and the drilled shaft piles. These mass concrete foundations can generate a large amount of heat during the curing process. Thermal blankets, ice batching of the concrete and/or water pumped through embedded piping in the pile cap may be required to ensure proper concrete curing and to minimize cracking caused by large thermal gradients.

2.2. History

The roots of modern segmental bridge construction can be traced back to the iron and steel truss bridges of the 19th century. A prime example is the Firth of Forth Railway Bridge in Scotland, where individual truss members were erected using the previously constructed portions of the bridge as supports, as shown in Figure 2-12. Construction began at the piers and progressed outward toward midspan on either side in a balanced fashion to prevent the enormous structure from tipping.

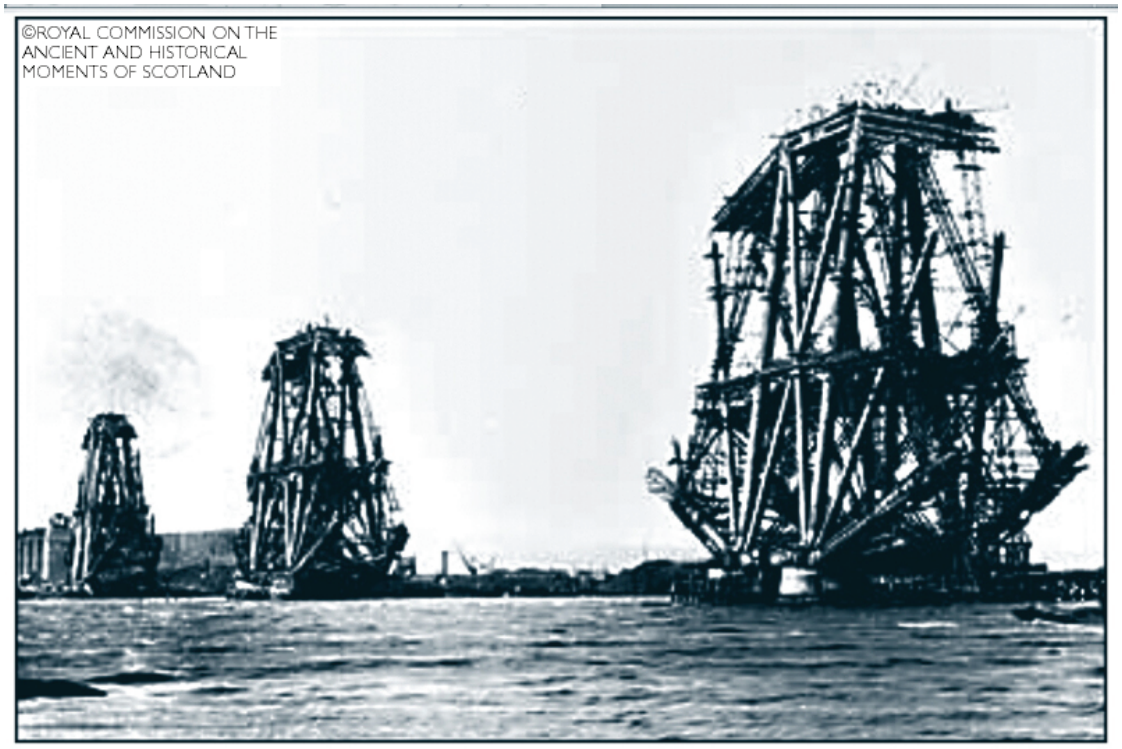

Figure 2-12 Segmental Construction Methods used on the Firth of Forth Bridge, Scotland - Constructed 1883-1890 (Murillo and Showers, 2004)

After World War II, Europe, particularly France and Germany, was in dire need of civil infrastructure, as many bridges and roads were severely damaged during the conflict (Murillo and Showers, 2004). In addition, factories were in disrepair, so large fabricated steel members, for use as final bridge members or as temporary supports during construction, were difficult to come by. It was within this landscape of large infrastructure demands and a shortage of materials that the first prestressed concrete segmental bridge was constructed across the Lhan River in Balduinstein, Germany in 1951 (Murillo and Showers, 2004).

By the mid 1960s more than 300 cast-in-place prestressed concrete segmental bridges had been constructed. This first generation of segmental bridges typically utilized box girder cross sections, midspan deck hinges and due to improvements in prestressing steel technology, was able to span nearly 500 feet. The midspan deck hinges allowed the superstructure to creep under its self-weight without developing large internal stresses. These creep deformations, however, generated noticeable undulations of the bridge that affected serviceability. To address this problem, closure joints between cantilevers from adjacent piers were constructed to make the spans continuous. The first multi-span continuous segmental bridge was the Bouguen Bridge in France and was opened to traffic in 1963 (Murillo and Showers, 2004).

The development of precasting technology in the early 1960s allowed the concrete superstructure segments to be fabricated away from the bridge site and then transported to the site when required. This technology allowed for improved curing of the concrete, reduced influence of weather on production rates, and a shorter construction schedule as the superstructure could be fabricated and stored off site while the foundations were being constructed. The first precast segmental concrete

bridge was the Choisy-Le-Roi Bridge across the Seine River in Paris, which was opened to traffic in 1964 (Murillo and Showers, 2004).

The use of segmental bridge construction methods have been spreading around the world since the 1960s. The first precast segmental bridge in the United States was built in 1973 in Corpus Christy, Texas. The first CIP segmental bridge in the United States was the Pine Valley Bridge along Interstate 8 in San Diego, County, which was opened to traffic in 1974. (Murillo and Showers, 2004)

Figure 2-13 Pine River Bridge, San Diego, CA - The First Cast-in-Place Segmental Bridge in the United States (Opened to Traffic 1974)

Over the years alternatives to the balanced cantilever method of construction were developed to expand the use of segmental bridges. These methods include,

span-by-span construction, progressive placement, incremental launching and cable stayed construction. These methods will be discussed in greater detail in Chapter 2.3

2.3. Construction Methods

The design of segmental bridges is highly dependent on the construction method to be used. The various construction methods for segmental bridges are discussed below.

2.3.1. Cast-in-Place vs. Precast

In CIP segmental construction, the superstructure segments are constructed on the bridge in their final position. Mild steel reinforcement crosses the joint between segments. Prestressing tendons are installed as needed to support the new segments during construction. This construction method is typically cost effective for bridges that have a relatively short total length and have easy access to a concrete batch plant.

In precast segmental construction, the segments are fabricated and stored at a special facility that is typically away from the bridge site. The segments are then delivered to the site as required and installed in their final position using post-

tensioned tendons. The surface between the segments may be covered with epoxy to increase strength and durability and to lubricate the joints for ease of fit during construction. The segments are often steam cured and aged for a month or more prior to installation to minimize creep and shrinkage deformations. The precast segments can be extremely large and will typically require heavy lifting equipment to maneuver and install. This equipment requires a large upfront cost for the contractor. The precast construction method can be very economical for very long bridges where a repetitive assembly line procedure is most efficient and can offset the upfront costs of the heavy lifting equipment. Precast methods allow for improved quality control, reduced weather dependence on production rates and reduced construction time as work on the superstructure and substructure can be performed simultaneously. Precast superstructure segments do not have mild steel reinforcement across the segment joints.

2.3.2. Balanced Cantilever

In the balanced cantilever construction method, segments are placed one at a time beginning at the piers and proceeding outward towards midspan on both sides simultaneously. As construction progresses the negative moment on each cantilever

increases, thus PT tendons are required most at the top of the section near the piers. Eventually the cantilevers from adjacent piers meet at midspan and are connected with a closure joint or an expansion joints. The balanced cantilever method of construction can be performed with either CIP (see Figure 2-14) or precast segments (see Figure 2-15 and Figure 2-16) and has an economical span range of up to 750 feet (Madani, 2006). As mentioned in Section 2.3.1, precast construction methods require heavy lifting equipment to maneuver the large segments during construction. One way to do this is with a moveable overhead gantry as shown in Figure 2-15. Another method utilizes span mounted lifting equipment, as shown in Figure 2-16. For additional photos of segmental bridge construction, see Appendix E.

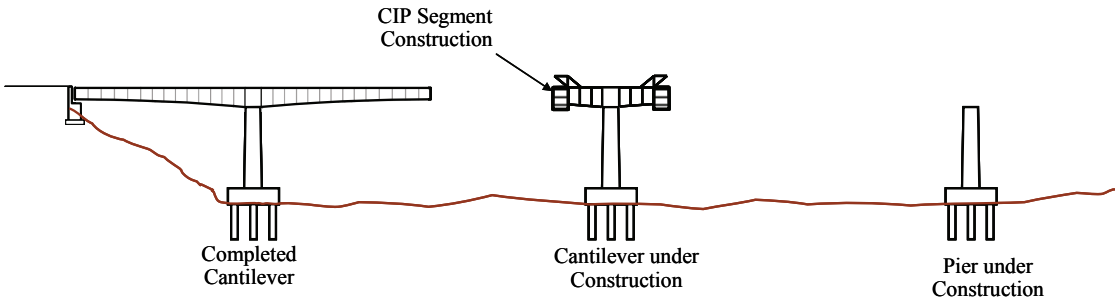

Figure 2-14 Schematic of Balanced Cantilever Construction with CIP Segments

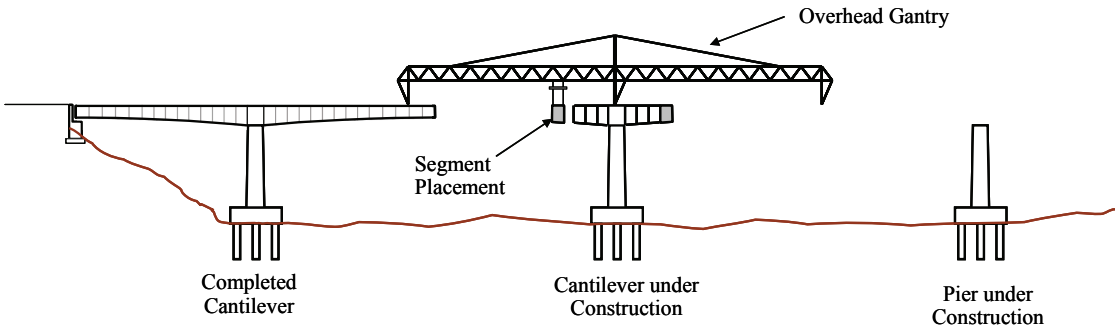

Figure 2-15 Schematic of Balanced Cantilever Construction with Precast Segments and an Overhead Gantry

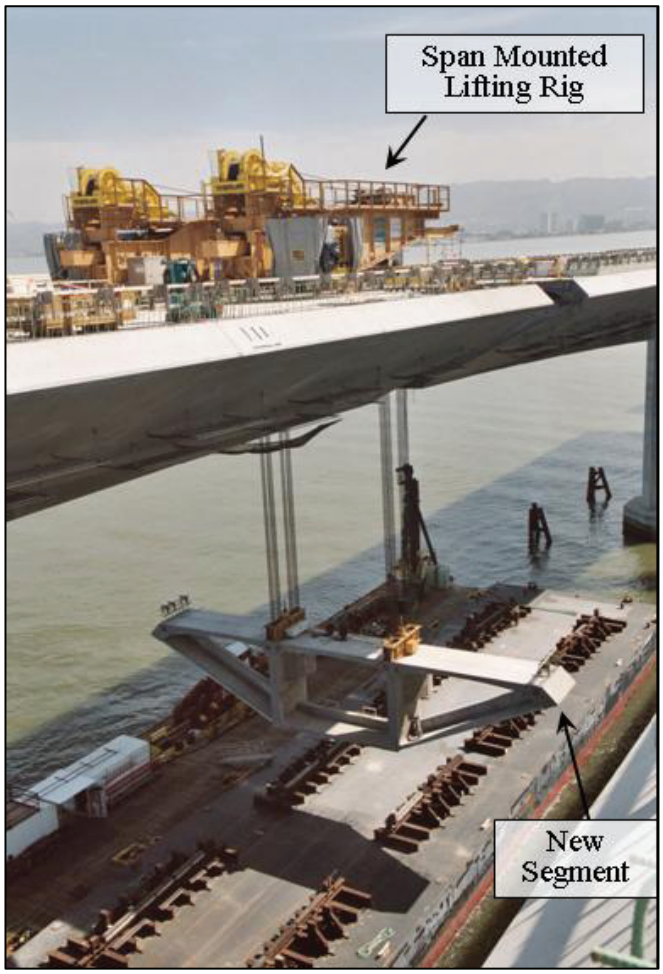

Figure 2-16 Lifting Operation for Balanced Cantilever Construction with Precast Segments and Span Mounted Lifting Equipment

2.3.3. Span-by-span

The span-by-span method, shown in Figure 2-17, typically requires falsework to cross a full span length. Once a span is constructed, post-tensioned and self-supporting, the falsework is release and moved on to the next span. Another variation of the span-by-span method is to construct full spans on the bridge site and then lift full spans in place using heavy lifting equipment. The dead load moment diagram is similar to that of a simply supported beam, thus the PT is heaviest at the bottom of the girder near midspan. The span-by-span method of construction can be performed with either CIP or precast segments and has an economical span range of up to 160 feet (Madani, 2006).

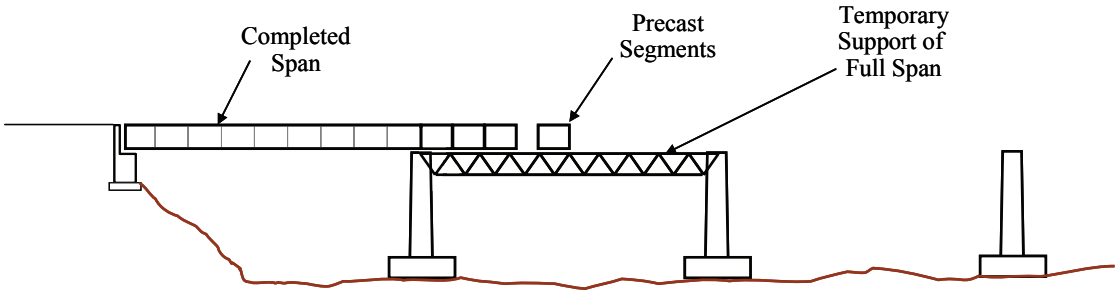

Figure 2-17 Schematic of Span-by-Span Construction with Precast Segments

2.3.4. Progressive Cantilever

The progressive placement method, shown in Figure 2-18, is similar to the span-by-span method in that it begins from one end of the bridge and proceeds

towards the other in a progressive manner. The difference is that segments are placed one at a time, rather than full spans at time. A moveable temporary stay arrangement is typically required to support the cantilever end during construction. The progressive cantilever method of construction is typically performed with precast segments and has an economical span range of up to 200 feet (Madani, 2006).

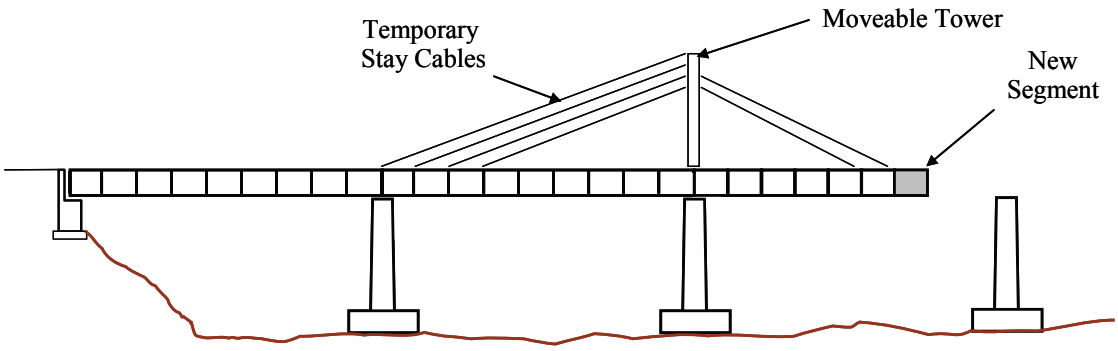

Figure 2-18 Schematic of Progressive Cantilever Construction

2.3.5. Incrementally Launched

The incrementally launched method of construction, shown in Figure 2-19, typically begins at one abutment where a segment is added to the previously built superstructure and then the entire superstructure is pushed outward towards the other abutment, making room for the next segment. This method of construction requires a steel launching nose at the leading edge of the superstructure to reduce the

variations in construction stresses. The incrementally launched method of construction is typically performed with CIP segments and has an economical span range of up to 240 feet (Madani, 2006).

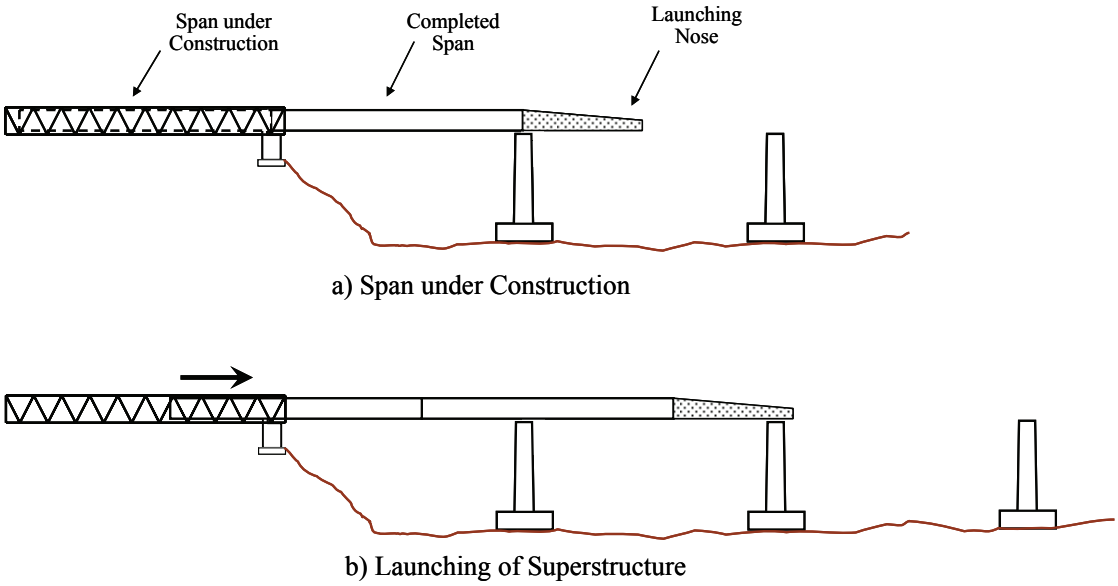

Figure 2-19 Schematic of Incrementally Launched Construction

2.3.6. Cable Stay

Cable stayed bridges are a special type of segmental bridges (see Figure 2-20). In cable stayed bridges the superstructure, or deck as it is more commonly called, is supported from tall pylons by cables. The deck construction begins after construction of the pylons and in a balanced fashion, one segment at a time, from either end of the pylon moving outward. The cantilever segments are supported by cables as they are placed. This allows for smaller deck cross sections, thus

minimizing materials, weight and cost. The cable stayed construction method can be performed with either CIP or precast segments and has an economical span range from 500 to 1500 feet (Madani, 2006).

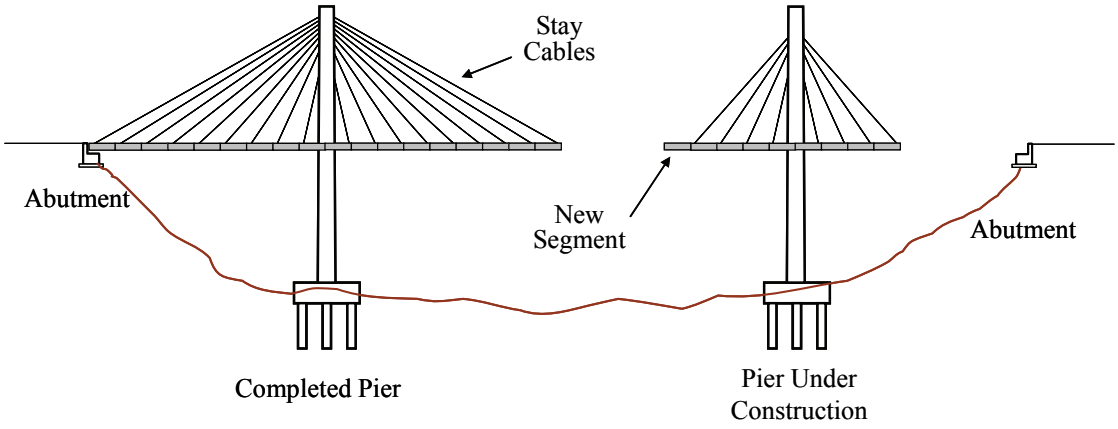

Figure 2-20 Schematic of Cable Stay Construction

2.4. Current Seismic Design Practice in California

The governing seismic design code in California is the Caltrans Seismic Design Criteria (SDC) (Caltrans, 2004). The SDC divides bridges into several classifications and requires different seismic performance and design calculations depending on the classification. All bridges in California are classified as either 'Important' or 'Ordinary'. 'Important' bridges are those that must remain functional after a seismic event. This may be because they are necessary to provide access to emergency facilities or because their loss will significantly impact the economics of the region. All bridges that are not 'Important' are considered 'Ordinary'.

‘Ordinary’ bridges are designed for a no collapse criteria. That is they can sustain significant damage and may require demolition following a significant seismic event, but they must not collapse during the seismic event.

All bridges are further classified as either ‘Standard or ‘Non-Standard’. The most common aspects of a ‘Standard’ bridge are spans less than 300 feet, normal weight concrete, minimal skew and in-plane curvature and a balanced stiffness distribution between piers. Examples of ‘Non-Standard’ bridge features include irregular geometry, unusual framing, or unusual geologic conditions.

The Caltrans SDC applies to ‘Ordinary-Standard’ bridges only. All other bridges require a project specific design criteria to address their specific needs. The seismic demands for ‘Ordinary-Standard’ bridges are obtained using relatively simple response spectrum analyses and are compared with capacities that are calculated based on strain limits.

The project specific design criteria for ‘Important’ or ‘Non-Standard’ bridges will typically outline the specific seismic design requirements, such as strain limits and types of analyses to perform. The irregular features of ‘Non-Standard’ bridges can lead to complex seismic response, thus time history analyses may be required

depending on the 'Non-Standard' features of the bridge. Similarly, it is not uncommon for non-linear time history analyses to be required for 'Important' bridges. When time history analysis is required the seismic demands are typically based on the worst case from three different ground motion sets (T.Y. Lin International and Moffatt & Nichol Engineers, 2001).

Bridges in California are typically designed to be flexible so that they can withstand the displacements imposed by seismic events. This is done by designing in a failure mechanism in the bridge by allowing the development of plastic hinges in the columns. The columns are selected because they are typically the easiest to inspect and repair following an earthquake. The superstructure and foundations are designed using capacity design principles, to be stronger than the columns to force the desired failure mechanism to occur.

Segmental bridges are considered 'Non-standard', and may be either 'Ordinary' or 'Important'. Thus the seismic design requirements will vary depending on the bridge. Time history analyses may or may not be required. In general, however, the current seismic design practice is to follow capacity design

principles, set forth in the SDC, and protect the superstructure and footing from inelastic behavior by forcing the non-linear response into the columns.

CHAPTER 3. LITERATURE REVIEW

Several topics are relevant to the investigations presented in this dissertation. These topics include ground motion selection and scaling, the vertical components of ground motion, the development length of PT strands and the seismic performance of segmental bridges. Literature regarding these topics is discussed in this chapter.

3.1. Ground Motion Selection and Scaling

It is generally understood that the earthquake ground motions used as input in non-linear time history analyses can dramatically impact the seismic response of the structure being studied. Thus realistic representations of the most likely earthquake scenario (i.e. magnitude, distance, fault mechanism, soil type etc.) are critical to the accuracy of the analyses. It is for this reason that real recordings of historic earthquakes are commonly used as input for time history analyses. The scarcity of naturally occurring records with site characteristics similar to the design level seismic event, typically a 1000-2500 year return event, forces engineering seismologists to increase the intensity of records on hand. This is commonly achieved using one of two approaches. The records may be amplitude scaled such

that they are representative of the design response spectra at a specific period or over a period range, or the records are altered, either in the time or frequency domain, to match the design response spectrum. Amplitude scaling preserves the naturally occurring peaks and troughs in the response spectra while spectrum matching smoothes the response spectrum to be compatible with the design spectrum. The effects of these scaling methods on structural response have been studied by a number of research teams.

A number of different techniques have been used to generate spectrum compatible ground motions. One method alters the frequency content of white noise to create a synthetic ground motions. This approach has been criticized for generating ground motions that are not physical with regard to the number of cycles, phase content and duration of the record, and are not recommended (Hancock et al., 2006). A second technique utilizes recordings of actual earthquakes as the starting point and alters the record in the frequency domain by adjusting the Fourier amplitude spectrum (Rizzo et al., 1975; Sliva and Lee, 1987). While this approach is a noticeable improvement over synthetic ground motions, this approach significantly alters the velocity and displacement time series and can result in motions with

unrealistically high energy content (Naeim and Lew, 1995). A third technique modifies actual earthquake records in the time domain using wavelets (Abrahamson, 1992; Lilhanand and Tseng, 1987; Lilhanand and Tseng, 1988; Mukherjee and Gupta 2002a; Mukherjee and Gupta 2002b; Suarez and Montejo, 2003; Suarez and Montejo, 2005). This approach tends to preserve the displacement and velocity time series and introduces less energy into the ground motion than frequency domain methods (Hancock et al., 2006).

Bazzurro and Luco (2003) extensively studied the non-linear response of SDOF and MDOF buildings of different periods and strengths to real unscaled records, amplitude scaled records, and spectrum-compatible records which were generated using wavelets in the time domain (Abrahamson, 1993). The 31 unscaled records were earthquakes with moment magnitude between 6.5 and 6.7 and were within 16 km of the fault. The researchers showed that amplitude scaling tends to make the records slightly more damaging, up to 25%, while spectrum matching makes the record more benign, up to 30%, when compared to the unscaled naturally occurring records. They also showed that spectrum matching reduced response

variability by 60%-80%, and thus needs far fewer analyses to achieve the median response of a structure with the same level of accuracy.

Hancock et al. (2006), corroborated the findings of Bazurro and Luco and stated that matched records exhibit greatly reduced variability, yet scaled records may be preferable if the characteristics of real ground motions are of interest.

Watson-Lamprey and Abrahamson (2006a) studied the response of simple bi-linear SDOF oscillators and found that the main reason for using spectrum compatible records is that they suppress variability and reduce the number of records required to obtain a median response.

Bazzurro and Luco (2006) reiterated their earlier findings and showed that spectral matching has a tendency to soften the near source effect of ground motions by smoothing out the velocity pulses, while amplitude scaled records are typically more aggressive than naturally occurring near field records.

Bommer and Acevedo (2001) recommended limits on record scaling between 2 and 4. Watson-Lamprey and Abrahamson (2006a), however, suggested that these limits were based on comfort level and not quantitative evaluations. They then proposed a method of time series selection that is appropriate for non-linear systems

and showed that large scale factors, in some cases up to 12, can produce reasonable results provided the record is not selected solely based on magnitude and distance, but rather selected based on the characteristics of the scaled ground motions. These characteristics may include the shape of the scaled response spectra, the peak ground acceleration or peak horizontal or vertical spectral accelerations. The ability to use large scale factors increased the pool from which ground motion records may be selected.

The research outlined above on record scaling and spectrum matching is beginning to emerge in the bridge design codes. While the Caltrans SDC (Caltrans, 2004) is intended only for "Ordinary-Standard" bridges and thus does not discuss record selection for time history analyses, the current AASHTO LRFD (AASHTO, 2006) requires the use of five spectrum compatible time histories. However it does not specify whether the bridge is to be designed for the maximum or the mean of these five time histories, and makes no mention of multiple components of ground motion.

The proposed AASHTO Guide Specification for LRFD Seismic Bridge Design (AASHTO, 2007), provides more guidance than the current AASHTO

LRFD, and requires a minimum of three spectrum compatible time histories, each with all three components of motion. The designer is required to design the bridge for the maximum response obtained from the three time series sets. As an alternative, bridges may be designed for a minimum of seven time histories and designed for the mean response. In addition, the proposed AASHTO Guide Specification (AASHTO, 2007), states that near field effects, such as fling and forward directivity, must be considered when within six miles of a fault.

No studies were found that investigated the effect of different methods of amplituded scaling, such as scaling the lateral motion to a single period or scaling the lateral ground motion across a period range, on the structural response.

3.2. Vertical Ground Motion

A number of studies have investigated the impact of the vertical component of ground motion on the response of highway bridges (Saadeghvaziri and Foutch, 1991; Broekhuizen, 1996; Yu et al., 1997; Gloyd, 1997). In general they studied conventional prestressed concrete bridges and showed that vertical motion can

significantly affect the axial load demand on the columns as well as the moment demand on the superstructure.

Yilmaz et al. (2006) performed a number of analyses on the response of typical California highway bridges to vertical accelerations. They noted the importance of vertical acceleration, especially for near field events and commented on the lack of guidance from bridge design codes with respect to vertical acceleration.

The Caltrans SDC (Caltrans, 2004) requires vertical static analysis based on 0.25g for 'Ordinary-Standard' bridges where the peak horizontal rock acceleration is 0.6g or greater. It states that combined vertical and horizontal load analysis is not required for 'Ordinary-Standard' bridges, however the SDC mentions that the effect of vertical is required for 'Non-Standard' and 'Important' bridges, but provides no guidance on how to determine the vertical component.

The current AASHTO LRFD (AASHTO, 2006) does not mention the vertical component of ground motion. The proposed AASHTO Guide Specification for LRFD Seismic Bridge Design (AASHTO, 2007), on the other hand, requires all three components of motion to be used in time history analyses. The commentary

mentions that the high short period spectral content of near-source vertical ground motions should be considered, however guidance for obtaining a vertical design spectrum or vertical time histories is not given.

Design codes for the building industry provide more guidance than bridge codes with regard to vertical earthquake motion. FEMA (FEMA, 2000) recommends determining the vertical design spectrum by scaling the lateral design response spectrum by a factor of 2/3 over the entire period range. The vertical design spectrum, however, is not used for time history analyses. Instead FEMA requires scaling of the horizontal components of ground motion for a best fit with the design spectrum over a period range. It is unclear what scale factor is to be used on the vertical component of ground motion, but presumably it is the same as the horizontal.

A number of studies (Niazi and Bozorgnia, 1989; Niazi and Bozorgnia, 1990; Niazi and Bozorgnia, 1991; Niazi and Bozorgnia, 1992) showed that a constant reduction of 2/3 is not accurate for near source events and revealed that a vertical-to-horizontal (V/H) ratio greater than unity can occur in the low period range. Campbell and Bozorgnia (2004) studied over 400 real accelerograms and developed

a near-source attenuation relationship for horizontal and vertical components of ground motion. Bozorgnia and Campbell (2004) found that the vertical-to-horizontal response spectral ratio is very sensitive to period, distance to fault and soil type and somewhat insensitive to magnitude and style of faulting (see Figure 3-1). They proceeded to use their attenuation model, as well as other notable attenuation relationships, to develop simple V/H ground motions models and a simple procedure to develop a tentative vertical design spectrum.

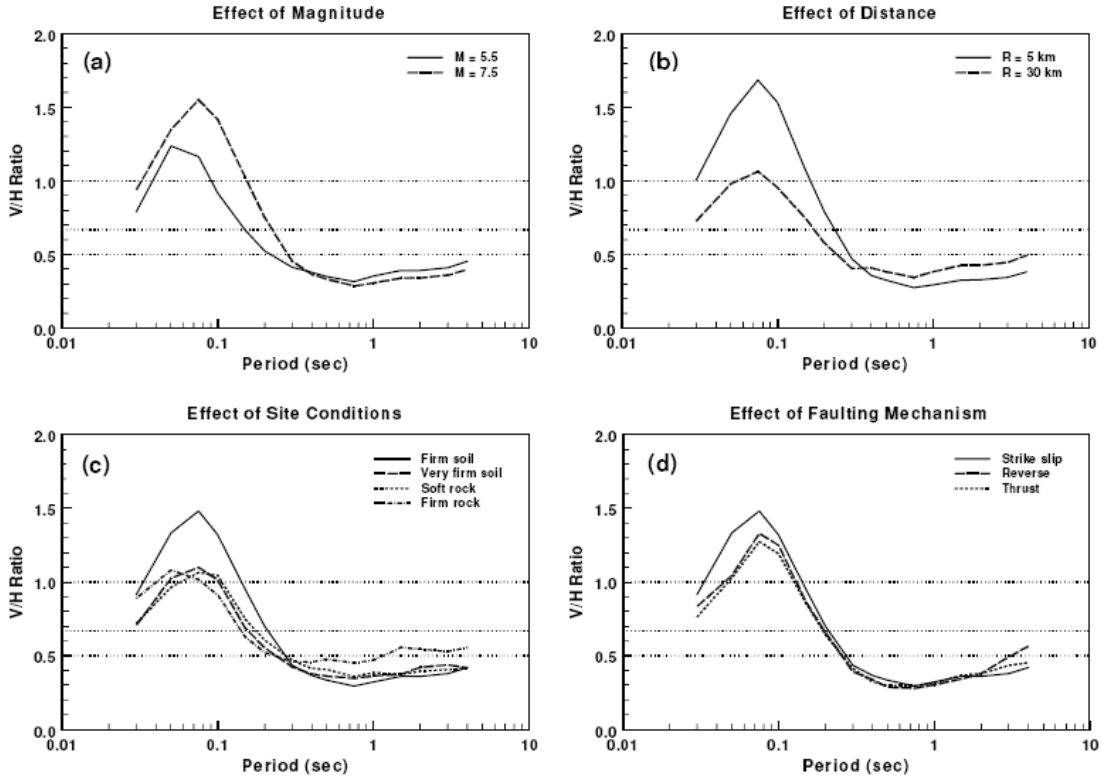

Figure 3-1 V/H ratio for Various Parameters (from Bozorgnia and Campbell, 2004)

Yilmaz et al. (2006) developed an alternative method for determining a vertical design spectrum. Their proposed method is based on a period shift and amplitude scaling of the horizontal design spectrum. The magnitude of the amplitude scale factor is based on distance from the fault.

3.3. Development length of Post tensioning strands

As segment joints in a precast segmental bridge open, the strain in the PT tendons crossing the segment joints must increase to accommodate the deformations. The increased tendon strains penetrate into the segments and will cause debonding of the tendon strands within the grouted duct. It will be shown in Section 4.3.1 that the length of debonding significantly impacts the rotation capacity of precast segmental bridge joints, thus determining this length is critical to accurately estimate the deformation capacity of segmental joints with bonded tendons.

There have been a number of studies (Ghosh and Fintel, 1986; Tabatabai, and Dickson, 1993; Russell, and Burns, 1996; Barnes et al., 2003) that investigated the development length of single PT strands in precast pre-tensioned beams. The development length is defined as the sum of the transfer length, L_t, and the flexural bond length, L_b (Naaman, 2004). The mechanics behind these two parameters are

very different. The transfer length is based on bond stresses generated by the expansion of the strand diameter as the strand withdraws into the concrete, L_w, after release from the stressing rig at the ends of pretensioned beams (see Figure 3-2). The debond length, on the other hand, is based on an expanded tendon length and contracting strand diameter as the tendons stress increases as shown in Figure 3-3.

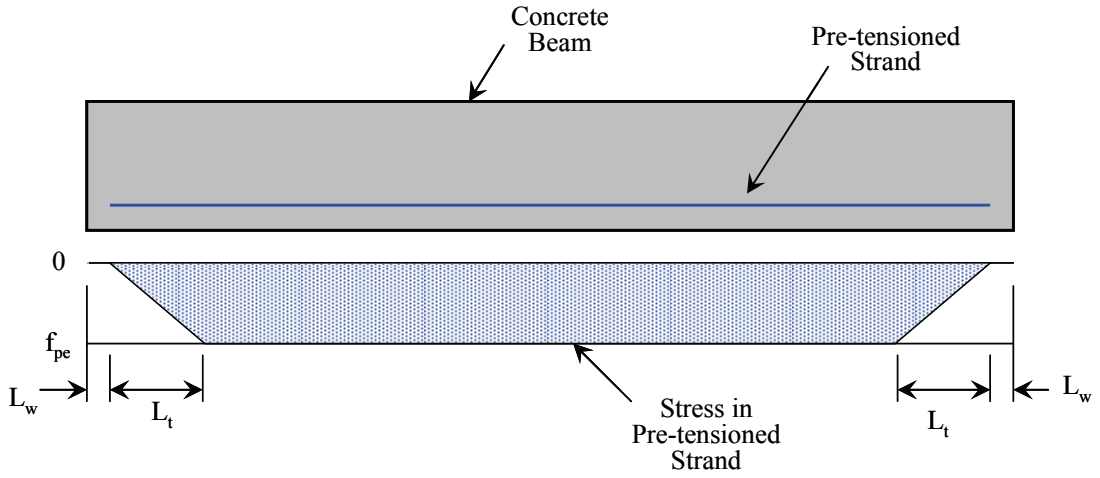

Figure 3-2 Transfer Length in Pre-Tensioned Beams

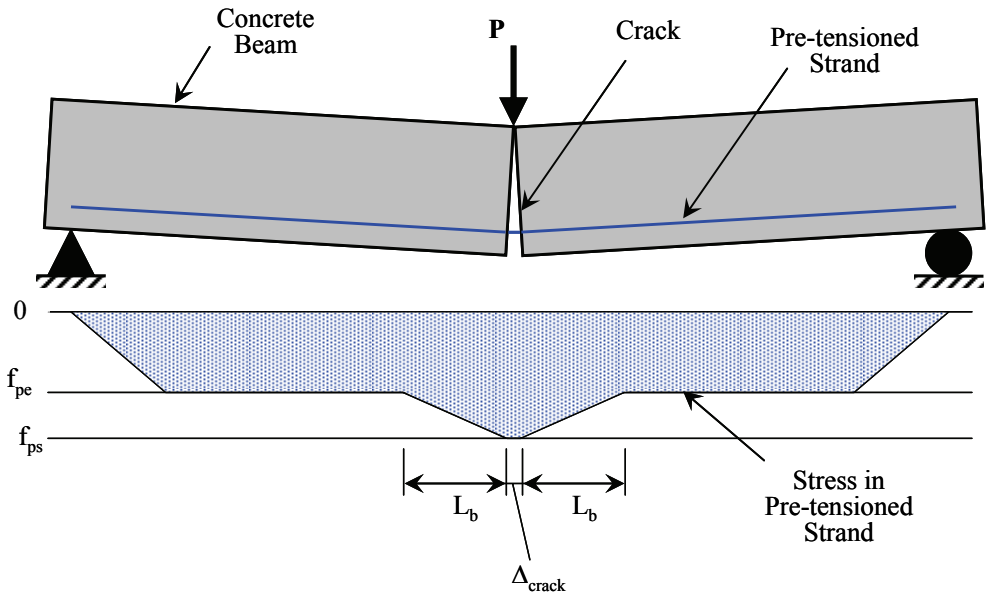

Figure 3-3 Flexural Bond Length in Pre-Tensioned Beams

The flexural bond length equation, developed by Zia and Mostafa (1977) after extensive study of previous research, is the most appropriate estimate of the debonded length for analysis of precast segmental bridges.

$$L_b = 1.25\left(f_{ps} - f_{pe}\right)d_b \qquad \textbf{3-1}$$

Where f_{ps} is the full design strength of post-tensioning strand, f_{pe} it the effective stress in post-tensioning strand and d_b is the diameter of the strand. This equation is applicable to seven wire strand and is based on an assumed bond stress of 250 psi.

While Equation 3-1 can give an estimate of the debond length on either side of a segment joint crack, it was developed for a single seven wire strand and may be inappropriate for multi-strand tendons. This is because the strands in a tendon tend

to cluster together and act as a group. The effective bond surface of the group is not a simple multiple of the strand bond area, but rather the surface are of the whole group, as shown in Figure 3-4. Thus multi-strand tendons may show a debond length larger than that indicated by Equation 3-1.

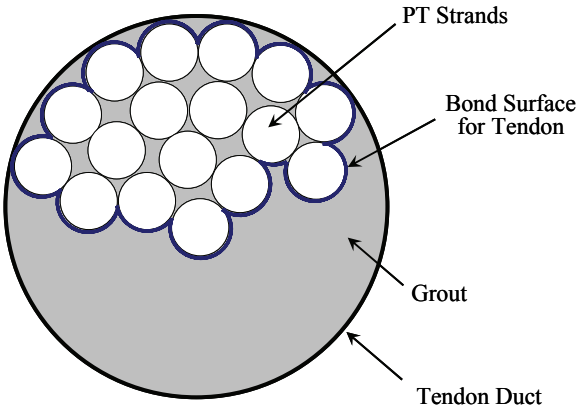

Figure 3-4 Bond Surface Area for PT Tendons

3.4. Segmental Bridges

There is a large body of research studying segmental superstructures. These studies investigated the shear and flexural behavior of segmental bridges with external PT using epoxy and dry joints (Ramirez et al., 1993; Hindi et al., 1995), shear studies on the behavior of multiple and single shear key segment joints (Aparicio et al., 2002; Turmo et al., 2006a), modeling of unbonded PT with dry joints (Turmo et al., 2006b), proof testing of full scale segments with unbonded PT and dry joints (Tassin et al., 1996; Takebayashi et al., 1994), to name a few. The

vast majority of this research, however, addressed strength considerations for service load conditions using monotonic push testing techniques, and did not address the cyclic response expected during a significant seismic event. The only research found in the literature addressing the seismic performance of segmental bridge superstructures was performed at the University of California at San Diego (UCSD) and is outlined below.

3.4.1. UCSD Segmental Superstructure: Phase I – High Moment and Low Shear Experiments

Four 2/3 scale test units were tested under vertical loading to failure to investigate the performance of precast segments in superstructure regions of high moment and low shear (Megally et al., 2002). The test set-up is shown in Figure 3-5. The test units investigated different post tensioning layouts as shown in Figure 3-6. In addition, one test unit was constructed with a cast-in-place deck closure and 100% internal tendons. All test units achieved large rotations prior to failure. The Failure modes varied from rupture of the PT, to crushing of the extreme concrete fibers to buckling of the deck rebar and subsequent compression failure of the cast-in-place deck.

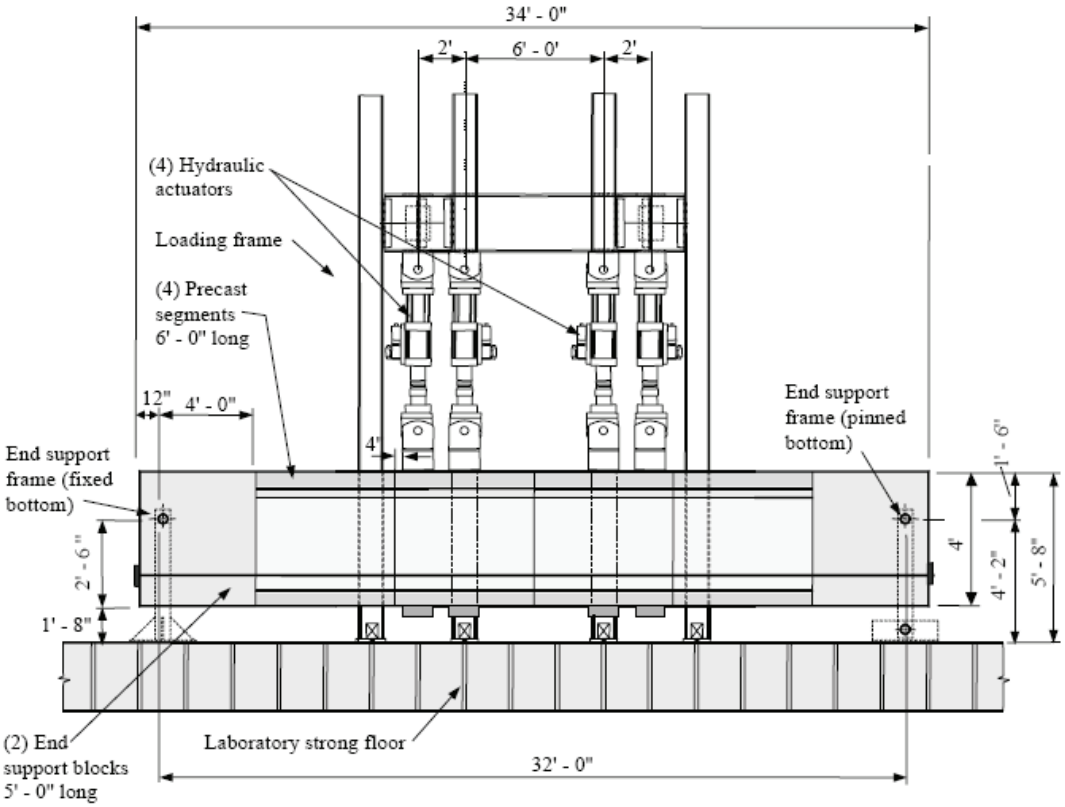

Figure 3-5 Phase I Experimental Test Set-Up (Megally et al., 2002)

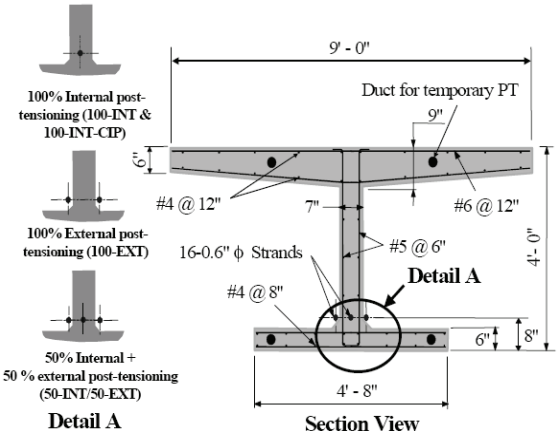

Figure 3-6 Phase I Test Unit Cross Section (Megally et al., 2002)

3.4.2. UCSD Segmental Superstructure: Phase II – High Moment and High Shear Experiments

This phase of the research program utilized similar test units as in Phase I, but with different PT details and test set-up (Megally et al., 2002). The test units and test set-up are shown in Figure 3-7 and Figure 3-8, respectively. The results of this phase are similar to the previous phase in that all test units achieved large rotations prior to failure. In addition, no relative shear slip between segments was observed prior to flexural failure. All test units experienced crushing of the bottom soffit under negative bending. The final failure, however, varied from crushing of the top flange to rupture of the PT tendons.

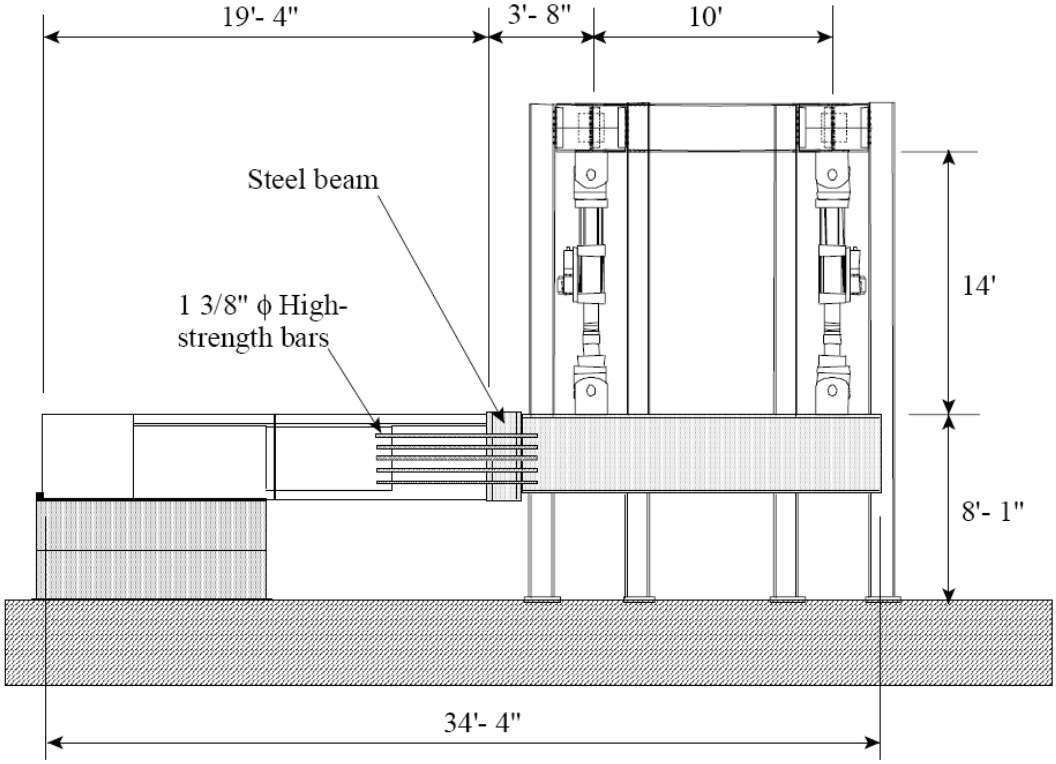

Figure 3-7 Phase II Test Set-Up (Megally et al., 2002)

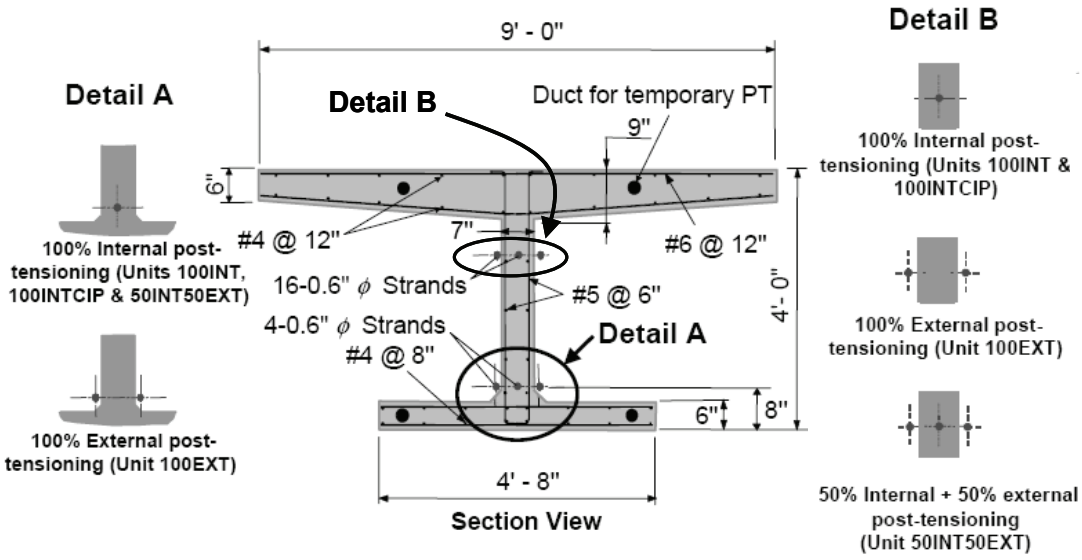

Figure 3-8 Phase II Test Unit Cross Section (Megally et al., 2002)

3.4.3. UCSD Segmental Superstructure: Phase III – System Test

This phase of the research program looks into the performance of a half-scale superstructure-pier system (Burnell et al., 2005). The test set-up and superstructure cross section are shown in Figure 3-9 and Figure 3-10, respectively. The testing program for this phase was split into two stages. The first stage achieved a column displacement ductility of 4 and utilized 100% of the design post-tensioning as well as 100% of the superstructure dead load. The results from this stage indicate that there is no significant opening of the segment-to-segment joints. A hairline crack was observed at a displacement ductility of 4, but this was adjacent to the cast-in-place closure pour, so the crack was likely initiated by shrinkage. The second stage of testing continued from displacement ductility 4 up to ductility 8 and utilized 175% of the superstructure dead load, to simulate the effect of vertical ground accelerations, and approximately 75% of the longitudinal superstructure PT. The results from this stage indicated that segment-to-segment joints open during testing, but they close when the earthquake demands are removed.

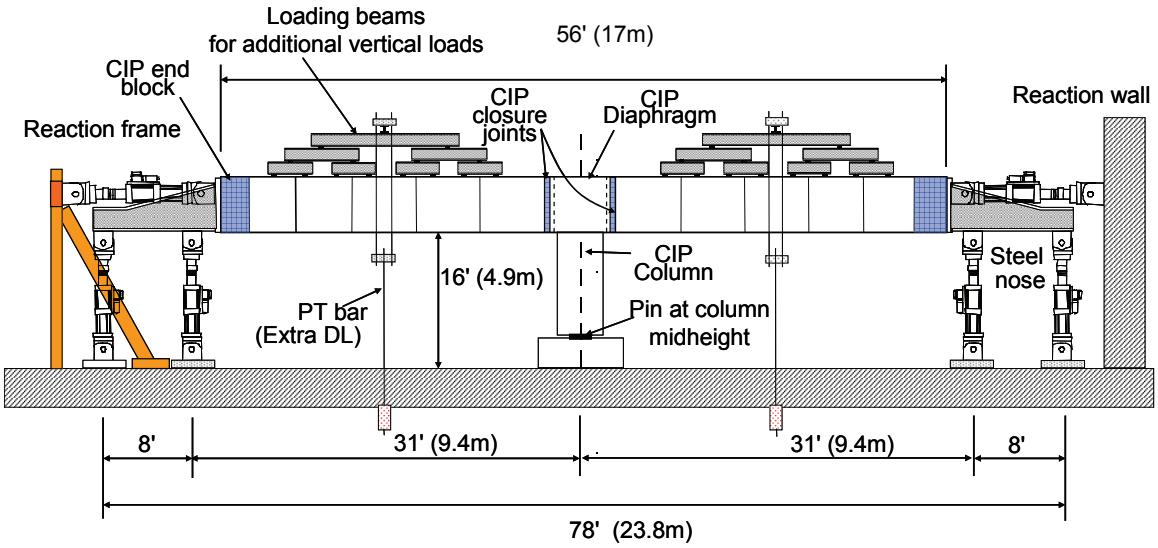

Figure 3-9 Phase III Experimental Test Set-Up (Burnell et al., 2005)

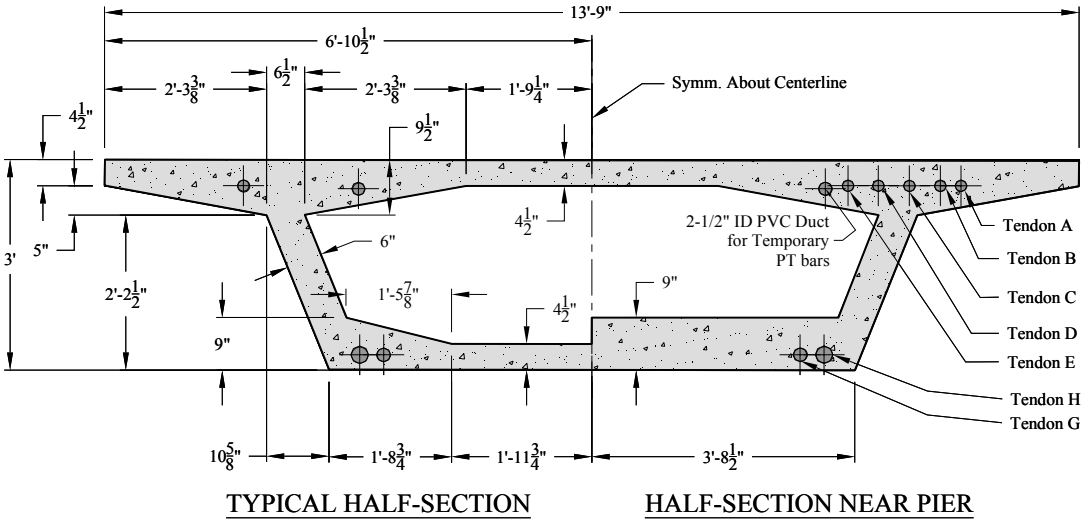

Figure 3-10 Phase III Test Unit Superstructure Cross Section (Burnell et al., 2005)

3.4.4. UCSD Segmental Superstructures with Lightly Stressed Deck Tendons

Densley et al. (2003) studied the performance of precast segmental superstructure with low stressed auxiliary tendons in the deck slab. The purpose of these tendons was to minimize the likelihood of residual joint opening following a seismic event. The test set-up was exactly the same as the Phase I experiments by Megally et al. (2002). The design details of the test unit were similar to those of the San Francisco-Oakland Bay Bridge Skyway thus this test unit was also a proof test of designs in place in high seismic zones of California.

The results from this experiment were compared with the Phase I results by Megally et al. (2002). The results showed that continuity of precast segmental superstructures can be achieved by the use of low-stressed auxiliary prestressing tendons in the deck and that these tendons reduce the permanent openings of the segment joints in the deck when compared to CIP closure joints.

CHAPTER 4. JOINT MODEL VALIDATION

To ensure that the analytical model accurately represents the physical world, the joint model must be validated with physical experiments. Two detailed finite element models of test unit 100-INT from the Phase I experiment by Megally et al. (2002), were created using the computer software Ruaumoko (Carr, 2004). Ruaumoko was selected because of its extensive library of non-linear hysteresis and damping rules. These models were developed to capture numerous physical characteristics of the segment-to-segment joints. These characteristics include: crushing of extreme concrete fibers, yielding of PT tendons at the true limit of proportionality, and energy dissipation due to bond slip of the grouted internal tendons.

4.1. Single Joint Model

The first model, shown in Figure 4-1, captured the moment rotation response of a single segment-to-segment joint. To concentrate deformations at the midspan joint, the rotations of the girder nodes were slaved to the rotation at the supports. Rigid elements between the superstructure girder elements and the PT were used to

ensure accurate PT deformations. At the joint locations, however, rigid elements were not used. Rather, the vertical deformations of the PT nodes were slaved to the girders. This allowed for tendon slip caused by strain penetration into the segments.

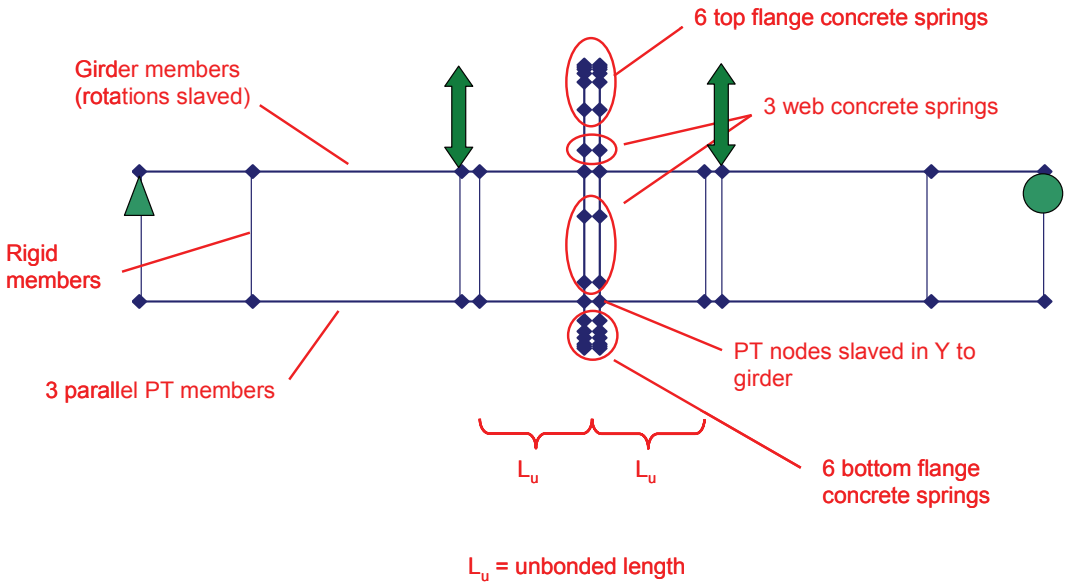

Figure 4-1 Single Joint Model

4.1.1. Segment Joint Concrete Elements

The compressive strength of the concrete was based on 85% of day of test $f_c^{'}$ with crushing occurring at a strain of 0.17%. The tensile strength was based on 15% of the modulus of rupture, f_r , calculated as $3.5\sqrt{f_c^{'}(psi)}$ to match the strength of concrete after the onset of cracking. Thus the model did not predict the initial cracking strength of the section. The length of the concrete joints springs were

defined to be six inches based on estimates from photographs of the Phase I experiments by Megally et al. (2002).

The joint was modeled with six truss elements at the top and bottom flanges and three truss elements at the web. Each element captures concrete crushing and tensile cracking using an origin centered hysteresis rule to capture the loss of stiffness after cracking and crushing (see Figure 4-2).

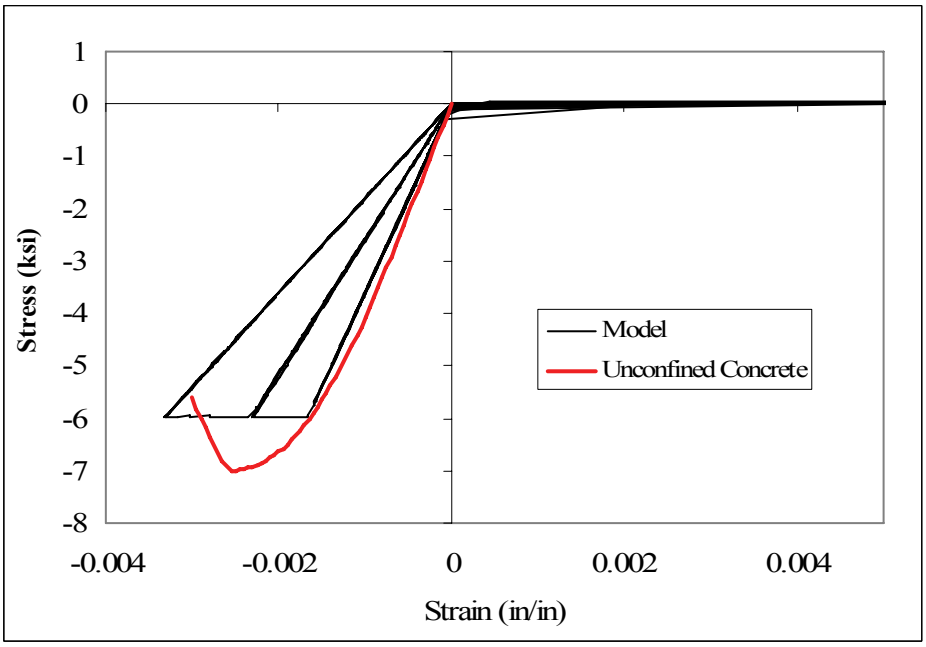

Figure 4-2 Joint Concrete Hysteresis Model

4.1.2. Segment Joint PT Elements

It was believed that the energy dissipation observed at small joint rotations in the Phase I experiments by Megally et al. (2002) was due to friction caused by bond

slip between the PT strands and the grout. When a segment joint opens due to seismic demands, the PT tendons crossing the joint must elongate to accommodate the gap opening. As the tendons stretch and contract under cyclic seismic loading the strands lose their bond with the grout. Thus as the joints open and close the tendons slide relative to the surrounding grout, dissipating energy due to friction.

The energy dissipation at large rotations was believed to be dominated by yielding of the PT tendons. The yield strain of high strength steel is often determined using the 0.2% offset rule (Naaman, 2004). This method, however, does not capture the true limit of proportionality of high strength steel and will not accurately predict when inelastic behavior begins (see Figure 4-3).

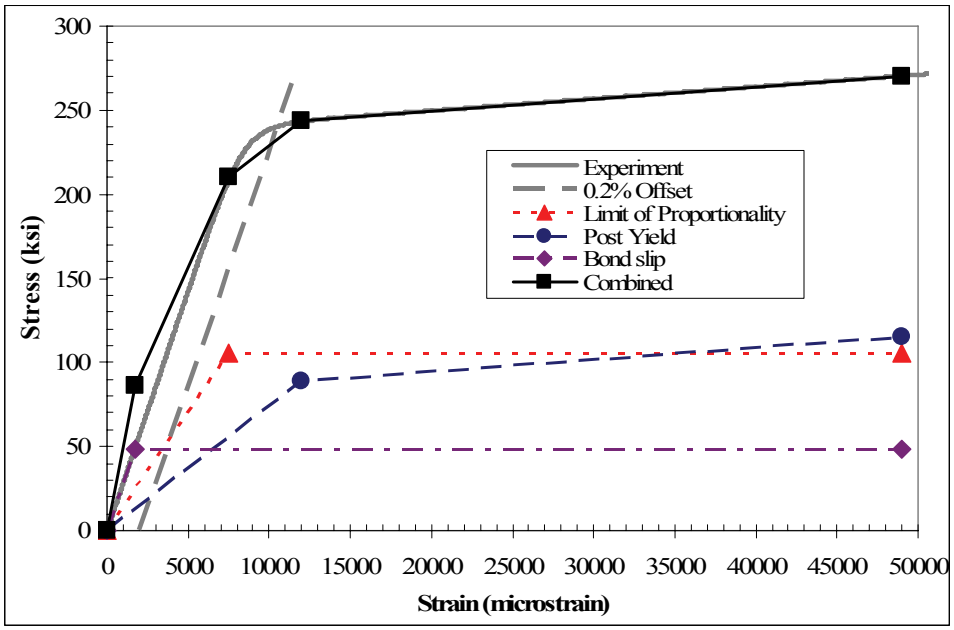

Figure 4-3 PT Tendon Modeling

To accurately capture the onset of inelastic response in the PT and friction due to bond slip, the tendon across the joint was modeled with three separate elements (see Figure 4-3). One element captured the early onset of yielding at the true limit of proportionality of ASTM A416 (270 ksi) steel which was taken to be 210 ksi (= 0.78 f_u). A second element captured the response of PT between the limit of proportionality and the idealized yield stress, assumed to be a strain of 1.2%, as well as the post yield response of PT strands. The third element captured the bond slip behavior of PT across the joint. The cyclic response of the combined PT members is shown in Figure 4-4.

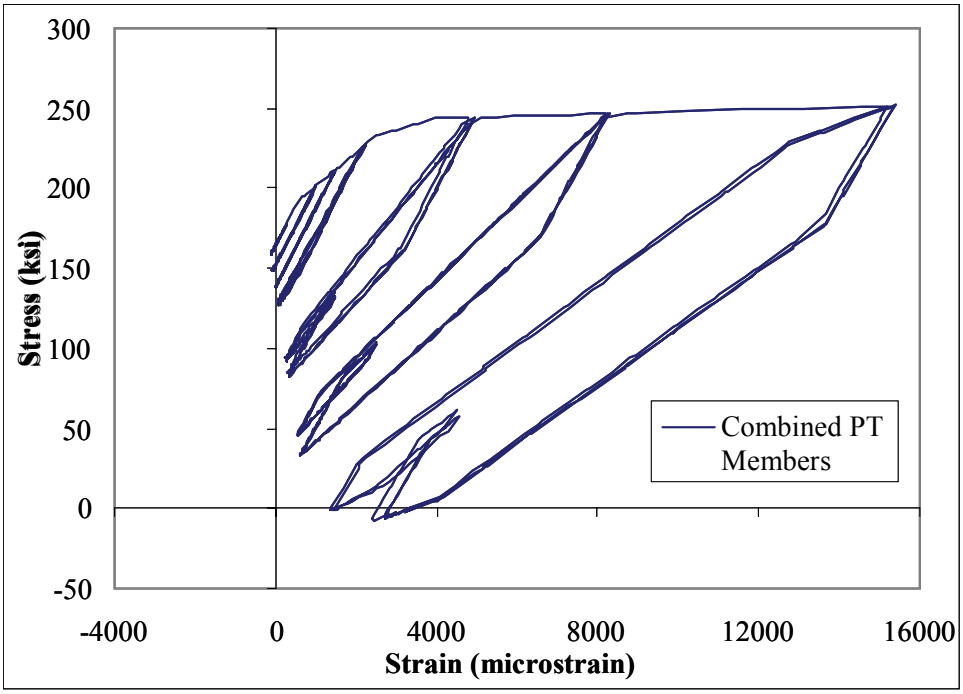

Figure 4-4 Combined PT Hysteresis Model – Includes Bond Slip

Because of the lack of knowledge, a bond-slip relationship for multi-strand tendons, as discussed in Section 3.3, was obtained by a trial and error process to match the experimental data. This process is described in detail in Section 4.3.1.

4.1.3. Comparison with Experimental Results

Results from the single joint model are shown in Figure 4-5. The backbone curve, yield rotation and energy dissipation match very accurately the experimental results, especially in the small rotation range where seismic rotation demands were expected to be. Differences between the model and the experiment at large rotations are such that the residual rotations in the model are larger than observed in the tests.

Therefore the residual rotations obtained from the analyses will be accurate if not over-predicted.

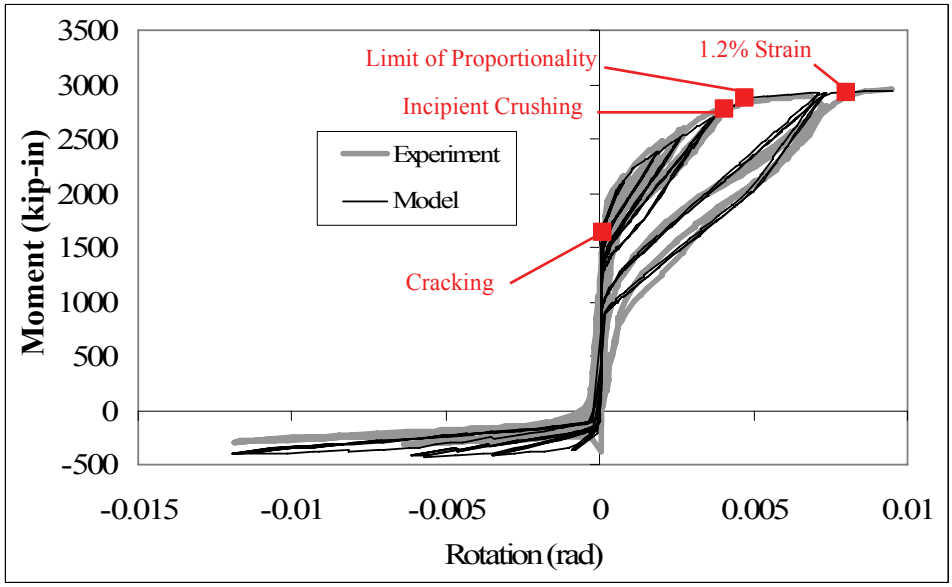

a) Small Rotations

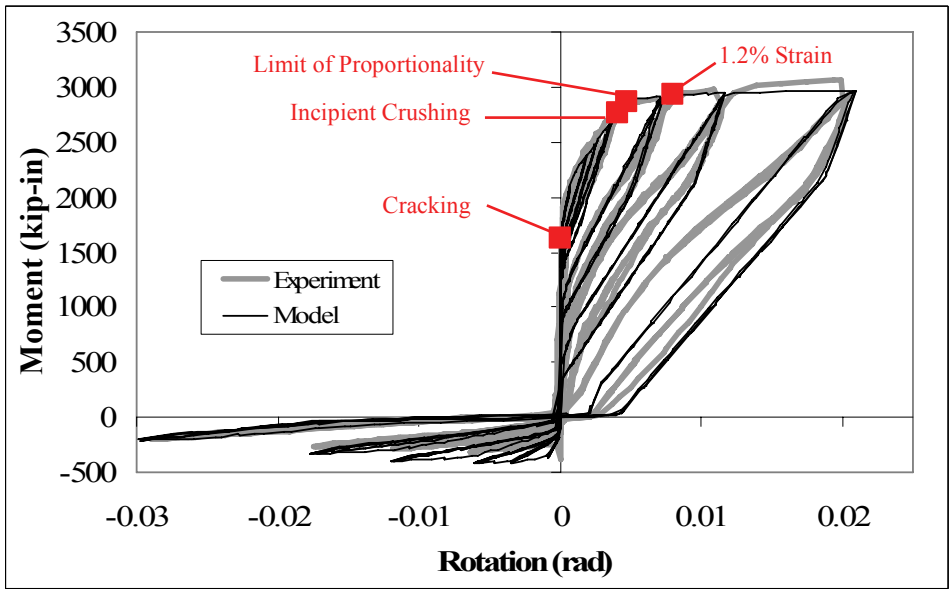

b) Large Rotations

Figure 4-5 Moment-Rotation Diagrams of Single Joint Model

4.2. Multiple Joint Model

The second validation model, shown in Figure 4-6, captured the response at the multiple segment level including deformations of the precast segments and joint opening. This model allows the superstructure girders to crack and captured shear deformations of the girders using a concentrated flexibility approach. That is, all the shear deformations were concentrated in two non-linear element located at segment-to-segment joints 2 and 4. Note that shear deformations were not expected to be significant in a full size bridge superstructure, because the shear span of a full size bridge is much larger. These elements were added to the model to capture effects observed in the experiment. The properties of the non-linear shear springs were estimated using the modified compression field theory (Collins and Mitchell, 1991).

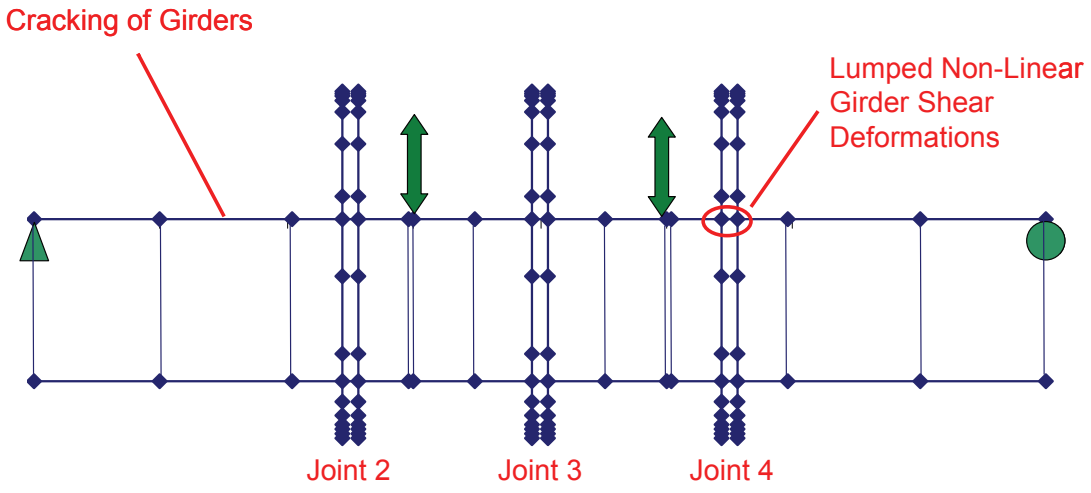

Figure 4-6 Multiple Joint Model

Results from the multi-joint model are shown in Figure 4-7 and Figure 4-8. Figure 4-7a shows the Moment-Rotation of the midspan joint for small rotations (less than 0.005 radians). This plot suggests that the computer model slightly under-predicted the joint rotation. This, however, is not the case because the target displacement for the 1 inch cycle was not reached, as can be seen in Figure 4-7b.

Figure 4-8a shows the segment-to-segment Moment-Rotation diagram for large rotations (greater than 0.0075 radians), while Figure 4-8b shows the Girder Shear-Midspan Deflection diagram. These diagrams indicate that the model overestimated the midspan joint rotations while matching the midspan vertical deformations. This suggests that the finite element model will provide conservative joint rotation estimates and was considered acceptable.

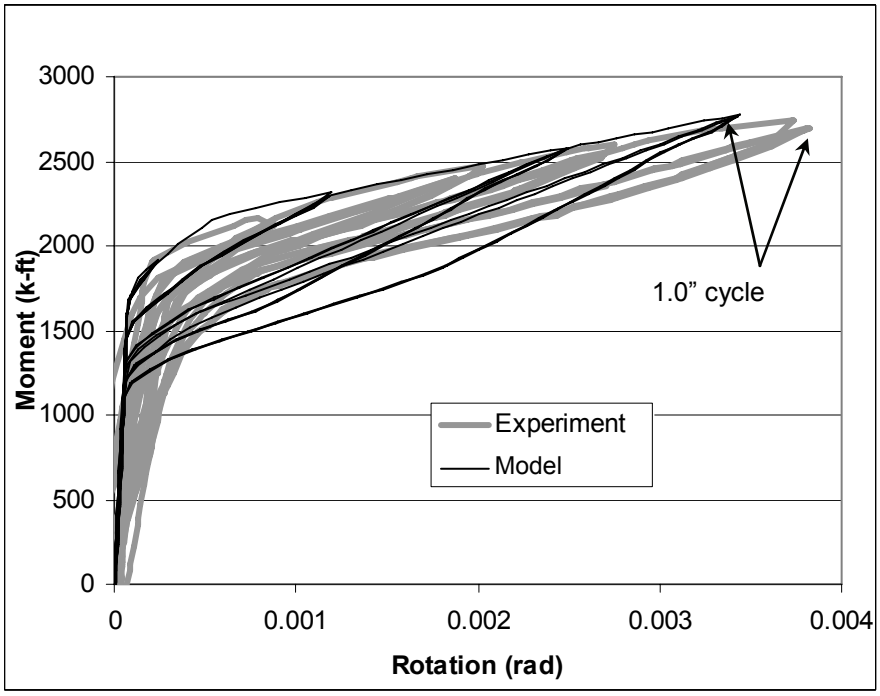

a) Midspan Moment-Rotations

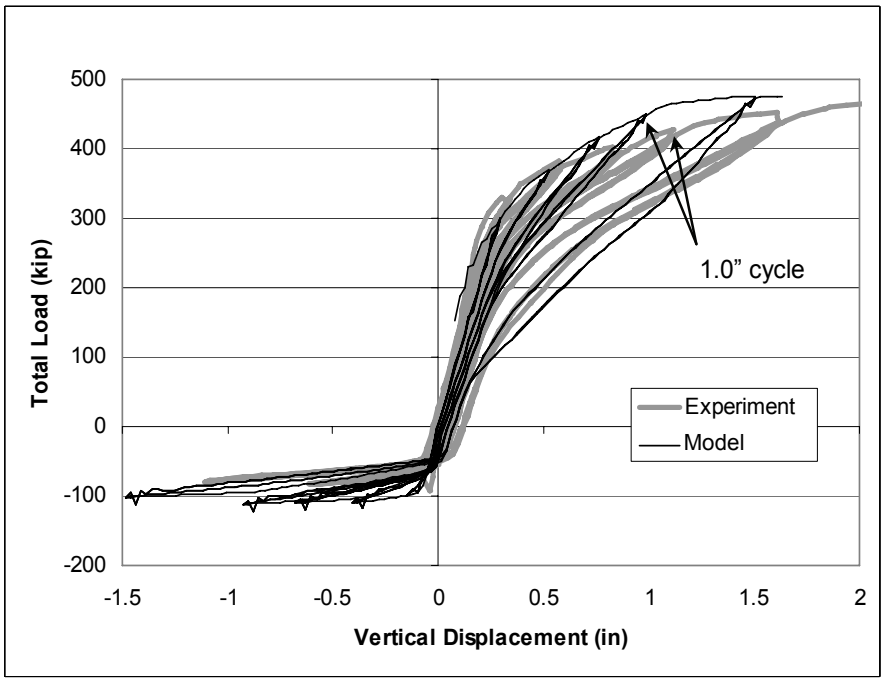

b) Girder Shear-Midspan Deflection

Figure 4-7 Small Deformation Results from the Multiple Joint Model

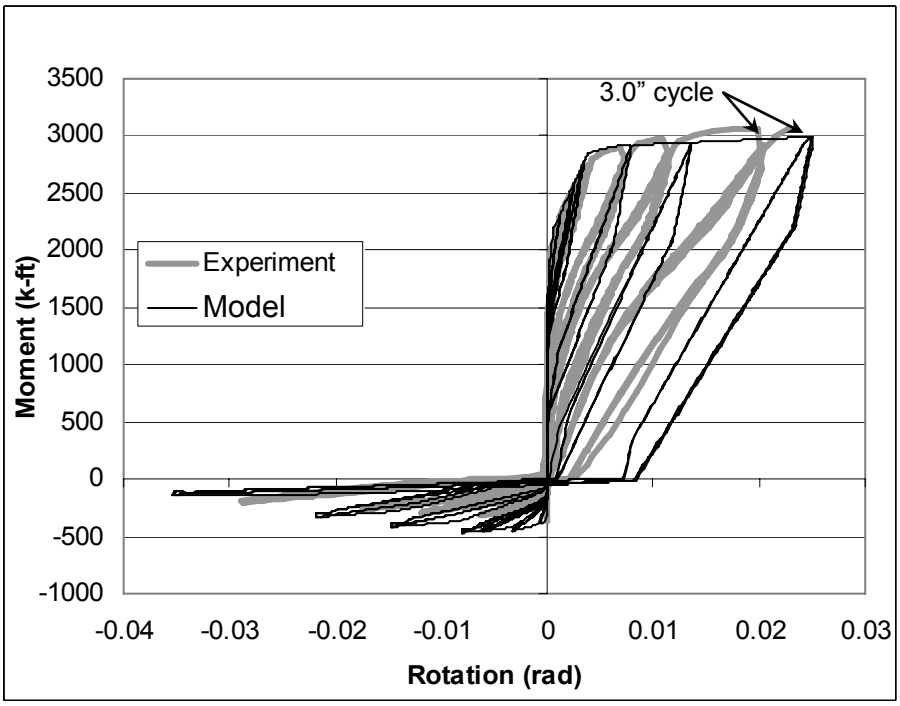

a) Midspan Moment-Rotations

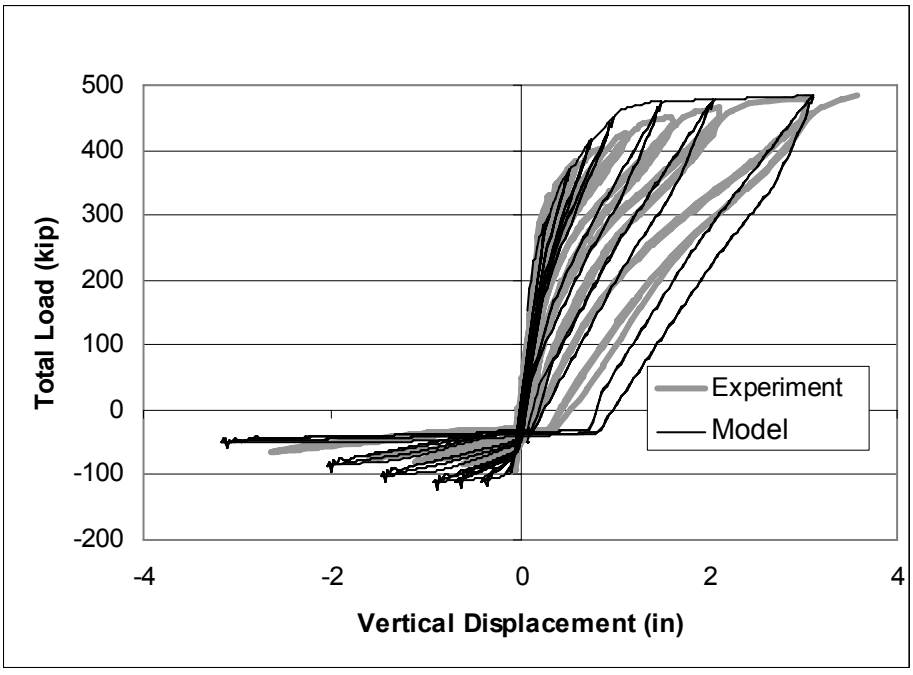

b) Girder Shear-Midspan Deflection

Figure 4-8 Large Deformation Results from the Multiple Joint Model

4.3. Sensitivity Studies

Three separate parameter studies were performed to investigate the influence of various variables and to optimize performance. The parameters studied included the number of concrete springs across the segment-to-segment joints, the unbonded length of the grouted PT tendons, and the amount and type of damping.

4.3.1. Unbonded Length of the PT

The stress gradient generated along the PT tendon (see Figure 3-3) due to friction along the tendon during joint opening was difficult to model. For simplicity, an equivalent unbonded length, L_u, was used to match the stiffness of the tendons over the flexural bond length (see Figure 4-9). The stiffness of the segment joints after cracking and opening is highly dependant on the unbonded length of the PT tendon crossing the joint. Thus, to accurately estimate the rotation at which the tendons yield, we must start with a good approximation of the unbonded length. The unbonded length will likely be approximately 50% of the flexural bond length based on strain energy comparisons. However, PT strands tend to group at either the top or bottom of the duct depending on the curvature of the duct. This grouping of strands can make it difficult for grout to penetrate between the individual strands. Thus,

empirical equations that estimate the flexural debond length of single strands are inappropriate for multi-strand tendons. It was for this reason that the unbonded length of the PT tendons was determined using a trial and error approach to match the results from the Phase I experiments by Megally et al. (2002).

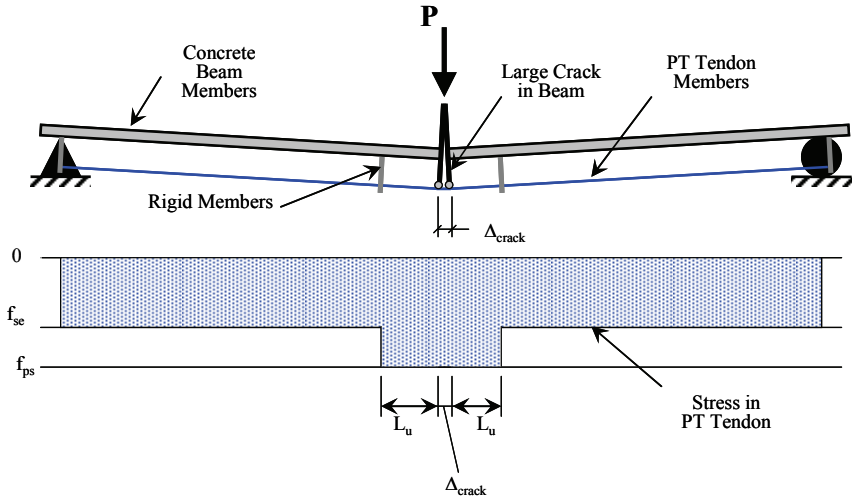

Figure 4-9 Modeling of Unbonded Length of PT Tendon

The unbonded length was increased in 5 inch increments from 10 inches up to 45 inches, and the moment-rotation response of the joint was compared to the experimental results. Figure 4-10 to Figure 4-12 show the comparisons of the 10 inch, 25 inch, and 40 inch unbonded lengths to test unit 100-INT of the Phase I experiment (Megally et al., 2002). An unbonded length of 25 inches matched the experiment best, particularly at rotations smaller than 0.01 radians and provided a good match at larger rotations. The PT tendons of the model and the experiment

yielded at the same rotation and the energy dissipation was comparable. The 10 inch unbonded length was too stiff after joint opening and significantly under-predicted the yield rotation of the tendon. Conversely, the 40 inch unbonded length was too soft upon joint opening and significantly over predicted the yield rotation of the tendon.

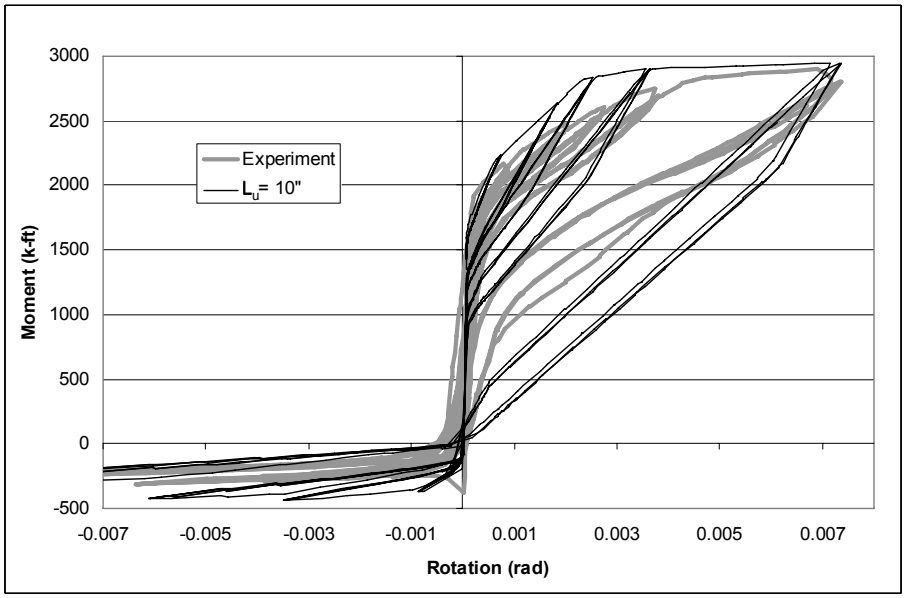

a) Small Rotations

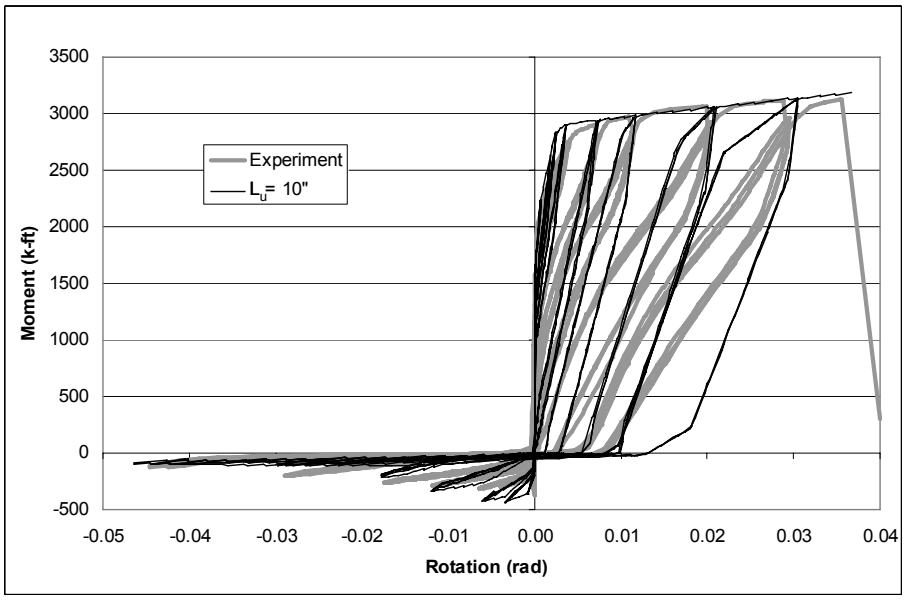

b) Large Rotations

Figure 4-10 Moment - Rotation Diagrams with 10" Unbonded Length

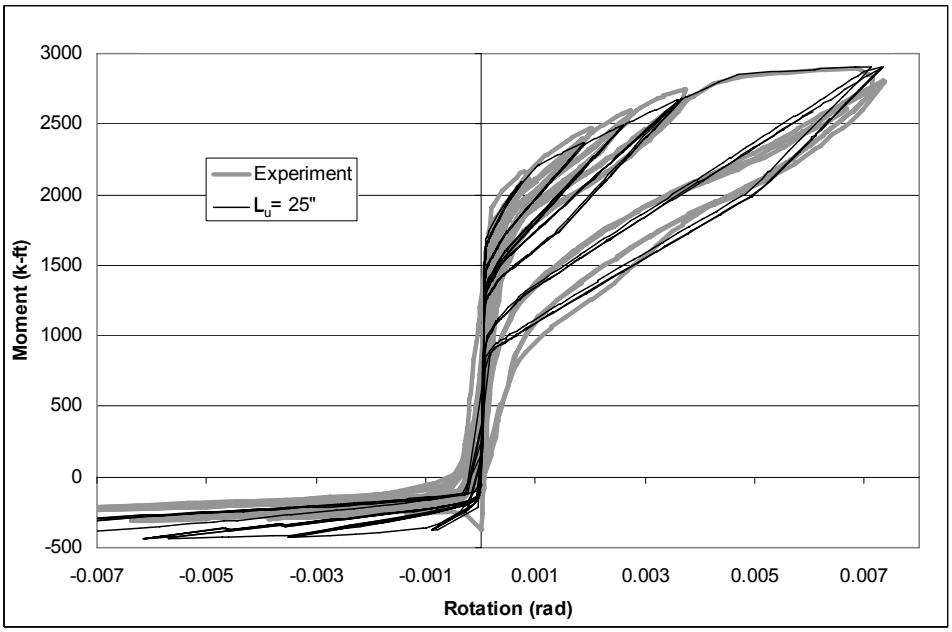

a) Small Rotations

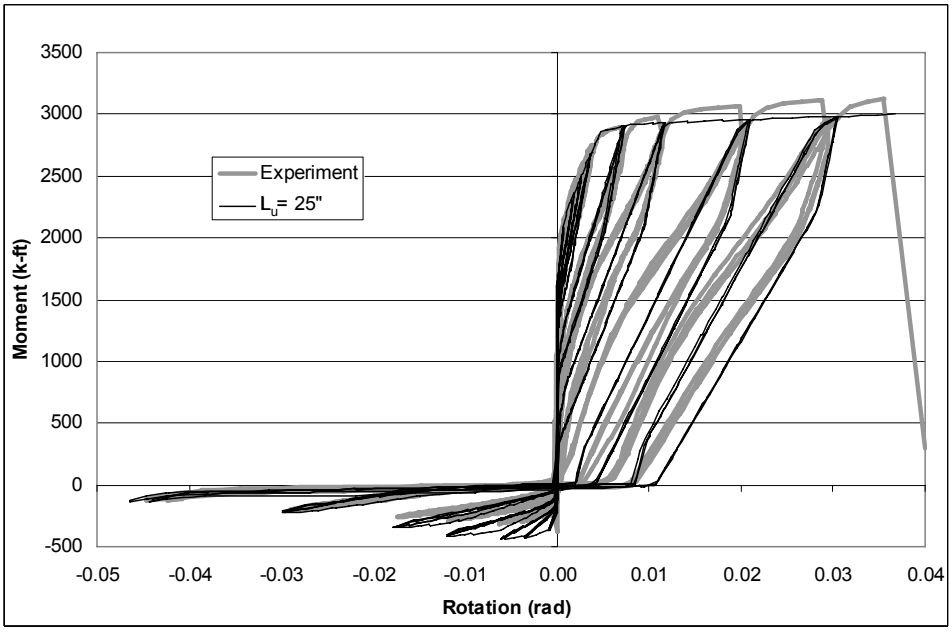

b) Large Rotations

Figure 4-11 Moment - Rotation Diagrams with 25" Unbonded Length

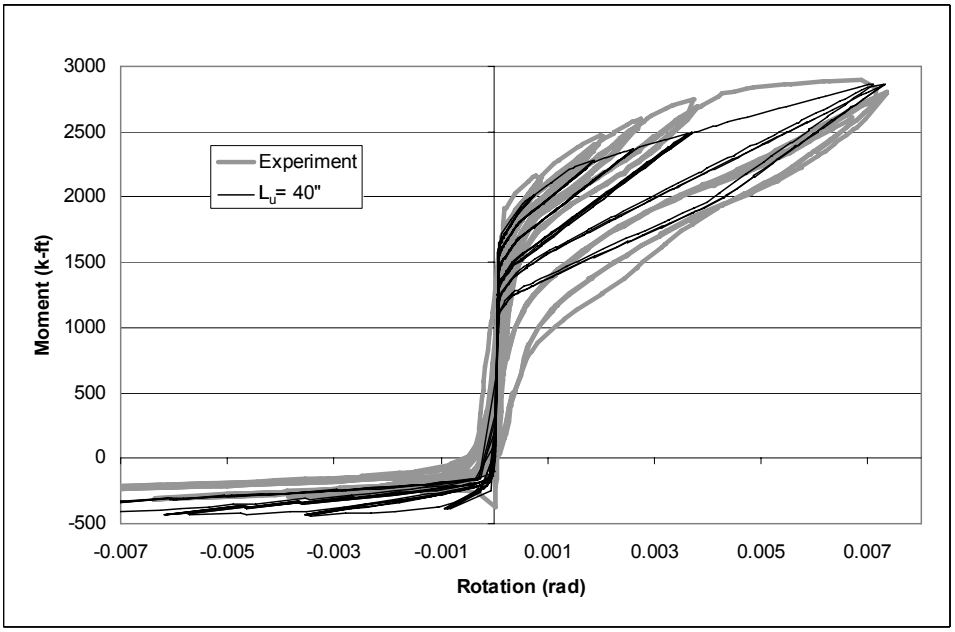

a) Small Rotations

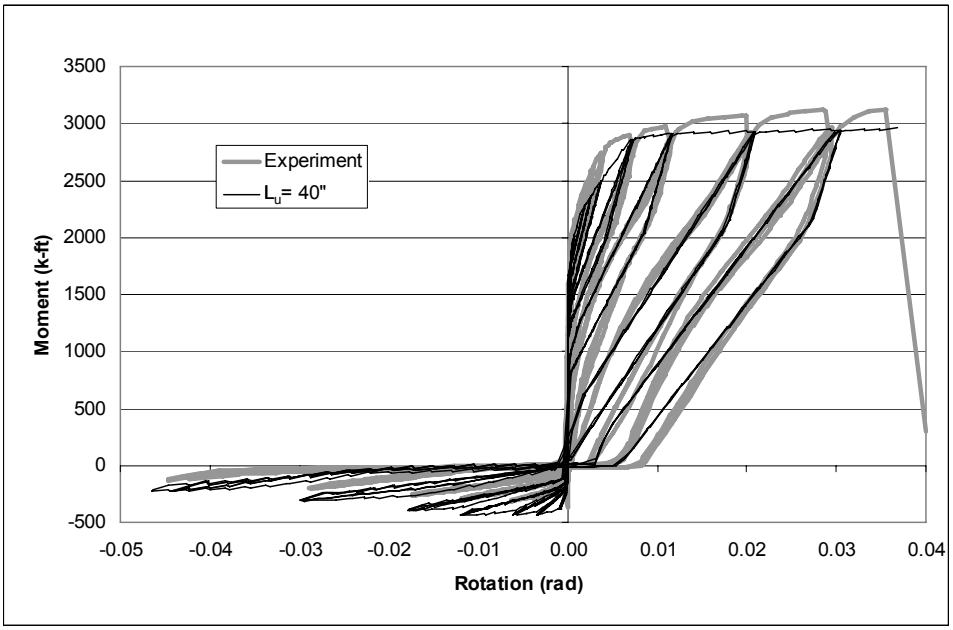

b) Large Rotations

Figure 4-12 Moment - Rotation Diagrams with 40" Unbonded Length

4.3.2. Number of Joint Springs

The initial number of concrete springs across the segment-to-segment joints was selected somewhat arbitrarily to be fifteen (i.e. six in both the top and bottom flanges and three in the web). The intention was to capture the energy dissipation and loss of stiffness due to crushing of the extreme concrete fibers. Using fifteen concrete springs across each joint will result in a very large stiffness matrix in a full bridge model. This may increase the likelihood of convergence problems and will require significant computational effort. If the number of concrete springs can be reduced without compromising the accuracy of the results, much time and effort will be saved.

With the goal of optimizing the number of concrete springs across the segment-to-segment joints, several models were developed with flange springs ranging from one to six and web springs ranging from one to three. Comments about each model are listed in Table 4-1.

Table 4-1 Joint Spring Parameter Study Summary

Total Joint Springs	Flange Springs	Web Springs	Comments
15	6	3	Reference model.
14	6	2	No visible change in response.
13	6	1	No visible change in response.
11	5	1	Essentially no change.
9	4	1	Essentially no change. Stable if only 2 flange springs crush.
7	**3**	**1**	**Essentially no change. Stable if only 1 flange spring crushes.**
5	2	1	Slightly understimates the yield moment. Numerical problems at large rotations.
3	1	1	Understimates the yield moment. No concrete crushing

The seven spring model (i.e. three flange springs and 1 web spring, identified as 3-1) produced the best results as can be seen in Figure 4-13. The joint response was nearly identical to the fifteen spring model (i.e. six flange springs and 3 web springs, identified as 6-3), with a slight deviation at the onset of joint opening. The yield rotation and energy dissipation were essentially identical. Further reducing the number of flange springs increased the likelihood of numerical instability and inaccuracies in the moment due to difficulties in modeling the centroid of the compression toe.

It should be noted that for tall girders, multiple web springs may be required in order to accurately model the bending stiffness of the girder across the joints. By using only axial springs across the joint, the moment of inertia is calculated solely with the parallel axis theorem. For very large webs, the moment of inertia of the web itself (i.e. $bd^3/12$) is significant. Breaking the web up into smaller areas will reduce the error. It is for this reason that multiple web springs were used in the full bridge models.

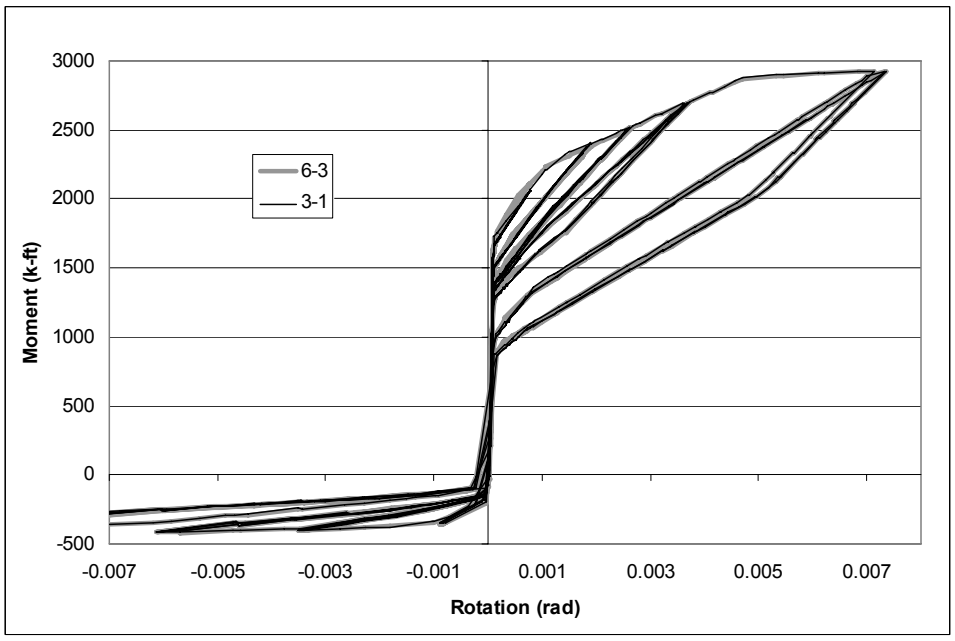

a) Small Rotations

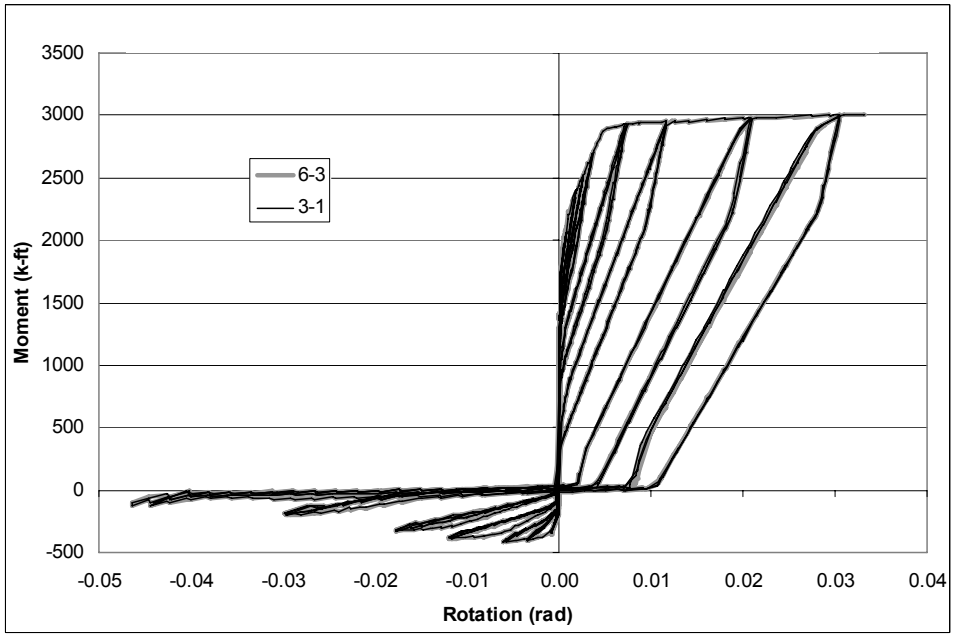

b) Large Rotations

Figure 4-13 Moment - Rotation Diagram - Comparison of 15 and 7 Joint Springs

4.3.3. Damping

The type and amount of damping can play a significant role in the accuracy of jointed models excited dynamically beyond their initial closed status. To fully understand the role of damping in the structure we must begin with the equations of motions

$$m\ddot{u} + c\dot{u} + ku = -m\ddot{u}_g \qquad \textbf{4-1}$$

where m is the mass matrix, c is the damping matrix, k is the stiffness matrix, $\ddot{u}$ is the acceleration vector, $\dot{u}$ is the velocity vector, u is the displacement vector and $\ddot{u}_g$ is the ground acceleration. The formation of the damping matrix depends on the type of damping used in the analysis.

Rayleigh damping generates the damping matrix based on proportionality with the mass and stiffness matrices.

$$c = a_0 m + a_1 k \qquad \textbf{4-2}$$

where a_0 and a_1 are mass and stiffness proportionality coefficients, respectively. The relationship between the damping ratio and frequency is

$$\xi_n = \frac{a_0}{2\omega_n} + \frac{a_1 \omega_n}{2} \qquad \textbf{4-3}$$

where ξ_n is the percentage of critical damping of the nth mode and ω_n is the circular frequency of the nth mode

The proportionality coefficients can be determined by solving Equation 4-3 simultaneously after defining the damping ratio for two anchor frequencies. It is clear that the amount of damping will vary depending on frequency, as shown in Figure 4-14, thus it is important to select these two anchor modes carefully to ensure that critical modes are not damped out, or for that matter, underdamped.

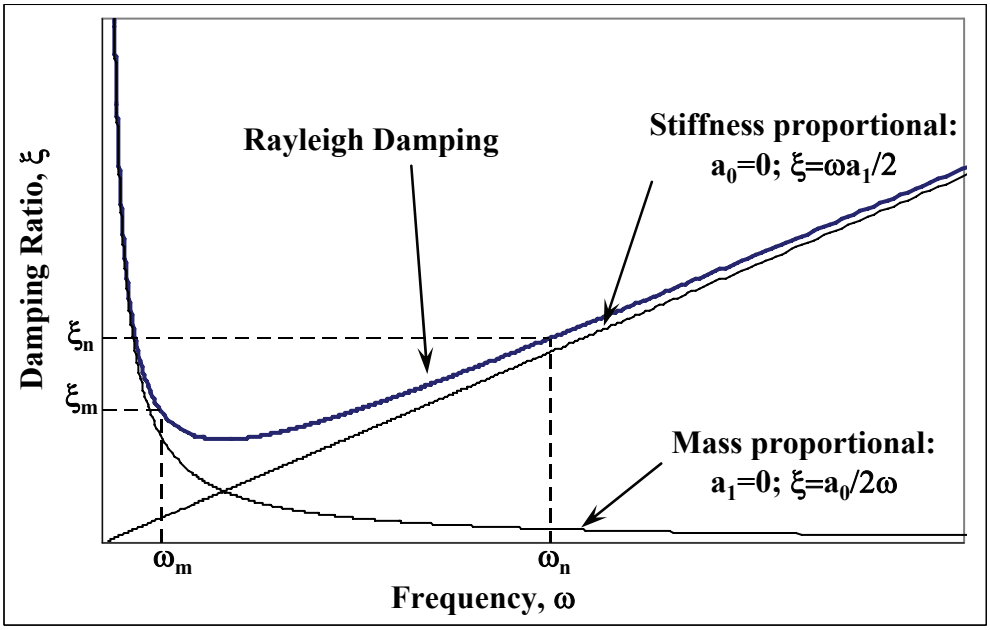

Figure 4-14 Rayleigh Damping (Clough and Penzien, 1993)

Initial stiffness Rayleigh damping generated the damping matrix based on the initial stiffness matrix of the structure. The damping matrix, c, remains constant throughout the analyses and is banded.

Tangent stiffness Rayleigh damping generates the damping matrix, based on the tangent stiffness of the structure. Thus the damping matrix, c, is changing continually during the analyses.

Numerical problems may arise from the use of initial and tangent stiffness Rayleigh damping for jointed structures from the fact that as segment joints open, the frequency of the dominant mode reduces to near zero and, as shown in Figure 4-14, the damping ratio for very low frequencies is very high. This very high damping ratio can generate large non-physical damping forces.

The use of tangent stiffness Rayleigh damping may compensate for the increased damping expected due to shifting of the structural period. As the segment joint opens, the stiffness matrix reduces, thereby reducing the stiffness proportional component of the damping matrix. However, additional numerical problems may arise due to the use of tangent stiffness Rayleigh damping. As the segment joints open, the stiffness matrix reduces and the damping matrix approaches a purely mass

proportional state, where high frequency modes receive little to no damping. Impact between segments upon closure of the segment joints can excited these higher modes, significantly altering the joint response.

4.3.3.1. Damping Study Details and Results

To investigate and understand the effects of the damping model on a simple segmental joint bridge subsystem, a number of analyses were performed with different types and amount of damping. The two damping types selected were initial stiffness Rayleigh damping and tangent stiffness Rayleigh damping as described above. Damping levels were varied from 0.1% up to 10%.

The North-South component of the Rinaldi record from the 1994 Northridge earthquake was used as the excitation in the damping sensitivity study. The single joint model was used to ensure that observations were due solely to the modeling of the joint and not due to other modeling effects. Mass was added to the model at midspan to obtain a realistic primary vertical period of 0.4 seconds (see Figure 4-15). The record was reduced down to a PGA of 0.7g and then further reduced by a factor of 1/8 to account for scaling effects as this was a model of a half-scale experiment. This reduction in the excitation produced reasonable joint rotations that ranged from

0.005 radians (i.e. the yield rotation) with 10% damping up to 0.03 radians with 0.1% damping.

It is important to note that the integration time-step is a critical analysis parameter. A time-step that is too large can converge on an incorrect solution. A typical rule of thumb is to use a time step that is $1/10^{th}$ the period of interest. A time-step of 0.001 seconds was used for all analyses in this study and was significantly smaller than the 0.04 second time step obtained using the rule of thumb. A time step of 0.0001 seconds was also investigated, but this reduced time step had no effect on the results, yet increase the run time significantly.

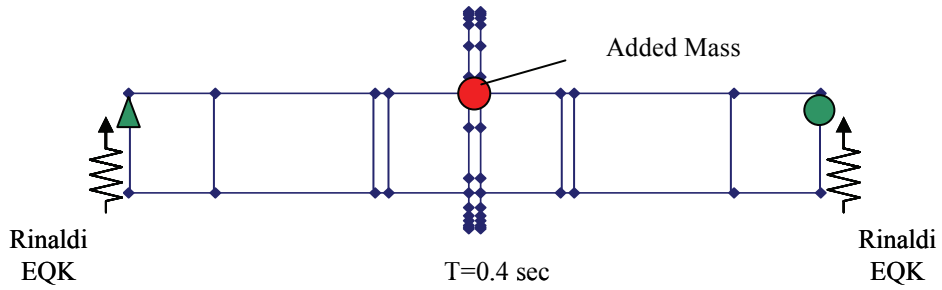

Figure 4-15 Damping Sensitivity Study Model

Results from the damping study are summarized on Figure 4-16. The tangent stiffness Rayleigh damping typically generated girder shear forces that were significantly higher than the initial stiffness Rayleigh.

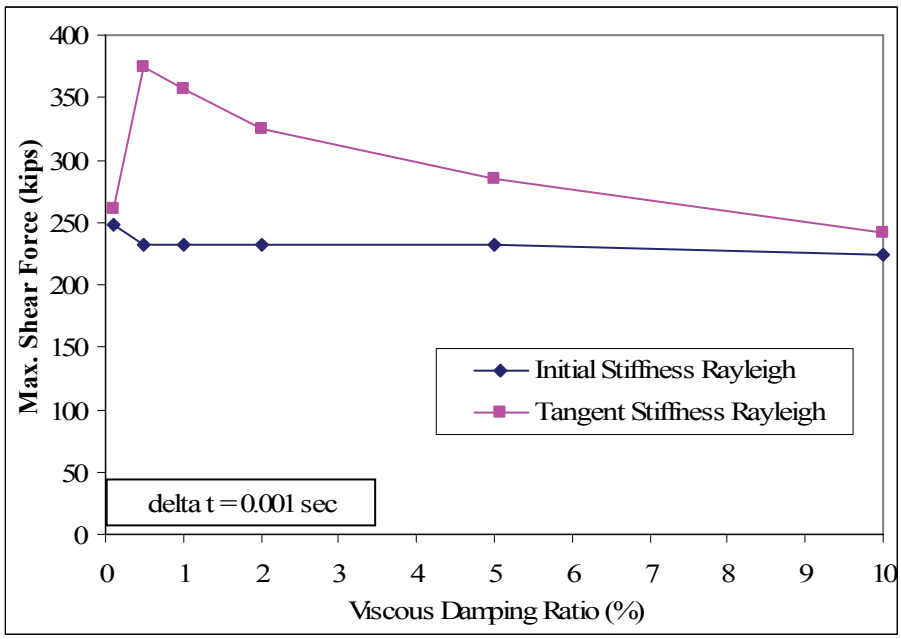

Figure 4-16 Influence of Amount of Damping on Peak Girder Shear Force

Figure 4-17 to Figure 4-19 compare the girder shear and midspan displacement time histories of the two damping models with damping values of 0.1%, 2%, and 10%, respectively. The initial stiffness Rayleigh and the tangent stiffness Rayleigh show significant differences. Tangent stiffness Rayleigh exhibited spikes in the girder shear forces as well as a markedly different displacement response at damping ratios greater than 0.5%.

The initial stiffness Rayleigh damping model appears to be the most stable. For these reasons, the initial Rayleigh damping model with 1% damping was selected as the damping model of choice for all future analyses.

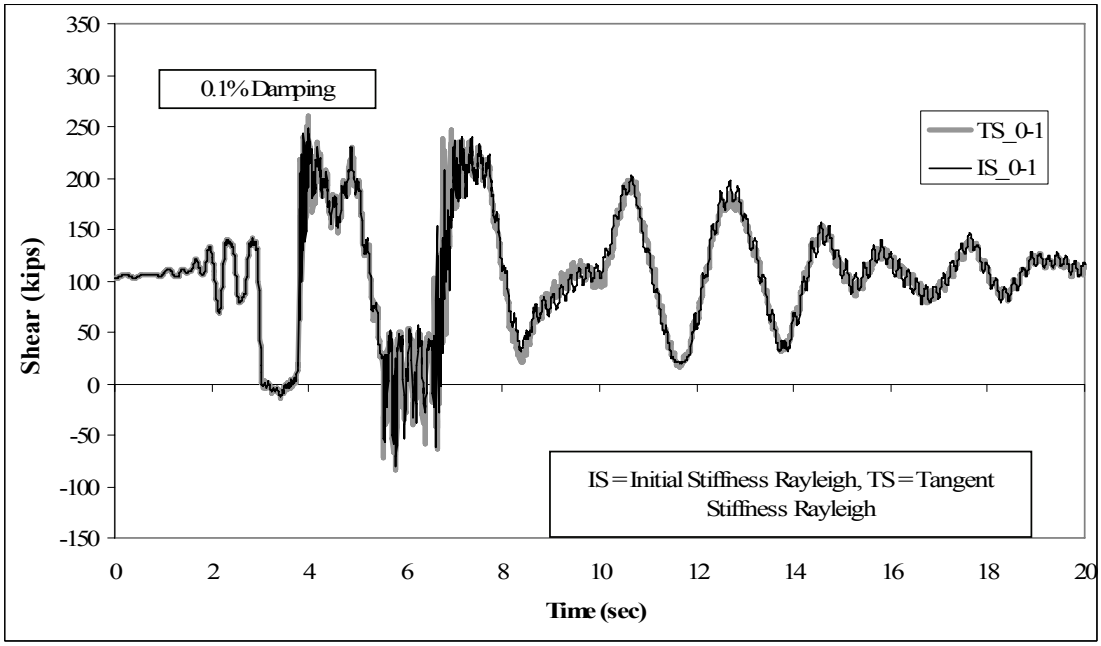

a) Girder Shear Force

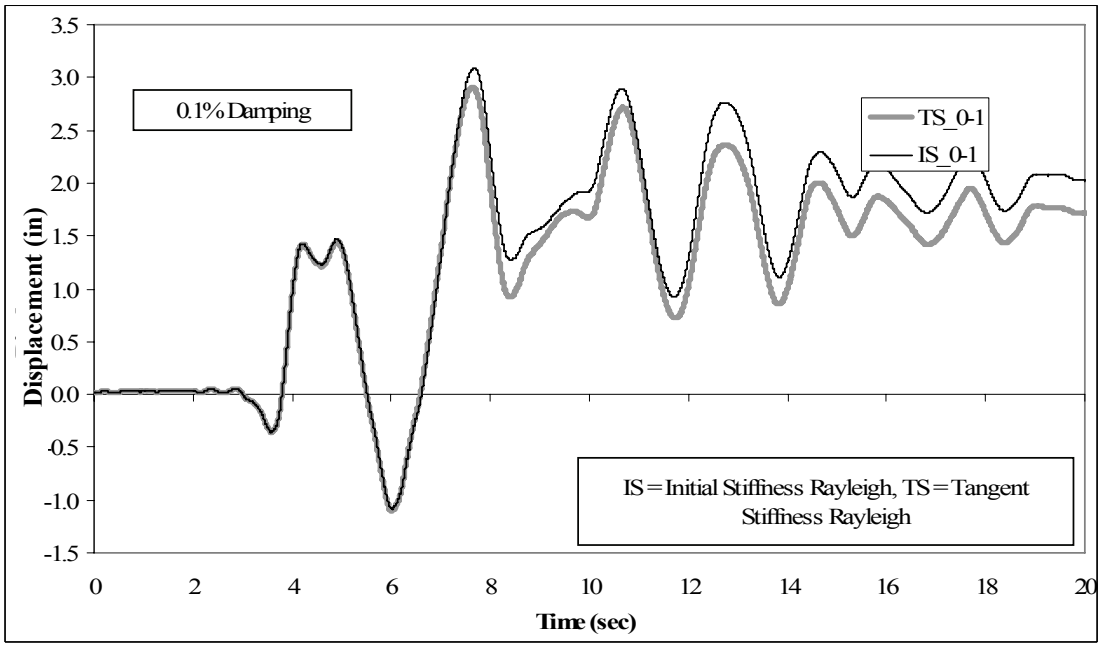

b) Midspan Deflection

Figure 4-17 Damping Model Time History Comparison (0.1% Damping Ratio)

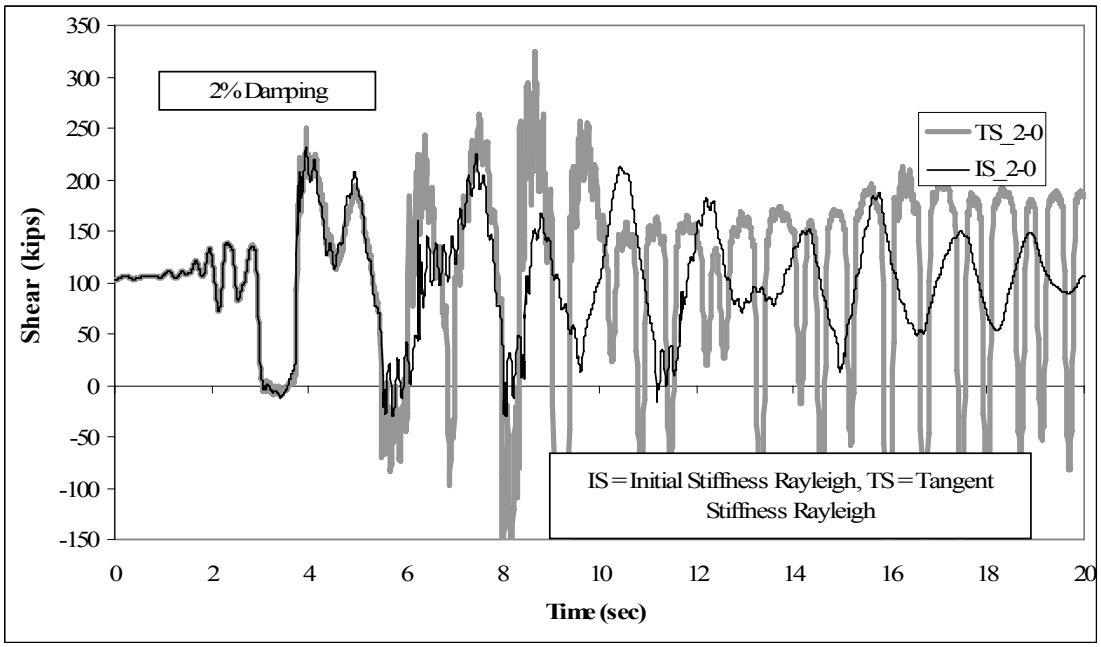

a) Girder Shear Force

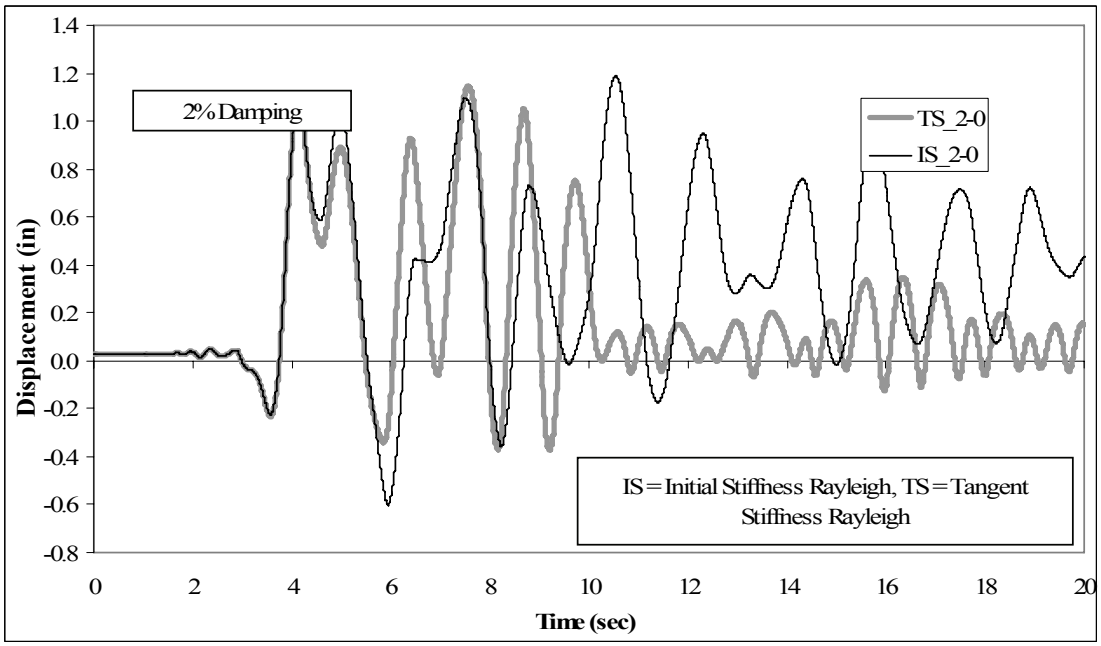

b) Midspan Deflection

Figure 4-18 Damping Model Time History Comparison (2% Damping Ratio)

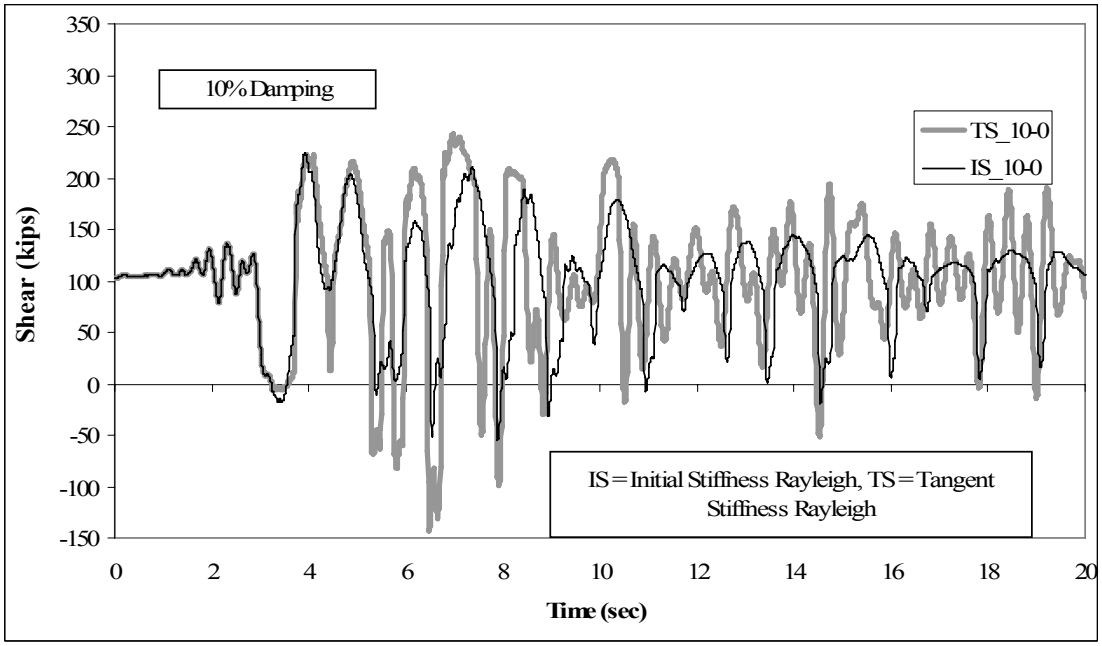

a) Girder Shear Force

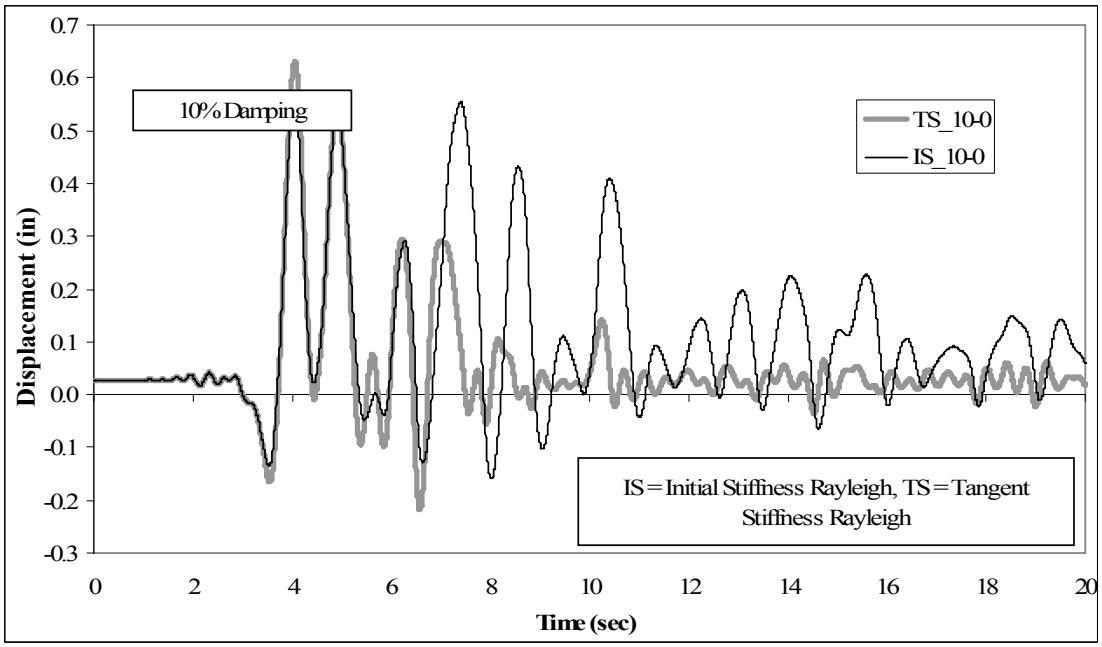

b) Midspan Deflection

Figure 4-19 Damping Model Time History Comparison (10% Damping Ratio)

CHAPTER 5. EARTHQUAKE EXCITATIONS

This chapter discusses the characteristics of the assumed site location for the full bridge models and summarizes the ground motions records selected for the non-linear time history analyses. Two different methods for scaling the ground motion records to the design spectrum for the site are outlined and the characteristic of the scaled records are presented and compared. The chapter concludes with a discussion on the vertical to horizontal spectral response ratio for the selected earthquake records.

5.1. Site Location and Record Selection

The assumed site location for the bridge was chosen to be 6 miles from a strike-slip fault capable of producing a moment magnitude 8 seismic event with a peak ground acceleration (PGA) of 0.7g. In addition, the site was assumed to be situated on Caltrans soil type D, as this type of soil maintains frequency content at higher periods and thus will be critical for long span bridge structures. The design spectrum was selected from the Caltrans Seismic Design Criteria (SDC) based on the

chosen site characteristics and represented a 5% in 50 year (approximately 1000 year return period) seismic event.

Twenty near field records were selected as input into the full scale bridge models with the goal of obtaining the median seismic response. All records were from stations that were within 15 miles (25 kilometers) of the fault rupture surface and several of the ground motions included significant near field effects (i.e. fling and forward directivity). These records were representative of a typical governing design scenario seismic event in California and were selected because they were from a similar earthquake scenario (i.e. magnitudes and distance) to the assumed design event for the bridge site and because they typically exhibited a modest amount of frequency content near the natural period of the bridge structures. Table 5-1 lists the earthquakes used and summarizes various parameters of each ground motion. These ground motions were amplitude scaled to the design spectrum and not spectrum matched because variability in the response of the bridge, while not the focus of the investigation, was of some interest (See Section 3.1 for a discussion of amplitude scaling versus spectrum matching). Two different scaling methods were

used to investigate the effect of the method of record scaling on the response of the bridge system.

Table 5-1 Summary of Earthquake Ground Motion Records

Earthquake	Station	Abbrev.	Date	Mw	Closest Dist to Rupture Surface (mi)	PGA - horiz (g)	PGA - vert (g)	Duration (sec)	Component
Chi Chi	TCU065	T65	9/20/1999	7.6	0.6	0.60	0.27	71	NS
Chi Chi	TCU068	T68	9/20/1999	7.6	0.7	0.57	0.49	71	EW
Duzce	Bolu	BOL	11/12/1999	7.1	10.6	0.74	0.21	50	NS
Erzincan, Turkey	Erzincan	ERZ	3/13/1992	6.7	1.1	0.50	0.25	21	EW
Iran	Tabas	TAB	9/16/1978	7.4	1.8	0.84	0.70	32	NS
Irpinia, Italy	Calitri	CAL	11/23/1980	6.5	11.4	0.18	0.15	40	NS
Kobe	Takarazuka	TAK	1/16/1995	6.9	0.7	0.70	0.44	30	NS
Kobe	Takatori	TAT	1/16/1995	6.9	0.2	0.63	0.28	30	EW
Loma Prieta	Gilroy Historic	GIL	10/17/1989	7.0		0.28	0.15	30	EW
Loma Prieta	Lexington Dam Abutment	LEX	10/17/1989	7.0	3.8	0.44	0.14	30	NS
Loma Prieta	Los Gatos Presentation Center	LOS	10/17/1989	7.0	2.1	0.64	0.89	22	EW
Loma Prieta	Saratoga Aloha Ave	SAR	10/17/1989	7.0	5.0	0.51	0.40	30	NS
N. Palm Springs	Morongo Valley	MOR	7/8/1986	6.0	6.1	0.22	0.45	20	NS
Northridge	Rinaldi	RIN	1/17/1994	6.7	4.3	0.84	0.86	15	NS
Northridge	Sylmar	SYL	1/17/1994	6.7	3.8	0.61	0.55	30	EW
Northridge	Sylmar Converter	SCS	1/17/1994	6.7	3.7	0.62	0.60	30	EW
Northridge	West Pico Cyn.	WPC	1/17/1994	6.7	4.3	0.33	0.30	25	NS
Northridge-01	Newhall Fire Station	NFS	1/17/1994	6.7	4.3	0.60	0.57	35	NS
San Fernando	Pacoima Dam	PAC	2/9/1971	6.6	1.7	1.25	0.71	20	NS
Superstition Hills	Wildlife Liquef.	WIL	11/24/1987	6.7	14.6	0.21	0.43	42	NS

It is important to note that the duration of each record was extended by fifteen seconds to allow the bridge response to damp out so that residual joint rotations and pier drift ratios could be obtained. In addition, the two ground motions components were assumed to act at all foundations simultaneously. That is, incoherent ground motions were not considered.

5.2. Ground Motions Scaled to Natural Period

One method of record scaling was to scale the horizontal earthquake records to match the design spectrum at the primary natural period of the structure. This same scale factor was used on the vertical ground motion to keep the components of the seismic event consistent with motions that occur in nature. The period of the primary longitudinal mode for both the 300 foot span and the 525 foot span bridge structures was approximately 2.0 seconds. It is important to note that the longitudinal response of the bridges may be greatly affected by the presence of the abutments after closure of the thermal expansion gap and engaging the abutment backwall. The period of free vibration found from the modal analysis did not consider the bridge-abutment interaction. This record scaling approach was used by the Pacific Earthquake Engineering Research Center (PEER) in the PEER Testbed projects (www.peertestbeds.net).

The results of this scaling method are shown below. Table 5-2 lists the scale factors and various properties of the ground motions after they were scaled to match the design spectrum at the dominant longitudinal natural period of the bridge. Figure 5-1 and Figure 5-2 show the longitudinal and vertical acceleration response spectra

for the suite of earthquakes after scaling. Note that the median spectra of the longitudinal motion, matches the design spectra fairly well and is more evident in Figure 5-7. Figure 5-3 shows the displacement response spectra for the scaled suite of earthquakes.

Table 5-2 Ground Motions Parameters – Scaled to Natural Period

			Scaled to T=2 sec			
Earthquake	**Station**	**Abbrev.**	**Sa @ T=2.0 sec**	**Scale Factor**	**PGA - horiz (g)**	**PGA - vert (g)**
Chi Chi	TCU065	T65	0.584	**1.240**	0.75	0.34
Chi Chi	TCU068	T68	0.582	**1.246**	0.71	0.61
Duzce	Bolu	BOL	0.280	**2.592**	1.91	0.54
Erzincan, Turkey	Erzincan	ERZ	0.378	**1.917**	0.95	0.48
Iran	Tabas	TAB	0.534	**1.358**	1.15	0.95
Irpinia, Italy	Calitri	CAL	0.135	**5.355**	0.95	0.79
Kobe	Takarazuka	TAK	0.477	**1.519**	1.07	0.67
Kobe	Takatori	TAT	0.864	**0.839**	0.52	0.23
Loma Prieta	Gilroy Historic	GIL	0.202	**3.591**	1.02	0.54
Loma Prieta	Lexington Dam Abutment	LEX	0.081	**9.005**	3.93	1.25
Loma Prieta	Los Gatos Presentation Center	LOS	0.444	**1.633**	1.05	1.46
Loma Prieta	Saratoga Aloha Ave	SAR	0.296	**2.451**	1.26	0.98
N. Palm Springs	Morongo Valley	MOR	0.243	**2.984**	0.66	1.35
Northridge	Rinaldi	RIN	0.574	**1.262**	1.06	1.08
Northridge	Sylmar	SYL	0.451	**1.608**	0.98	0.88
Northridge	Sylmar Converter	SCS	0.633	**1.145**	0.70	0.69
Northridge	West Pico Cyn.	WPC	0.395	**1.835**	0.60	0.55
Northridge-01	Newhall Fire Station	NFS	0.439	**1.653**	0.99	0.94
San Fernando	Pacoima Dam	PAC	0.483	**1.501**	1.88	1.07
Superstition Hills	Wildlife Liquef.	WIL	0.348	**2.085**	0.43	0.89

It should be noted that the peak ground acceleration and the spectral response below 1.0 seconds for one particular earthquake record was extremely high and will likely not occur naturally. This record was selected based on its response near the natural period of the structure. The displacement response at a period of 2.5 seconds

was greater than the majority of other records, thus this record helped to push the median response closer to the design spectrum at periods above 2.0 seconds.

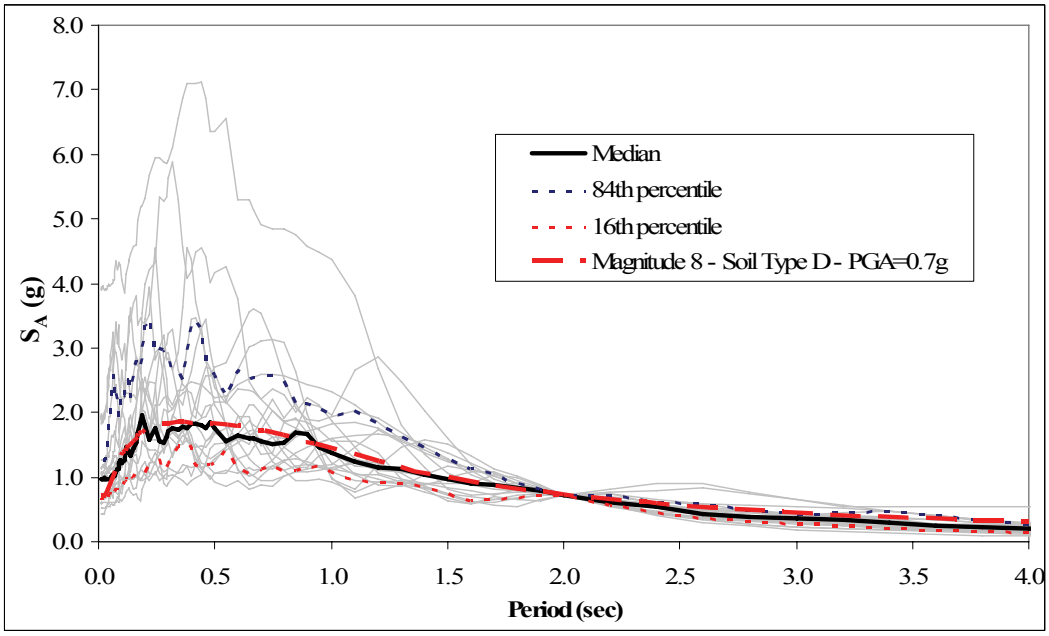

Figure 5-1 Longitudinal Acceleration Response Spectrum – Scaled to Natural Period

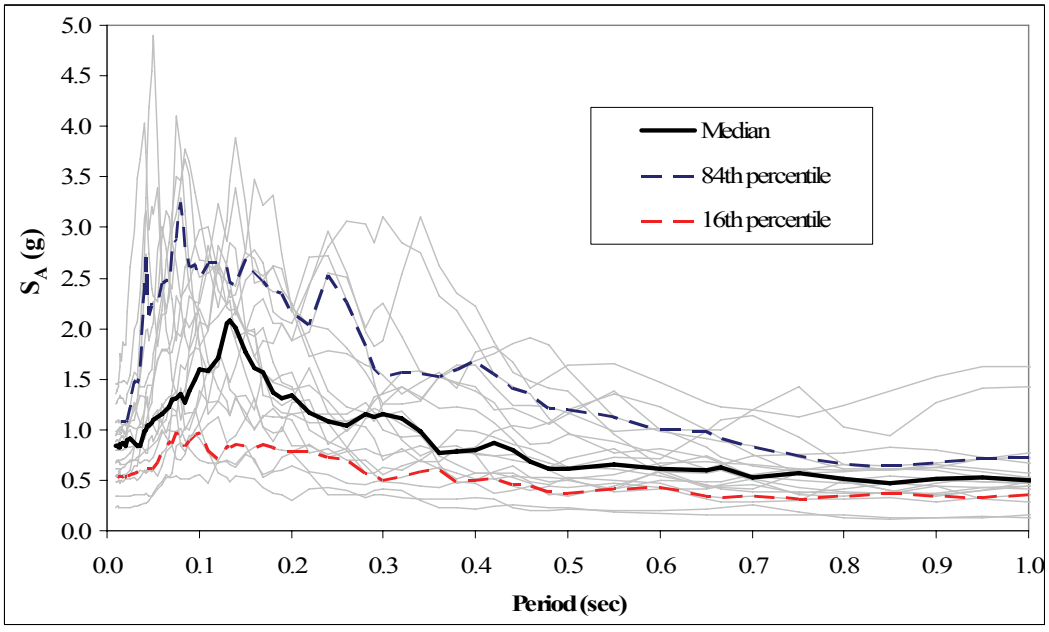

Figure 5-2 Vertical Acceleration Response Spectrum – Scaled to Natural Period

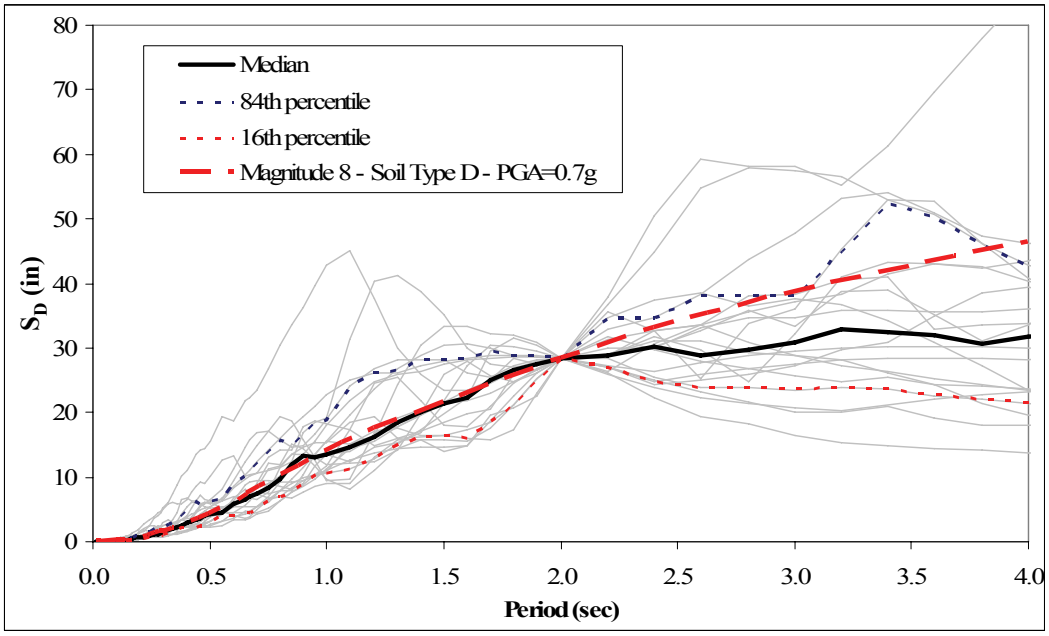

Figure 5-3 Displacement Response Spectrum – Scaled to Natural Period

5.3. Ground Motions Scaled to Period Range

In addition to the ground motion scaling method described in Section 5.2, the lateral ground motions were also scaled to match a period range. This same scale factor was then used to scale the vertical ground motion component to keep the records consistent with nature. The lower bound of the period range was selected to be near the period of the dominant vertical modes of the bridge models, while the upper end of the range was selected to be above the period of free vibration of the structure to allow for softening of the bridge due to inelastic response. This approach is similar to the approach outlined in the Uniform Building Code (UBC

1997). The scale factor was selected based on a least squares fit between the scaled displacement response spectra and the design displacement spectra over a period range of 0.5 seconds to 2.5 seconds.

The results of this scaling method are shown below. Table 5-3 lists the scale factors and various properties of the ground motion after they were scaled for the best fit with the design spectrum over a period range. Figure 5-4 and Figure 5-5 show the longitudinal and vertical acceleration response spectra for the suite of earthquakes after scaling. Figure 5-6 shows the displacement response spectra for the scaled suite of earthquakes.

Table 5-3 Ground Motions Parameters – Scaled to Period Range

			Scaled to Range (0.5sec - 2.5 sec)		
Earthquake	**Station**	**Abbrev.**	**Scale Factor**	**PGA - horiz (g)**	**PGA - vert (g)**
Chi Chi	TCU065	T65	**1.254**	0.76	0.34
Chi Chi	TCU068	T68	**1.145**	0.65	0.56
Duzce	Bolu	BOL	**2.649**	1.96	0.55
Erzincan, Turkey	Erzincan	ERZ	**2.115**	1.05	0.53
Iran	Tabas	TAB	**1.487**	1.26	1.04
Irpinia, Italy	Calitri	CAL	**3.894**	0.69	0.58
Kobe	Takarazuka	TAK	**1.551**	1.09	0.69
Kobe	Takatori	TAT	**0.838**	0.52	0.23
Loma Prieta	Gilroy Historic	GIL	**3.187**	0.91	0.48
Loma Prieta	Lexington Dam Abutment	LEX	**5.742**	2.50	0.80
Loma Prieta	Los Gatos Presentation Center	LOS	**1.537**	0.98	1.37
Loma Prieta	Saratoga Aloha Ave	SAR	**2.543**	1.31	1.02
N. Palm Springs	Morongo Valley	MOR	**2.611**	0.57	1.18
Northridge	Rinaldi	RIN	**1.120**	0.94	0.96
Northridge	Sylmar	SYL	**1.636**	1.00	0.89
Northridge	Sylmar Converter	SCS	**1.116**	0.69	0.67
Northridge	West Pico Cyn.	WPC	**1.932**	0.63	0.57
Northridge-01	Newhall Fire Station	NFS	**1.433**	0.86	0.81
San Fernando	Pacoima Dam	PAC	**1.412**	1.77	1.01
Superstition Hills	Wildlife Liquef.	WIL	**2.275**	0.47	0.97

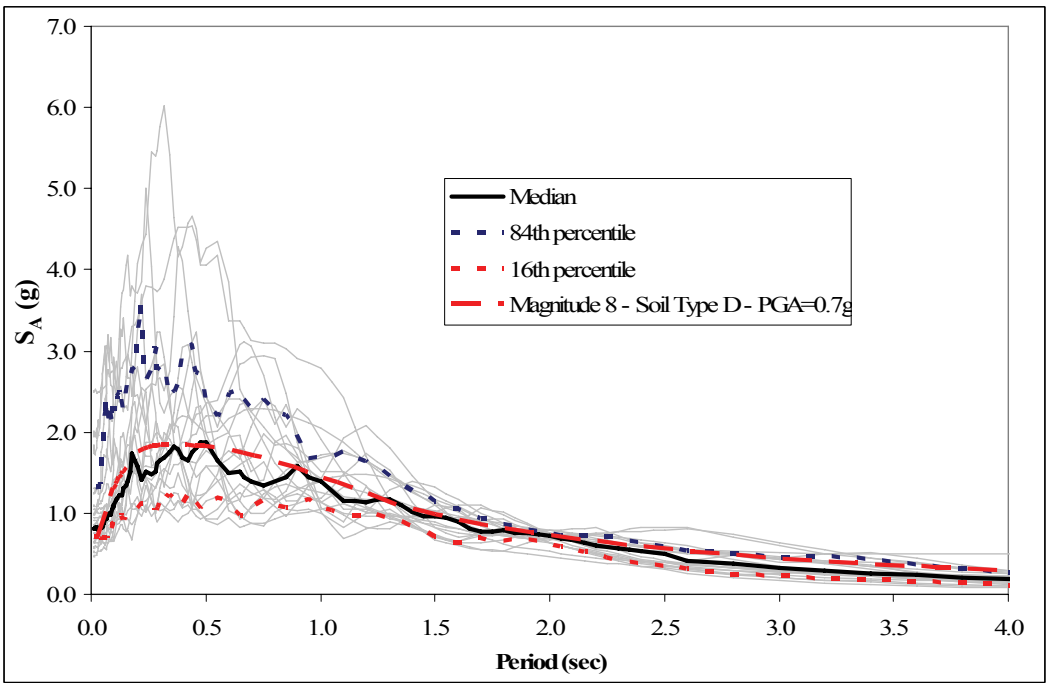

Figure 5-4 Longitudinal Acceleration Response Spectrum – Scaled to Period Range

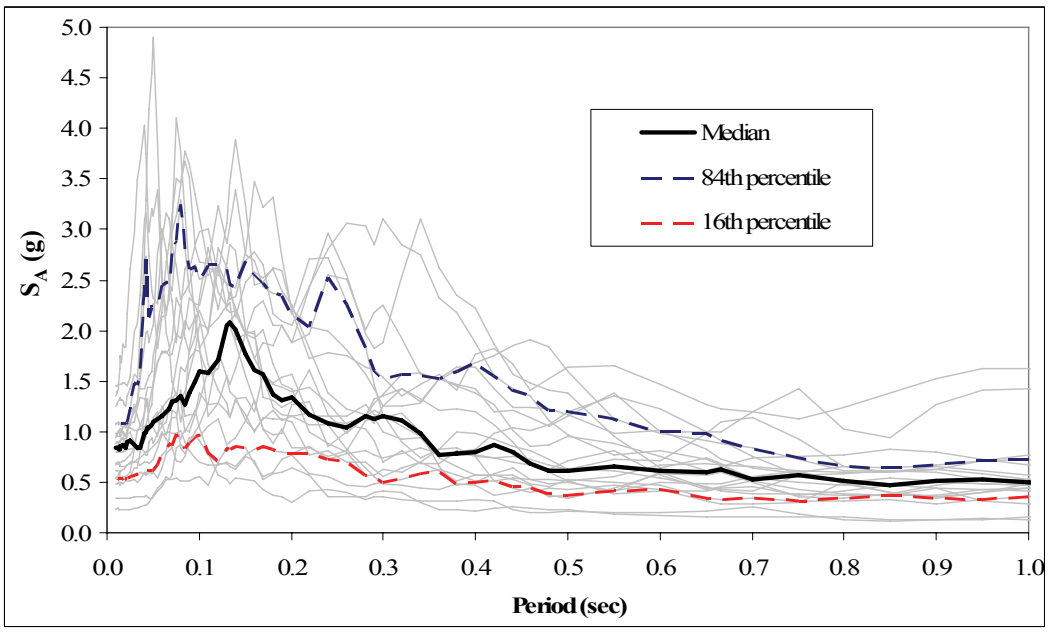

Figure 5-5 Vertical Acceleration Response Spectrum – Scaled to Period Range

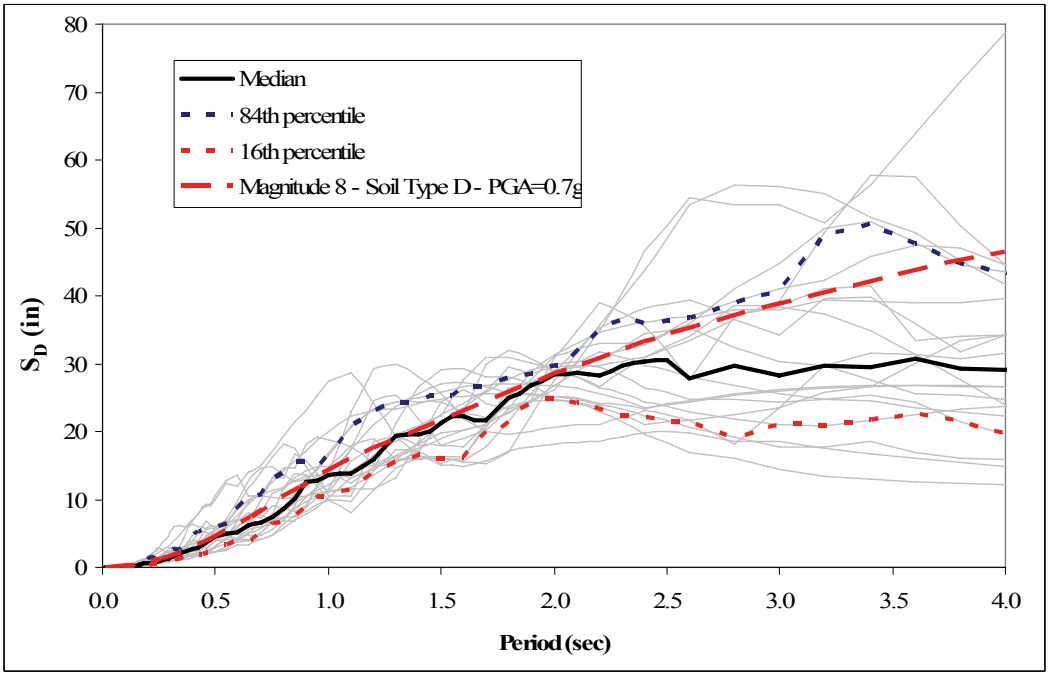

Figure 5-6 Displacement Response Spectrum – Scaled to Period Range

5.4. Comparison of Record Scaling Methods

Figure 5-7 to Figure 5-9 compare the median horizontal acceleration, vertical acceleration and horizontal displacement response spectra for the two different record scaling methods. It is clear from these diagrams that the method of records scaling will not significantly alter the median structural response. On average the scale factors for records scaled to a period range were 4% smaller than the scale factors for records scaled to the natural period of the structure. Thus the median response of the structure due to range scaled earthquake motions were expected to be slightly smaller than period scaled motions.

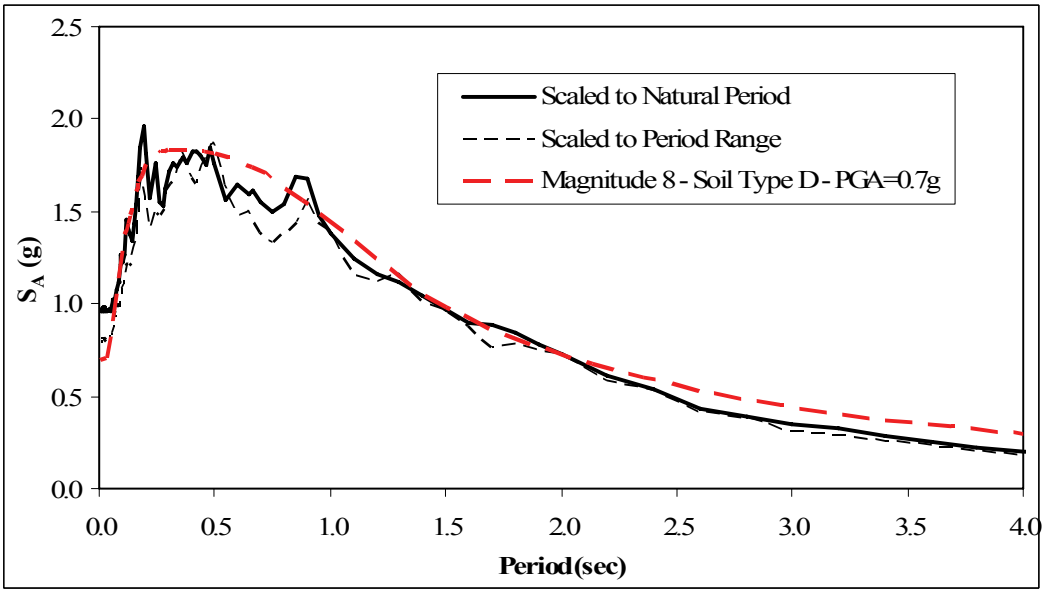

Figure 5-7 Comparison of Median Horizontal Acceleration Response Spectrum

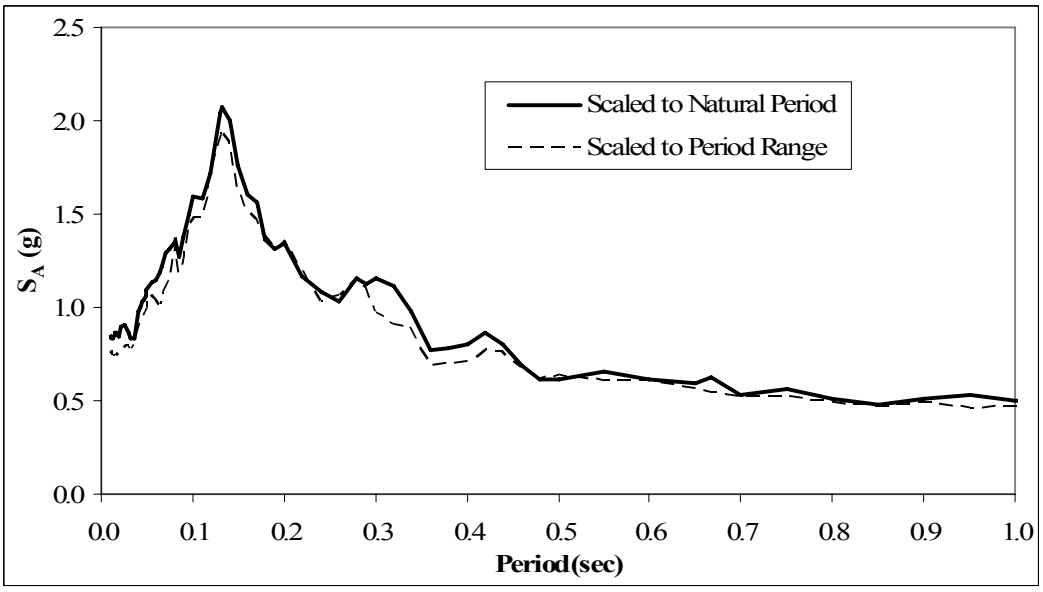

Figure 5-8 Comparison of Median Vertical Acceleration Response Spectrum

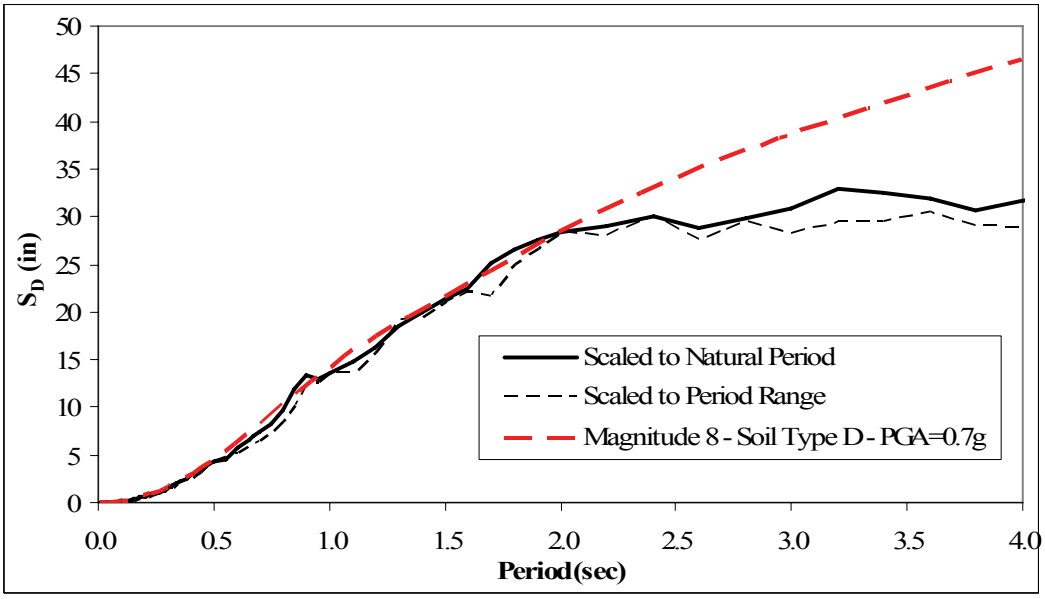

Figure 5-9 Comparison of Median Horizontal Displacement Response Spectrum

Figure 5-10 and Figure 5-11 show the coefficient of variation (COV) for the horizontal and vertical ground motions respectively of the two different scaling methods studied. The COV is defined as the standard deviation divided by the mean and is a measure of scatter. In general, scaling to a period range reduces the COV by as much as 30%. This in not true, however, for horizontal ground motions at periods greater than 1.7 seconds, where scaling to the natural period exhibited a smaller COV.

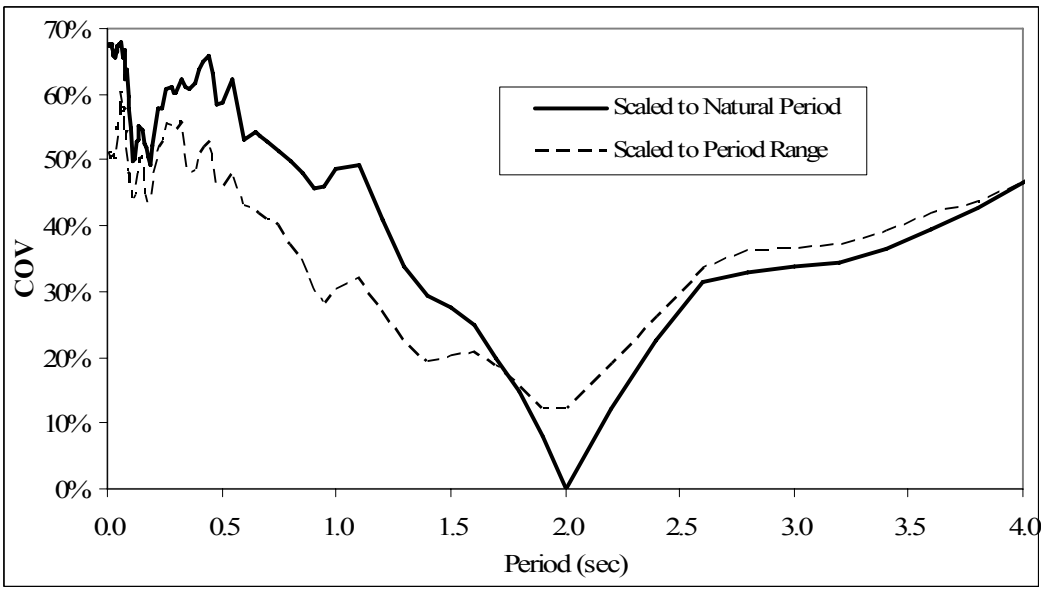

Figure 5-10 COV for Horizontal Ground Motions Records

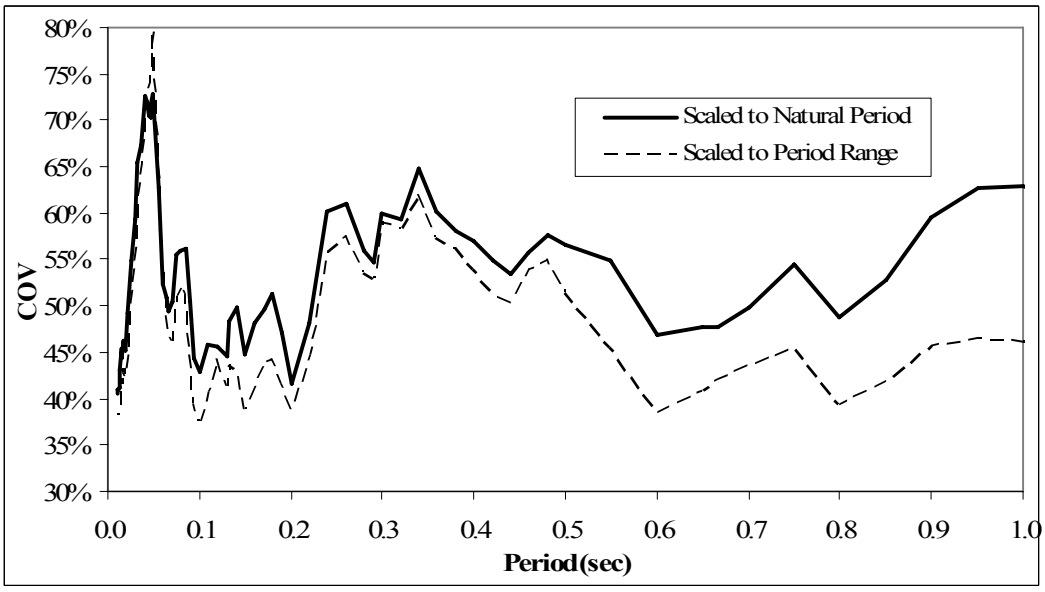

Figure 5-11 COV for Vertical Ground Motions Records

5.5. Spectral Response at Periods above the Natural Period

The median scaled ground motions discussed in Sections 5.2 through 5.4 matched the horizontal design spectrum reasonably well up to a period of 2.0 seconds. The horizontal response at periods above 2.0 seconds, however, was significantly below the design spectrum. This is most evident in the displacement response spectrum shown in Figure 5-9. The primary concern with this characteristic of the earthquake suite is that the structure will soften once yielding of the piers occurs and will be subjected to input energy that is less than that required by the design spectrum. This may result in displacement demands on the structure that are smaller than specified in the design criteria. Complicating the issue is the fact that impact with the abutment, or between adjacent frames, will stiffen the structural response and may negate any softening effects due to pier yielding.

To study the impact of the response above 2.0 seconds, three spectrum compatible records were developed, using the program WAVGEN (Mukherjee and Gupta, 2002b). This program modified the time history in the time domain using wavelets. The three ground motions with the smallest least square error with the design spectrum of a period range from 0.5 seconds to 2.5 seconds were selected to

minimize alterations of the original motion. The horizontal target was the median response of the range scaled records up to 2 seconds. Beyond 2.0 seconds the target was the design spectrum. The frequency content of the vertical motions were modified as well and the target was the median vertical response of the range scaled records.

Figure 5-12 to Figure 5-14 show the horizontal acceleration, vertical acceleration and horizontal displacement response spectra, respectively, for the three spectrum compatible motions. Figure 5-14 clearly indicates that these motions are a better fit to the design spectrum at periods above 2.0 seconds.

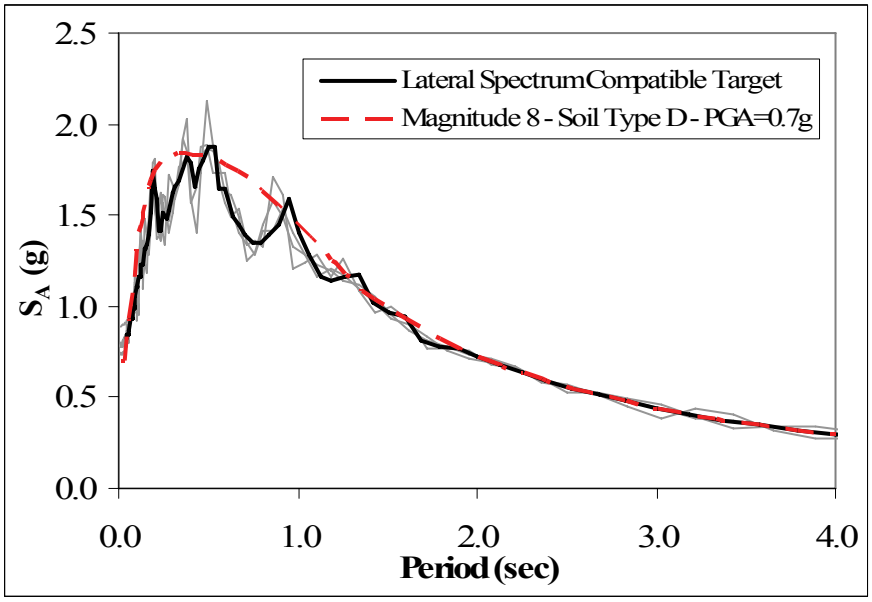

Figure 5-12 Longitudinal Acceleration Response Spectrum - Spectrum Compatible

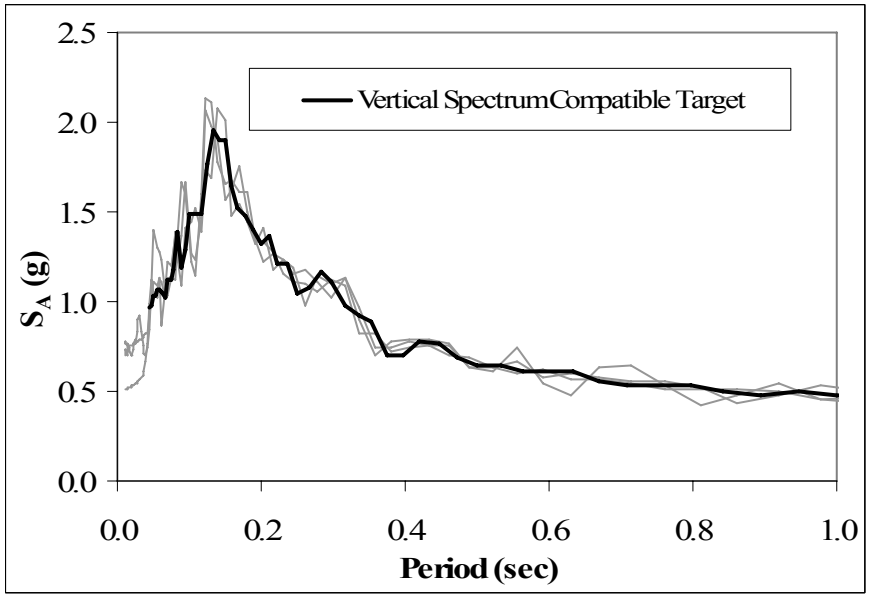

Figure 5-13 Vertical Acceleration Response Spectrum - Spectrum Compatible

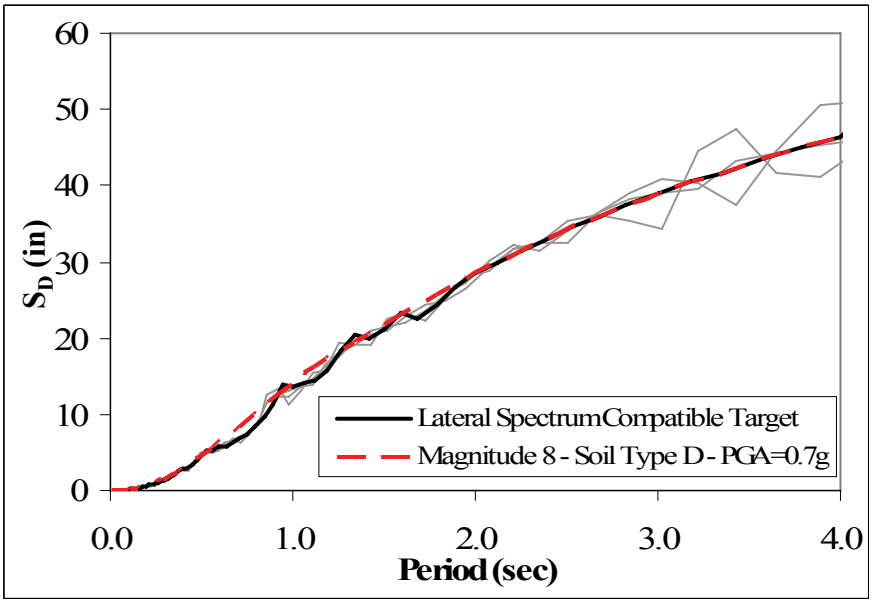

Figure 5-14 Longitudinal Displacement Response Spectrum - Spectrum Compatible

The results of the analyses with these input ground motions indicated that the longitudinal response was within 2% of the response obtained by range scaled records (see Section 7.4). Based on these results, the ensemble of scaled historical

records discussed in Sections 5.2 through 5.3 was used to perform the majority of analyses in this dissertation.

5.6. Vertical to Horizontal Response Spectral Ratio

The ground motion scaling methods used were based on the lateral component of the seismic event, with the intent of developing a suite of earthquake records that represent a 1000 year return event for the assumed bridge site. It will be shown in Chapter 7.1 that the vertical component contributes significantly to the seismic response for the superstructure segments joints, thus it is important to ensure that the vertical component of the ground motion is also consistent with a 1000 year return event.

As discussed in Section 3.2, design spectra or vertical hazard curves are typically not generated. Rather the vertical response is best obtained based on the vertical-to-horizontal (V/H) response spectral ratio. Figure 5-15 compares the V/H response spectral ratio for the suite of records used in this study with the V/H predicted by the Bozorgnia and Campbell attenuation model (Bozorgnia and Campbell 2004), based on properties that are consistent with the assumed bridge site

location (i.e. Soil Type D, 6 miles from fault). The median V/H ratio matched the attenuation model very well. Thus, on average, the V/H ratio of the ground motions selected for this study were typical of naturally occurring events for the assumed site location, and the vertical ground motion records were consistent with a return period of 1000 years.

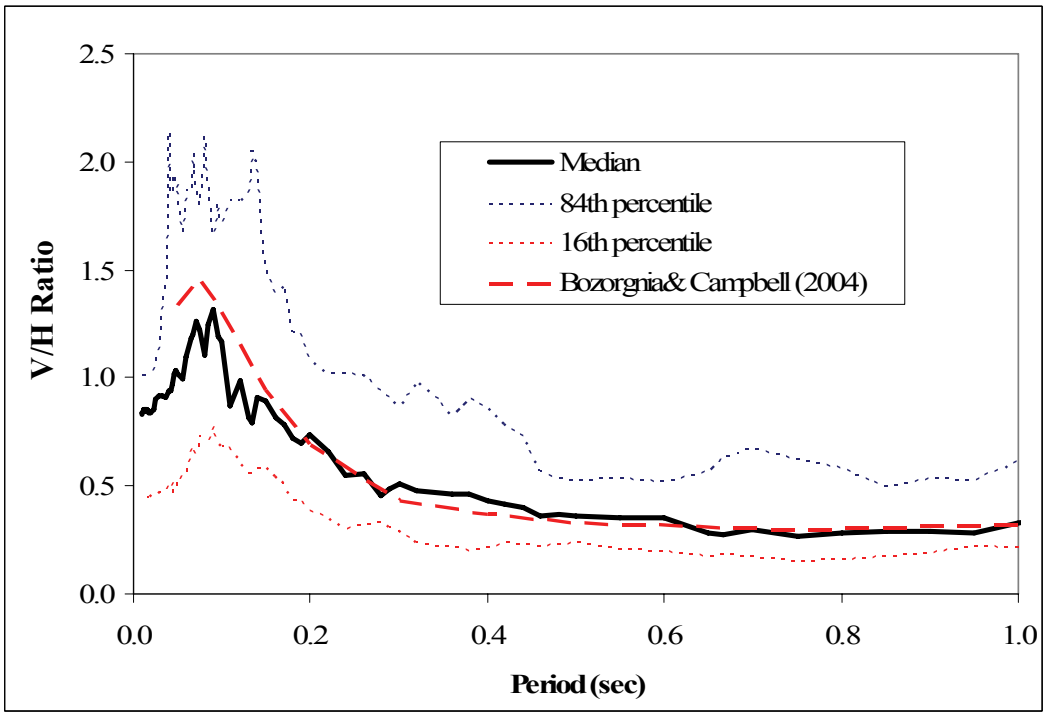

Figure 5-15 Vertical-to-Horizontal Spectral Response Ratio

It should be noted that since the ground motion records use the same scale factor for both the vertical and lateral components of motion, for both record scaling methods, the V/H ratio will be the same regardless of scaling method.

CHAPTER 6. FULL BRIDGE MODELS

Two full scale bridge models were developed to study the seismic response of superstructure segment joints. One with nominal interior span lengths of 300 feet and the other with spans lengths of 525 feet. These spans were selected because they were considered to be within the range where precast segmental construction methods are the most economically competitive in California. Spans less than 250 feet will likely be under bid by conventional cast-in-place methods while spans greater than 525 feet will likely be competing with cable stayed bridges. Both bridge models were assumed to use the balanced cantilever construction method as this method will be the most economical for the span lengths considered.

The primary purpose of these bridge models was to obtain realistic estimates of the effect of various parameters (i.e. vertical earthquake motion, pre-earthquake segment joint stress-state, record scaling, etc.) on the seismic response of the superstructure segment joints of precast segmental bridges. To that end, the models were developed based on design and construction details from segmental bridges currently under construction in California. These models, however, were not

intended to represent the actual bridges, nor are the results presented in this dissertation intended to be a design check of the actual bridges.

6.1. Analysis Control Parameters

All the time history analyses used the Newmark constant acceleration integration method, large displacement theory and 1% initial stiffness Rayleigh damping at mode 1 (i.e., a period of 2.0 seconds) and at a period of 0.1 seconds (see Figure 6-1). Newton-Raphson iterations in Ruaumoko appeared to set-up physical reversals during the convergence process and was deemed to be inappropriate for these analyses. Instead the integration time step was kept small at 0.001 seconds. A parameter study on the time step was performed and this time step was considered to be optimal. The 300 foot span model consisted of 1228 nodes, 1637 elements and 119 member properties while the 525 foot span model consisted of 1557 nodes, 2282 elements and 210 member properties.

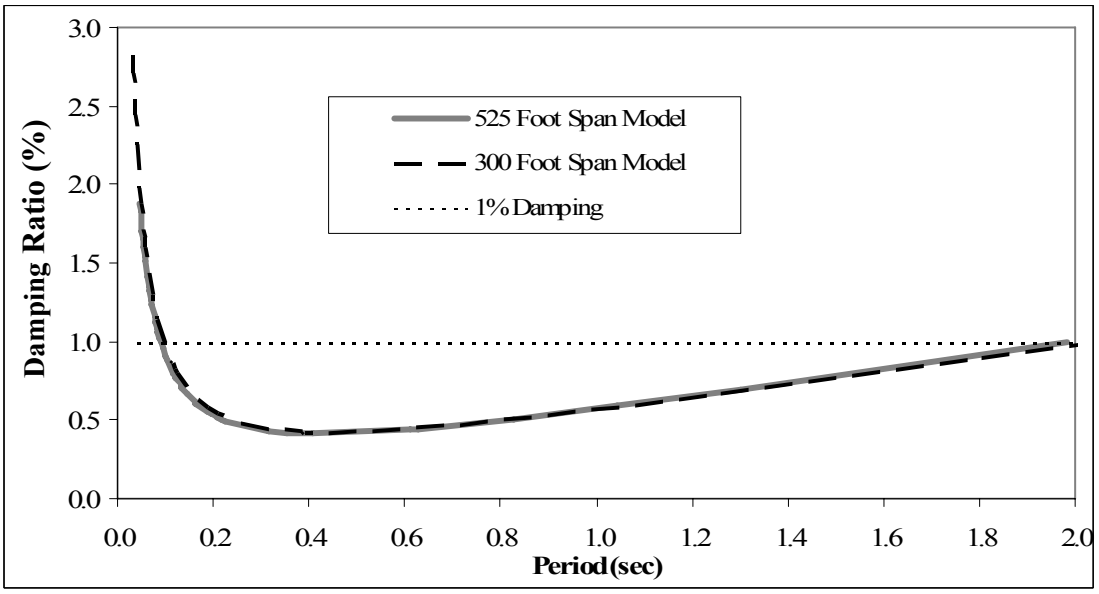

Figure 6-1 Initial Stiffness Rayleigh Damping Models Used in Full Bridge Analyses

6.2. 300 Foot Span Model Discretization

The 300 foot span model was based on the Otay River Bridge, currently under construction in San Diego County, California. The Otay River Bridge is 0.6 miles long and consists of four longitudinal frames and eleven tapered piers. The bridge consists of two parallel precast segmental superstructures that are joined at the top flange with a cast-in-place closure. The superstructure segments are 36 feet wide and vary in depth from 10 feet at midspan to 16 feet at the piers. Thus the span-to-depth ratio varies from 19 to 30.

An analytical model of a five span frame was developed as shown in Figure 6-2. The interior spans are 297 feet and the exterior spans are 176 feet. Approximately 40% (i.e., 11 of 29 joints per span) of all superstructure segment joints were modeled.

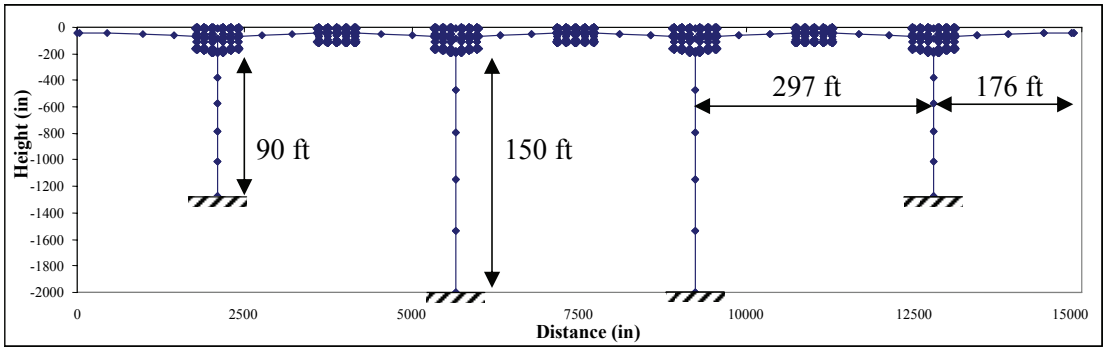

Figure 6-2 300 Foot Span Model (not to scale)

6.2.1. Boundary Conditions

The beginning and end of the frame were modeled as abutments. They were modeled with vertical roller supports and longitudinal non-linear compression only spring to capture the response of the soil behind the abutment, see Figure 6-3. The abutment soil spring properties were calculated based on the Caltrans Seismic Design Criteria (Caltrans, 2004) using an initial stiffness of 20 kips per inch and an ultimate stress of 5 ksf. The compression only longitudinal abutment springs were not engaged until the 9.8 inch thermal expansion gap was closed. The base of the

piers were modeled as fully fixed with no consideration for soil structure interaction, because the piers were tall and flexible relative to the span lengths, thus adding additional flexibility in the foundation will not significantly alter the response of the superstructure.

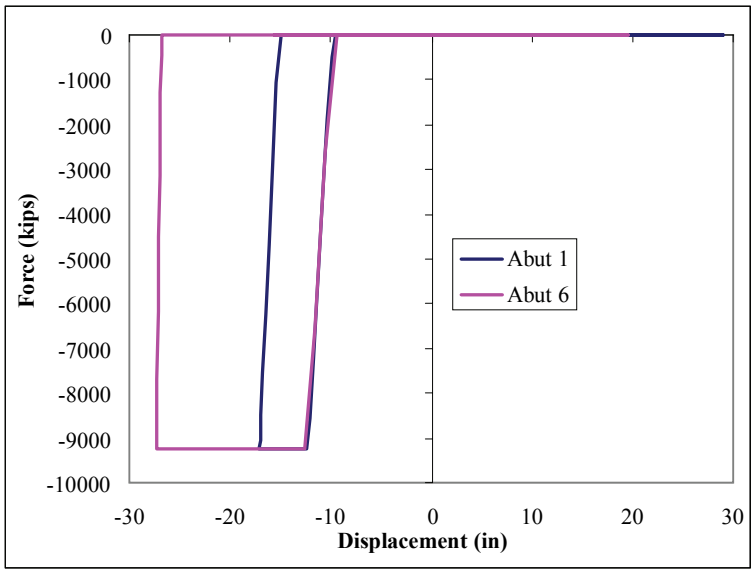

Figure 6-3 300 Foot Span - Abutment Hysteretic Behavior

6.2.2. Piers

The top and bottom of the piers were modeled with non-linear 2-component Giberson beam elements (Giberson, 1969). Giberson beam elements are computationally very effective because they can describe complex hysteretic behavior that is typical of reinforced concrete members using lumped plasticity. The Clough hysteresis rule was used to model the plastic hinging of the columns as

shown in Figure 6-4. The moment capacity of the piers was determined based on moment-curvature analyses using the program XTRACT (Chadwell and Imbsen, 2002). The plastic hinge length, L_p, of the piers were determined by

$$L_p = 0.08L + 0.3D + 0.15 f_y d_{bl} \quad \textbf{6-1}$$

where L is the column shear span length, D is the depth of the column, f_y is the yield strength of the reinforcement, and d_{bl} is the diameter of the longitudinal reinforcement bars of the column. This equation was developed by Hines et al. (1999) based on large scale experiments of structural wall with confined corner elements which was part of a larger research project studying the behavior of hollow column with confined corner elements.

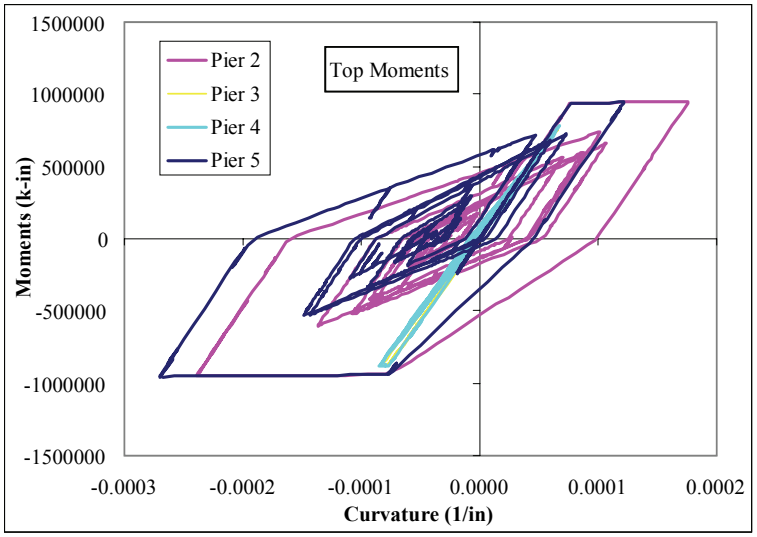

Figure 6-4 300 Foot Span - Pier Hinge Hysteretic Behavior

The Clough hysteretic rule did not capture axial force-bending moment coupling of the columns (see Figure 6-5). Since the focus of this investigation was the response of segment joints, and the longitudinal moment demand on the superstructure is generated by the moment at the top of the column, it was important to subject the superstructure to the largest reasonable column moment. This moment will occur when the axial load on the column is at its maximum. Thus the yielding moments of the piers were increased by 25% above the dead load moment capacity to account for the fact that vertical earthquake motion will increase the axial force on the piers which will in turn increase the moment capacity of the piers. The 25% increase was based on a preliminary run of the model using vertical and lateral components of 100% of the Rinaldi record from the 1994 Northridge earthquake.

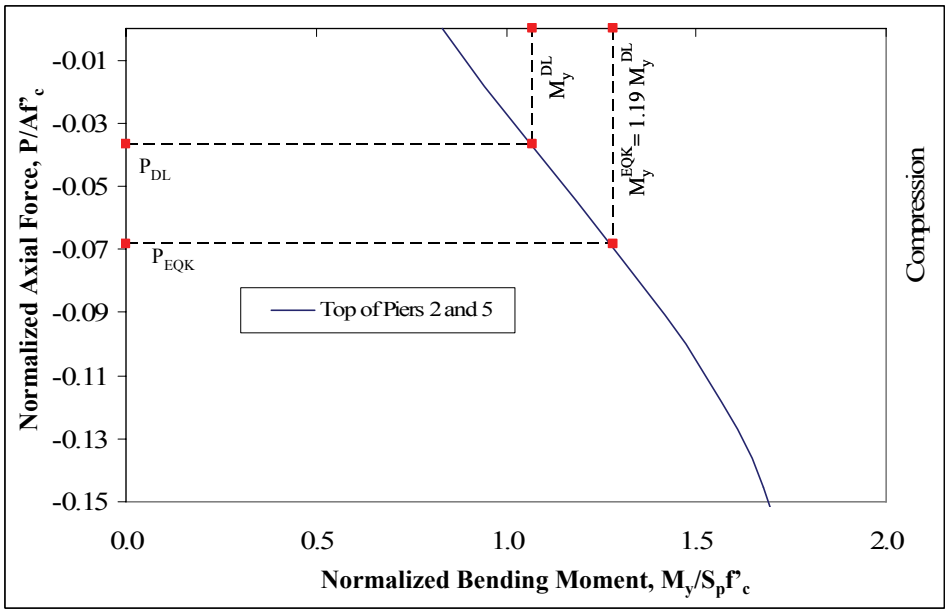

Figure 6-5 300 Foot Spans – Normalized Axial Force–Bending Moment Interaction Diagram for Piers 2/5

As a check of the amplified pier moment capacity, the normalized peak compressive forces and the corresponding normalized yield moment capacity for all twenty earthquake records are shown in Figure 6-6 and Figure 6-7, respectively. The median axial compressive force during an earthquake, P_{EQK}, for Piers 2 and 5 was plotted on the axial force-bending moment interaction diagram and the pier yield moment during an earthquake, M_y^{EQK}, was determined. This moment was 19% higher than the yield moment based on the dead load axial load, M_y^{DL}, and is 6% less than the value used in the model. This indicated that when the column plastic

mechanism forms, the model will subject the superstructure to a moment that is 6% larger than the median axial force on the column predicts.

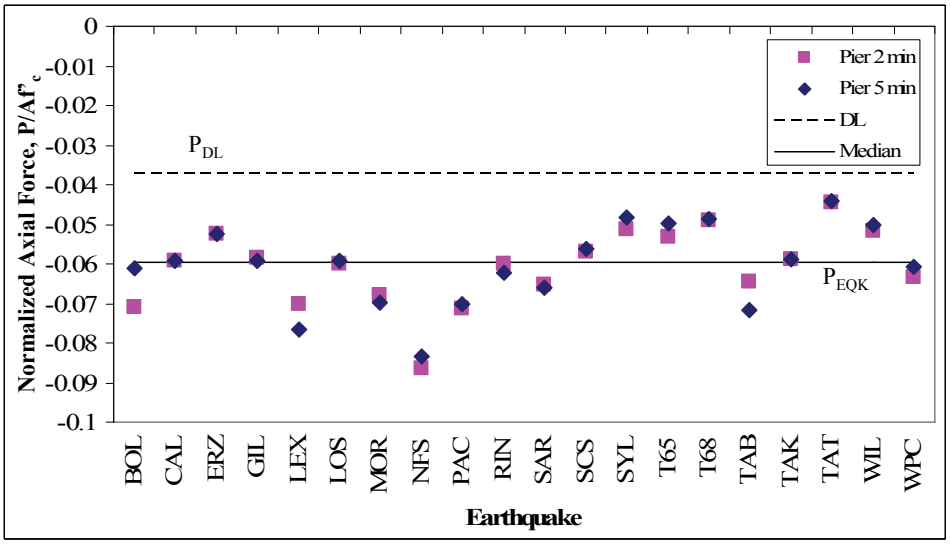

Figure 6-6 300 Foot Span – Normalized Peak Compression Axial Force in Piers 2 and 5

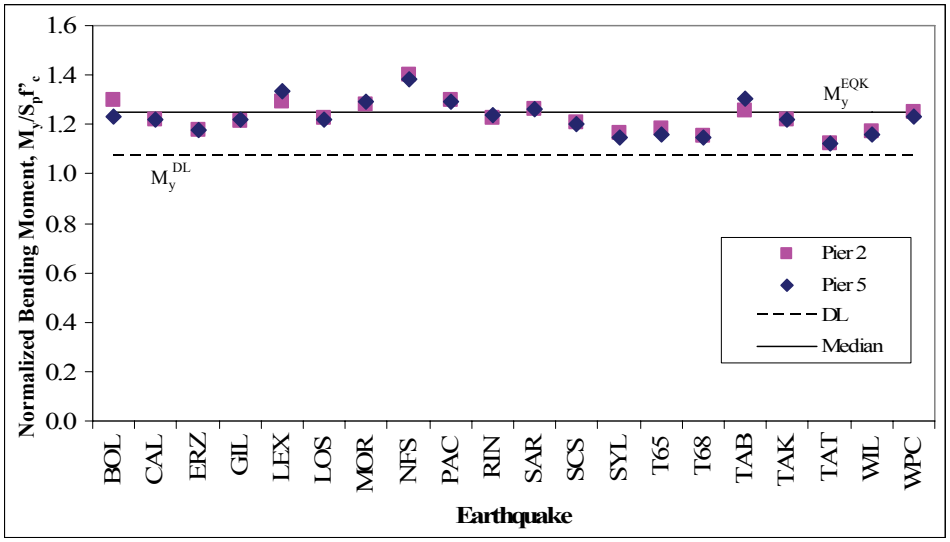

Figure 6-7 300 Foot Span – Normalized Bending Moment in Piers 2 and 5 Considering Interaction with Axial Load

Presland (1999) and Ang et al. (1985) noted that the nominal moment capacity predicted by ACI-318 (ACI, 2002) typically underestimated the capacity observed in tests on well confined columns. Figure 6-8 shows the moment capacity enhancement observed by these researchers. This moment enhancement was due to a number of reasons. ACI-318 does not account for strain hardening of reinforcement or for the effect of confinement on concrete strength and strain. In addition, the confinement effect of adjacent members, which can shift the location of the critical section on the column and effectively increase the moment capacity, was not considered. Presland also noted that dynamics effects can increase the actual capacity of a column. While moment-curvature analyses can account for the strain hardening of steel and the effect of confinement reinforcement on the ultimate strength and strain of concrete, confinement from adjacent members and dynamic effects on the column moment capacity were not considered in this dissertation. Thus the increase of 6% on the yield moment was justified for these lightly loaded well confined columns.

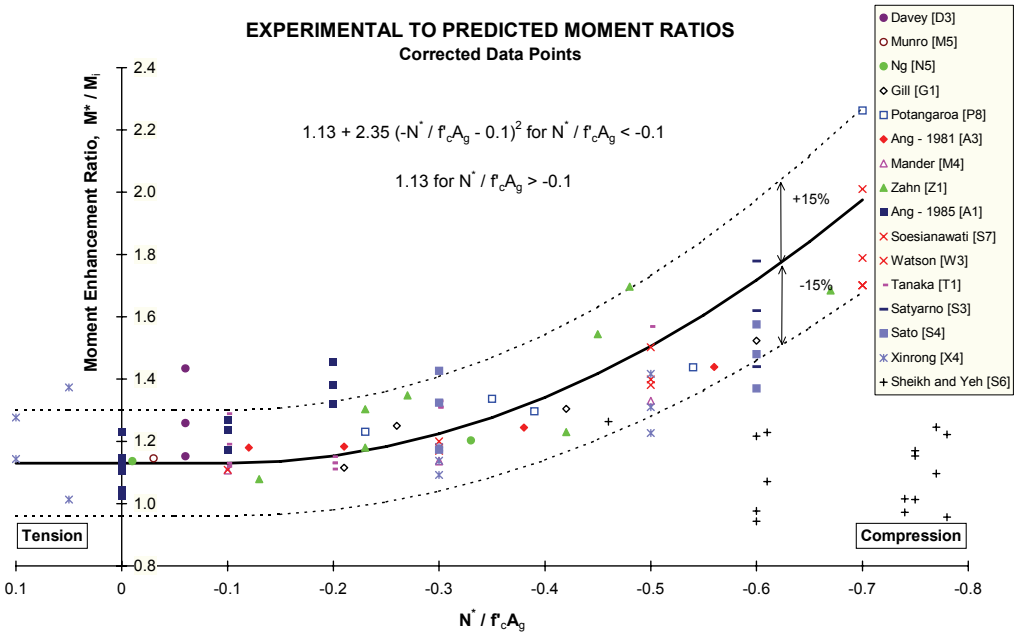

Figure 6-8 Influence of Axial Load on Moment Enhancement Ratio (Presland, 1999)

6.2.3. Superstructure Joints

A typical pier cantilever for a 300 foot span is shown in Figure 6-9. Twenty-eight superstructure segments formed the 300 foot span, thus there were twenty-nine segment joints per span. Eleven of these segment joints were modeled, six segment joints at each pier and five segment joints at midspan as shown in Figure 6-10 and Figure 6-11. These joints were modeled in a similar manner as the validation models discussed in Chapter 4 and were considered to be epoxied together and thus were able to take tension until cracking of the section occurred. Non-linear shear deformations of the superstructure were neglected because the shear spans were very

large (i.e., M/V > 70 feet) and thus shear deformations would be very small. Cracking of the segments between joints was also neglected to simplify the model. This approach was justified by large scale experimental results (Megally et al., 2002; Densley et al., 2003; Burnell et al., 2005) that indicated that very little flexural cracking occurred between segment joints.

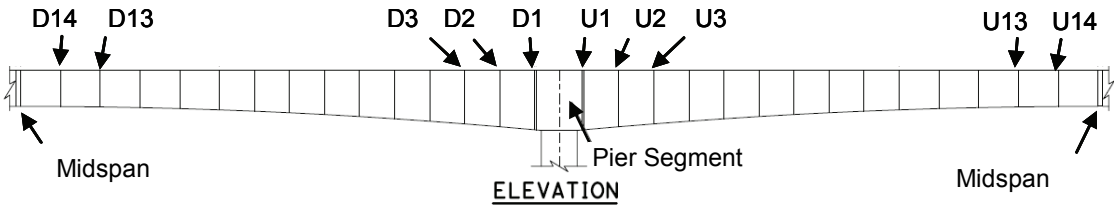

Figure 6-9 300 Foot Span - Segment Joint Identification

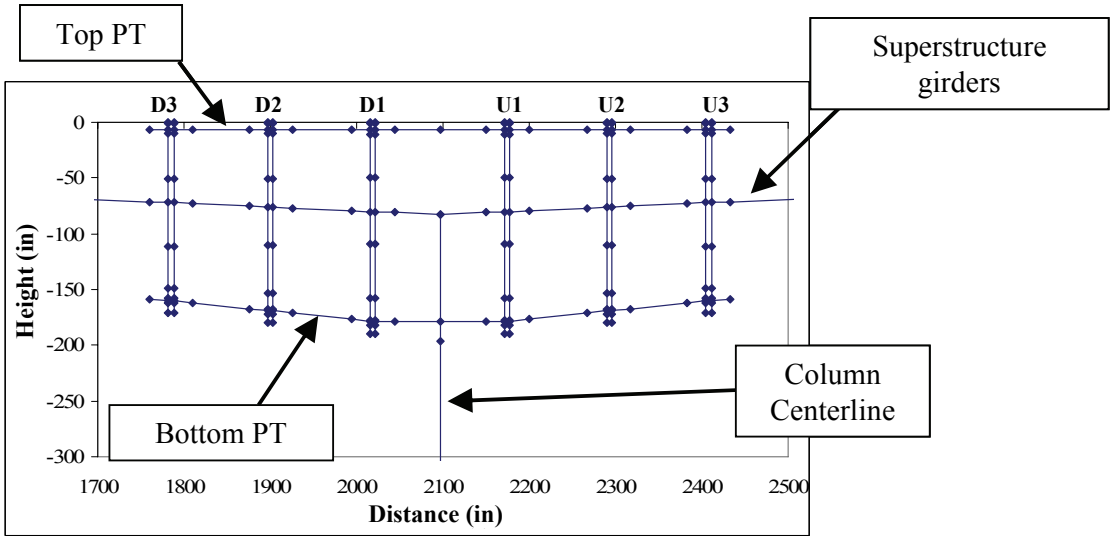

Figure 6-10 300 Foot Span Model Adjacent to Piers

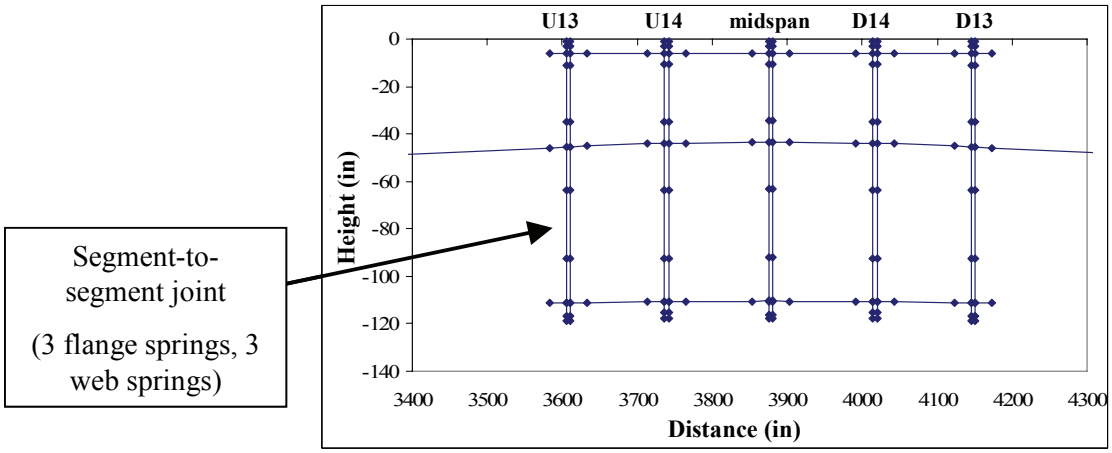

Figure 6-11 300 Foot Span Model Near Midspan

6.2.4. Superstructure Tendons

To ensure that the forces in the tendons were realistic, the tendons were preloaded in the model according to the jacking forces shown on the Otay River Bridge construction drawings. The model inherently accounted for elastic shortening losses, but not for losses due to friction or anchorage seating. To address this issue, the PT losses due to friction and anchorage seating were estimated for all tendons, based on the provisions outlined in Section 9.16 of the AASHTO Standard Specification for Highway Bridge (AASHTO, 2002). A sample tendon stress diagram is shown in Figure 6-12. Figure 6-13 summarizes the tendon losses based on their length. The losses for all tendons crossing a joint were averaged and the pretension load reduced accordingly. For example, 14 cantilever tendons crossed the

joint closest to the pier (i.e. Joint D1 or U1). The average loss in the PT member in the model was thus the average loss of all 14 tendons and was 17.8 ksi. This approach was used for all joints in the model. The losses range from 16 ksi to 21 ksi depending on the joint. It is important to note that time dependant losses (i.e. creep, shrinkage, and relaxation) were not inherently considered in the analyses. Rather they were considered separately as discussed in Section 6.2.5.2

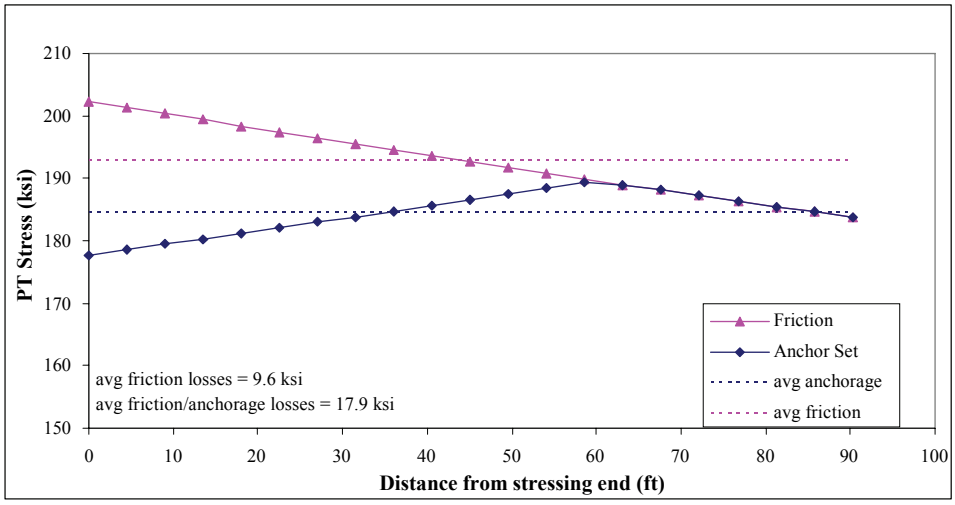

Figure 6-12 300 Foot Span - Anchorage and Friction Losses of a Typical Tendon

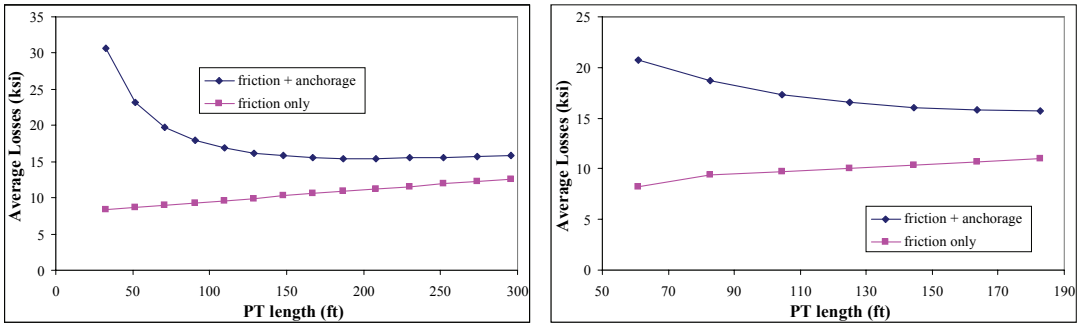

a) Cantilever Tendons **b) 'B' Tendons**

Figure 6-13 300 Foot Span - Summary of Tendon Losses

6.2.5. Pre-Earthquake Segment Joint Stress-State

One of the parameters of interest is the impact of the pre-earthquake stress-state on the response of segment joints. The pre-earthquake stress-state of the structure depends on the construction method and on creep, shrinkage and temperature variations. Creep and shrinkage is dependant on a number of variables, that included the compression stress on the section, the age of the concrete when the stress is applied, the duration of the load and the relative humidity, among other. To accurately estimate the effect of all these variables on a structure where every segment is constructed at different times and the loading at each segment joint changes during the construction process, clearly requires a very detailed analysis. Thus, the results from a full longitudinal construction staging analysis (LCA) of the Otay River Bridge were obtained from the designers, to ensure that the pre-earthquake stress-state of the segment joints were realistic.

6.2.5.1. Calibration Process

A comparison of the top and bottom superstructure stresses, at the end of construction (EOC), between the analytic model developed in this study and the designers LCA calculations are shown in Figure 6-45 and Figure 6-46, respectively.

The model overestimated the top stress and underestimated the bottom stresses. This difference was due to construction staging effects and indicates that the stress state in different section of the structure is highly dependant on the method of construction.

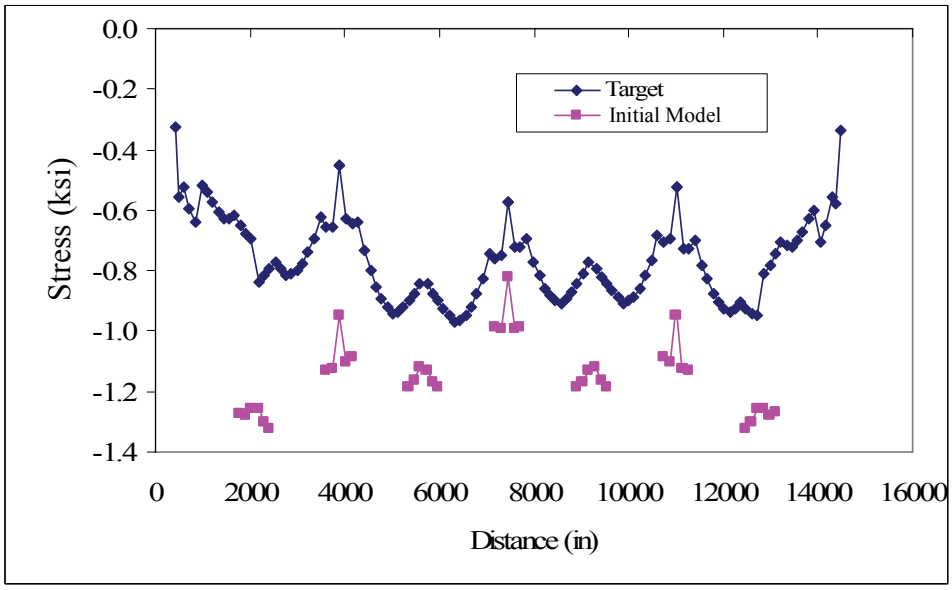

Figure 6-14 300 Foot Span - Comparison of Superstructure Top Stresses at EOC Prior to Calibration

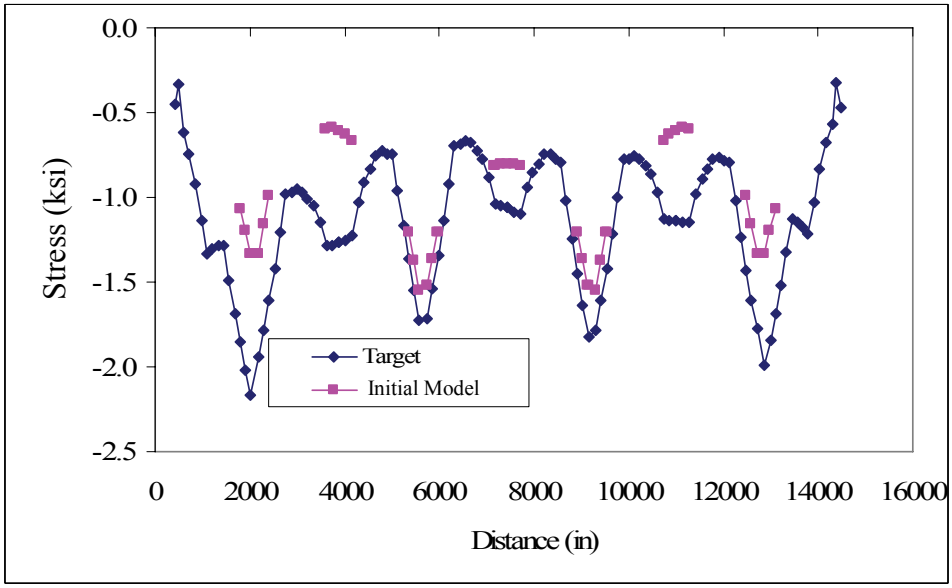

Figure 6-15 300 Foot Span - Comparison of Superstructure Bottom Stresses at EOC Prior to Calibration

The bridge was constructed using the balanced cantilever construction method (see Section 2.3.2). In this method, the superstructure behaves as a cantilever until continuity is built in at midspan. Thus, this method results in very large negative dead load bending moments at the pier faces, see Figure 6-16. The analytical model, on the other hand, assumes that all concrete is placed in a single placement operation and all PT tendons are stressed simultaneously, on a fully continuous frame structure. This will generate significantly smaller negative dead load bending moments at the piers and positive dead load bending moments at midspan, as shown in Figure 6-17. Clearly, such a model does not reflect the

construction method and staging, and must be adjusted to ensure accurate representation of the joint stress-state.

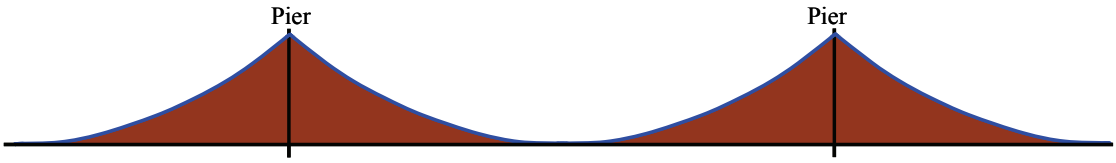

Figure 6-16 Dead Load Bending Moment Diagram for Balanced Cantilever Construction

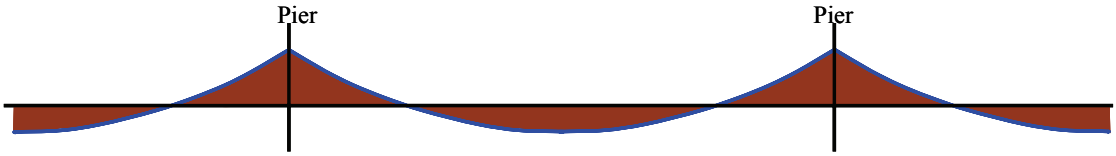

Figure 6-17 Dead Load Bending Moment Diagram for Continuous Frame Analytical Model

To more accurately represent the stress-state of the joints after construction, equal and opposite redistribution forces (i.e. bending moments and axial forces) were applied across each segment joint in the analytical model (See Figure 6-18). The magnitude of these forces was iterated until convergence with the designers's stress-state was achieved. The iteration process is as follows.

1. Run model with current segment joint forces. On the first iteration, these forces are zero.
2. Given the known target and current stresses at the extreme top and bottom fibers of the section and the section properties, calculate the axial load

and moment on the segment joints using simple solid mechanics relationships.

3. Calculate the difference between the current and target segment joint forces (i.e., axial loads and bending moments) at every segment joint
4. Determine the section forces for the next iteration by adding the difference calculated in step 3 to the current forces and check for convergence. Convergence was defined as a median change in segment joint forces of less than 0.1% from the previous iteration. .
5. Repeat steps 1 to 4 until convergence.

The process will typically converge in five iterations. A sample iteration process is shown in Appendix A.

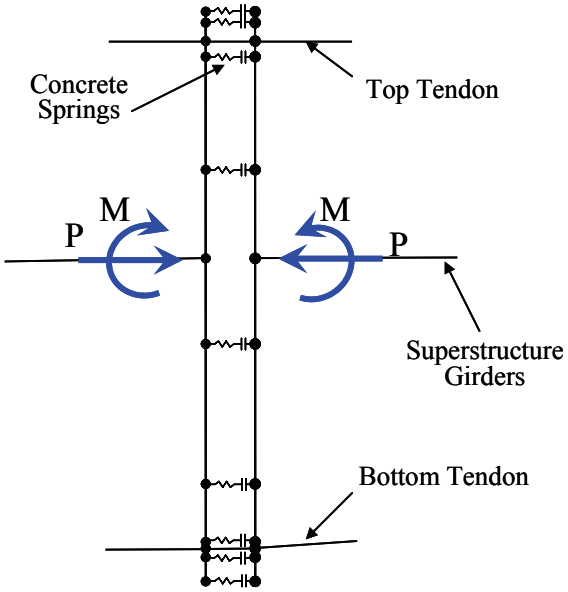

Figure 6-18 Sketch of Applied Segment Joint Forces

Figure 6-19 and Figure 6-20 show a comparison of the top and bottom stresses at the end of construction and after the iteration process described above.

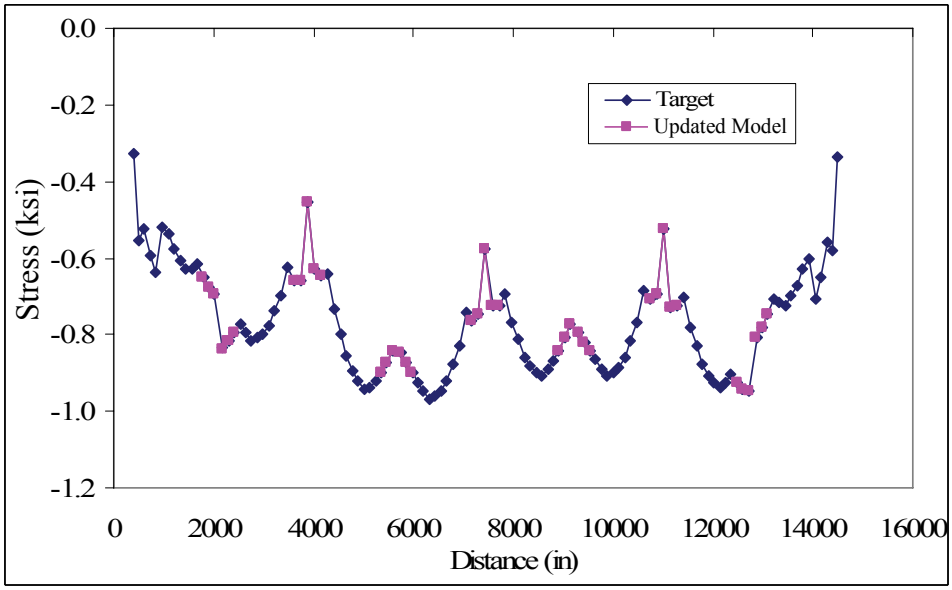

Figure 6-19 300 Foot Span - Comparison of Superstructure Top Stresses after Calibration to EOC

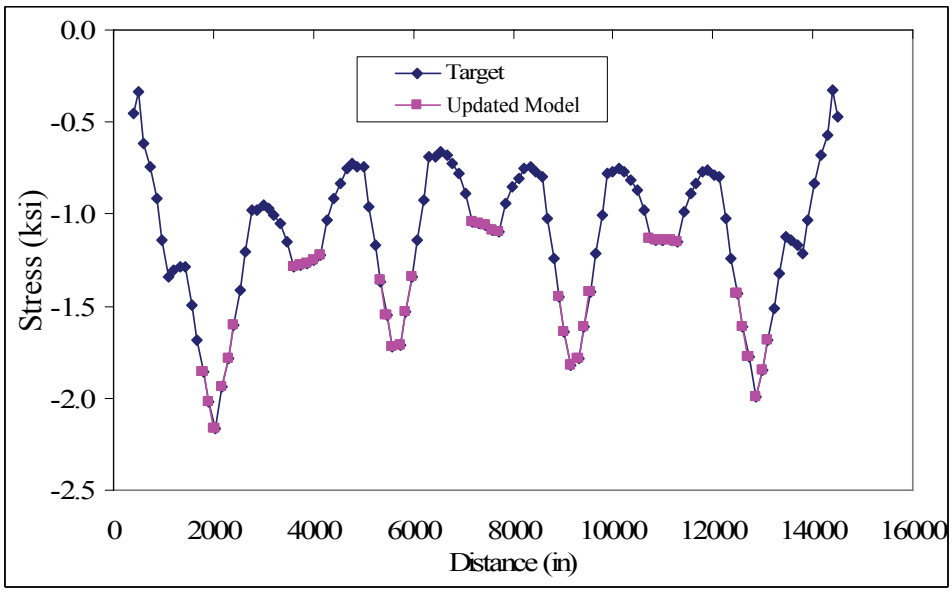

Figure 6-20 300 Foot Span - Comparison of Superstructure Bottom Stresses after Calibration to EOC

6.2.5.2. Considerations for Variations in the Pre-Earthquake Stress-State

Numerous influences, namely creep, shrinkage, relaxation, and temperature, will change the stress-state of the segment joints continually over the life of the bridge. To investigate the effect of the pre-earthquake stress-state on the seismic response, several pre-earthquake stress-states were investigated. These stress-states were developed in a systematic fashion based on the effect of creep and shrinkage. The changes in the stress-state due to creep and shrinkages of each segment joint was obtained from the designer's LCA and are summarized in Figure 6-21. On average the top and bottom fiber stresses increased, that is, lost compression, at the piers and

at the bottom of the midspan joints, while the compressive stresses increased in the top fibers of the midspan joints. This change in stress was used to generate four different pre-earthquake stress configurations that were intended to represent the range of stresses that may occur during the life of the superstructure. The stress-state in the piers remained essentially unchanged. These four configurations are as follows:

1. **–CS**: The stress at end of construction minus the change in stress due to creep and shrinkage. This stress configuration represented a potential state of stress near the end of construction (i.e. beginning of service life) with considerations for possible inaccuracies in the LCA as well as for considerations for the effect of temperature, particularly temperature gradients, on the bridge superstructure.
2. **EOC**: The best estimate of the stress-state at the end of construction and considers construction staging effects as well as volumetric changes that occur during construction.
3. **+CS**: The best estimate of the state of stress after the majority of creep and shrinkage has occurred, i.e. end of service life. This stress-state also

considered the effects of relaxation but the majority of the stress changes occurred from creep and shrinkage.

4. **+2CS**: The stress at EOC plus twice the change in stress due to creep and shrinkage. This stress configuration represented a potential stress-state towards the end of the service life of the bridge with considerations for possible inaccuracies in the LCA and creep and shrinkage calculations as well as for considerations for the effect of temperature on the bridge superstructure.

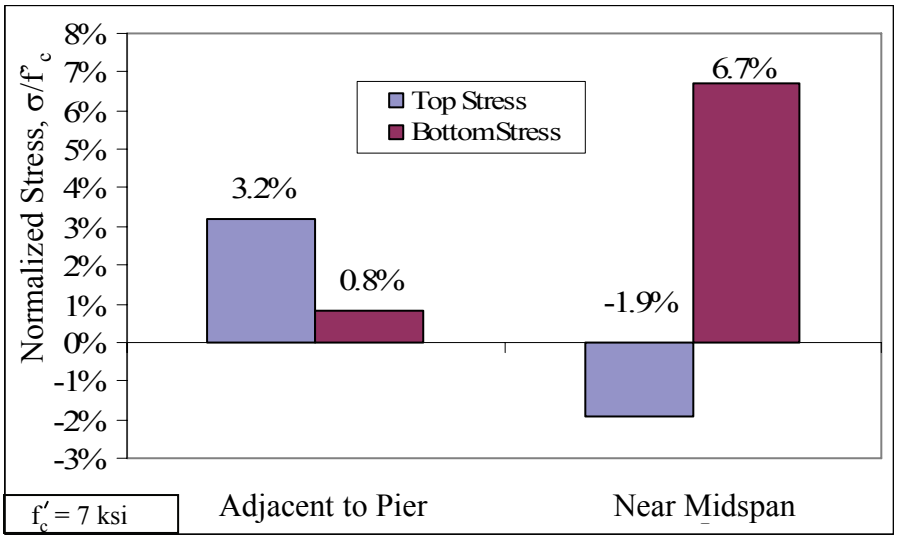

Figure 6-21 300 Foot Span - Average Normalized Stress Change due to Creep and Shrinkage

Figure 6-22 and Figure 6-23 show the top and bottom segment joints stresses for the four different initial stress configurations. The stress variation is most dramatic at midspan and at the top of the piers.

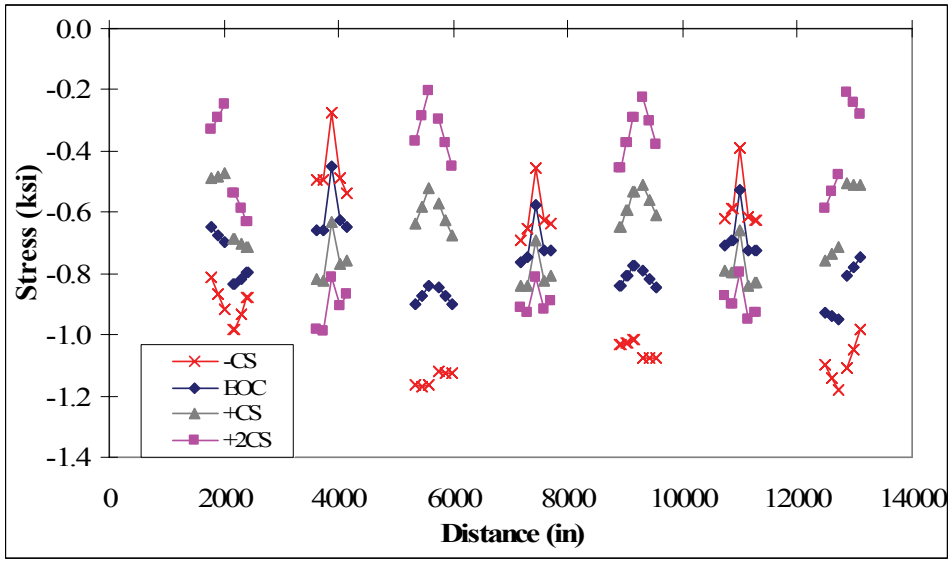

Figure 6-22 300 Foot Span – Top Fiber Stresses for Various Pre-Earthquake Stress-State Configurations (Negative Stress = Compression)

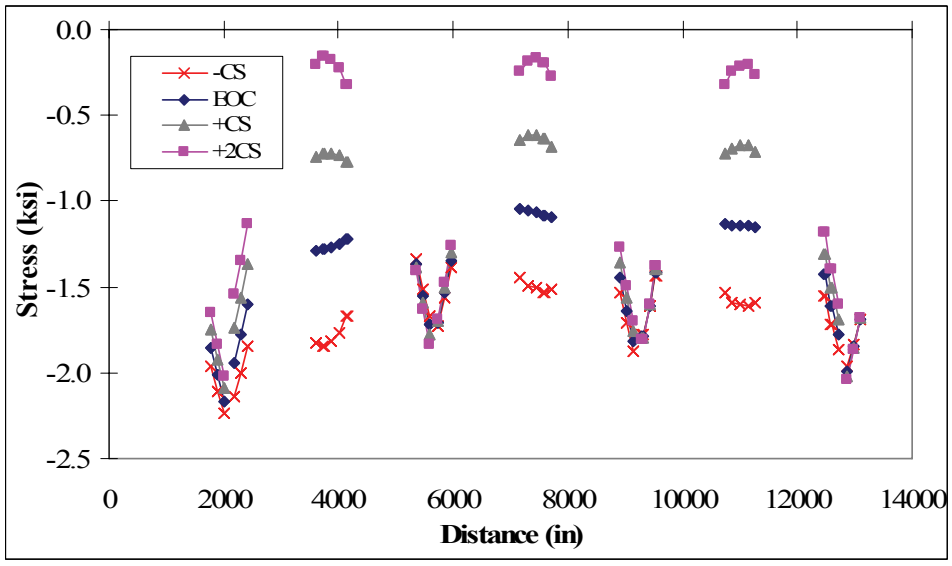

Figure 6-23 300 Foot Span – Bottom Fiber Stresses for Various Pre-Earthquake Stress-State Configurations (Negative Stress = Compression)

6.3. 300 Foot Span Model Characteristics

6.3.1. Dead Load Joint Stresses

The state of stress in the segment joints prior to a seismic event will likely affect the response of the joint. The stress profiles of the segment joints at Pier 2 and Span 3 for the four different pre-earthquake stress configurations are shown in Figure 6-24 through Figure 6-27. These profiles included dead load, PT loads, and losses due to elastic shortening, creep, shrinkage, relaxation, friction, anchorage seating, and the effects of construction staging. The stress profiles shown are typical of all segment joints in the model and are considered reasonable. The peak stresses are well below the AASHTO limit of $0.45 f_c^{'}$ (AASHTO, 1999). The average compression stresses across the joints as a percentage of $f_c^{'}$ are shown in Table 6-1. The average compression stress for segment joints adjacent to the piers ranged from 20% to 14% of $f_c^{'}$, while the average compression stress near midspan ranged from 16% to 8%.

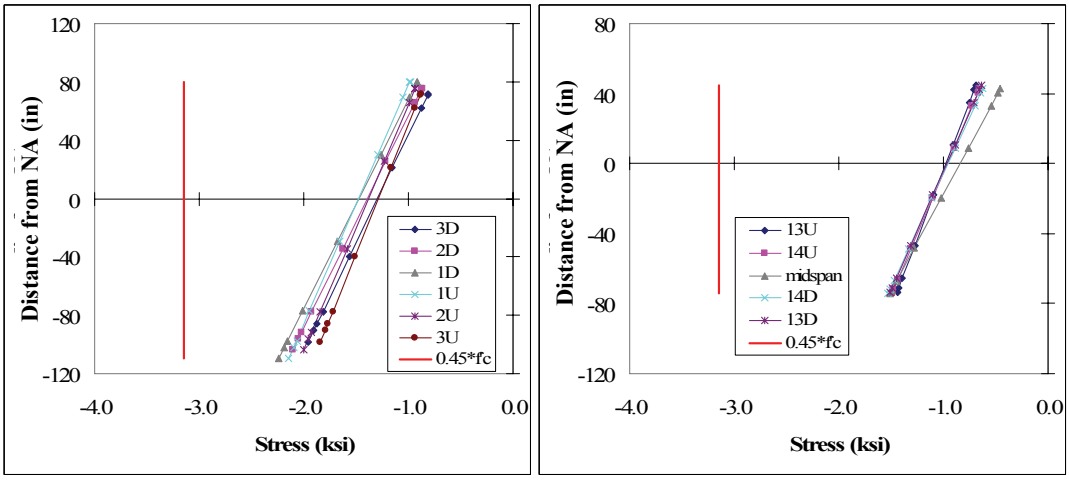

a) Pier 2 **b) Span 3**

Figure 6-24 300 Foot Span - Typical Dead Load Stress Profiles of Segment Joints at -CS

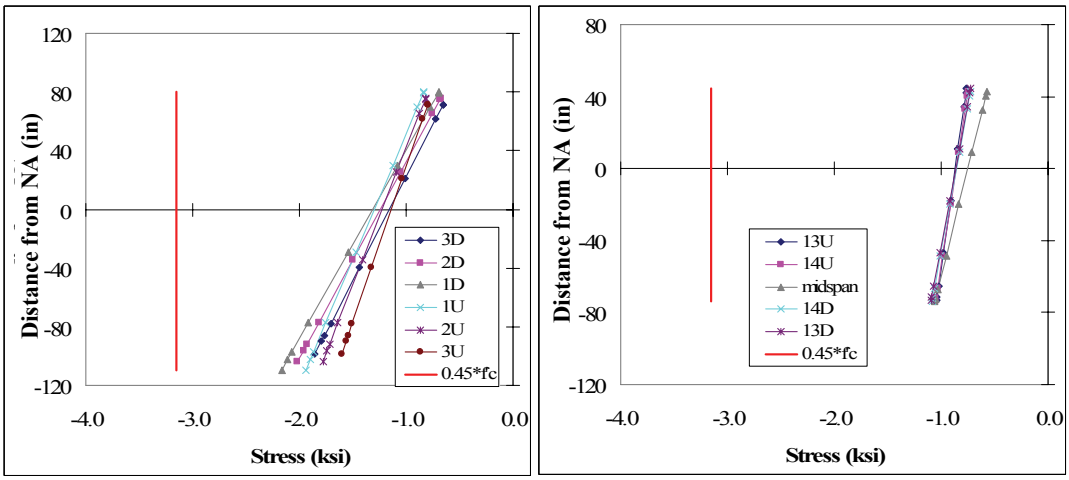

a) Pier 2 **b) Span 3**

Figure 6-25 300 Foot Span - Typical Dead Load Stress Profiles of Segment Joints at EOC

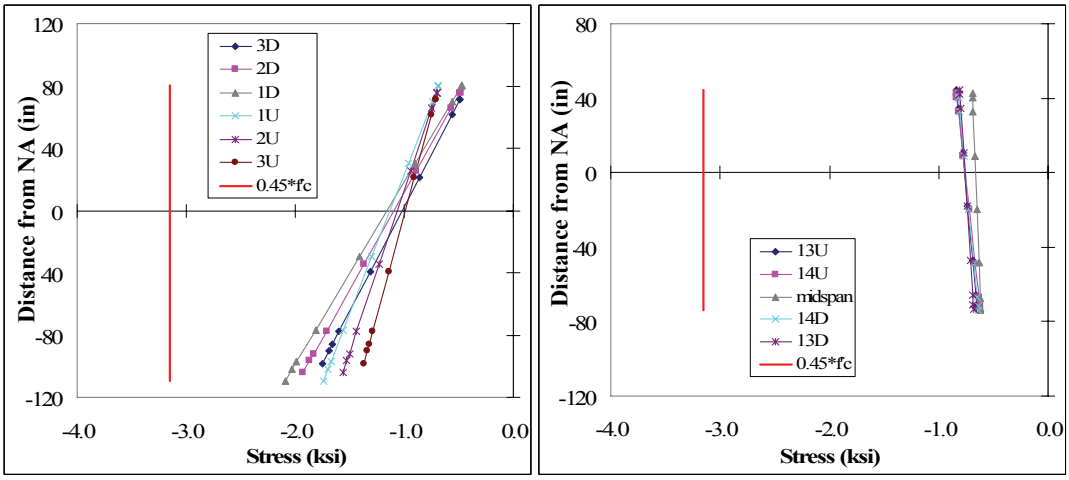

a) Pier 2 **b) Span 3**

Figure 6-26 300 Foot Span - Typical Dead Load Stress Profiles of Segment Joints at +CS

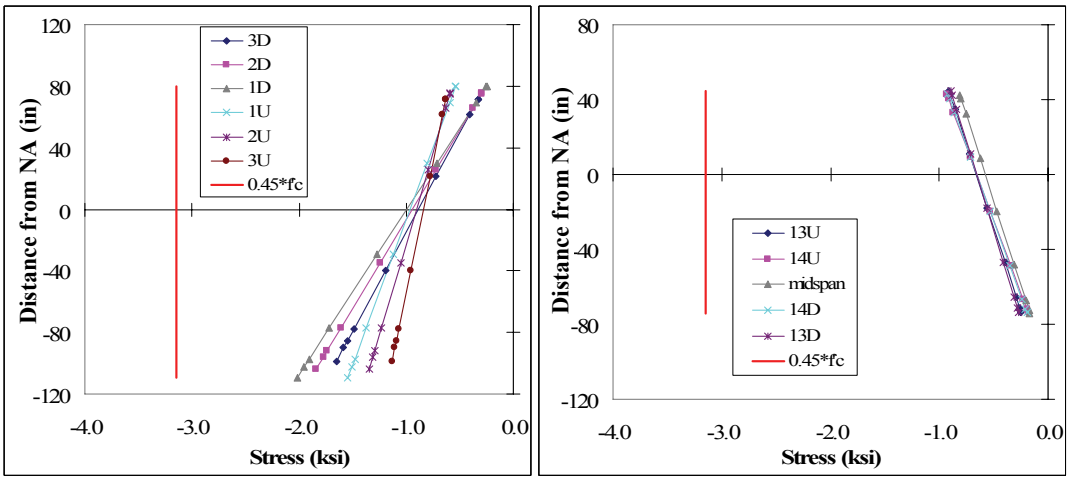

a) Pier 2 **b) Span 3**

Figure 6-27 300 Foot Span - Typical Dead Load Stress Profiles of Segment Joints at +2CS

Table 6-1 300 Foot Span - Summary of Average Superstructure Compression Stress (% of $f_c^{'}$)

Pre-Earthquke Stress Configuration	Adjacent to Piers	Near Midspan
-CS	20%	16%
EOC	18%	13%
+CS	16%	10%
+2CS	14%	8%

6.3.2. Mode Shapes

The period of the primary longitudinal mode was 2.0 seconds and had a modal mass of 86% of the total bridge mass (see Figure 6-28). It is important to note that the primary longitudinal mode at 2 seconds assumes no active engagement with the abutments. Since the abutments will likely be engaged during strong shaking, this mode shape is practically meaningless. The period of the dominant vertical modes, shown in Figure 6-29 and Figure 6-30, were 0.5 and 0.3 seconds and captured 18% and 22% of the total bridge mass, respectively.

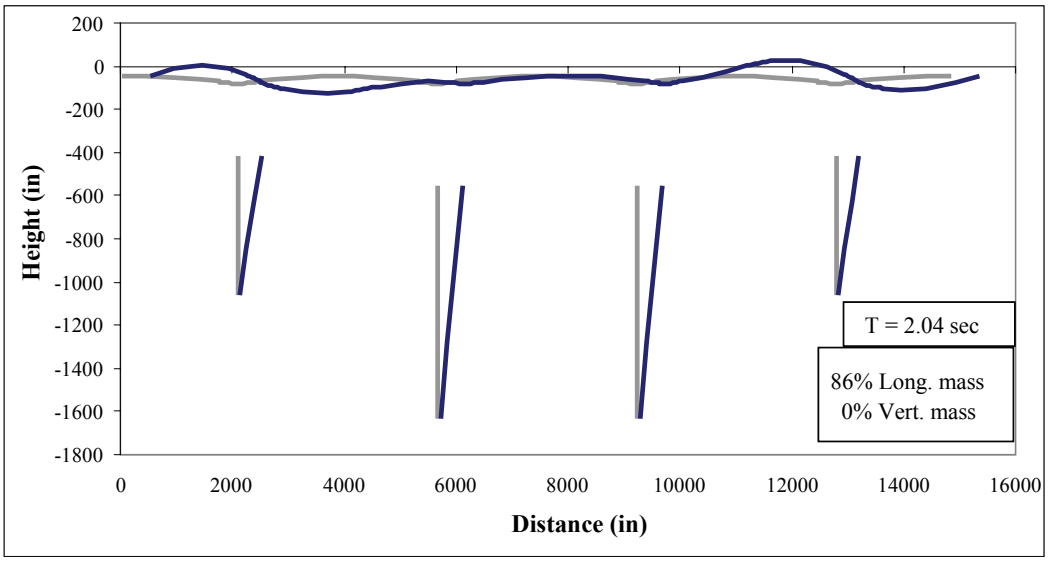

Figure 6-28 300 Foot Span - Primary Longitudinal Mode Shape

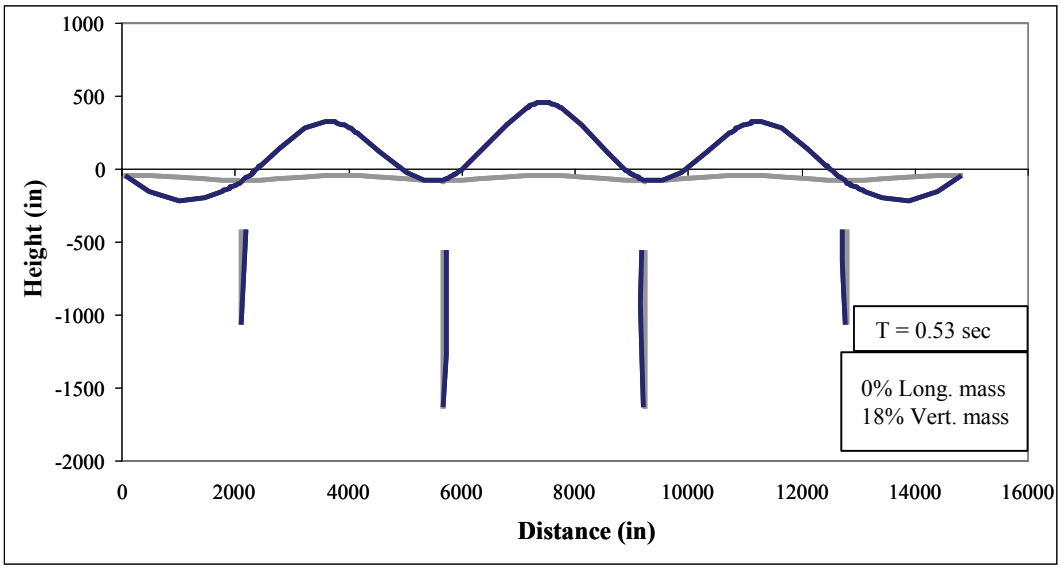

Figure 6-29 300 Foot Span - Primary Vertical Mode Shape – Mode 4

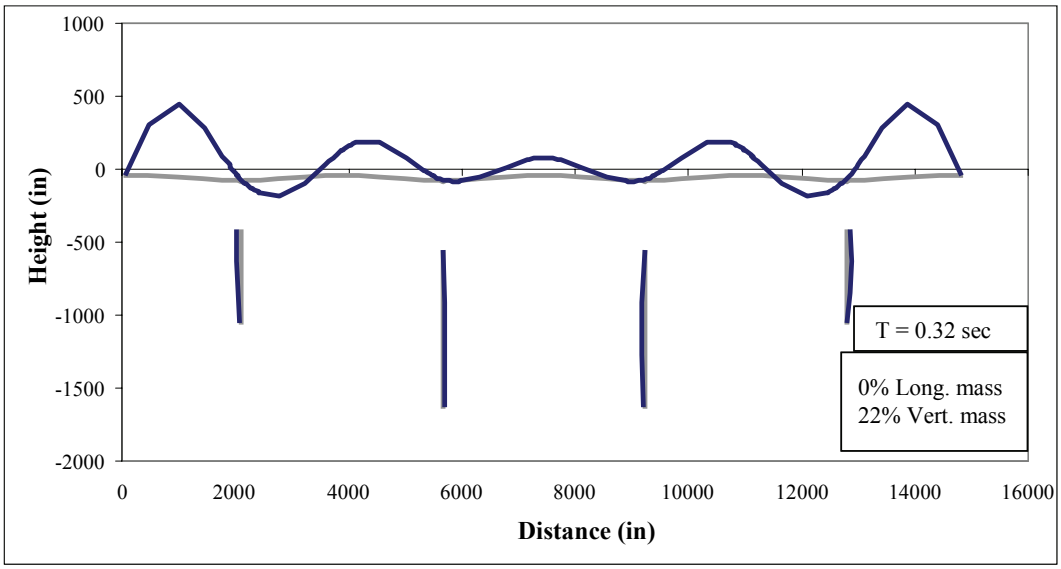

Figure 6-30 300 Foot Span - Primary Vertical Mode Shape – Mode 8

6.3.3. Longitudinal Pushover Analysis

A longitudinal pushover analysis was performed to understand the hinging sequence of the frame. The results of this analysis are shown in Figure 6-31. It is clear that the abutment soil spring is engaged prior to any column hinging. However the short piers yield and the onset of soil non-linear response behind the abutment occur at similar displacements. The tall piers begin to yield when the short pier has reached a displacement ductility of about 2. Note that a 10 inch superstructure displacement corresponds to a short pier drift of 1%.

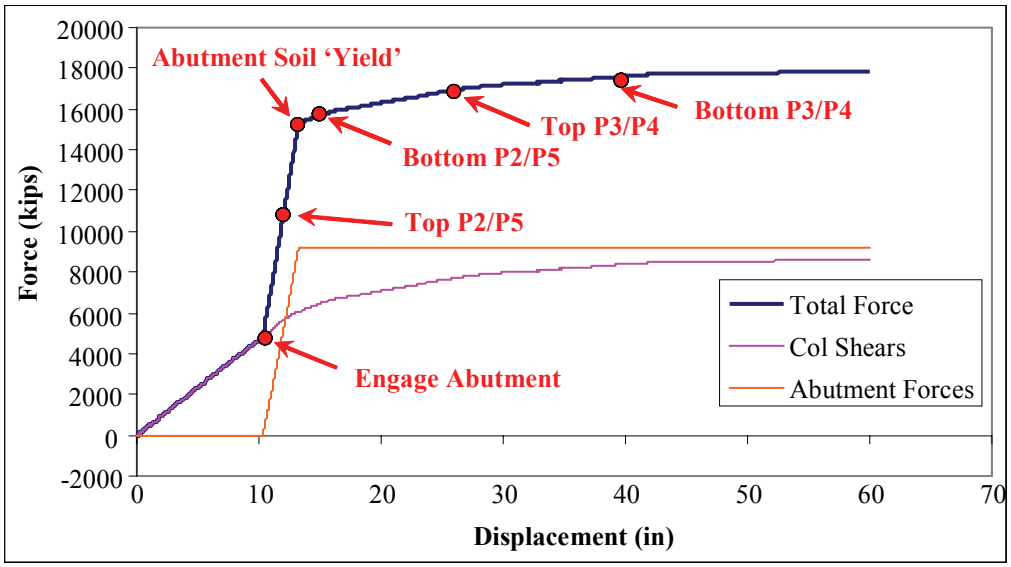

Figure 6-31 300 Foot Span - Longitudinal Push Results

6.3.3.1. Pier Performance Limit States

Pier performance limit states were identified based on the longitudinal pushover and moment-curvature analyses of the pier sections using the program XTRACT (Chadwell and Imbsen, 2002). These limits states represent crushing and spalling of the cover concrete, first yielding of the reinforcement and full plastic hinge development. Table 6-2 summarizes the performance limit states, outlines the consequences of exceeding each limit state and identifies the longitudinal drift ratio of Piers 2 and 5, for each limit state. For convenience and simplicity, the drift ratios of the shortest pier were used to identify the limit states, because the shortest piers tend to accumulate the most damage.

Table 6-2 300 Foot Span – Piers 2 and 5 Performance Limit States

Limit State	Pier 2/5 Drift Ratio	Description	Consequences
P-C1	**1.2%**	Incipient crushing of cover concrete, $\varepsilon_c = -0.002$	Patching of concrete may be required,
P-C2	**2.1%**	Spalling of cover concrete, $\varepsilon_c = -0.004$	Patching of concrete required, Operational performance level
P-C3	**5.7%**	Crushing of core concrete, $\varepsilon_c = -0.011$	Fracture of confinement reinforcement. Life safety performance level
P-R1	**0.45%**	First yield of reinforcement	End of purely elastic region of reinforcement.
P-R2	**1.1%**	Idealized yield of section	Development of plastic hinge. Noticeable residual cracking. Pressure grouting may be required. Operational performance level
P-R3	**4.3%**	Buckling of long. reinforcement, $\varepsilon_s = 0.04$	Buckling of longitudinal reinforcement. Life safety performance level

6.3.4. Segment Joints Behavior

6.3.4.1. Segment Joint Performance Limit States

Vertical pushover analyses were performed to obtain the backbone curve for the moment-rotation behavior of each segment joint, and to identify the rotation where various performance limit states occurred. The limits states of interest were cracking of the section, crushing of the extreme concrete fibers, the limit of proportionality of the main PT tendons which was assumed to occur at a stress of

210 ksi, and a strain of 1.2% in the main PT tendons. The crushing limit state, C2, was defined as the strain at 85% of f'_c, as illustrated in Figure 4-2. The consequences of the various performance limit states are outlined in Table 6-3.

Table 6-3 300 Foot Span – Segment Joint Performance Limit States

Limit State	Description	Consequences
C1	Concrete cracking, $\varepsilon_c = 0.000012$	Onset of joint opening, no consequences
C2	Crushing of extreme concrete fibers, $\varepsilon_c = -0.0016$	Patching of concrete may be required, Operational performance level
MT1	Limit of proportionality (210 ksi) of main tendons	End of purely elastic region of PT. Begin to lose prestressing force. Operational performance level.
MT2	$\varepsilon_{pt} = 0.012$ in main tendons	Full tendon yielding. Lose significant PT force. Residual joint openings are likely. Life safety performance level.

6.3.4.2. Vertical Monotonic Pushover Analyses

Figure 6-32 and Figure 6-33 show the backbone curves and limit states for the segment joints near midspan and adjacent to the piers, respectively. Table 6-4 summarizes the rotations at which the limits states were met for the various segment joints. Due to the regularity of the design and the gradual variations of the sections, the rotation limits states of the joints near the piers show only small variations. The same is true for the joints near midspan.

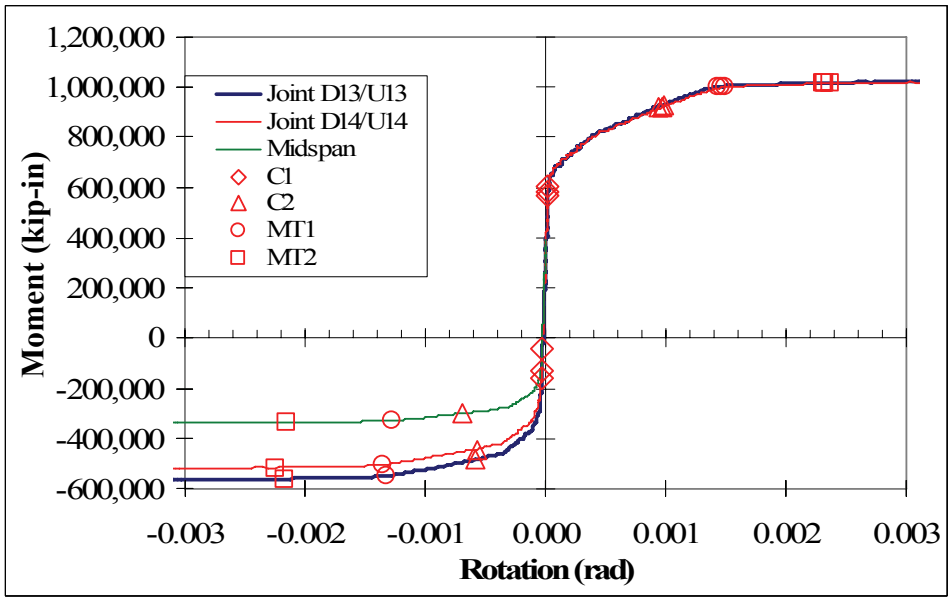

Figure 6-32 300 Foot Span - Behavior of Segment Joints Near Midspan

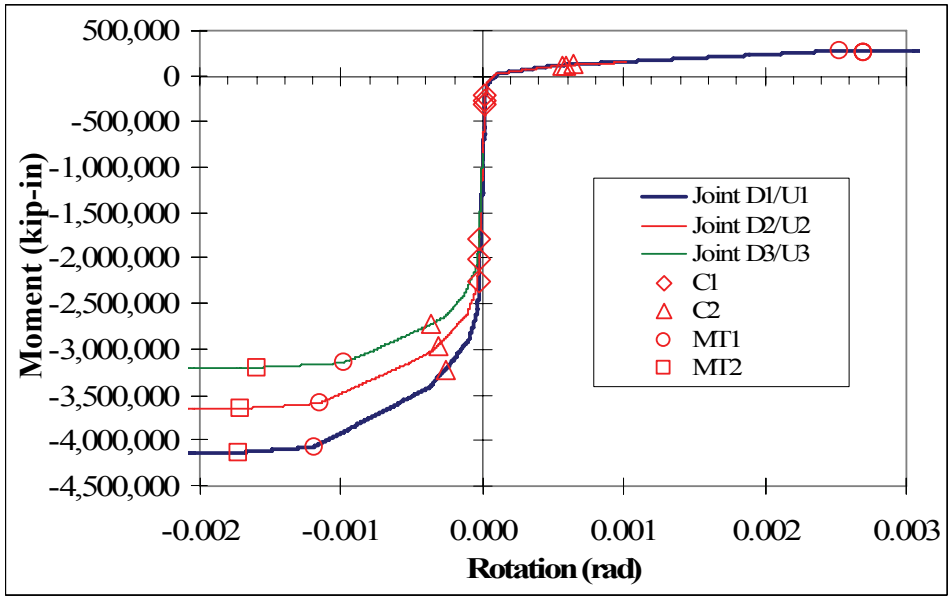

Figure 6-33 300 Foot Span - Behavior of Segment Joints Adjacent to Piers

Table 6-4 300 Foot Span - Summary of the Rotational Performance Limits States

			Segment Joint					
			D1/U1	**D2/U2**	**D3/U3**	**D13/U13**	**D14/U14**	**Midspan**
Performance Limit State	**C1**	**Negative**	-0.000024	-0.000025	-0.000025	-0.000033	-0.000034	-0.000031
		Positive	0.000017	0.000018	0.000018	0.000020	0.000020	0.000019
	C2	**Negative**	-0.00026	-0.00031	-0.00036	-0.00059	-0.00057	-0.00069
		Positive	0.00056	0.00060	0.00065	0.00093	0.00097	0.00098
	MT1	**Negative**	-0.00119	-0.00115	-0.00098	-0.00132	-0.00135	-0.00127
		Positive	0.00252	0.00270	0.00269	0.00143	0.00150	0.00147
	MT2	**Negative**	-0.00172	-0.00171	-0.00159	-0.00216	-0.00224	-0.00216
		Positive	0.00450	0.00364	0.00501	0.00232	0.00237	0.00231

All limit states above are in units of Radians

It is important to note that the pre-earthquake stress-state may alter the limit states slightly. Creep, shrinkage and relaxation are the dominant behaviors affecting the pre-earthquake stress-state in the long term, and will decrease the axial load on the sections as time progresses forward. A reduced compressive force on the section will reduce the moment capacity of the section slightly. The cracking rotation will also reduce up to 18% as shown in Appendix B. All other limits state were governed by the PT and remained essentially unchanged or increase up to 16%. For simplicity the limit states presented here and used in future section were defined based on the end of construction (EOC) stresses. For all limit states except cracking, this will be

slightly conservative for the CS and +2CS stress-state, yet non-conservative for the –CS stress-state.

6.3.4.3. Vertical Cyclic Pushover Analysis

A series of vertical reversed cyclic pushover analyses were performed to verify the cyclic moment-rotation behavior of the segment joints. Results from segment joint 1 (i.e., nearest the pier) and segment joint 15 (i.e., midspan) are shown in Figure 6-34 and Figure 6-35, respectively. The response captures joint opening, concrete crushing and PT yielding for both positive and negative bending directions.

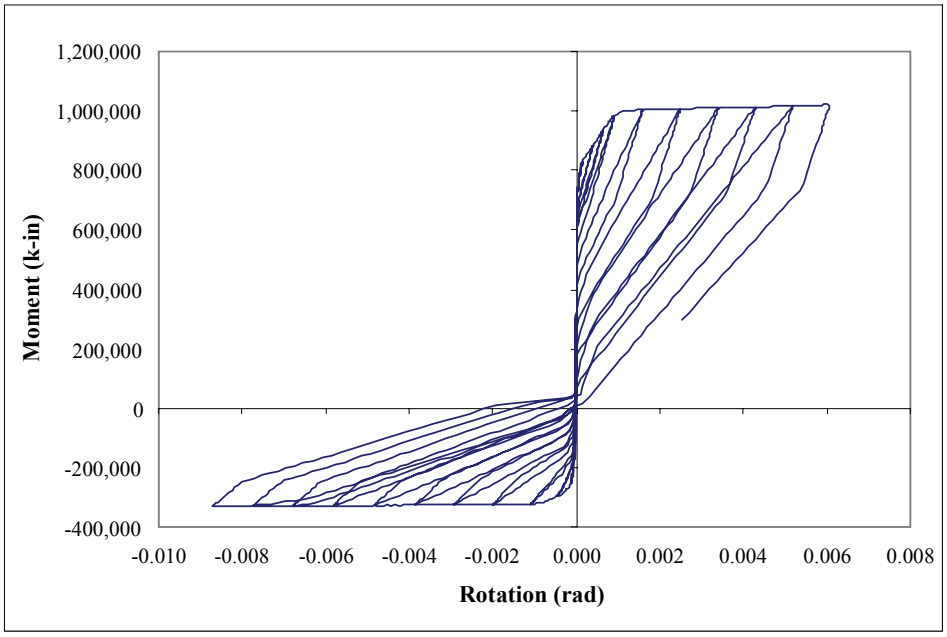

Figure 6-34 300 Foot Span - Midspan Moment-Rotation Diagram from Cyclic Analysis

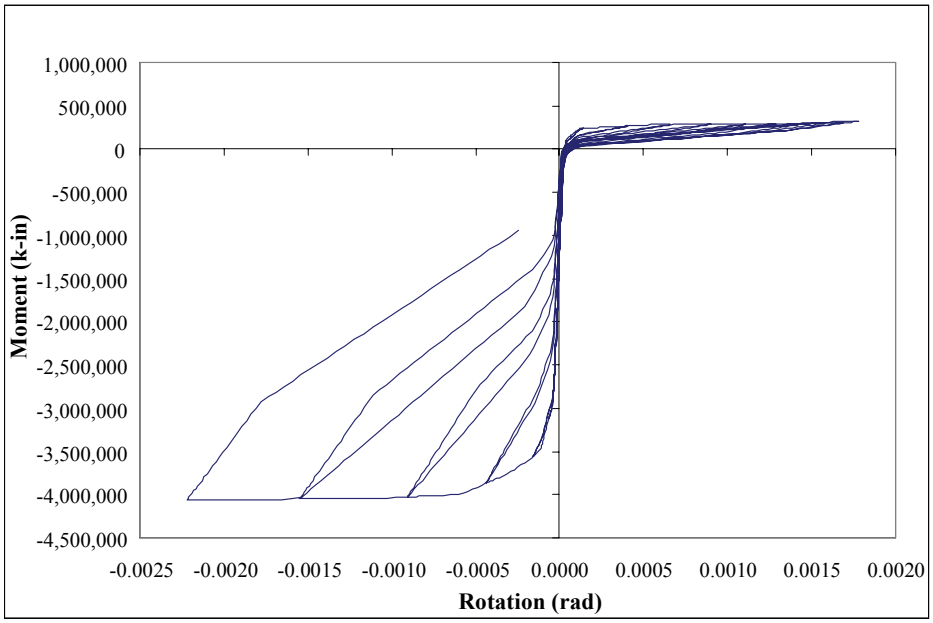

Figure 6-35 300 Foot Span – Joint 1 Moment-Rotation Diagram from Cyclic Analysis

6.3.4.4. Joint Rotation – Gap Width Relationship

The relationship between segment joint rotation and extreme fiber gap opening was obtained from the vertical push analyses and is shown in Figure 6-36. Positive rotations generated gaps at the bottom flange while negative rotations created gaps in the top flange. The positive and negative rotation relationships were essentially the same, thus only the positive rotation relationships are presented. Only Joint D1/U1 and midspan relationships are shown to ensure readability of the figure.

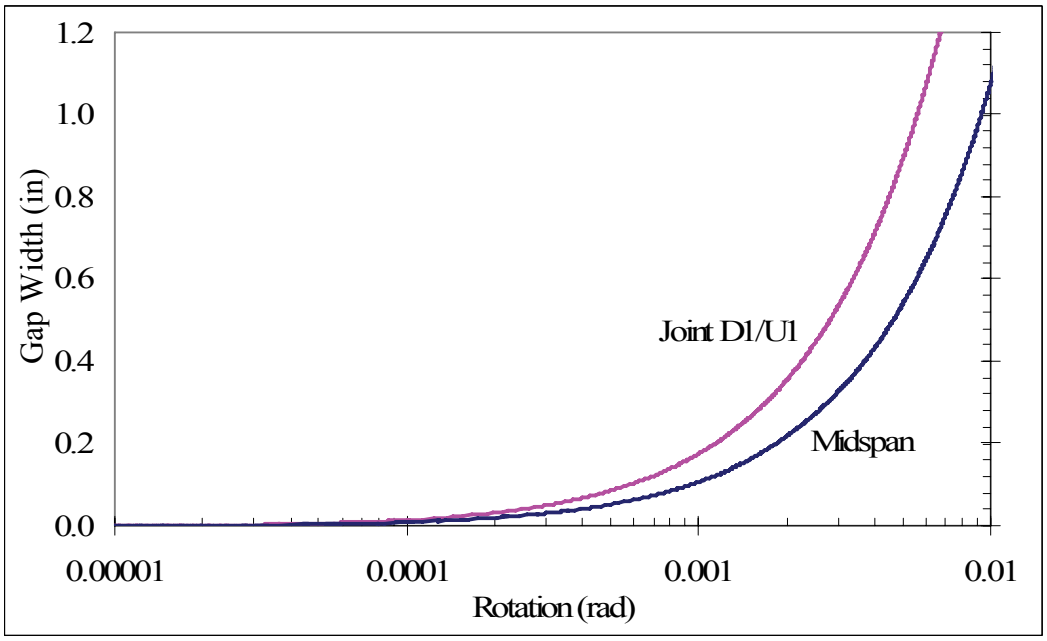

Figure 6-36 300 Foot Span – Joint Rotation vs. Gap Width Relationship

6.4. 525 Foot Span Model Discretization

The 525 foot span model is based on the San Francisco-Oakland Bay Bridge (SFOBB) Skyway, currently under construction in northern California. The SFOBB Skyway is 1.25 miles long and consists of four longitudinal frames and fourteen piers. The bridge consists of two parallel precast segmental superstructures that behave completely independent of each other. The superstructure segments are 87 feet wide and vary in depth from 18 feet at midspan to 30 feet at the piers. Thus the span-to-depth ratio varies from 18 to 29.

The framework for the 525 foot span model was the same as that of the 300' span model. Thus all modeling assumptions discussed in Section 6.2 apply to the 525 foot span model as well. An analytical model of a five span frame was developed based on details from the SFOBB Skyway as shown in Figure 6-37. Internal spans extended 525 feet in length while external spans stretched 350 feet. Pier heights varied from 80 feet to 110 feet. Approximately 60% (i.e., 11 of 19 joints per span) of all superstructure segment joints were modeled.

6.4.1. Boundary Conditions

As in the 300 foot span model, the beginning and end of the frame were modeled as abutments. The non-linear compression only longitudinal abutment springs, were engaged upon closing of the 19.7 inch thermal expansion gap.

The pier heights were short and stiff relative to the span length. Thus, soil structure interaction effects on the global bridge response were expected to be significant. To ensure reasonable results, foundation soil springs were obtained through the contractor of the SFOBB Skyway and incorporated into the model. These soil springs were also used by the designers of the prototype bridge. Coupling of the axial and bending springs was not considered in the model. While this is not

strictly correct, this approach was considered acceptable for the purposes of this investigation.

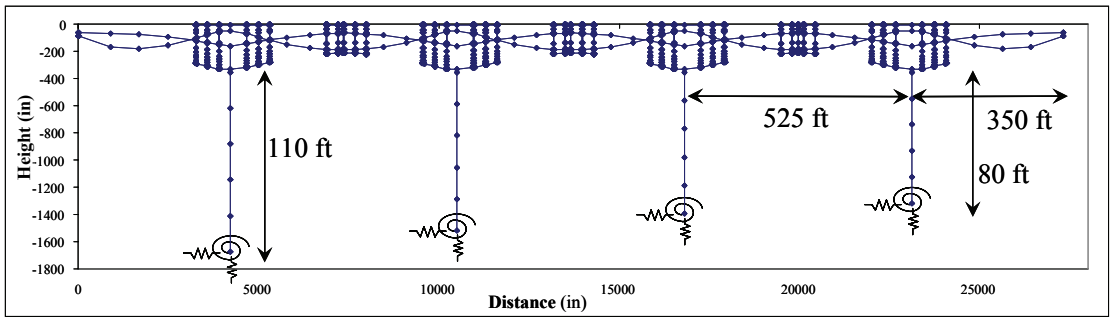

Figure 6-37 525 Foot Span Model (not to scale)

6.4.2. Piers

The piers were allowed to develop plastic hinges top and bottom and the moment capacity of the piers was increased by 23% to account for the axial load effect due to vertical earthquake motion (see Section 6.2.2). As a check of this amplified pier moment capacity, the peak normalized compressive forces and the corresponding normalized yield moment capacity, for all twenty records, are shown in Figure 6-38 and Figure 6-39, respectively. The median axial compressive force during an earthquake, P_{EQK}, was plotted on the axial force-bending moment interaction diagram shown in Figure 6-40 and the pier yield moment during an earthquake, M_y^{EQK}, was determined. This moment capacity was 16% higher than the yield moment based on the dead load axial load, M_y^{DL}, and is less than the value used

in the model. This indicated that when the column plastic mechanism forms, the model will subject the superstructure to a moment that is 7% larger than the median axial force on the column predicts. This 7% increase is justified based on research by Presland (1999) indicating 7that dynamic effects on material strength and the confinement of adjacent members can increase the moment capacity of lightly loaded well confined columns.

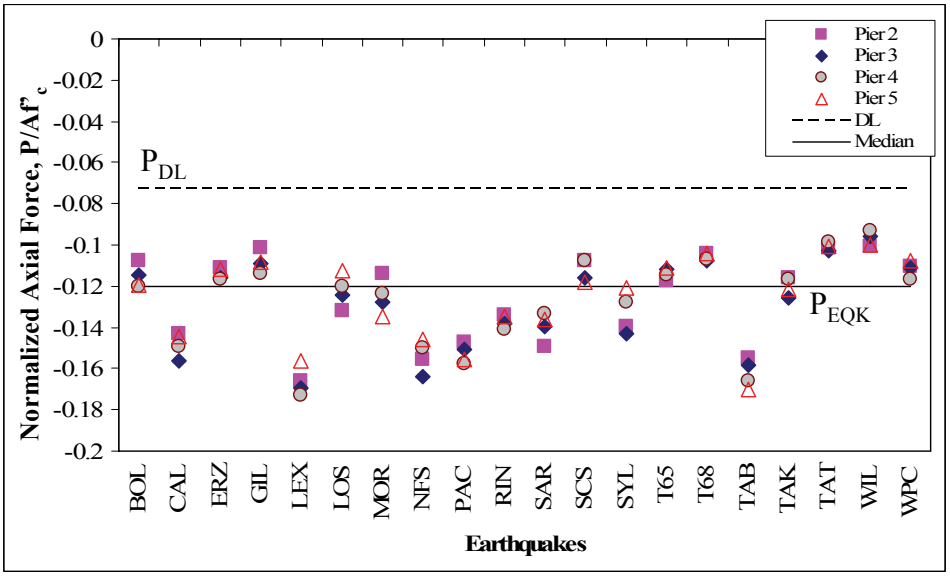

Figure 6-38 525 Foot Span – Normalized Peak Compression Axial Forces in Piers

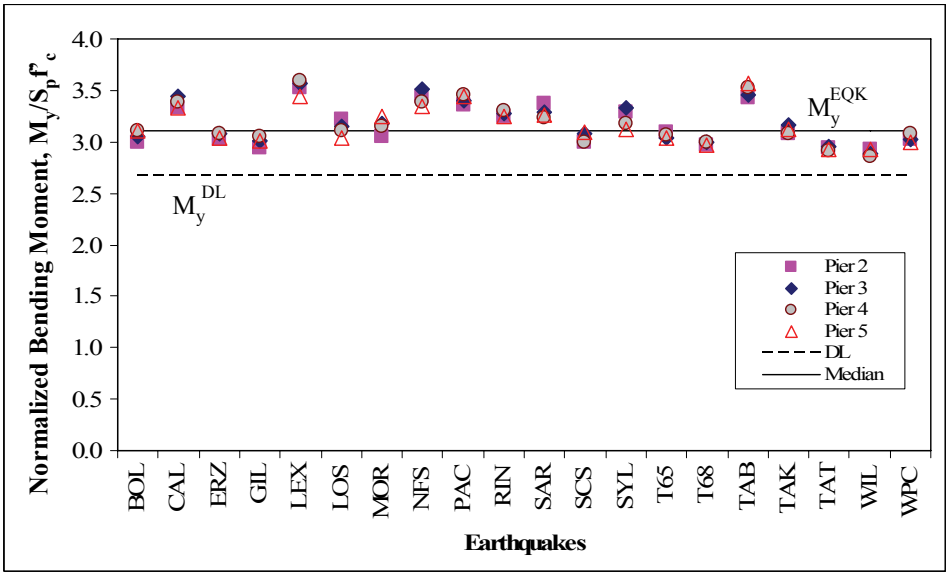

Figure 6-39 525 Foot Span – Normalized Bending Moments at Top of Piers Considering Interaction with Axial Load

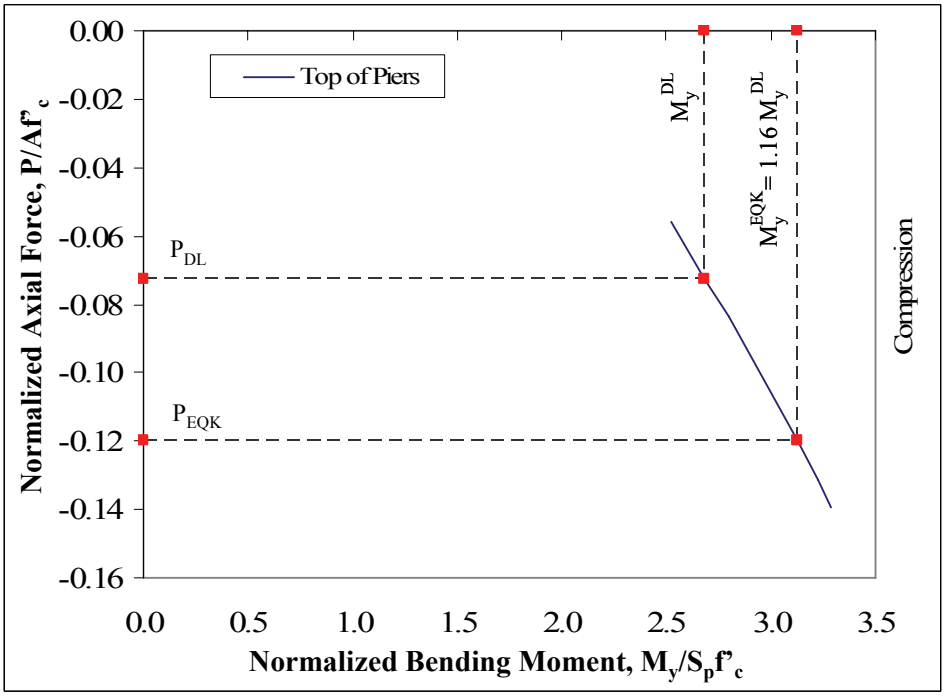

Figure 6-40 525 Foot Span – Normalized Axial Force-Bending Moment Diagram for Top of Piers

6.4.3. Superstructure Joints

A typical pier cantilever for a 525 foot span is shown in Figure 6-41. Note that the segments are not symmetric about the pier centerline to maximize construction efficiencies by maximizing the cantilever imbalance, thus reducing the number of segments per span. Eighteen superstructure segments were used to cross the 525 foot span, thus there were nineteen segment joints per span. Eleven of these segment joints were modeled, six segment joints adjacent to the piers and 5 segment joints near midspan, shown in Figure 6-42 and Figure 6-43, respectively. To improve numerical stability and to ensure accurate representation of the moment of inertia across the segment joints (see Section 4.3.2), three additional web springs were added to the joint modeling of the tall pier segment joints.

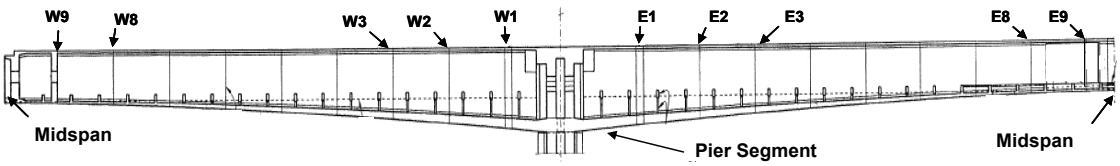

Figure 6-41 525 Foot Span - Segment Joint Identification

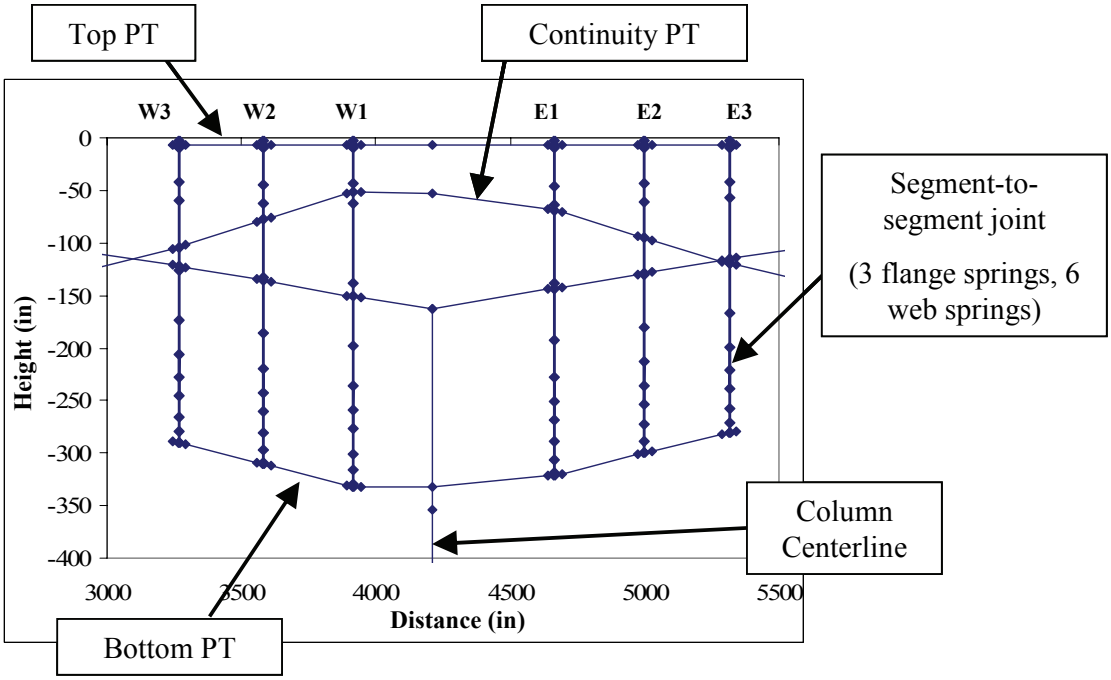

Figure 6-42 525 Foot Span Model Adjacent to Piers

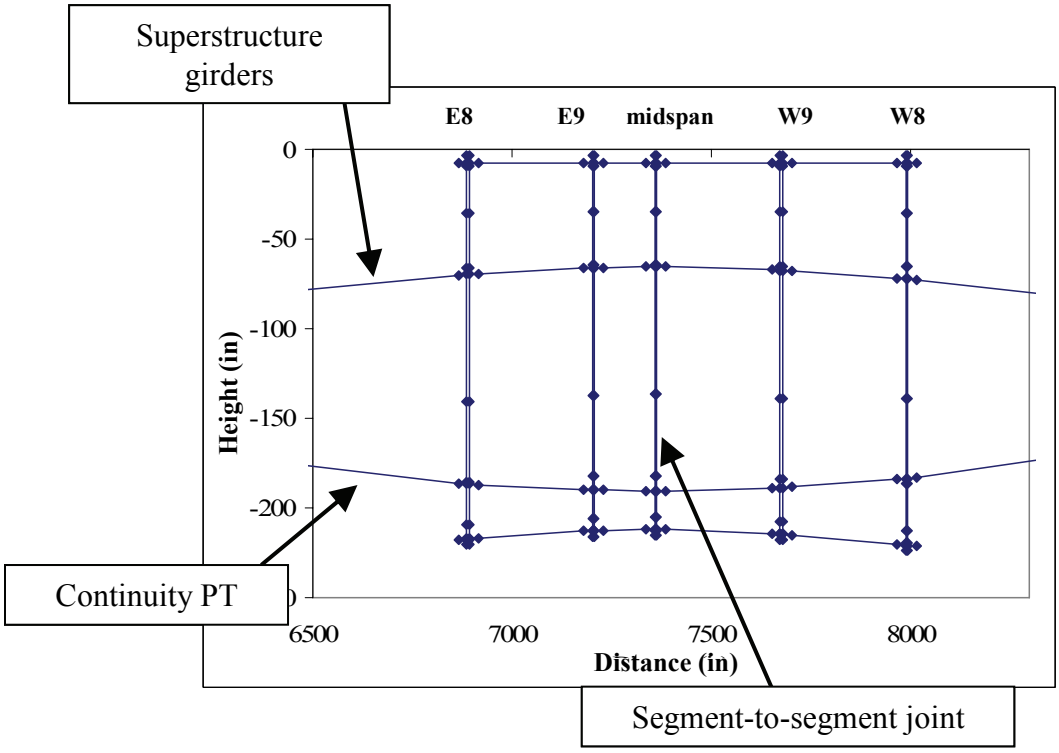

Figure 6-43 525 Foot Span Model Near Midspan

6.4.4. Superstructure Tendons

A typical long span precast segmental bridge utilizes various types of PT tendons (i.e., cantilever tendons, continuity tendons, top slab tendons, bottom soffit tendons, and auxiliary low-stressed deck continuity tendons), each with different jacking stresses and losses. To simplify the model, these various tendons were lumped together to generate three categories of PT; top tendons, bottom tendons and continuity tendons. Depending on when each tendon was stressed during the construction process, the tendon forces varied greatly. To ensure realistic modeling of tendon stresses, calculations from the SBOBB Skyway were obtained from the contractor. The initial jacking forces in the analytical model were adjusted until the losses at the end of construction matched the target calculated by the contractor of the SFOBB Skyway. The average results for all tendons at various segment joints are shown in Figure 6-44. On average the losses from the model and those determined by the contractors engineer were within 5%.

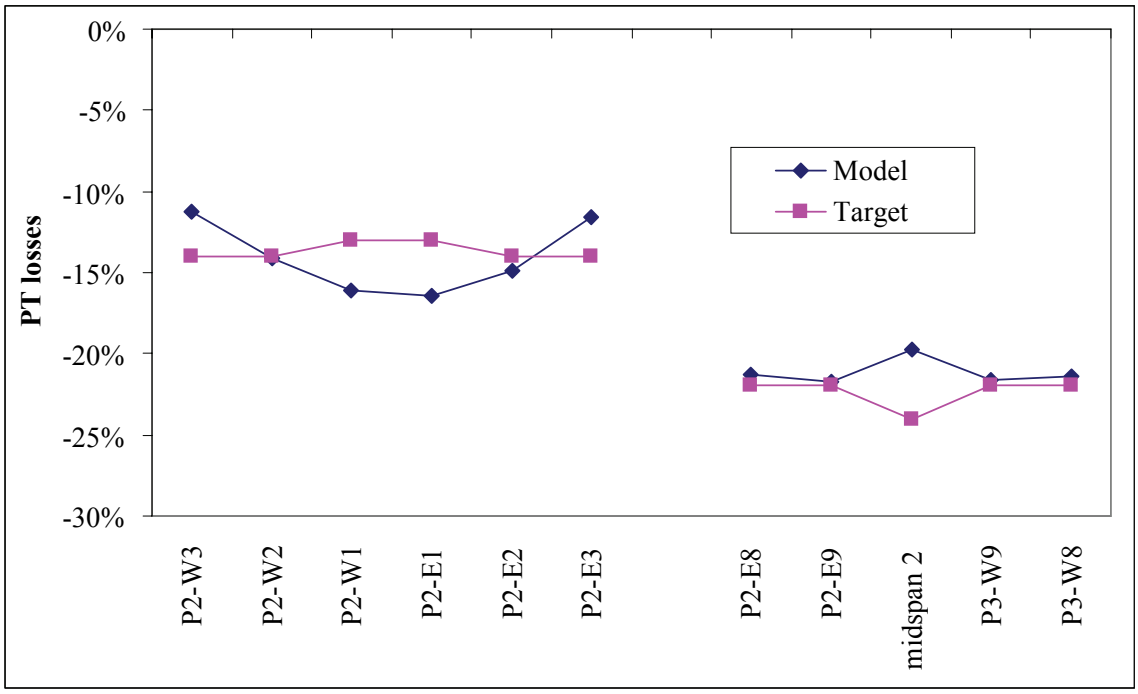

Figure 6-44 Comparison of Average PT Losses

6.4.5. Pre-Earthquake Segment Joint Stress-State

As discussed in Section 6.2.5 the pre-earthquake stress-state of the segment joints may affect the seismic response. The results from a full longitudinal construction staging analysis of the SFOBB skyway were obtained from the contractor to ensure that the pre-earthquake stress-state of the segment joints were realistic.

6.4.5.1. Calibration Process

A comparison of the top and bottom superstructure stresses, at the end of construction, between the analytical model developed in this study and the target

from the contractor's LCA are shown in Figure 6-45 and Figure 6-46, respectively. The analytical model overestimated the top stresses and underestimated the bottom stresses. As discussed in Section 6.2.5.1, this difference was due to construction staging effects. The model does not account for the fact that the bridge behaves as a cantilever structure for the majority of its construction, and not as a continuous frame. Rather, the analytical model effectively placed all the concrete and stressed all the PT tendons simultaneously, for the entire bridge. Clearly, the model is not correct as it is and must be adjusted to ensure accurate representation of the joint stress-state.

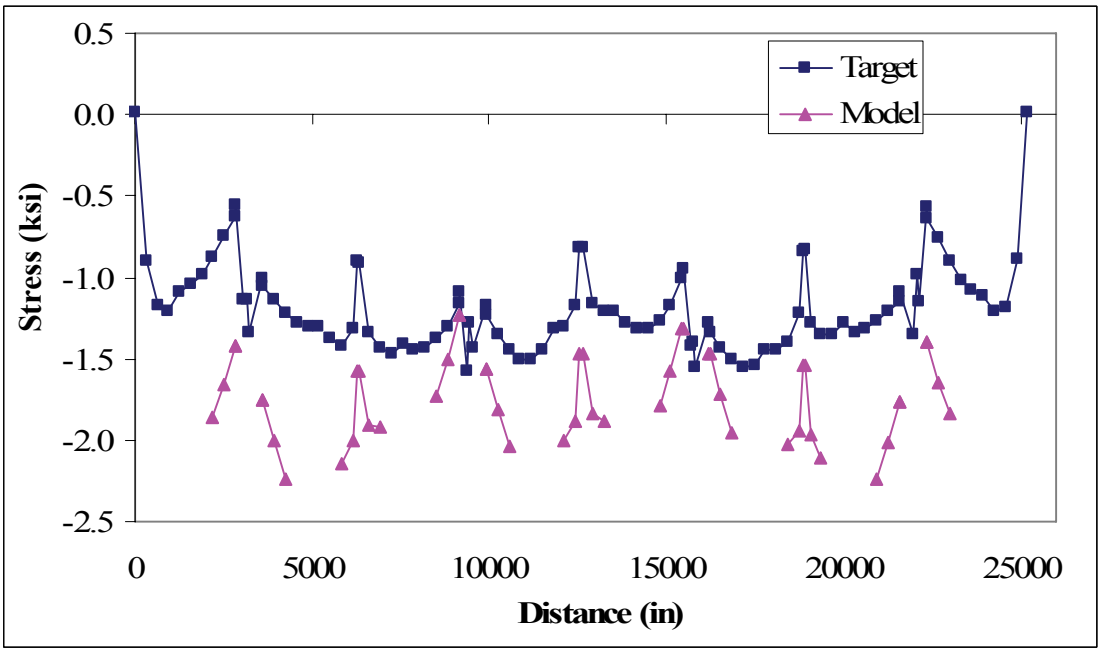

Figure 6-45 525 Foot Span - Comparison of Superstructure Top Stresses Prior to Calibration (EOC)

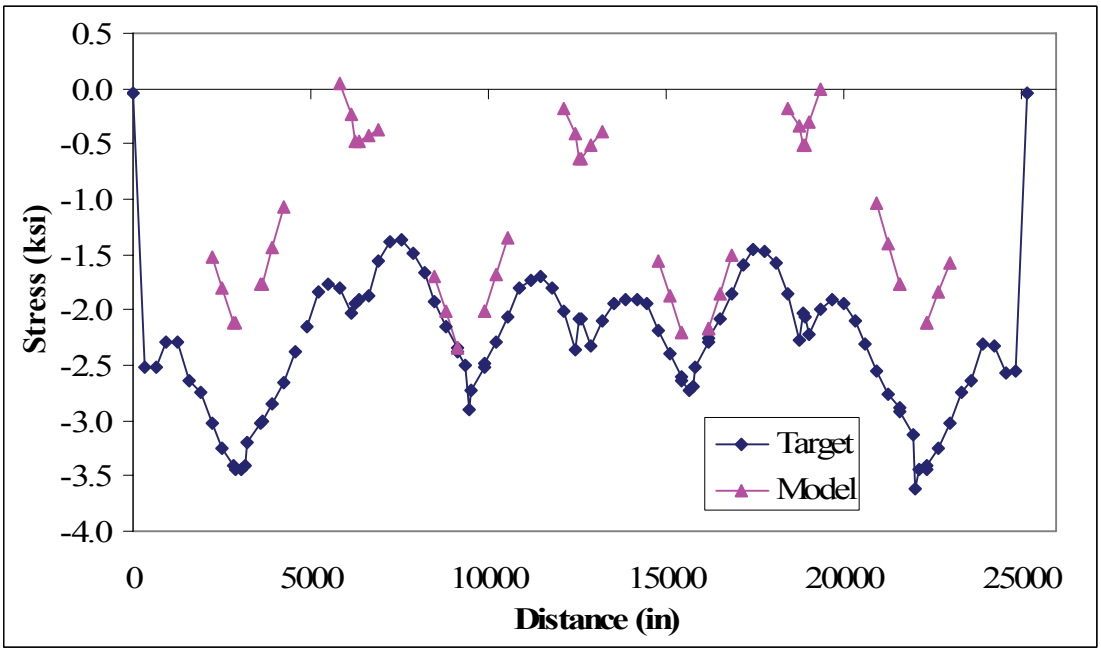

Figure 6-46 525 Foot Span - Comparison of Superstructure Bottom Stresses Prior to Calibration (EOC)

To more accurately represent the stress-state of the joints after construction, equal and opposite forces and moments were applied across each segment joint in the analytical model (see Figure 6-18). The value of these forces was iterated until convergence with the target stress-state was achieved. See Section 6.2.5 for a detailed description of the iteration process, and Appendix A for a sample of the iteration procedure.

Figure 6-47 and Figure 6-48 show a comparison of the top and bottom stresses after calibration to the end of construction stresses.

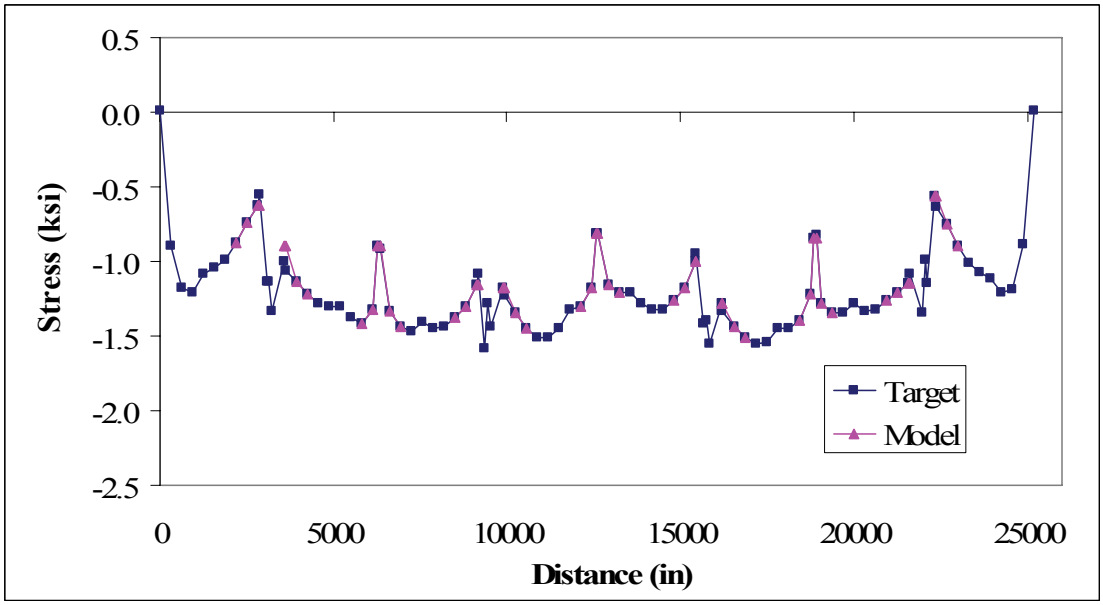

Figure 6-47 525 Foot Span - Comparison of Superstructure Top Stresses after Calibration (EOC)

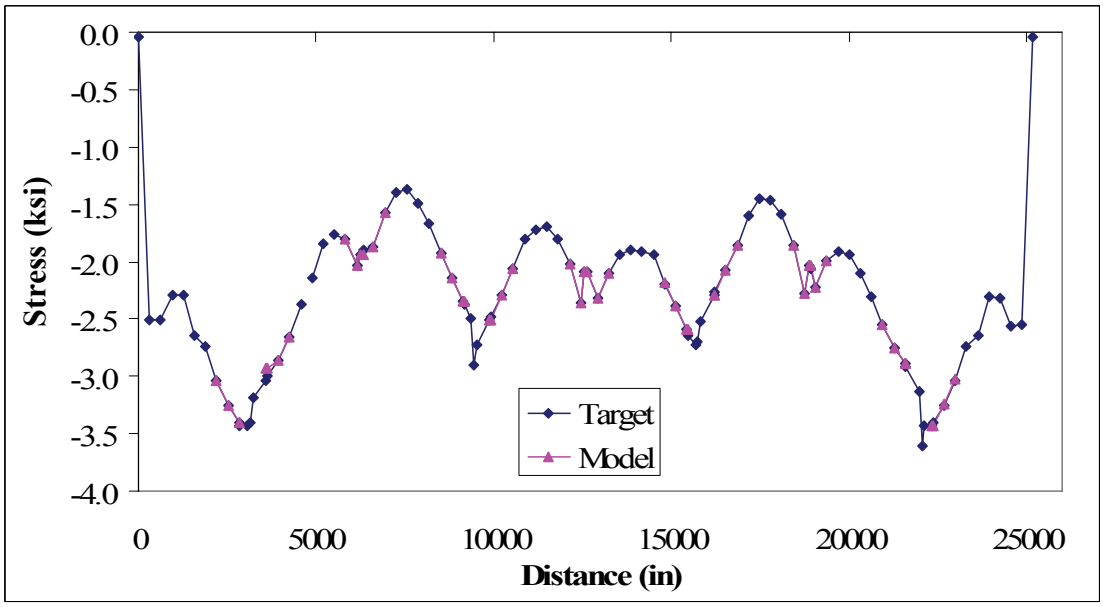

Figure 6-48 Comparison of Superstructure Bottom Stresses after Calibration (EOC)

6.4.5.2. Considerations for Variations in the Pre-Earthquake Stress-State

Numerous influences will change the stress-state of the segment joints continually over the life of the bridge. To assess the impact of the pre-earthquake stress-state on the seismic response of segment joints, four pre-earthquake stress-states were defined as described in Section 6.2.5.2 based on the effects of creep and shrinkage as obtained from the contractor's LCA. On average the top and bottom stresses increased, that is, lost compression, at the piers and at the bottom of the midspan joints, while the stresses decreased in the top fibers of the midspan joints, see Figure 6-49.

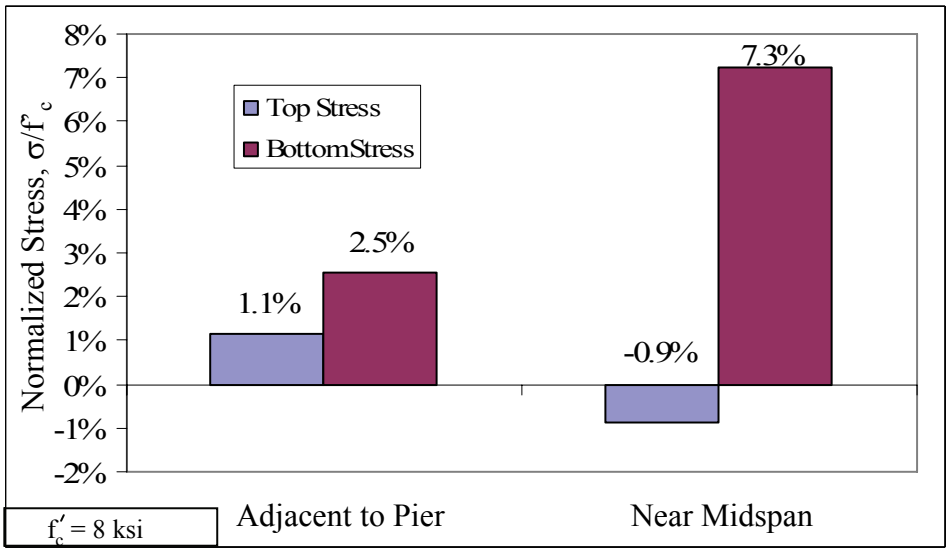

Figure 6-49 525 Foot Span - Average Normalized Stress Change due to Creep and Shrinkage

Figure 6-50 and Figure 6-51 show the top and bottom joint stresses for the four initial stress configurations. The largest stress variations occur at midspan.

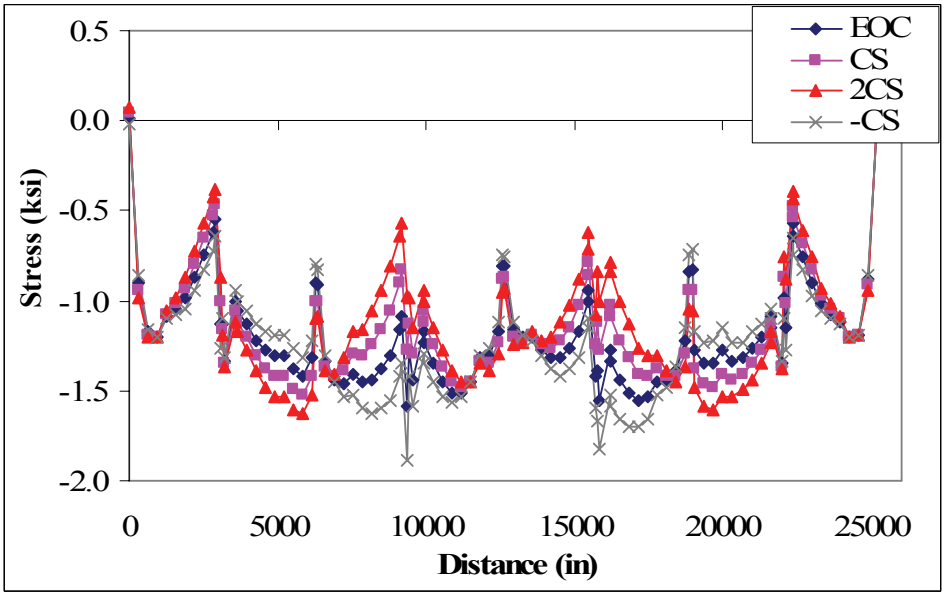

Figure 6-50 525 Foot Span – Top Stresses for Various Pre-Earthquake Stress-State Configurations

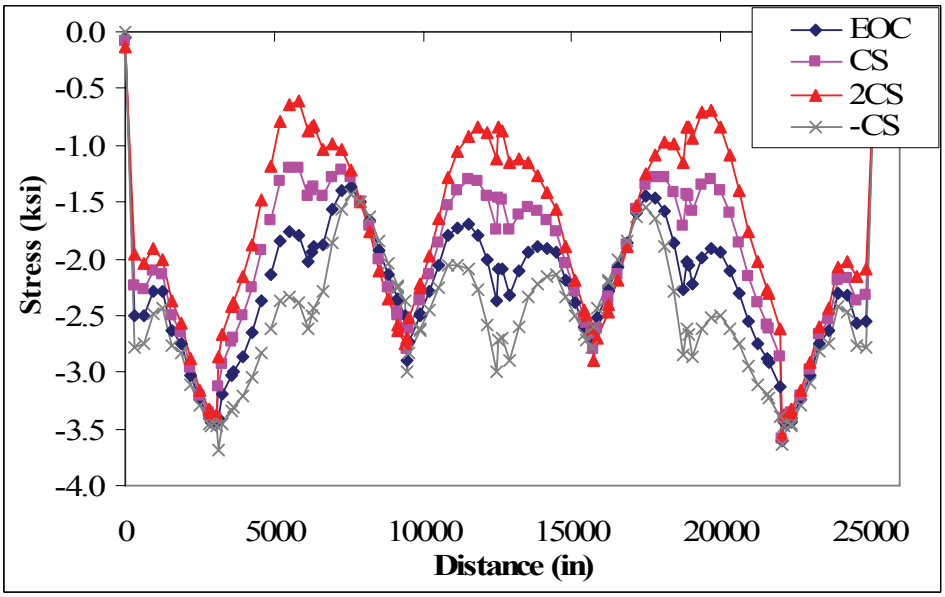

Figure 6-51 525 Foot Span – Bottom Stresses for Various Pre-Earthquake Stress-State Configurations

6.5. 525 Foot Span Model Characteristics

6.5.1. Dead Load Joint Stresses

The dead load superstructure segment joint stress profiles at pier 2 and span 3 are shown in Figure 6-52 to Figure 6-55 for the four pre-earthquake stress configurations. These profiles included the contributions of dead load, PT loads, losses due to elastic shortening, creep, shrinkage, relaxation, friction, anchorage seating, and the effects of construction staging. The stress profiles shown were typical of all segment joints in the model and were considered reasonable. The peak stresses were well below the AASHTO limit of 0.45 $f_c^{'}$ (AASHTO, 1999).

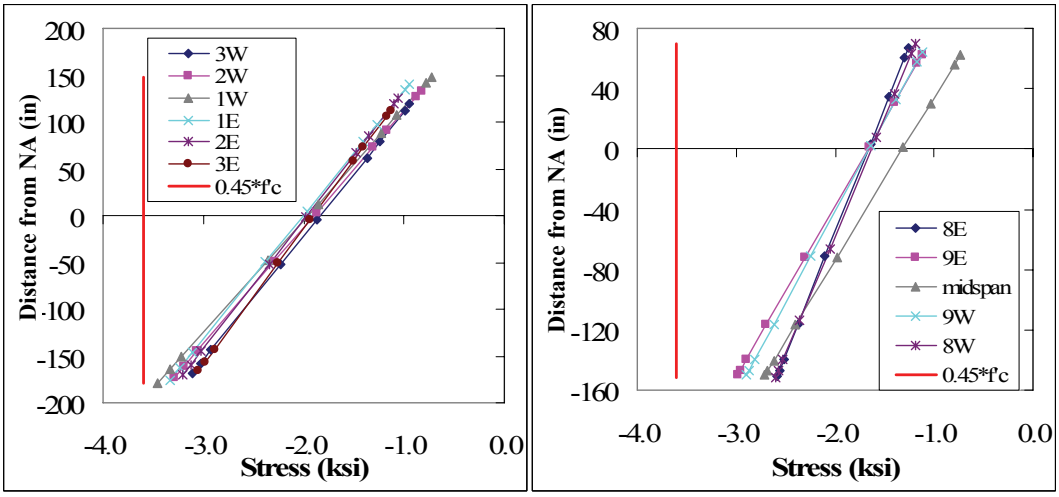

a) Pier 2 **b) Span 3**

Figure 6-52 525 Foot Span - Dead Load Superstructure Stress Profile for Typical Piers and Spans (-CS)

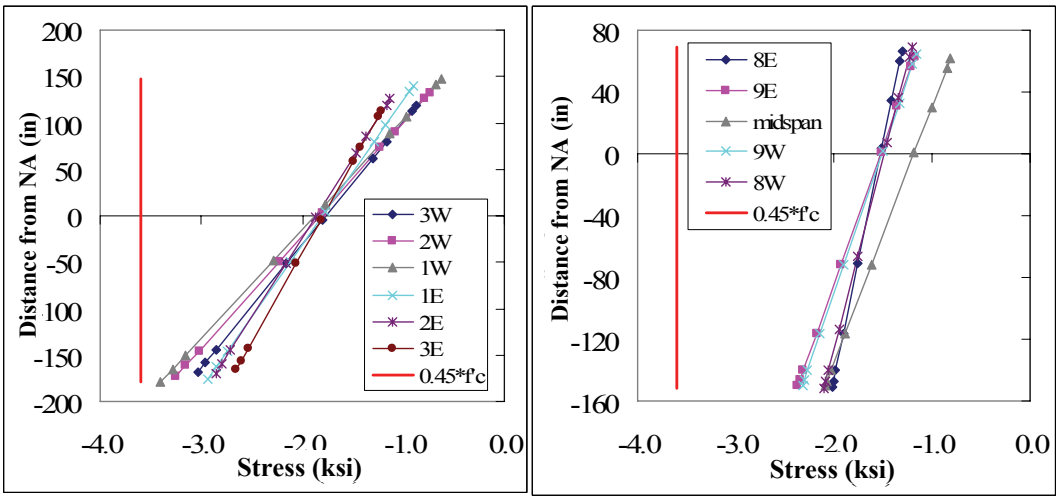

a) Pier 2 b) Span 3

Figure 6-53 525 Foot Span - Dead Load Superstructure Stress Profile for Typical Piers and Spans (EOC)

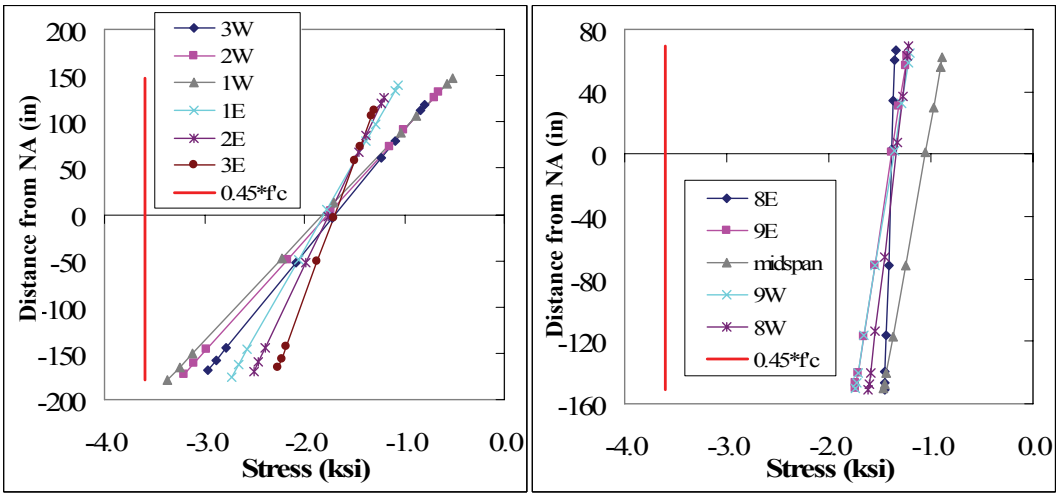

a) Pier 2 b) Span 3

Figure 6-54 525 Foot Span - Dead Load Superstructure Stress Profile for Typical Piers and Spans (+CS)

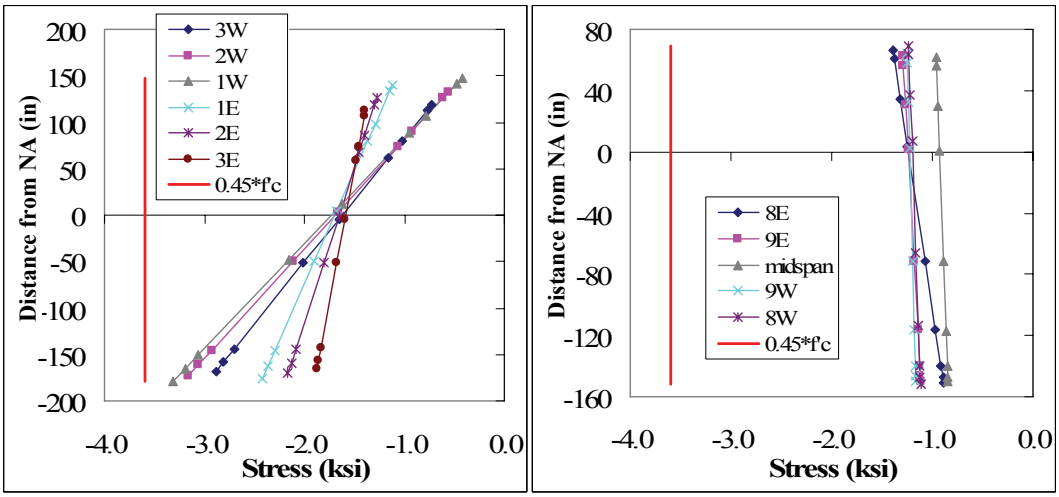

a) Pier 2 **b) Span 3**

Figure 6-55 525 Foot Span - Dead Load Superstructure Stress Profile for Typical Piers and Spans (+2CS)

The average compression stresses across the joints, as a percentage of $f_c^{'}$, are shown in Table 6-5. The average compression stress for segment joints adjacent to the piers ranged from 21% to 24% of $f_c^{'}$, while the average compression stress near midspan ranged from 14% to 24%.

Table 6-5 525 Foot Span - Summary of Average Superstructure Compression Stress (% of $f_c^{'}$)

Initial Stress Configuration	Adjacent to Piers	Near Midspan
-CS	24%	24%
EOC	23%	21%
+CS	22%	17%
+2CS	21%	14%

6.5.2. Mode Shapes

The primary longitudinal and vertical mode shapes are shown in Figure 6-56 and Figure 6-57, respectively. The natural period of the primary longitudinal mode was 2.0 seconds and engaged 93% of the total bridge mass. The period of the dominant vertical mode was 0.66 seconds and captured 41% of the total bridge mass.

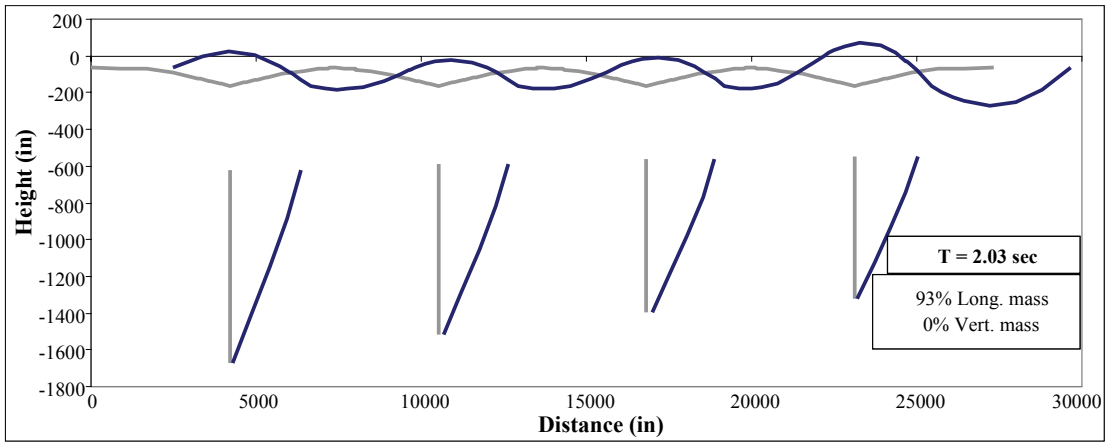

Figure 6-56 525 Foot Span - Primary Longitudinal Mode

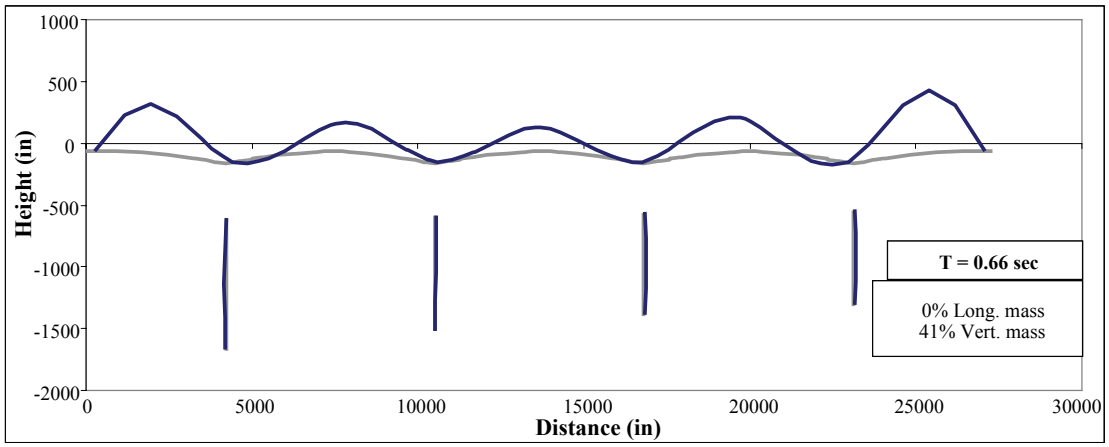

Figure 6-57 525 Foot Span - Primary Vertical Mode

6.5.3. Longitudinal Pushover Analysis

A longitudinal push-over analysis was performed in order to understand the hinging sequence of the frame, see Figure 6-58. The top of the piers hinge first, prior to engaging the abutment soil springs. The bottom of the piers hinged when the top hinges reached a displacement ductility of about 5. Note that a 10 inch short pier (i.e. Pier 5) displacement corresponds to a drift ratio of approximately 1%.

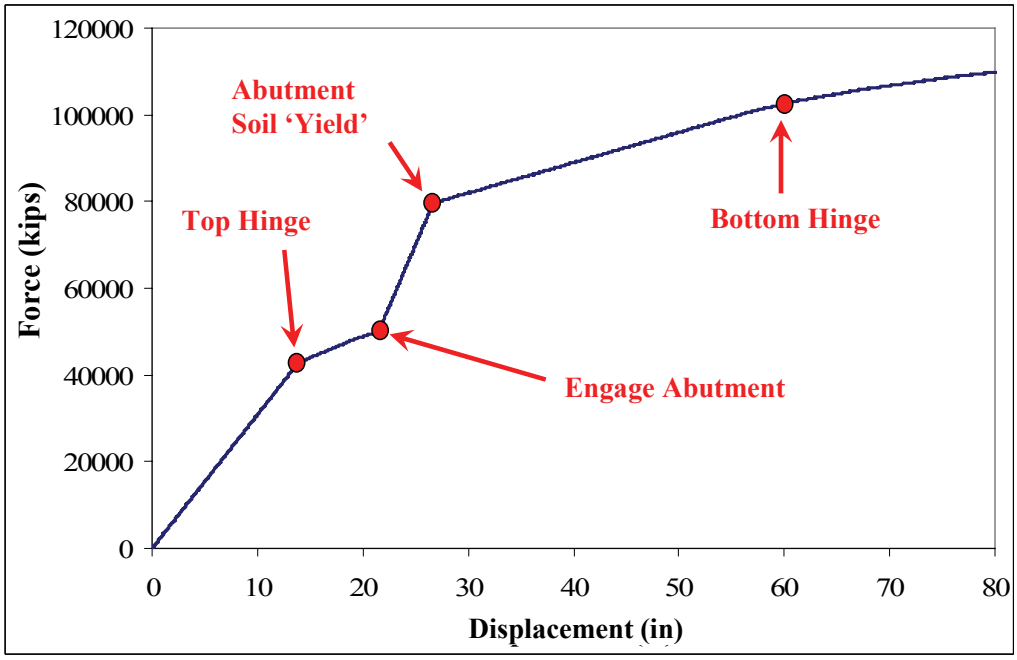

Figure 6-58 525 Foot Span - Longitudinal Push Analyses

6.5.3.1. Pier Performance Limit States

Pier performance limit states were identified based on the longitudinal pushover and moment-curvature analyses of the pier sections. These limits states

represented crushing and spalling of the cover concrete, first yielding of the reinforcement and full plastic hinge development. Table 6-6 summarizes the performance limit states, outlines the consequences of exceeding each limit state and identifies the longitudinal drift ratio of Piers 5 for each limit state. For convenience and simplicity the drift ratios of the shortest pier were used to identify the limit states as this pier accumulated the largest damage.

Table 6-6 525 Foot Span – Pier 5 Performance Limit States

Limit State	Pier 5 Drift Ratio	Description	Consequences
P-C1	**1.8%**	Incipient crushing of cover concrete, $\varepsilon_c = -0.002$	Patching of concrete may be required.
P-C2	**2.4%**	Spalling of cover concrete, $\varepsilon_c = -0.004$	Patching of concrete. Operational performance level
P-C3	**4.1%**	Crushing of core concrete, $\varepsilon_c = -0.011$	Fracture of confinement reinforcement. Life safety performance level
P-R1	**0.9%**	First yield of reinforcement	End of purely elastic region of reinforcement.
P-R2	**1.2%**	Idealized yield of section	Development of plastic hinge. Noticeable residual cracking. Pressure grouting may be required. Operational performance level
P-R3	**4.5%**	Buckling of long. reinforcement, $\varepsilon_s = 0.04$	Buckling of longitudinal reinforcement. Life safety performance level

6.5.4. Segment Joints Behavior

6.5.4.1. Segment Performance Limit States

Vertical pushover analyses were performed to obtain the backbone curve for the moment-rotation behavior of each segment joint, and to identify the rotation of various performance limit states. These limits states, shown in Table 6-7, were the same as those defined for the 300 foot span model, except that two additional limit state were required to assess the performance of the continuity tendons. It should be noted that the crushing limit state, C2, was defined as the strain at 85% of as illustrated in Figure 4-2. This strain is larger than the strain used in the 300 foot span model because the concrete was assumed to be stronger, thus the strain at $0.85f'_c$ was also increased.

Table 6-7 525 Foot Span – Segment Joint Performance Limit States

Limit State	Description	Consequences
C1	Concrete cracking, $\varepsilon_c = 0.000010$	Onset of joint opening, no major consequences
C2	Crushing of extreme concrete fibers, $\varepsilon_c = -0.0021$	Patching of concrete may be required, Operational performance level.
MT1	Limit of proportionality (210 ksi) of main tendons	End of purely elastic region of PT. Begin to lose prestressing force. Operational performance level.
MT2	$\varepsilon_{pt} = 0.012$ in main tendons	Full tendon yielding. Lose significant PT force. Residual joint openings are likely. Life safety performance level.
CT1	Limit of proportionality (210 ksi)of continuity tendons	End of purely elastic region of PT. Begin to lose prestressing force. Operational performance level.
CT2	$\varepsilon_{pt} = 0.012$ in continuity tendons	Full tendon yielding. Lose significant PT force. Residual joint openings are likely. Life safety performance level.

6.5.4.2. Vertical Monotonic Pushover Analyses

Figure 6-32 and Figure 6-33 show the backbone curves and limit states for the segment joints near midspan and adjacent to the piers, respectively. Table 6-8 summarizes the rotations at which the limits states were met for the various segment joints. In general, the limits states for the segment joints near midspan occurred at rotations similar to each other, with the exception of limit state C2 at midspan. The midspan positive rotation crushing limit state was approximately four times that of

the adjacent joints because of reduced total PT across the section which reduced the compression force across the joint, thereby allowing for an increased rotation to crush the extreme concrete fibers. Similarly, the limits states for the segment joints adjacent to the piers occurred at rotations similar to each other.

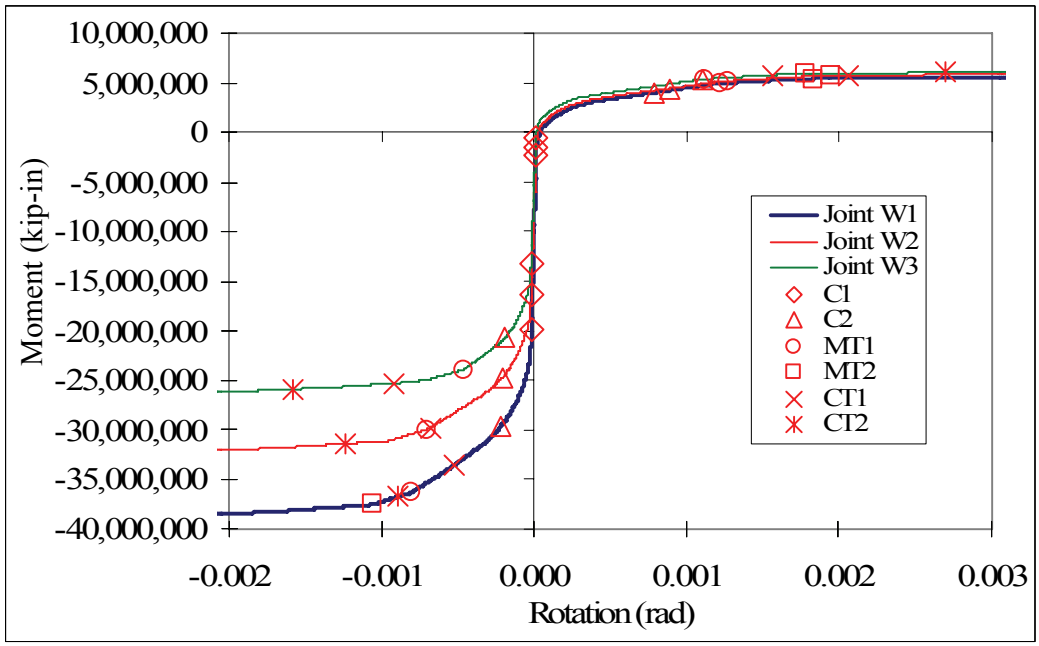

Figure 6-59 525 Foot Span - Behavior of Segment Joints Adjacent to Piers

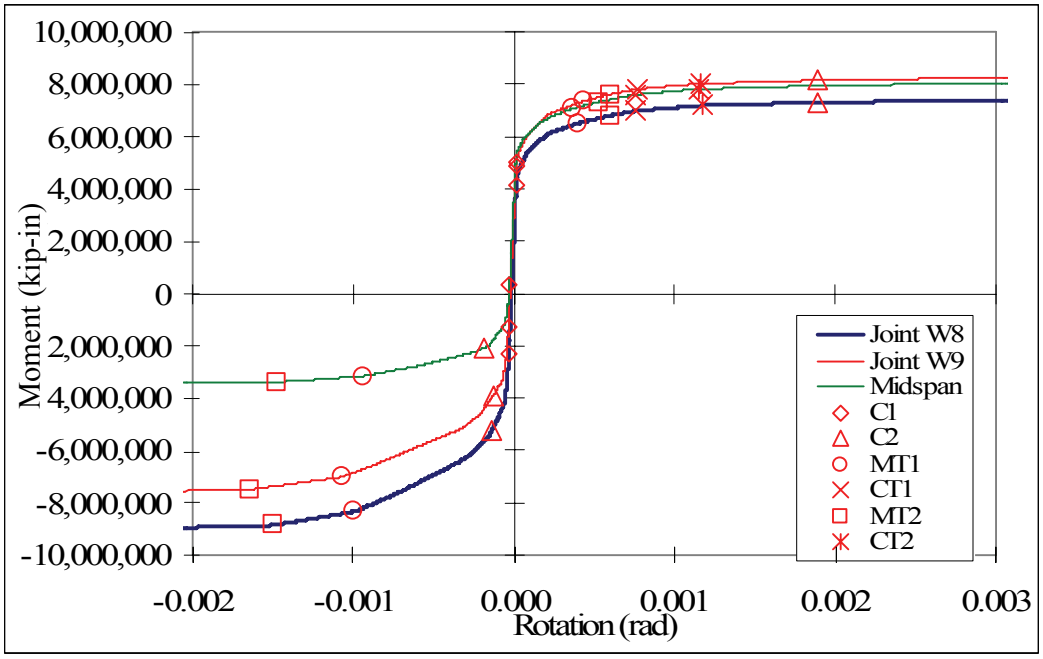

Figure 6-60 525 Foot Span - Behavior of Segment Joints Near Midspan

Table 6-8 525 Foot Span - Summary of the Rotational Performance Limits States

			Segment Joint					
			W1	W2	W3	W8	W9	Midspan
Performance Limit State	C1	Negative	-0.000017	-0.000019	-0.000021	-0.000031	-0.000034	-0.000027
		Positive	0.000013	0.000014	0.000013	0.000014	0.000015	0.000012
	C2	Negative	-0.00022	-0.00020	-0.00019	-0.00014	-0.00013	-0.00019
		Positive	0.00079	0.00088	0.00110	0.00189	0.00189	0.00946
	MT1	Negative	-0.00081	-0.00070	-0.00046	-0.00100	-0.00107	-0.00094
		Positive	0.00121	0.00127	0.00111	0.00040	0.00043	0.00036
	MT2	Negative	-0.00106	-0.00372	-0.00714	-0.00150	-0.00164	-0.00148
		Positive	0.00182	0.00195	0.00177	0.00060	0.00060	0.00053
	CT1	Negative	-0.00053	-0.00068	-0.00092	-0.00463	-0.00731	-0.00847
		Positive	0.00323	0.00206	0.00156	0.00076	0.00077	0.00076
	CT2	Negative	-0.00090	-0.00124	-0.00158	-0.00697	-0.01063	-0.01172
		Positive	0.00536	0.00367	0.00270	0.00118	0.00116	0.00115

All limit states above are in units of Radians

It is important to note that the pre-earthquake stress-state may alter the limit states. In general progressing in time from the EOC to the CS stress-states will

reduce the rotation at cracking up to 14%, while all other critical limits states remain essentially unchanged or reduce slightly (up to 5%), as shown in Appendix B. For simplicity the limit states presented here and used in future section were defined based on the end of construction (EOC) stresses. For all limit states except cracking, this will likely be conservative for the CS and +2CS stress-state, yet non-conservative for the –CS stress-state.

6.5.4.3. Vertical Cyclic Pushover Analysis

A series of vertical reversed cyclic pushover analyses were performed in order to verify the moment-rotation behavior of the segment joints. Results from segment joint W1 (i.e., nearest the pier) and segment joint 10 (i.e., midspan) are shown in Figure 6-61 and Figure 6-62, respectively. The response captures joint opening, concrete crushing and PT yielding for both positive and negative bending directions.

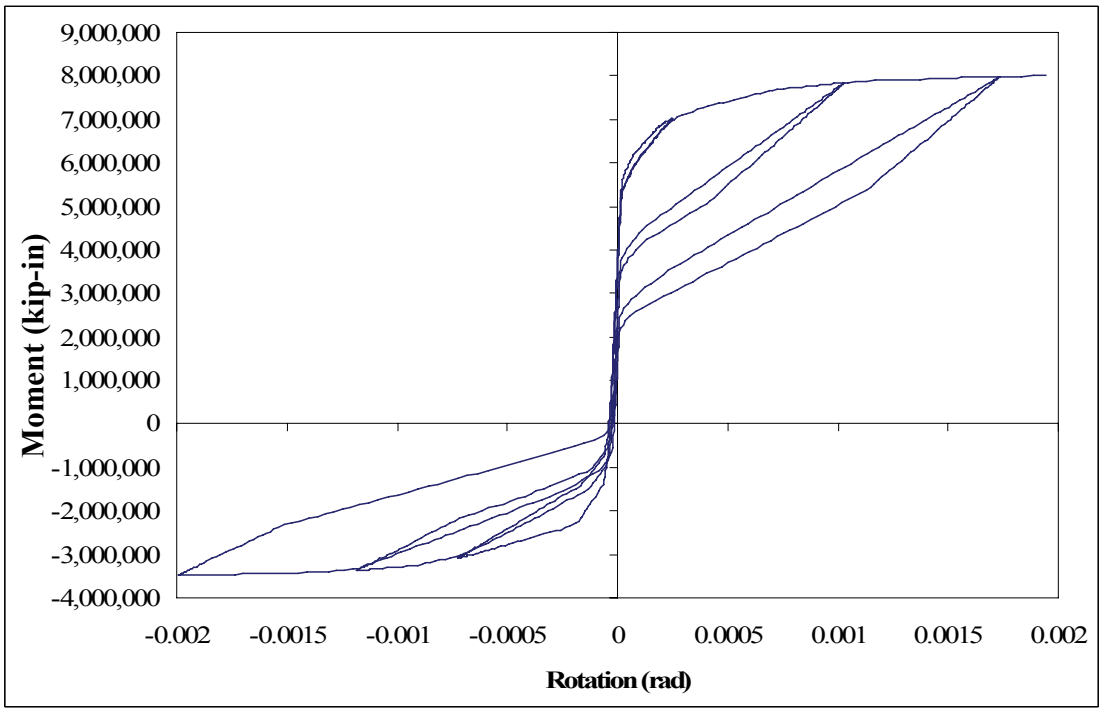

Figure 6-61 525 Foot Span - Midspan Moment-Rotation Diagrams from Cyclic Push Analysis

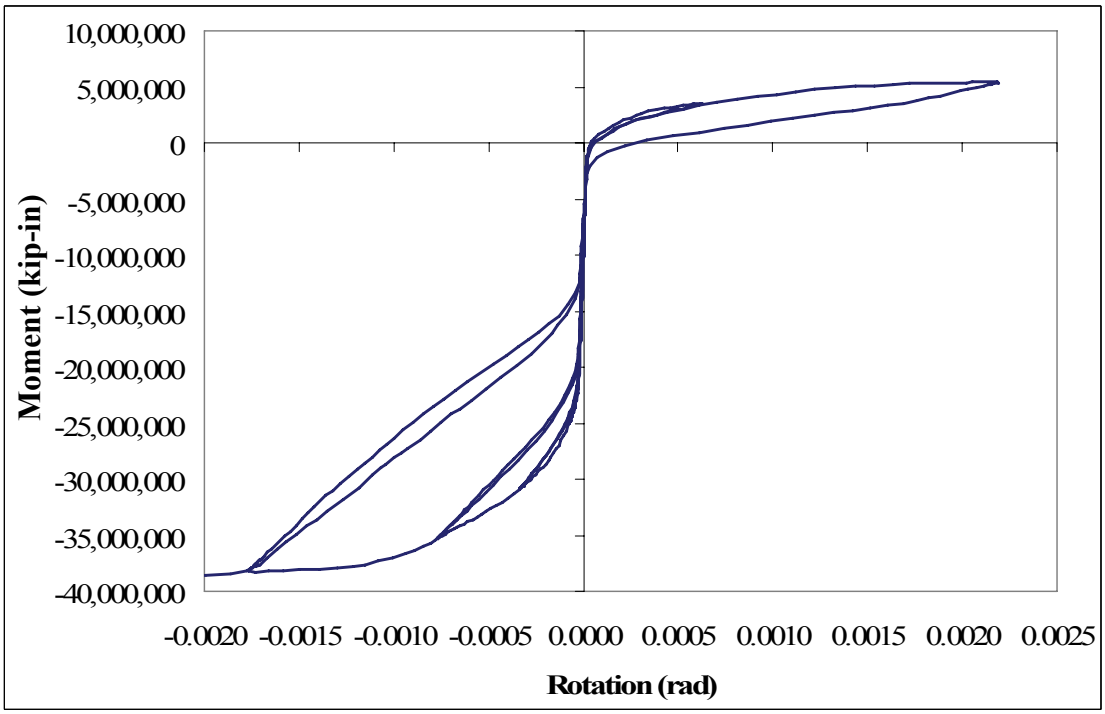

Figure 6-62 525 Foot Span – Joint W1 Moment-Rotation Diagrams from Cyclic Push Analysis

6.5.4.4. Joint Rotation – Gap Width Relationship

The relationship between segment joint rotation and extreme fiber gap opening was obtained from the vertical push analyses and is shown in Figure 6-63. Positive rotations generated gaps at the bottom flange while negative rotations created gaps in the top flange. The positive and negative rotation relationships were essentially the same, thus only the positive rotation relationships are presented. Only Joint W1 and midspan relationships are shown to ensure readability of the figure.

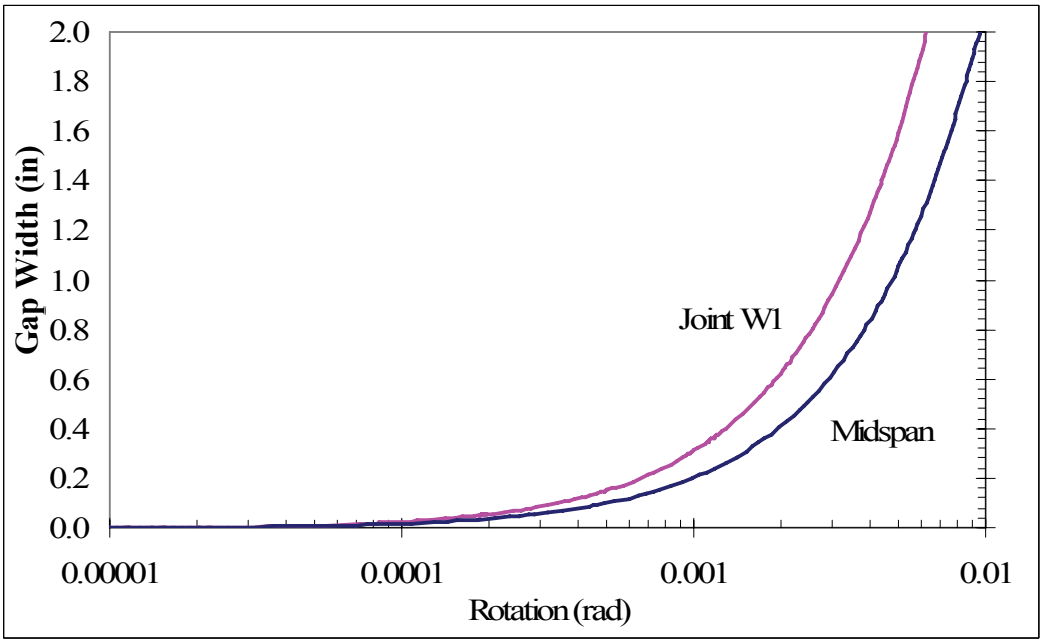

Figure 6-63 525 Foot Span - Joint Rotation - Gap Width Relationship

CHAPTER 7. FULL BRIDGE MODEL RESULTS

The impact of various parameters on the seismic response of segmental bridges, particularly the response of the superstructure segment joints, is presented in this chapter. The results are organized by the parameter of interest (i.e. vertical excitation, pre-earthquake stress-state, etc.) and by the span length.

7.1. Vertical Excitation

To quantify the contribution of the vertical ground motion on the segment joint response, the models were subjected to longitudinal motions only, as well as simultaneous longitudinal and vertical earthquake motions. All ground motions for the vertical excitation study were scaled using the method based on the primary natural period and the pre-earthquake joint stress-state was based on the best estimate of the stresses at the end of construction. Some of the figures in this section remind the reader of this fact with the notation "T=2" and "EOC" in the legend. The influences of record scaling and the pre-earthquake joint stress-state will be discussed in Sections 7.2 and 7.3, respectively.

7.1.1. 300 Foot Spans

The effect of vertical excitation on the 300 foot span model is shown in Figure 7-1 to Figure 7-3. In these figures each vertical bar represents the median response of the twenty earthquakes due to longitudinal only (i.e. "L_only")and due to both longitudinal and vertical (i.e. "L+V") ground motions. Figure 7-1 summarizes the median peak positive bending joint rotations for the six segment joints families. D1/U1 represents the first joint down-station or up-station from the pier, while D14/D14 is fourteen segment joints away from the pier and is adjacent to midspan, see Figure 6-9. It is clear that adding the vertical ground motion component significantly increases the joint rotation demand. By taking the median of the ratio of the "L+V" and "L_only" segment joint median responses, we find that the median positive bending rotations increased by 1000%. From similar plots, shown in Figure 7-2 and Figure 7-3, we find that median negative bending rotations increased by 250% and the residual rotations remained essentially unchanged.

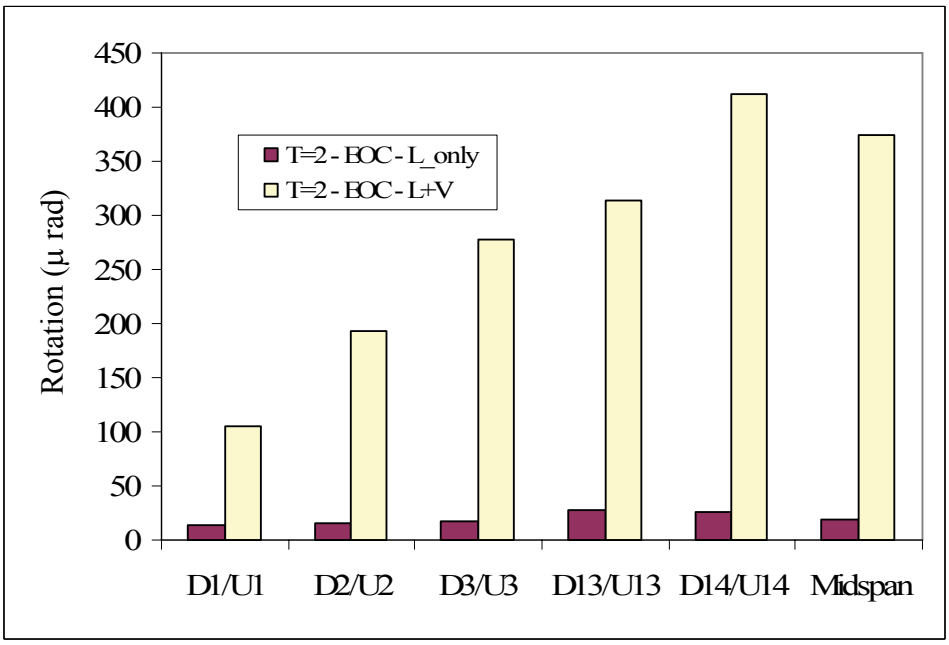

Figure 7-1 300 Foot Span – Influence of Vertical Ground Motion on the Median Peak Positive Segment Joint Rotations

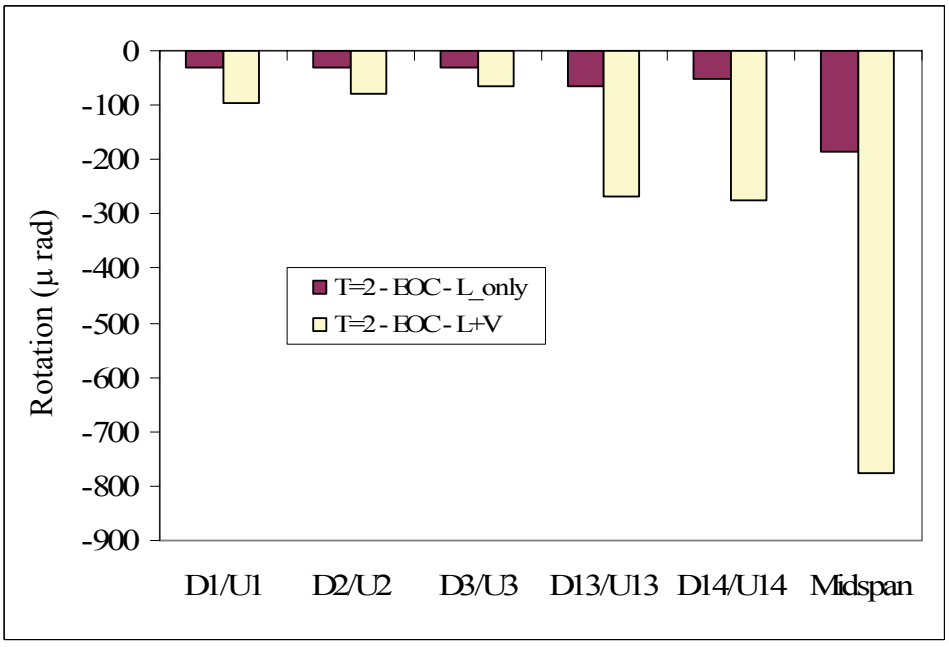

Figure 7-2 300 Foot Span – Influence of Vertical Ground Motion on the Median Peak Negative Segment Joint Rotations

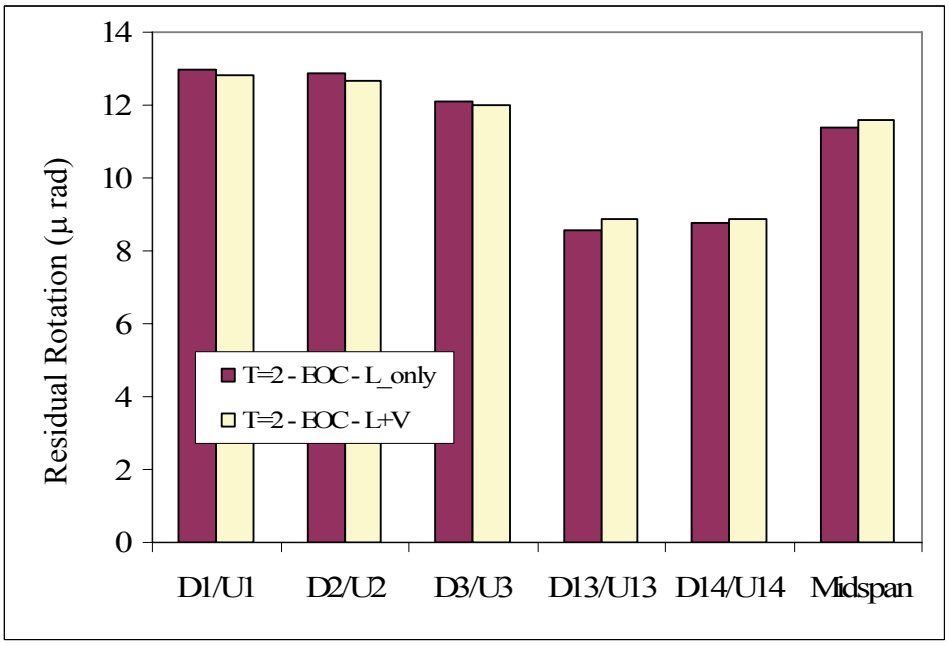

Figure 7-3 300 Foot Span – Influence of Vertical Ground Motion on the Median Residual Segment Joint Rotations

The reason for such large increases in the peak rotations can be explained by comparing the joint rotation data to the performance limits states as shown in Figure 7-4 and Figure 7-5. Each small dot represents the peak rotation from one earthquake. The square mark represents the median rotation. The diamond marks represent the 16^{th} and the 84^{th} percentiles and the vertical lines identify the various performance limit states. These percentile marks are shown to assess relative sensitivities based on the suite of ground motion records used in this study. It is important to note that a different set of ground motion records, or a different record scaling method, will likely have a different standard deviation, which can alter the variation in the joint

response presented here. Clearly, adding the vertical earthquake ground motions pushed the superstructure joints beyond the cracking limit state, C1, and into the non-linear range, were a small increase in bending moment produces a large increase in rotation.

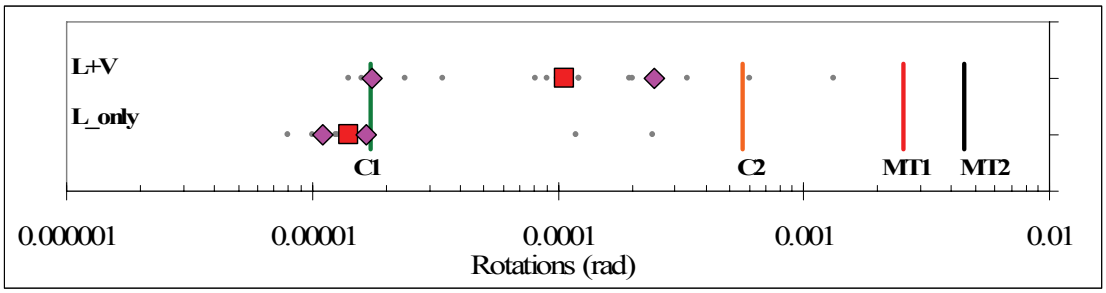

Figure 7-4 300 Foot Span – Influence of Vertical Ground Motion on Positive Joint D1/U1 Rotations

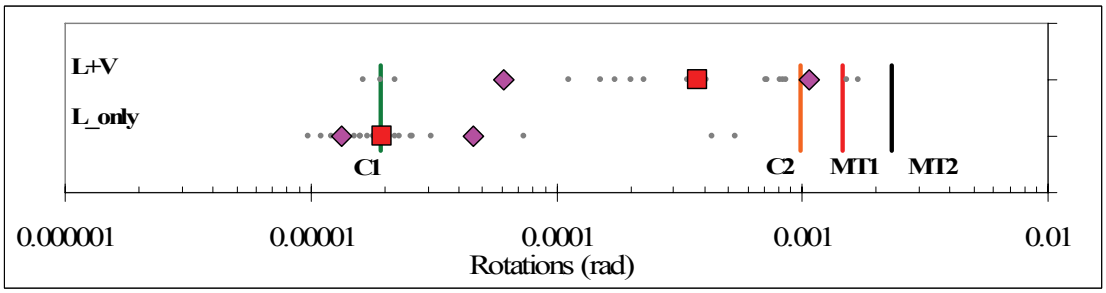

Figure 7-5 300 Foot Span – Influence of Vertical Ground Motion on Positive Midspan Rotations

The influence of the vertical ground motion on the piers is shown in Figure 7-6 and Figure 7-7. Figure 7-6 summarizes the median of the peak longitudinal drift ratios. Clearly, adding the vertical component of ground motion does not significantly impact the longitudinal response of the piers. Figure 7-7 summarizes

the median residual longitudinal drift ratios. The figure suggests that adding vertical motions reduces the residual drift ratio. However, the magnitude of the change is very small (0.06% drift at most), and is considered negligible.

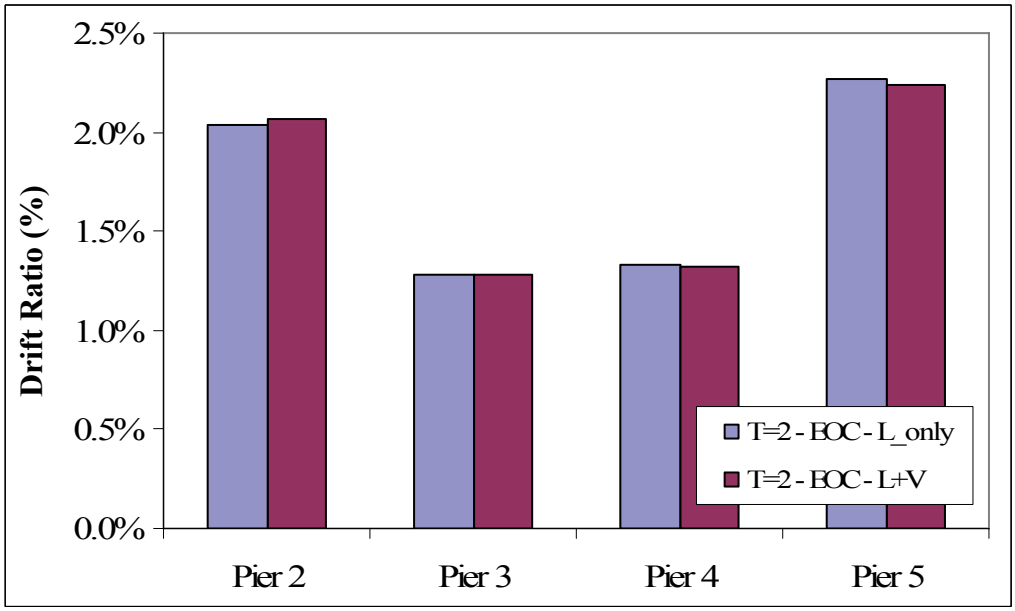

Figure 7-6 300 Foot Span - Influence of Vertical Ground Motion on the Median Peak Pier Longitudinal Drift Ratio

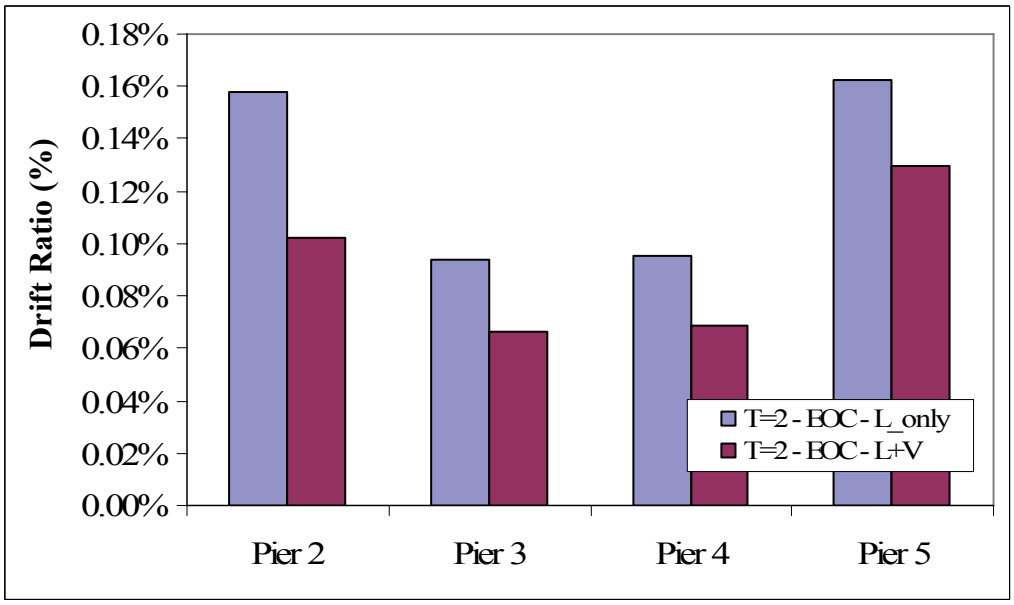

Figure 7-7 300 Foot Span - Influence of Vertical Ground Motion on the Median Residual Pier Longitudinal Drift Ratio

7.1.2. 525 Foot Spans

The impact of vertical excitation on the 525 foot span model is shown in Figure 7-8 to Figure 7-10. Figure 7-8 summarizes the median peak positive bending joint rotations for the six segment joints families due to longitudinal only (i.e., "L_only") and due to both longitudinal and vertical (i.e., "L+V") ground motions. W1/E1 represents the first joint down-station or up-station of the pier, while W9/E9 is nine segment joints away from the pier and is adjacent to midspan, see Figure 6-41. Clearly, the vertical component significantly increased the joint response. By taking the median of the ratio of the "L+V" and "L_only" segment joint median

responses, we find that the median positive bending rotations increased by 500%. From similar plots, shown in Figure 7-9 and Figure 7-10, we find that negative bending rotations increased by 140% and the residual rotations remained essentially unchanged.

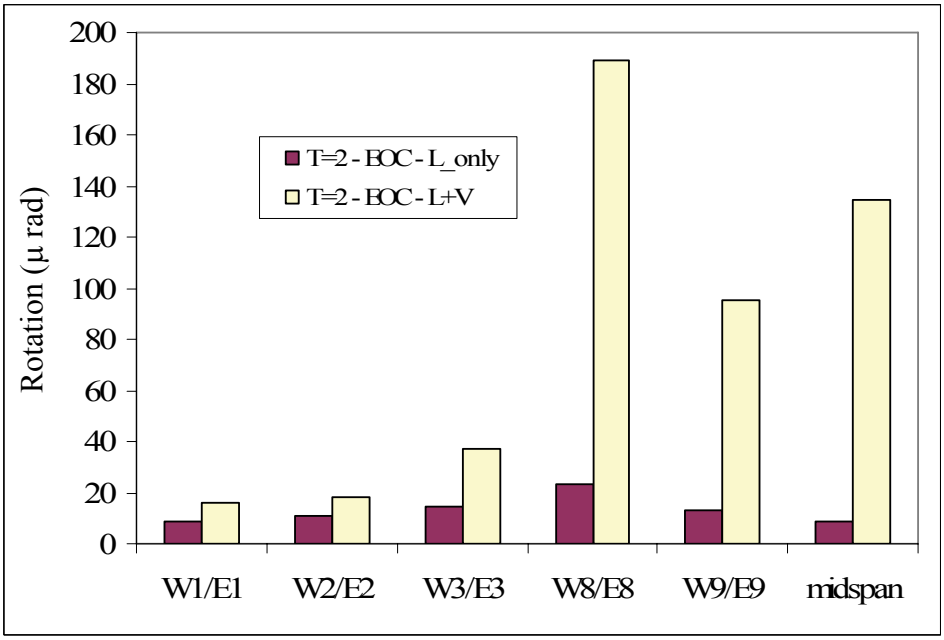

Figure 7-8 525 Foot Span – Influence of Vertical Ground Motion on the Median Peak Positive Segment Joint Rotations

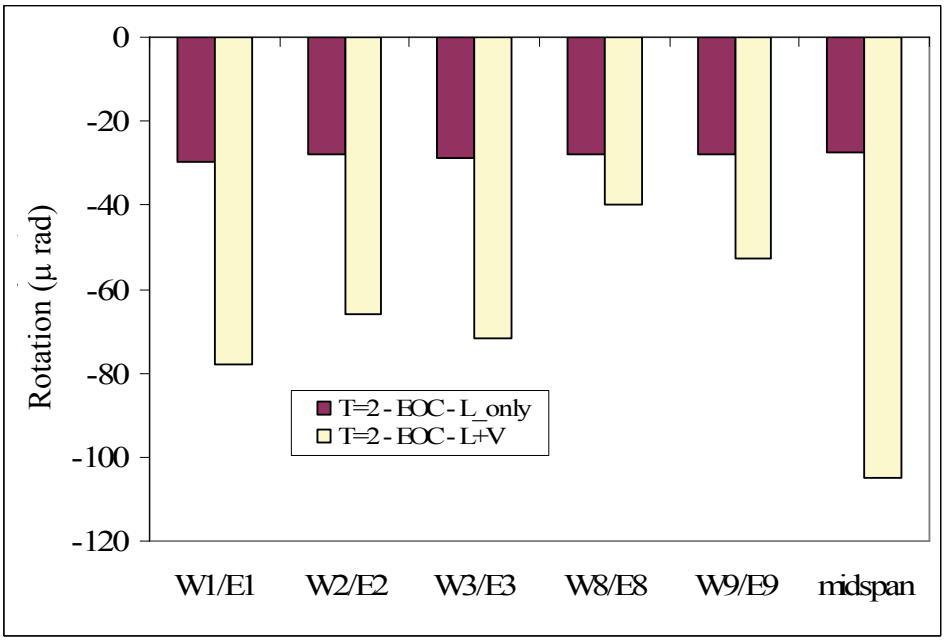

Figure 7-9 525 Foot Span – Influence of Vertical Ground Motion on the Median Peak Negative Segment Joint Rotations

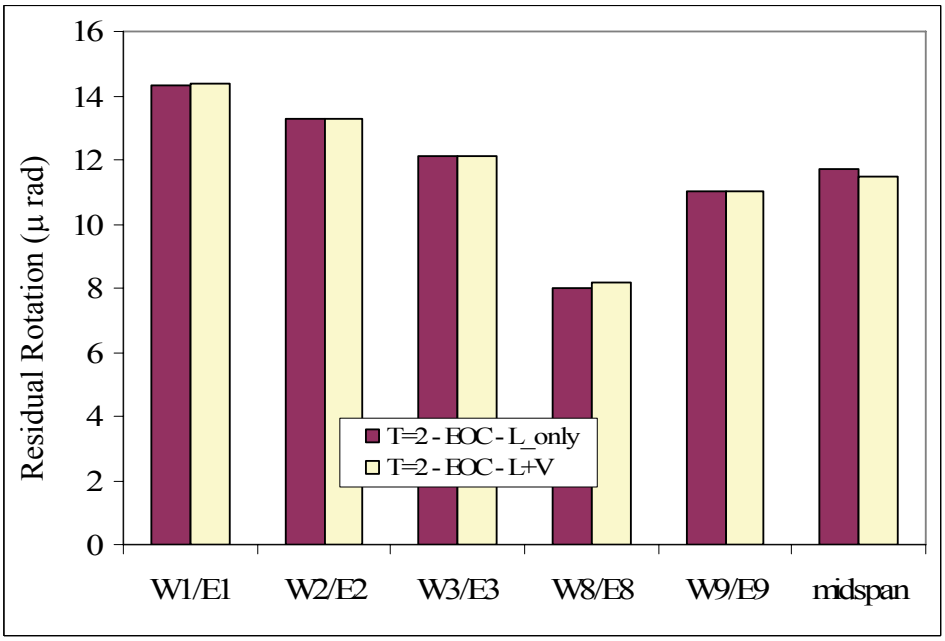

Figure 7-10 525 Foot Span – Influence of Vertical Ground Motion on the Median Residual Segment Joint Rotations

The reason for such large increases in the peak rotations are the same as described above for the 300 foot span model. That is, that the vertical earthquake ground motions pushed the superstructure joints beyond the cracking limit state, C1, and into the non-linear range, were a small increase in moment demand produced a large increase in joint rotation demand (see Figure 7-11 and Figure 7-12).

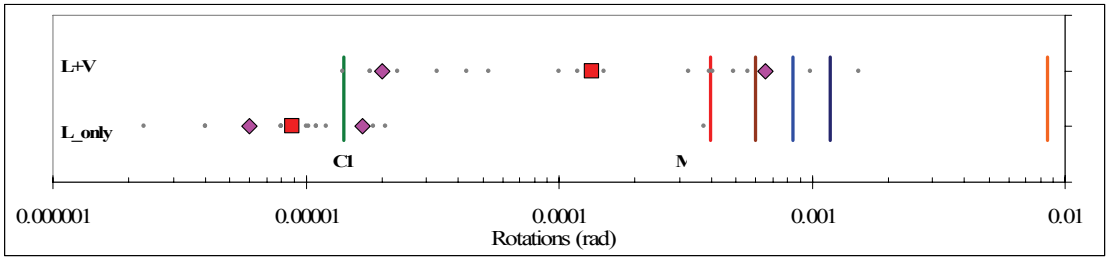

Figure 7-11 525 Foot Span – Influence of Vertical Ground Motion on Positive Midspan Rotations

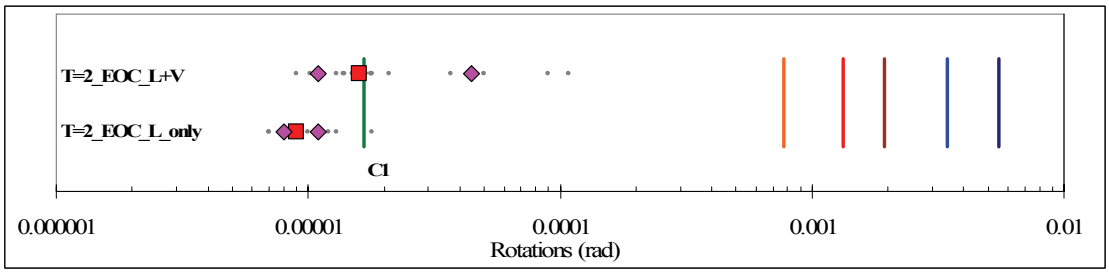

Figure 7-12 525 Foot Span – Influence of Vertical Ground Motion on Positive Joint W1/E1 Rotations

The influence of the vertical ground motion on the piers is shown in Figure 7-13 and Figure 7-14. Figure 7-13 summarizes the median of the peak longitudinal drift ratios while Figure 7-14 summarizes the median residual longitudinal drift

ratios. Clearly, adding the vertical component of ground motion does not significantly impact the longitudinal response of the piers.

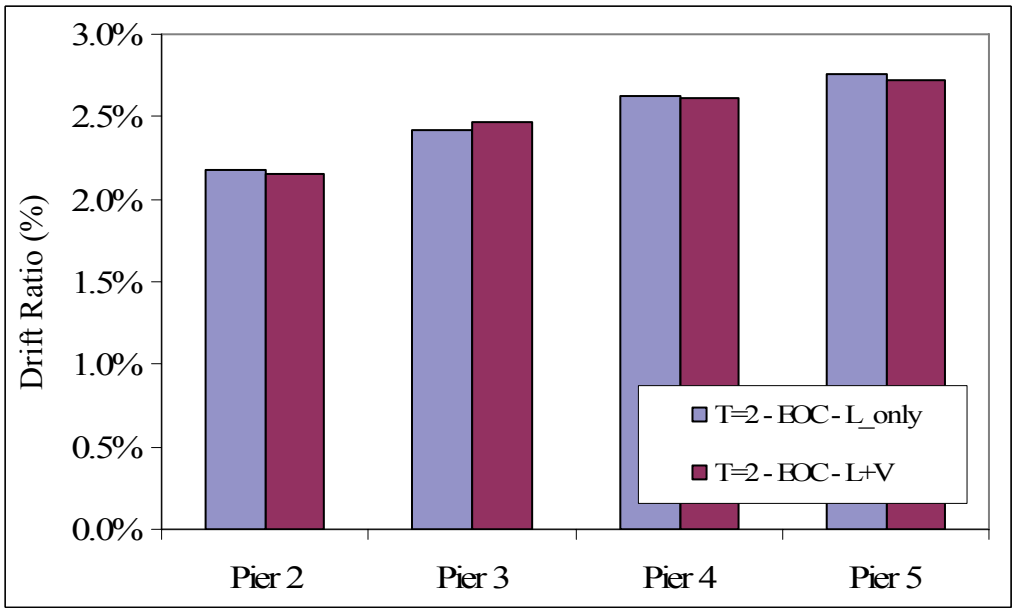

Figure 7-13 525 Foot Span - Influence of Vertical Ground Motion on the Median Peak Pier Longitudinal Drift Ratio

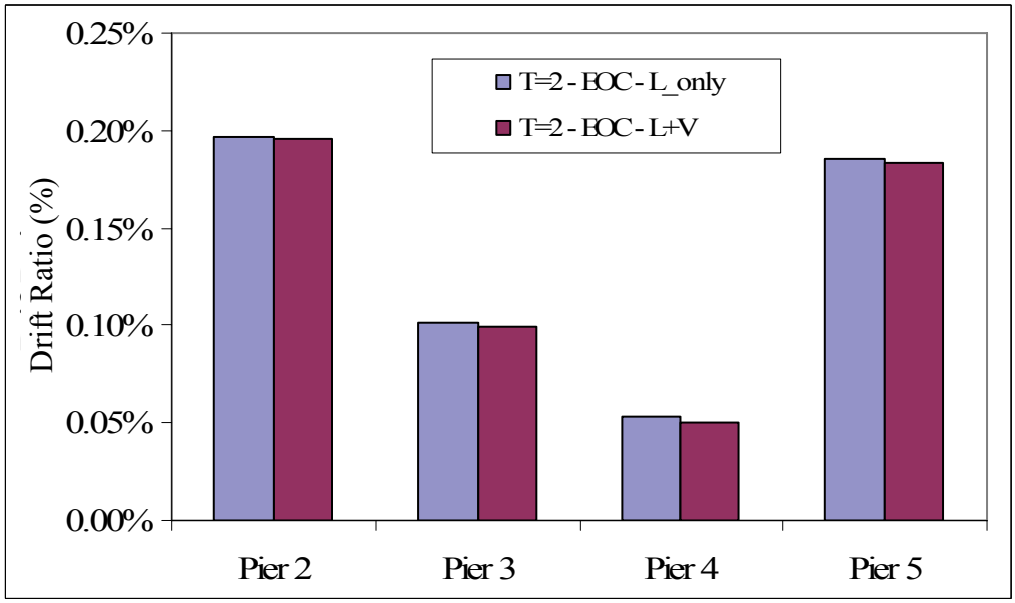

Figure 7-14 525 Foot Span - Influence of Vertical Ground Motion on the Median Residual Pier Longitudinal Drift Ratio

7.2. Record Scaling

One of the primary goals of this research was to study the impact of the method of record scaling on the response of precast segmental bridge structures. The effect on the segment joints due to the two different record scaling methods, described in Chapter 5, was investigated. The first method scaled the lateral ground motion to match the design spectrum at the natural period of the structure and the second method scaled the lateral motions for a least squares fit over a period range. Both record scaling methods scaled the vertical ground motion with the same scale factor as the lateral ground motion. This study utilized ground motions with both longitudinal and vertical components and were based on joint stresses at the end of construction, i.e. prior to creep and shrinkage losses. Some of the figures in this section remind the reader of this fact with the notation "L+V" and "EOC" in the legend.

It is important to recall (see Section 5.3) that the scale factors for the range scaled ground motions were generally 4% smaller than the scale factors for the ground motions that were scaled to the natural period. Thus a small reduction in the median response was expected in the results from range scaled excitations.

7.2.1. 300 Foot Spans

The results of the record scaling investigation for the 300 foot span bridge model are shown in Figure 7-15 and Figure 7-16 Figure 7-15 shows the median of the peak negative joint rotations for the six different joint families in the model. Clearly the median of the peak negative joint rotations does not change significantly. On average, scaling for the best fit over a period range reduced the median by 8%. This is slightly more than the 4% expected based on the median scale factor reduction, but is a small difference overall.

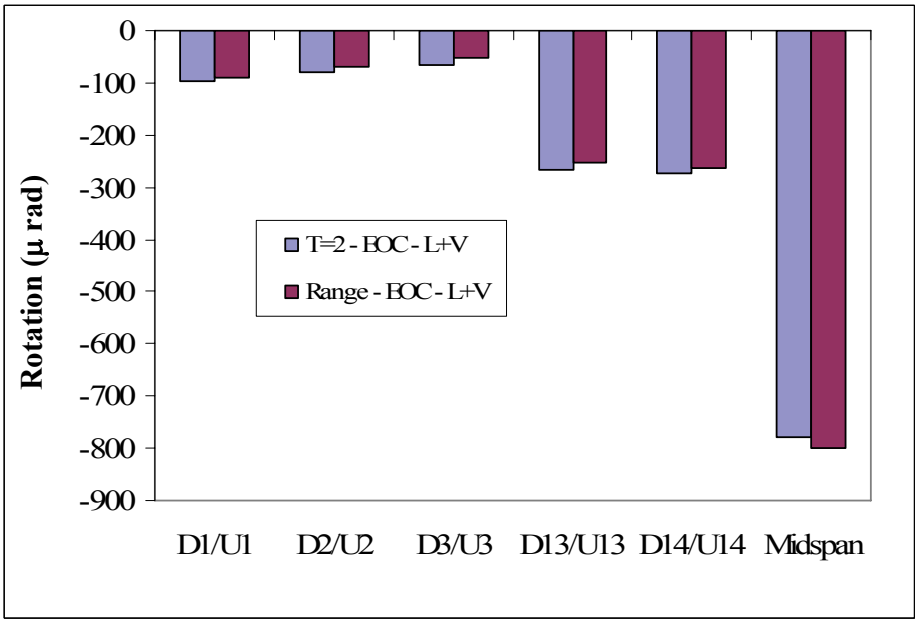

Figure 7-15 300 Foot Span - Influence of Record Scaling on Median of the Peak Negative Rotations

Figure 7-16 shows the coefficient of variation (COV) for the same set of data. The COV is defined as the ratio of the standard deviation divided by the mean for a set of data and is a measure of the scatter of the data. Clearly, the method of record scaling dramatically affects the COV. This is not surprising because the variation of the range scaled ground motions was smaller than the records scaled to the natural period as discussed in Section 5.4 and shown in Figure 5-11. While the results vary from segment joint to segment joint, on average scaling the record for a best fit over a period range, reduced the COV by 34% for peak negative bending of the superstructure joints.

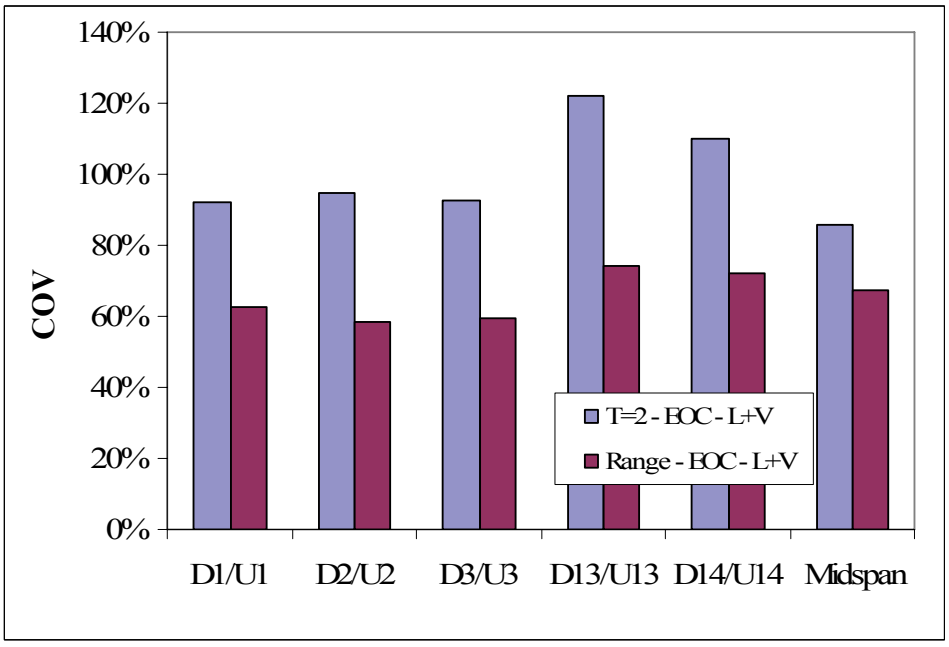

Figure 7-16 300 Foot Span – Influence of Record Scaling on COV for Peak Negative Joint Rotations

Similar figures of the peak positive segment joint rotations and residual rotations (see Appendix C) show scaling to a range reduced the median by 8% and 0% respectively, while the COV reduces by 14% and 4%, respectively. Table 7-1 summarizes the change in segment joint response between scaling to the natural period and scaling for the best fit over a period range.

Table 7-1 300 Foot Span - Change in Superstructure Response between Scaling to Natural Period and Scaling for Best Fit over a Period Range

	Peak Positive Rotations		Peak Negative Rotations		Residual Rotations	
	Median	**COV**	**Median**	**COV**	**Median**	**COV**
D1/U1	-15%	-33%	-8%	-32%	0%	-58%
D2/U2	-32%	-18%	-14%	-38%	-1%	-8%
D3/U3	-9%	-4%	-22%	-36%	0%	-21%
D13/U13	15%	-8%	-5%	-39%	2%	19%
D14/U14	-4%	-13%	-5%	-35%	0%	23%
midspan	-6%	-11%	3%	-22%	0%	23%
average ==>	**-8%**	**-14%**	**-8%**	**-34%**	**0%**	**-4%**

Table 7-2 summarizes the impact of the method of record scaling on the pier response. The results for the piers were similar to that of the superstructure segment joints. In general, scaling the records to match a period range reduced the median response modestly (less than 4%) while the COV reduced by 13% and 29% for the peak and residual drift ratios, respectively.

Table 7-2 300 Foot Span - Change in Pier Response between Scaling to Natural Period and Scaling for Best Fit over a Period Range

	Peak Longitudinal Drift Ratio		Residual Long. Drift Ratio	
	Median	**COV**	**Median**	**COV**
Pier 2	2%	-7%	7%	-23%
Pier 3	-3%	-10%	1%	-27%
Pier 4	-7%	-16%	-3%	-32%
Pier 5	-7%	-21%	-5%	-35%
average ==>	**-4%**	**-13%**	**0%**	**-29%**

A reduction in the COV of the pier response is somewhat unexpected when one compares the COV of the ground motions (see Figure 5-10) at a period of 2.0 seconds. If the structure responded at its natural period, the COV of the range scaled records should have been larger than the period scaled records. This result suggests that the abutments played a role in the longitudinal response of the bridge by stiffening the overall structural response. This is not surprising given the fact that the abutments were engaged at a displacement of only 10 inches (see Figure 6-31) and the expected displacement response of an equivalent elastic structure of 2.0 second period was 30 inches (see Figure 5-9).

7.2.2. 525 Foot Spans

The results of the record scaling investigation for the 525 foot span bridge model are presented below. Figure 7-17 shows the median of the peak negative joint

rotations for the six different joint families in the model. Clearly, the median of the peak negative joint rotations does not change significantly. On average scaling for the best fit over a period range reduced the median by 7%. This is comparable to the median reduction of the 300 foot span.

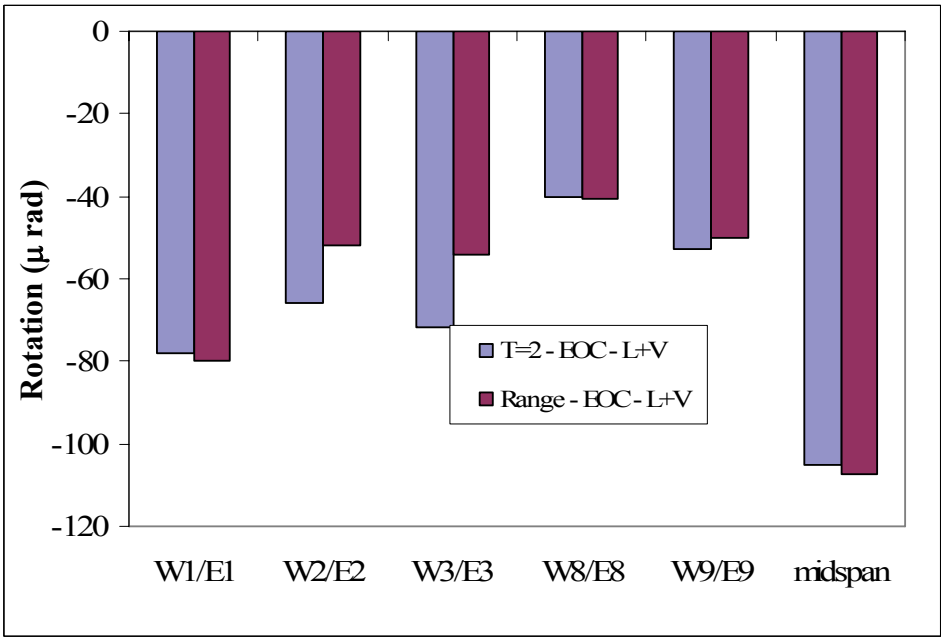

Figure 7-17 525 Foot Span - Influence of Record Scaling on Median of the Peak Negative Rotations

Figure 7-18 shows the coefficient of variation (COV) for the same set of data. Clearly, the method of record scaling significantly affected the COV, as expected based on the COV of the ground motion records themselves. While the influence of record scaling varied from joint to joint, on average scaling the record for a best fit

over a period range reduced the COV by 30% for peak negative bending of the superstructure joints.

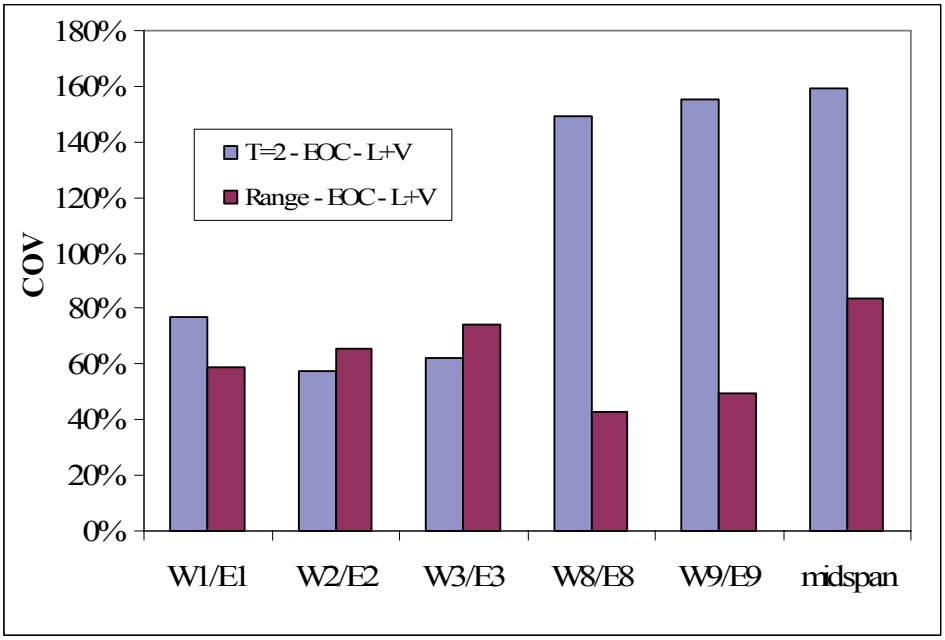

Figure 7-18 525 Foot Span – Influence of Record Scaling on COV for Peak Negative Rotations

Similar figures of the peak positive segment joint rotations and residual rotations (see Appendix C) show scaling to a range reduced their median responses by 2%, while the COV reduced by 22% and 29%, respectively. Table 7-3 summarizes the change in segment joint response between scaling to the natural period and scaling for the best fit over a range.

Table 7-3 525 Foot Span - Change in Superstructure Response between Scaling to Natural Period and Scaling for Best Fit over a Period Range

	Peak Positive Rotations		Peak Negative Rotations		Residual Rotations	
	Median	**COV**	**Median**	**COV**	**Median**	**COV**
W1/E1	-13%	-18%	3%	-24%	1%	-33%
W2/E2	-11%	-42%	-21%	14%	1%	-29%
W3/E3	-21%	-22%	-25%	19%	0%	-32%
W8/E8	-15%	-9%	1%	-71%	-4%	-27%
W9/E9	21%	-25%	-5%	-68%	-4%	-34%
midspan	24%	-16%	2%	-48%	-3%	-16%
average ==>	**-2%**	**-22%**	**-7%**	**-30%**	**-2%**	**-29%**

The impact of scaling the ground motions to a range is different for the piers, as shown in Table 7-4. The median response reduced modestly (3% for the peak longitudinal drift ratios and 5% for the residual drift ratios), as expected based on the reduced scale factor on the ground motions. However, the COV increased by 28% and 36% for the peak longitudinal and residual drift ratios, respectively. This is expected based on the COV of the ground motions near the natural period of the structure (see Figure 5-10). This result suggests that the abutments did not dominate the longitudinal response as they did in the 300 foot span model (see Section 7.2.1)/

Table 7-4 525 Foot Span - Change in Pier Response between Scaling to Natural Period and Scaling for Best Fit over a Period Range

	Peak Longitudinal Drift Ratio		Residual Long. Drift Ratio	
	Median	**COV**	**Median**	**COV**
Pier 2	0%	39%	0%	26%
Pier 3	-4%	39%	-1%	21%
Pier 4	-5%	24%	-19%	71%
Pier 5	-2%	10%	0%	28%
average ==>	**-3%**	**28%**	**-5%**	**36%**

It should be noted that the large percent changes in the residual longitudinal drift ratios for Pier 4 shown in Table 7-4, were due to the fact that the residual drifts for this pier were very small, thus any modest change generated a significant percentage difference.

7.3. Pre-Earthquake Stress-State

The stress-state of concrete bridges fluctuates on a daily basis due to temperature and over the service life of the bridge due to creep and shrinkage. The pre-earthquake stress-state of the superstructure segment joints may affect the seismic response. To investigate this effect four different pre-earthquake stress-states were studied. These stress-states represented the possible range of stresses that may occur during the service life of a segmental bridge and are defined and discussed in Sections 6.2.5 and 6.4.5.

The pre-earthquake stress-state study in this section utilized ground motions with both longitudinal and vertical components that were scaled based on the natural period of the bridge. Some of the figures in this section remind the reader of this fact with the notation "L+V" and "T=2" in the legend. These ground motions were selected because they were expected to produce the largest median segment joint response (see Section 7.1) as well as the largest variation in joint response (Section 7.2) of the ground motions options in this study.

7.3.1. 300 Foot Spans

The seismic response of the 300 foot span model based on four different pre-earthquake stress-states is presented below.

7.3.1.1. Abutment Response

Based on the Caltrans SDC (Caltrans, 2004) strength and stiffness estimates of the soil behind the abutment back wall and considering the thermal expansion joint, the abutment soil will yield at a displacement of approximately 13 inches. The peak abutment displacements were approximately 22 and 24 inches at Abutment 1 and 6, respectively. The unloading response of the abutment soil was assumed to be equivalent to the initial stiffness, thus a gap of 9 to 11 inches will likely be created

due to significant non-linear response of the soil behind the abutment back wall. This gap will be located between the superstructure and the abutment back wall. A gap of this size will significantly impact traffic flow and will likely require bridge closure for repair.

7.3.1.2. Pier Response

Figure 7-19 and Figure 7-20 compare the median response of the twenty earthquake records for the peak longitudinal and residual longitudinal drift ratios for the four pre-earthquake stress-states. Clearly the peak longitudinal drift is unaffected by the pre-earthquake stress-state of the superstructure segment joints. The residual longitudinal drift, however, shows some variation in response with the 2CS stress-state exhibiting the largest response. While there is up to a 40% variation, the residual drifts remain very small and are of no concern from a structural point of view.

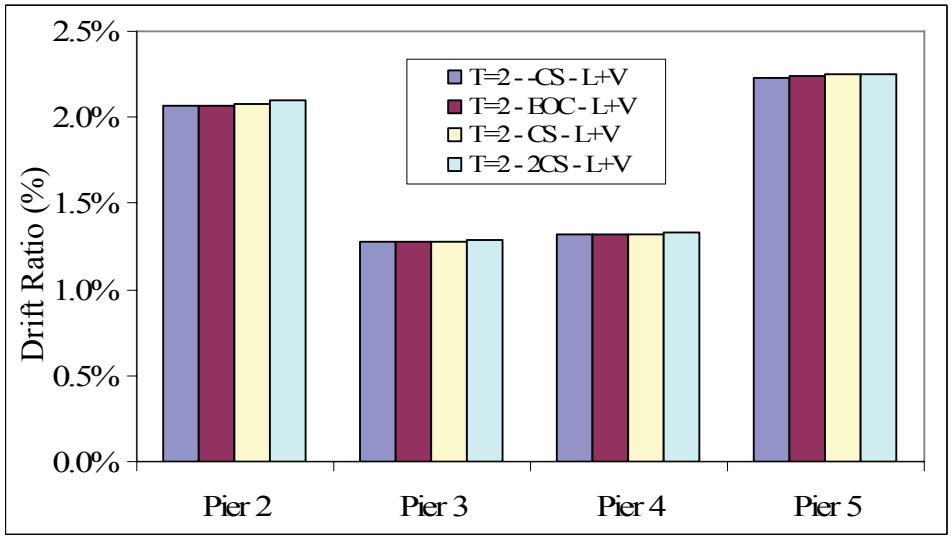

Figure 7-19 300 Foot Span – Influence of Pre-Earthquake Stress-State on Peak Longitudinal Drift Ratio

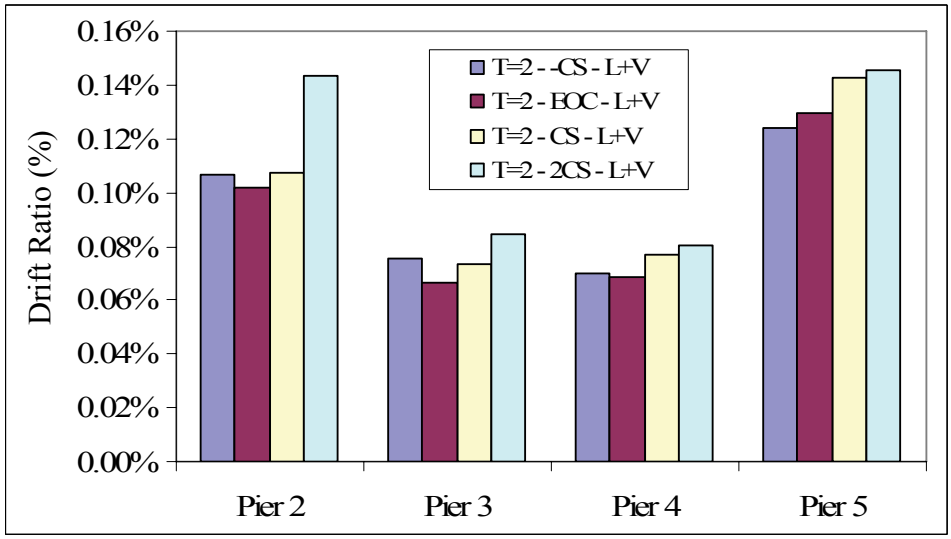

Figure 7-20 300 Foot Span – Influence of Pre-Earthquake Stress-State on Residual Longitudinal Drift Ratio

Comparing the peak drifts of Piers 2 and 5 in Figure 7-19 with the longitudinal push results (see Figure 6-31) and performance limits (see Table 6-2) it is clear that the short piers developed full plastic hinges (i.e., exceeded performance

limit state P-R1) and incipient spalling of cover concrete (i.e., exceeded performance limit state P-C2). This level of damage may not require closure of the bridge as the damage is below the roadway, but will require significant repair.

7.3.1.3. Superstructure Segment Joint Response

Figure 7-21 to Figure 7-23 compares the median segment joint rotations among the various joint families for the four pre-earthquake stress-states. Figure 7-21 presents the median response of the peak positive bending joint rotations. Clearly, the pre-earthquake stress-state impacts the joint response, particularly near midspan, where the 2CS stress-state exhibited the largest rotations. This is because the bottom of the midspan joint was under the least compression during pre-earthquake stress-state 2CS, and was the closest of the four pre-earthquake stress-states to opening under positive bending.

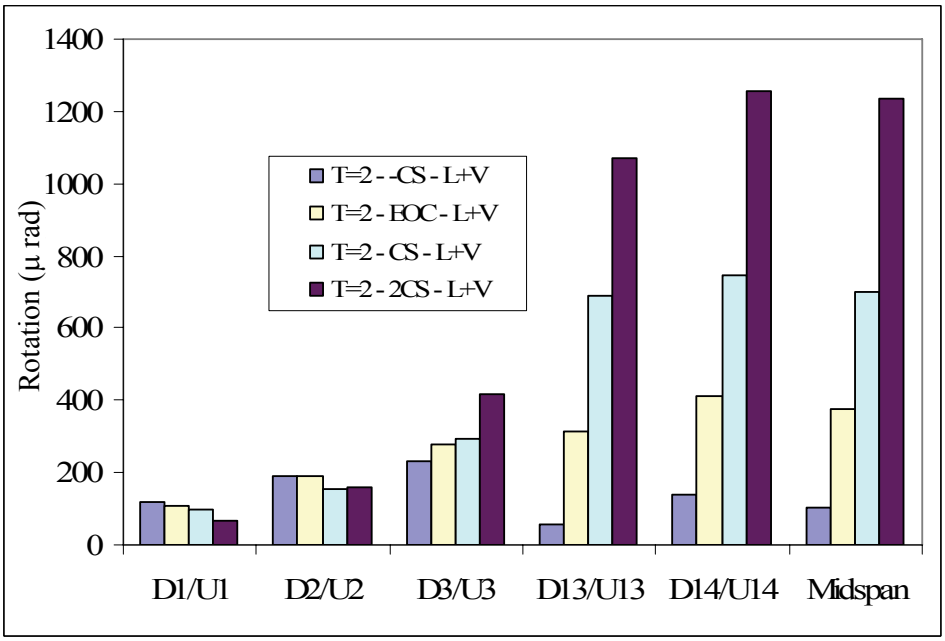

Figure 7-21 300 Foot Span – Influence of Pre-Earthquake Stress-State on Median Peak Positive Bending Joint Rotations

Figure 7-22 presents the median response of the peak negative bending joint rotations. Once again the midspan joints were the most impacted by the pre-earthquake stress-state, with the –CS stress-state generating the largest midspan rotations. This is because the top of the midspan joint was under the least compression for stress-state -CS, and was closest to opening under negative bending.

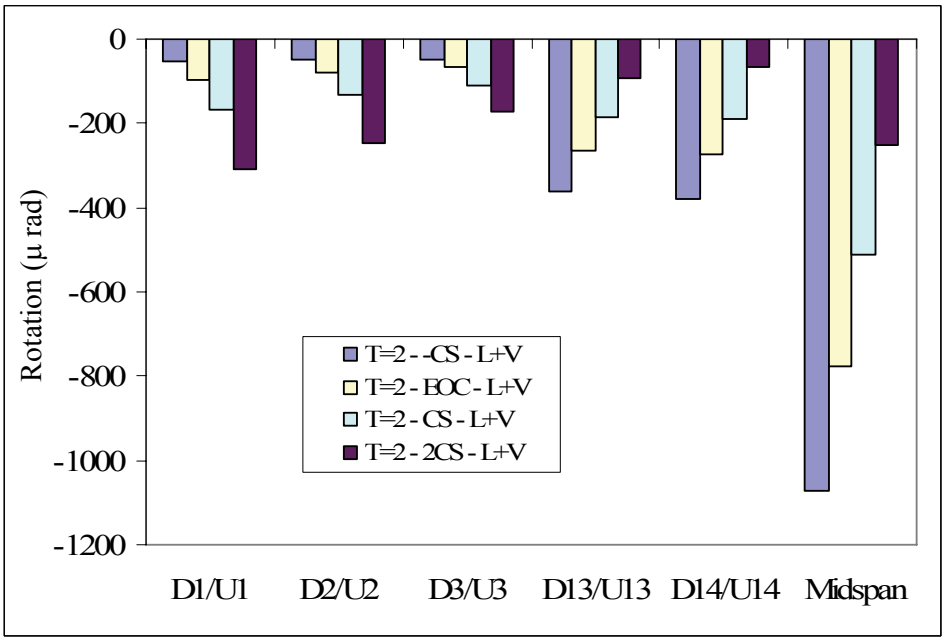

Figure 7-22 300 Foot Span – Influence of Pre-Earthquake Stress-State on Median Peak Negative Bending Joint Rotations

Figure 7-23 presents the median response of the residual joint rotations. Near the piers there was a gradual increase in residual drift as the stress-state moves from –CS to 2CS. This increase is relatively small indicating that the joints close completely for all stress-states. Near midspan, the extreme stress-states (i.e. –CS and 2CS) increased the median residual rotations significantly, indicating that the response was likely pushed beyond a limit state that generated damage.

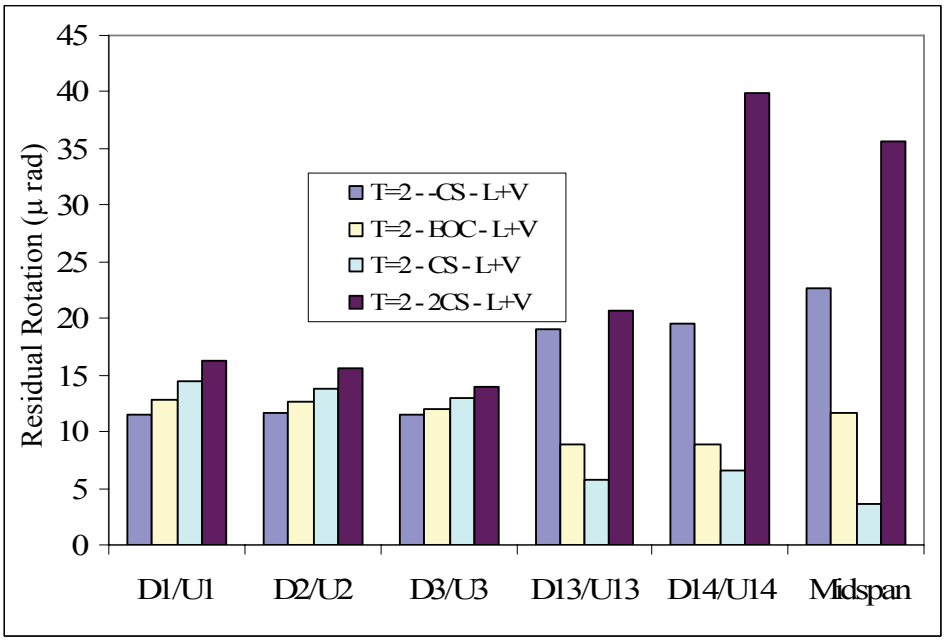

Figure 7-23 300 Foot Span – Influence of Pre-Earthquake Stress-State on Median Residual Joint Rotations

Figure 7-24 to Figure 7-26 compare the peak rotations based on the four pre-earthquake stress conditions with the performance limit states for the first joint adjacent to the piers, i.e., Joint D1/U1. The response of the other joints adjacent to the piers was similar and is shown in Appendix D. Each gray dot represents the peak rotation from one earthquake. The square marks represent the median rotation. The diamond marks represent the 16^{th} and the 84^{th} percentiles and the vertical lines identify the various limit states as defined in Section 6.3.4. In general, the median response for Joint D1/U1 stayed below the crushing limits state, C2, except for

stress-state 2CS under negative bending (see Figure 7-24 and Figure 7-25), which exceeded C2.

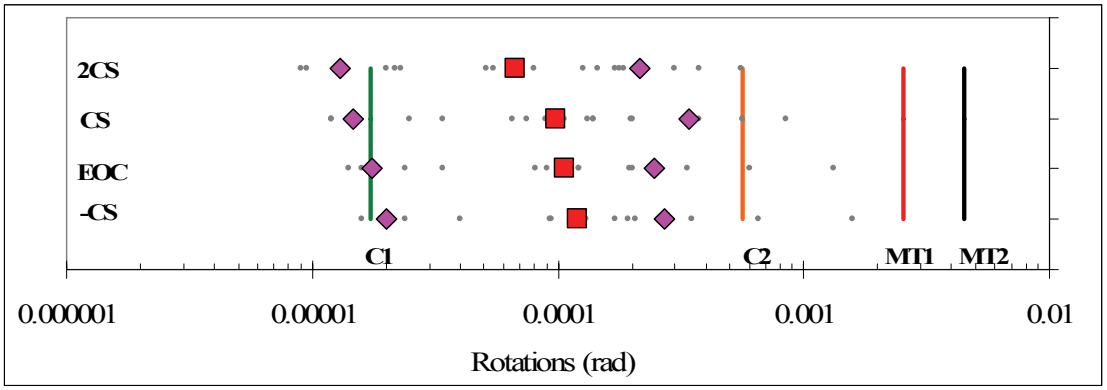

Figure 7-24 300 Foot Span – Influence of Pre-Earthquake Stress on Peak Positive Joint D1/U1 Rotations

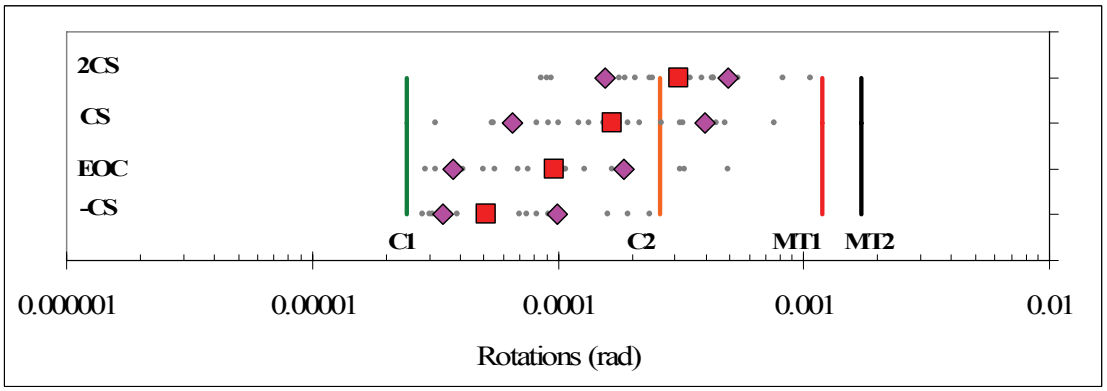

Figure 7-25 300 Foot Span – Influence of Pre-Earthquake Stress on Peak Negative Joint D1/U1 Rotations

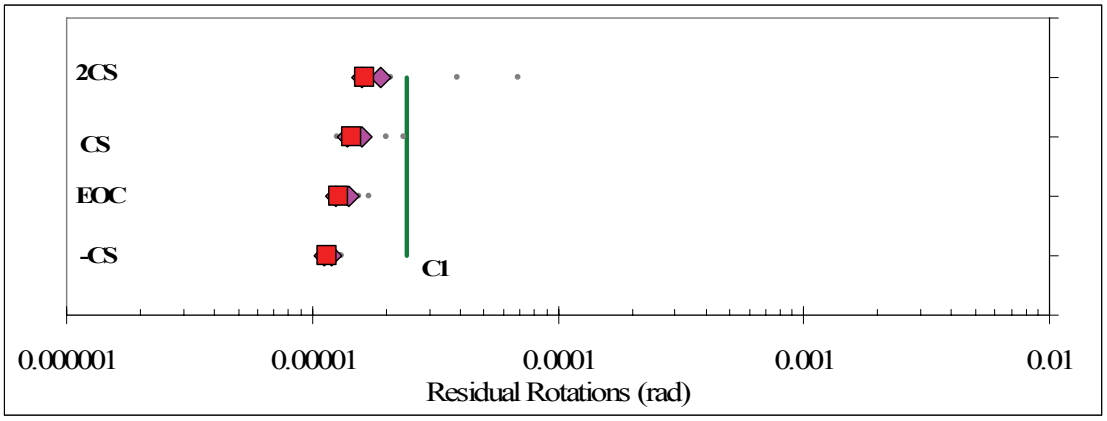

Figure 7-26 300 Foot Span – Influence of Pre-Earthquake Stress on Residual Joint D1/U1 Rotations

Figure 7-27 to Figure 7-29 compare the peak rotations based on the four pre-earthquake stress conditions with the performance limit states for the midspan joints. The response of the other joints near midspan was similar and is shown in Appendix D.

Figure 7-27 shows the influence of the pre-earthquake stress-state on the peak positive joint rotations at the midspan joints. The median response remained below the C2 limit state for all stress-states except for 2CS. In this case the median rotation approached, but do not exceed the limit of proportionality of the main tendons, i.e., MT1.

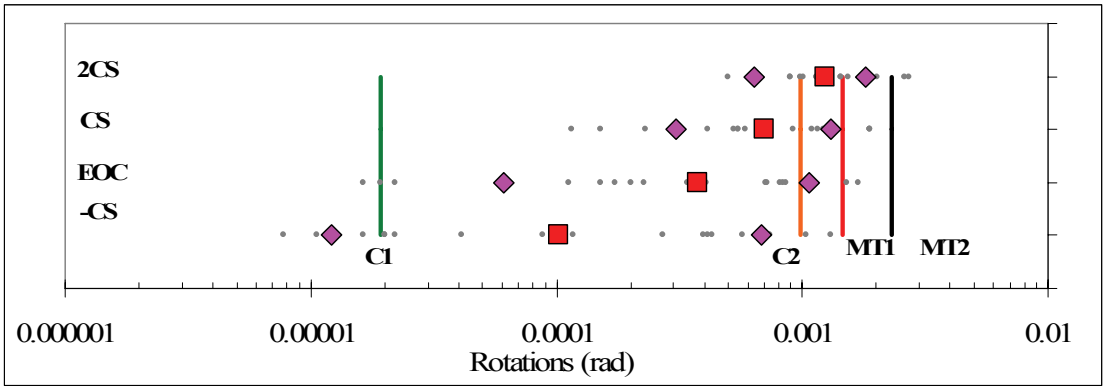

Figure 7-27 300 Foot Span – Influence of Pre-Earthquake Stress on Peak Positive Midspan Joint Rotations

Figure 7-28 shows the influence of the pre-earthquake stress-state on the peak negative joint rotations at the midspan joints. The absolute value of the negative rotations was taken so that the results could be plotted on a log scale. The median response remained below the C2 limit state for stress-states CS and 2CS, while stress-states EOC and –CS exceed the C2 limits state.

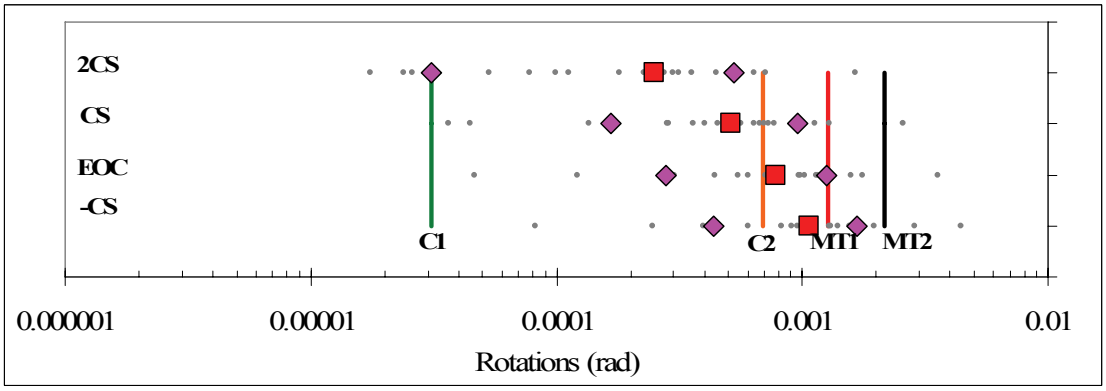

Figure 7-28 300 Foot Span – Influence of Pre-Earthquake Stress on Peak Negative Midspan Joint Rotations

Figure 7-29 illustrates the impact of the pre-earthquake stress-state on the residual midspan joint rotations. The median residual joint rotations of the extreme stress-states, namely 2CS and –CS were beyond the cracking limit state, indicating that the joint may maintain some amount of crack opening. The largest residual rotation was caused by crushing of the extreme concrete fibers in compression due to positive bending moments. At midspan the dead load of the structure generates a positive bending moment, thus the residual crack will be below the bridge and not on the riding surface. This residual crack width remained very small and was less than 0.01 inches. Crushed concrete, on the other hand, caused by positive bending moments exceeding the C2 limit state, will be on the riding surface and may affect serviceability.

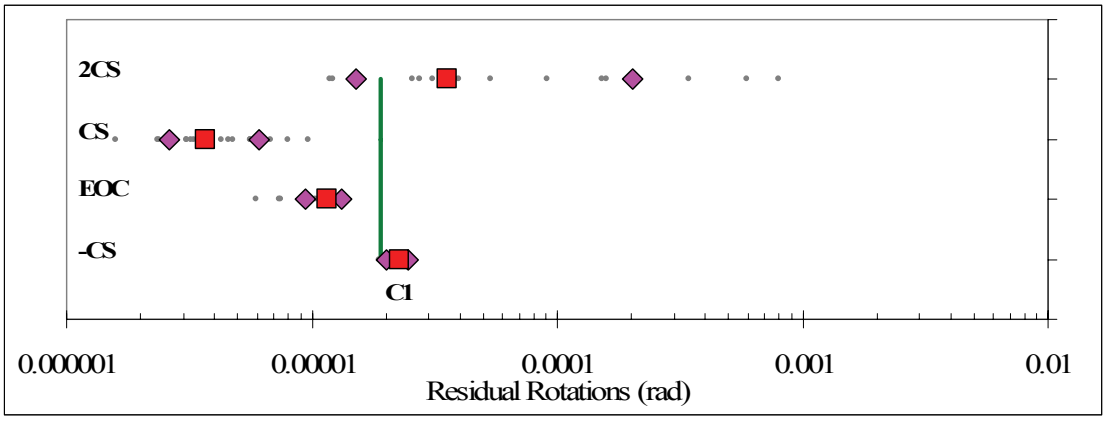

Figure 7-29 300 Foot Span – Influence of Pre-Earthquake Stress on Residual Midspan Joint Rotations

In summary, the pre-earthquake stress-state influenced the response of the 300 foot span segment joints and resulted in a median joint response that exceeds the crushing performance limits states. This occurred most often near midspan where the effects of creep and shrinkage were more pronounced. For example, cracking and joint opening is expected near the piers due to all pre-earthquake conditions, however crushing was observed only at the bottom flange near the piers due to the +2CS stress-state. Similarly, cracking and joint opening was observed at midspan due to all pre-earthquake stress-states, however, crushing of the bottom flange occurred only due to the +2CS stress-state, while crushing of the bottom flanges occurred only due to the EOC and the –CS stress-states.

The median response, both at the piers and near midspan, remained below the limit of proportionality of the PT. Thus loss of prestressing force did not occur.

It is important to consider that while the results indicated that crushing of the extreme superstructure fibers may occur (i.e. $\varepsilon_c < -0.0016$), the damage in the short piers exceeded the spalling limit state (i.e. $\varepsilon_c < -0.004$) and will require more repair than the superstructure.

7.3.1.4. Superstructure Segment Joint Response Summary

The median positive, negative and residual joint rotations, for the worst cast pre-earthquake stress state are summarized on the monotonic push results in Figure 7-30 and Figure 7-31 for the pier and midspan joints, respectively. These figures also indicate the performance limit states, thus the approximate level of damage is also shown in these figures. In general, the first joint adjacent to the pier and the joint at midspan exhibited the largest rotation demands and the most damage.

Figure 7-30 indicates that Joint D1/U1 exceeded the crushing limit state, C2, due to negative bending, while Joints D2/U2 and D3/U3 remained below the crushing limit state.

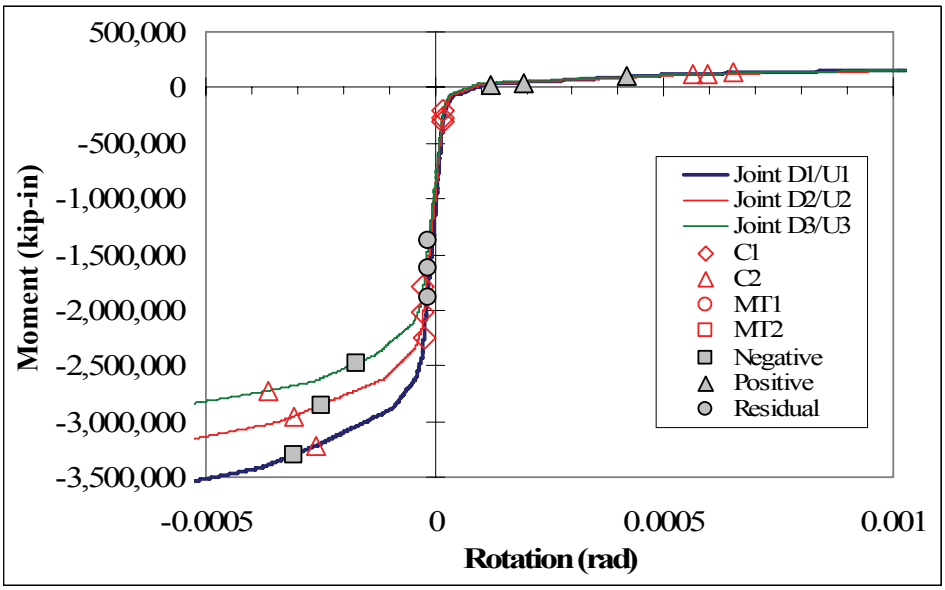

Figure 7-30 300 Foot Span - Summary of Worst-Case Joint Response Adjacent to the Pier

Figure 7-31 indicates that the joints near midspan received similar rotation demands due to positive bending and exceeded the C2 limit state. However, only the midspan joints exceeded the crushing limit state due to negative bending.

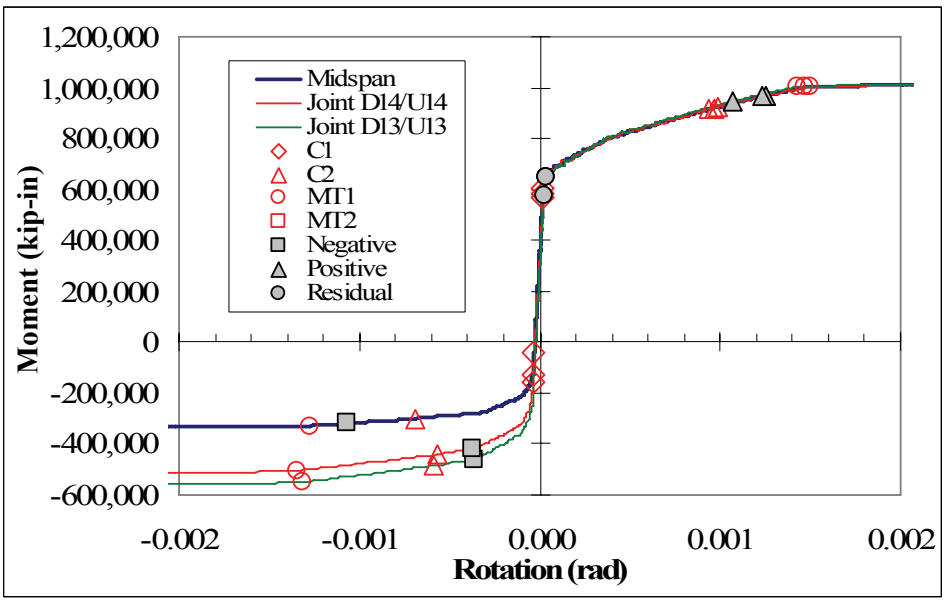

Figure 7-31 300 Foot Span - Summary of Worst-Case Joint Response Near Midspan

7.3.2. 525 Foot Spans

The seismic response of the 525 foot span model based on four different pre-earthquake stress-states is presented below.

7.3.2.1. Abutment Response

Based on the Caltrans SDC (Caltrans, 2004) strength and stiffness estimates of the soil behind the abutment back wall and considering the thermal expansion

joint, the abutment soil will yield at a superstructure displacement of approximately 27 inches. The peak longitudinal superstructure displacements were approximately 30 and 28 inches at abutments 1 and 6, respectively. The unloading response of the abutment soil was assumed to be equivalent to the initial stiffness, thus a gap of between 1 and 3 inches may be created due to failure of the abutment back wall and subsequent soil failure. A gap of 1 inch will likely not impact traffic flow, however, a gap of 3 inches can impact traffic flow and may require bridge closure for repair.

7.3.2.2. Pier Response

Figure 7-32 and Figure 7-33 compare the median response of the twenty earthquake records for the peak longitudinal and residual longitudinal drift ratios for the four pre-earthquake stress-states. Clearly the peak longitudinal drift is unaffected by the pre-earthquake stress-state of the superstructure segment joints. This result confirms the general understanding that volumetric changes do not impact the response of pier. The residual longitudinal drift ratio shows some variation in response, however, these variations remained very small and are of no concern from structural a point of view.

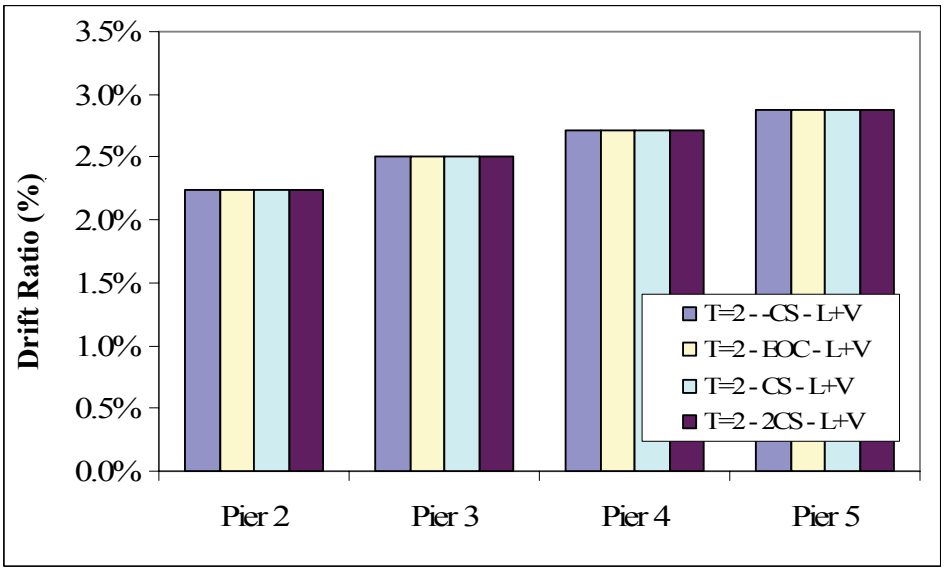

Figure 7-32 525 Foot Span – Influence of Pre-Earthquake Stress-State on Peak Longitudinal Drift Ratio

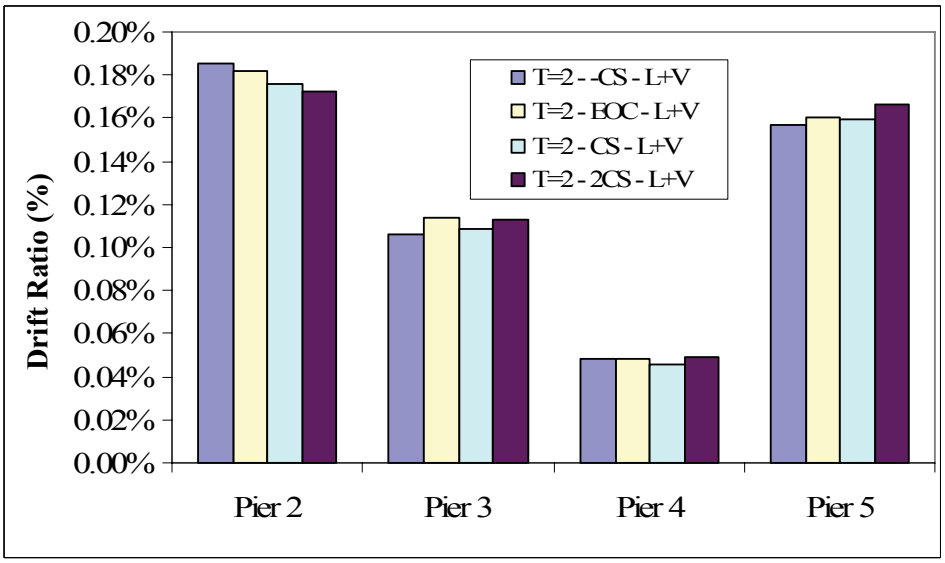

Figure 7-33 525 Foot Span – Influence of Pre-Earthquake Stress-State on Residual Longitudinal Drift Ratio

Comparing the peak Pier 5 drifts shown in Figure 7-32 with the longitudinal push results (see Figure 6-58) and performance limits (see Table 6-6) it is clear that

the short pier developed full plastic hinges (i.e. exceeded performance limit state P-R1) and will have spalling of cover concrete (i.e. exceeded performance limit state P-C2). This level of damage may not require closure of the bridge as the damage is below the roadway, but will require significant repair.

7.3.2.3. Superstructure Segment Joint Response

Figure 7-34 to Figure 7-36 compare the median segment joint rotations among the various joint families for the four pre-earthquake stress-states. Figure 7-34 presents the median response of the peak positive bending joint rotations. Clearly, the pre-earthquake stress-state affects the joint response, particularly near midspan, where the 2CS stress-state exhibited the largest rotations. This is because the bottom of the midspan joint was under the least compression for stress-state 2CS, and closest to opening under positive bending.

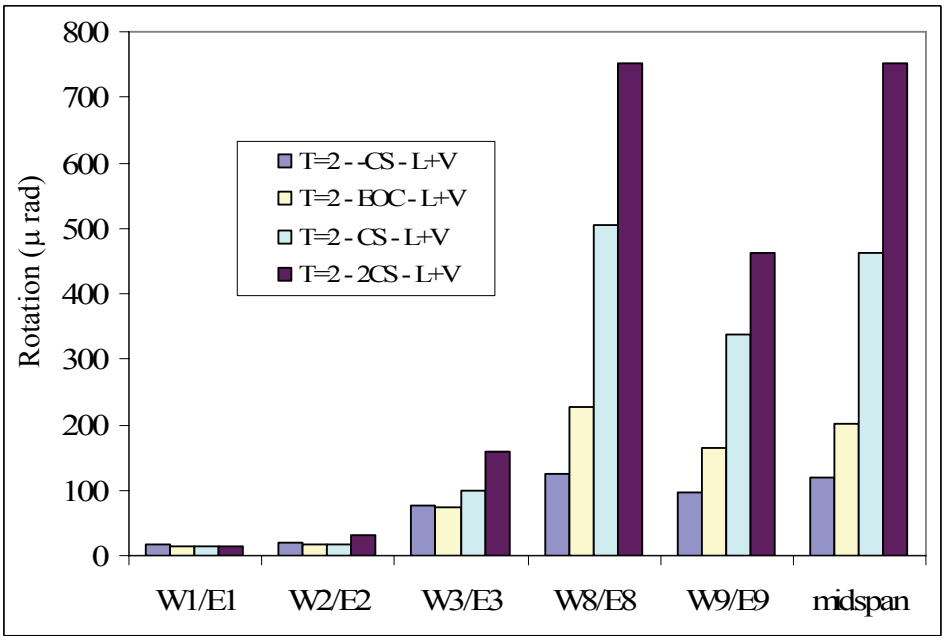

Figure 7-34 525 Foot Span – Influence of Pre-Earthquake Stress-State on Median Peak Positive Bending Joint Rotations

Figure 7-35 presents the median response of the peak negative bending joint rotations. Once again the midspan joints are the most effected by the pre-earthquake stress-state, with the –CS stress-state generating the largest midspan rotations. This is because the top of the midspan joint was under the least compression for stress-state -CS, and was closest to opening under negative bending.

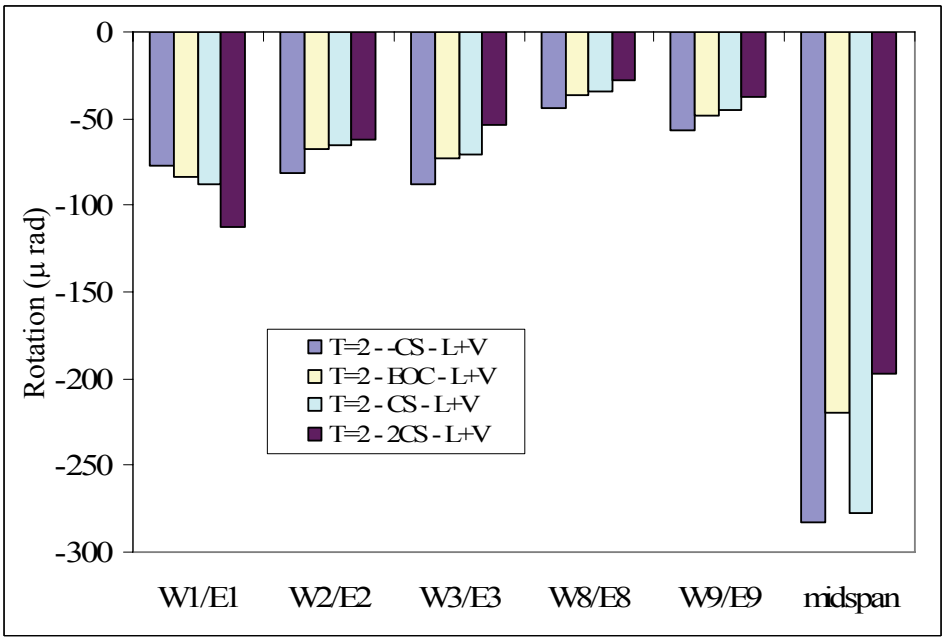

Figure 7-35 525 Foot Span – Influence of Pre-Earthquake Stress-State on Median Peak Negative Bending Joint Rotations

Figure 7-36 presents the median response of the residual joint rotations. In general there was a gradual increase in residual rotations near the piers as the stress-state moved from –CS to 2CS. A dramatic increase in residual rotations would suggest that a performance limit state was exceeded. Near midspan, the extreme stress-states (i.e. –CS and 2CS) increased the median residual rotations significantly, indicating that the response was likely pushed beyond a limit state that generated damage. This will be shown in greater detail later in this section.

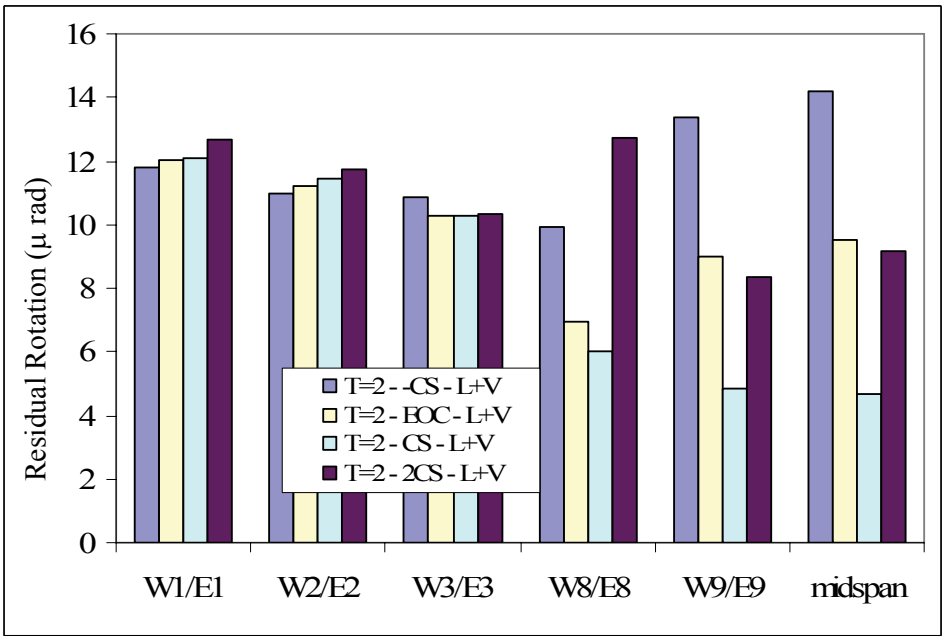

Figure 7-36 525 Foot Span – Influence of Pre-Earthquake Stress-State on Median Residual Joint Rotations

Figure 7-37 to Figure 7-42 compare the peak rotations from the four pre-earthquake stress conditions with the limit states for the joints nearest the piers, Joint W1/E1, and for the midspan joints. These two joint families were selected because they were representative of the response of joints adjacent to the piers and near midspan. The response of all segment joints are shown in Appendix D.

In general, the median response for Joint D1/U1 remained well below the crushing limits state, C2, and for positive bending the median response was near the cracking limit state (see Figure 7-37 and Figure 7-38). This was typical regardless of pre-earthquake stress condition. Thus joint family W1/E1 remained essentially

undamaged and closed completely following the seismic event as indicated by the very small residual joint rotation for all pre-earthquake stress conditions shown in Figure 7-39

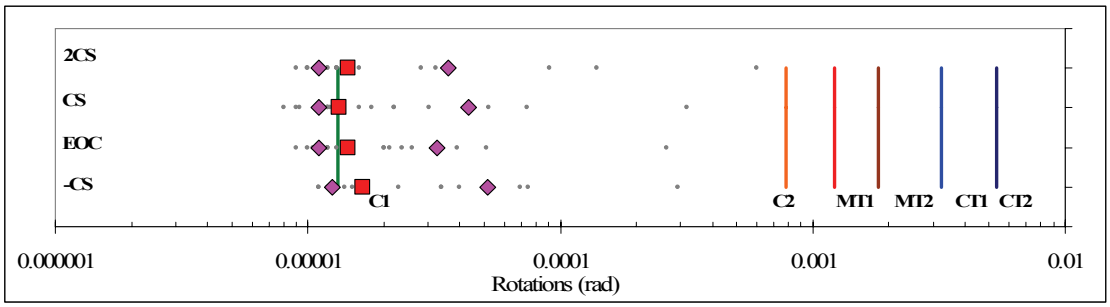

Figure 7-37 525 Foot Span – Influence of Pre-Earthquake Stress on Peak Positive Joint W1/E1 Rotations

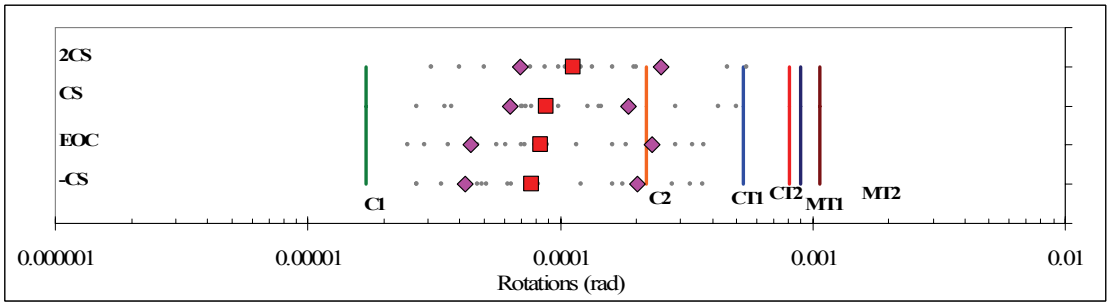

Figure 7-38 525 Foot Span – Influence of Pre-Earthquake Stress on Peak Negative Joint W1/E1 Rotations

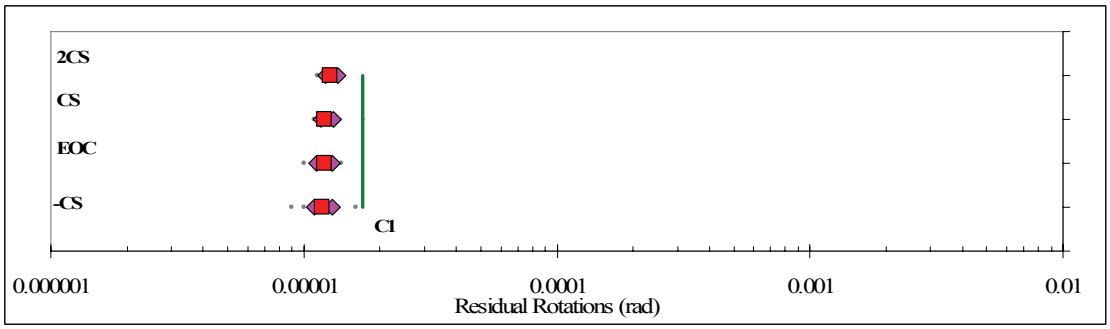

Figure 7-39 525 Foot Span – Influence of Pre-Earthquake Stress on Residual Joint W1/E1 Rotations

Figure 7-40 shows the influence of the pre-earthquake stress-state on the peak positive joint rotations at the midspan joints. The median response remained below the MT1 limit state for all stress-states except for the CS stress-state which exceeded MT1 and for the 2CS stress-state which reached CT1.

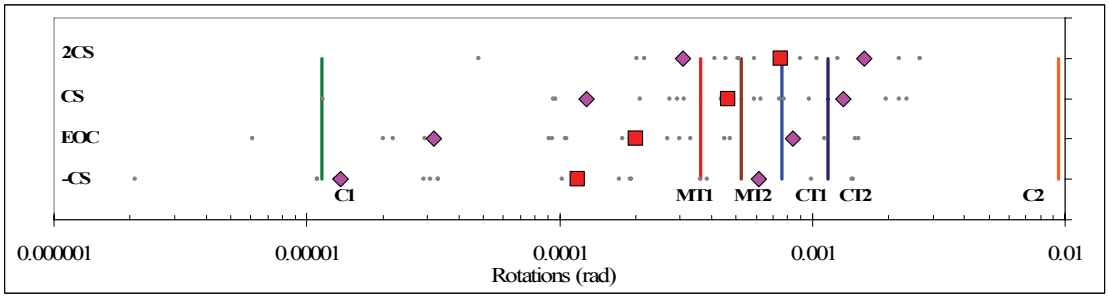

Figure 7-40 525 Foot Span – Influence of Pre-Earthquake Stress on Peak Positive Midspan Joint Rotations

Figure 7-41 shows the influence of the pre-earthquake stress-state on the peak negative joint rotations at the midspan joints. The absolute value of the negative rotations was taken so that the results could be plotted on a log scale. The median response slightly exceeded the C2 limit state for all stress-states.

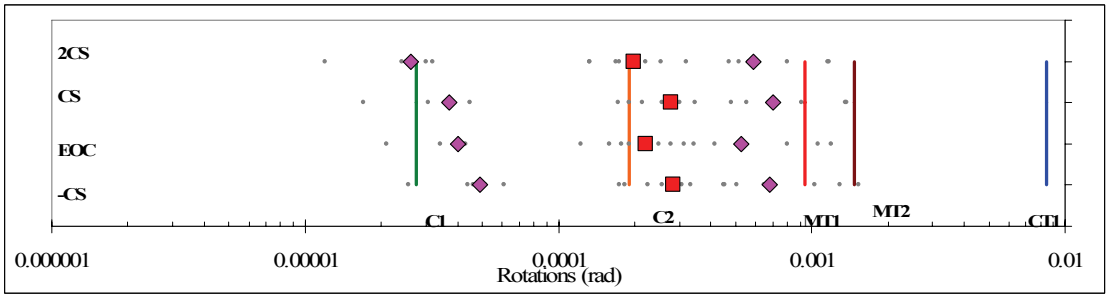

Figure 7-41 525 Foot Span – Influence of Pre-Earthquake Stress on Peak Negative Midspan Joint Rotations

Figure 7-42 illustrates the impact of the pre-earthquake stress-state on the residual midspan joint rotations. The median joint rotations of all pre-earthquake stress conditions were below the cracking rotation indicating that the joints typically closed completely. The variation of the median residual rotations between the pre-earthquake stress-states was due the differences in their initial rotations prior to the seismic event and not due to rotations caused by the earthquakes. It should be noted that the 2CS stress-state showed significant variability in response. This was due to the fact that the limits states for positive bending were very close to each other and a number of earthquake records exceeded the yield point of both the main tendons and the continuity PT.

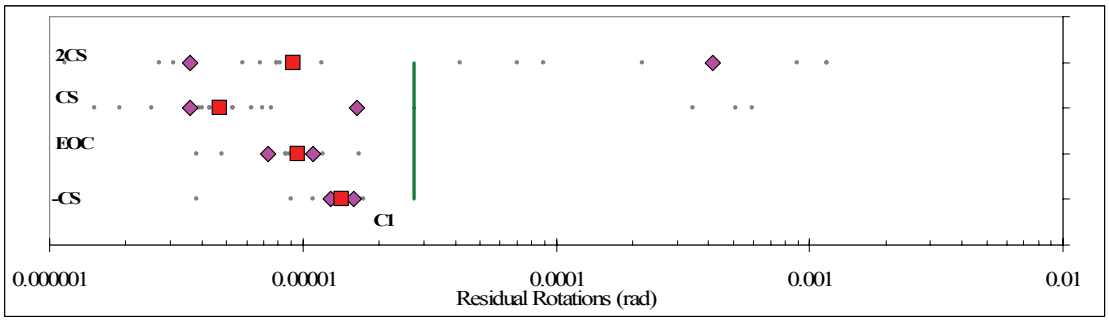

Figure 7-42 525 Foot Span – Influence of Pre-Earthquake Stress on Residual Midspan Joint Rotations

In summary, the pre-earthquake stress-state influenced the response of the 525 foot span segment joints and resulted in a median joint response that reached the

CT1 performance limits states. This occurred most often near midspan where the effects of creep and shrinkage were more pronounced. For example, cracking and joint opening was observed at midspan due to all pre-earthquake conditions, however yielding of the main tendons, i.e. limit state MT2, was exceeded only due to the +2CS stress-state.

It is important to consider that while the results indicated that crushing of the extreme superstructure fibers (i.e. $\varepsilon_c < -0.0021$) and yielding of the main tendons (i.e. $\varepsilon_{pt} > 0.012$) near midspan may occur, the damage at the top of Pier 5 developed a full plastic hinge and exceeded the spalling limit state (i.e. $\varepsilon_c < -0.004$) and will likely require more repair than the superstructure.

7.3.2.4. Superstructure Segment Joint Response Summary

The median positive, negative and residual joint rotations, for the worst cast pre-earthquake stress-state are shown on the monotonic push results in Figure 7-43 and Figure 7-44 for the pier and midspan joints, respectively. These figures also indicate the performance limit states, thus the approximate level of damage is also shown in these figures. In general, the first joint adjacent to the pier and the joint at midspan exhibited the largest rotational response and the most damage.

Figure 7-43 indicates that all joints adjacent to the piers performed in a similar manner, showing some joint opening, but not exceeding any significant damage limit state.

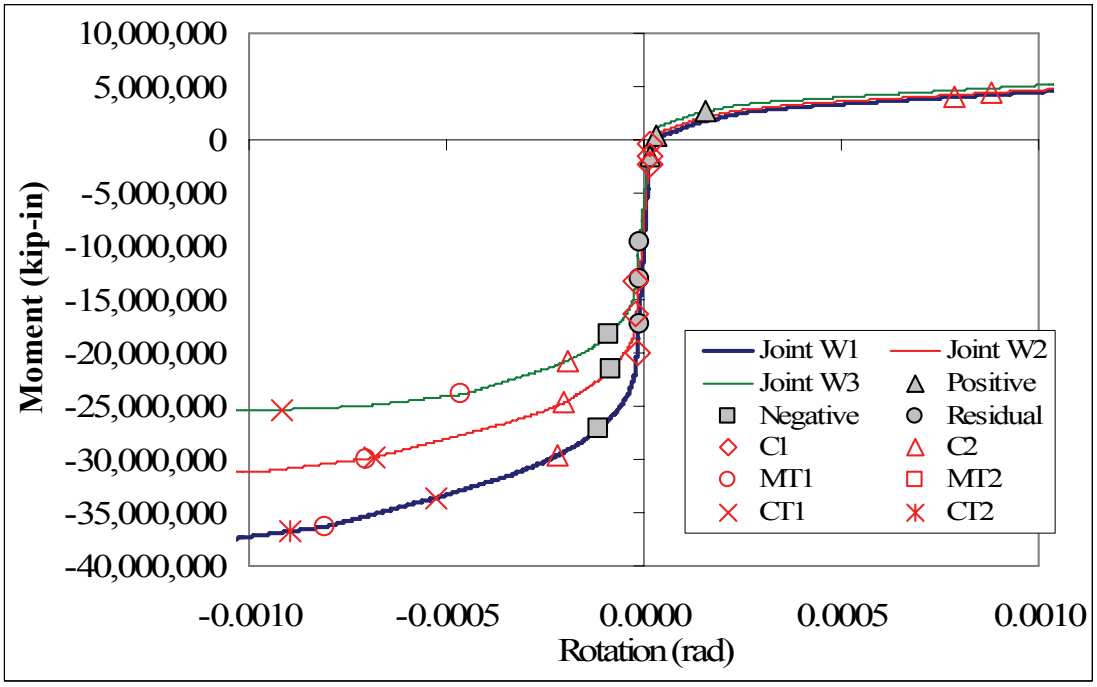

Figure 7-43 525 Foot Span - Summary of Worst-Case Joint Response Adjacent to Piers

Figure 7-44 indicates that all joints near midspan exceeded the limit of proportionality of the main tendons due to positive bending, with the midspan and the W8 joint families exceeding full yield of the main tendons and reaching the limit of proportionality of the continuity tendons. The W9 joint family showed less damage due to a larger pre-earthquake compression stress across the joint as shown

in Figure 6-52 to Figure 6-55. Under negative bending, only the midspan joint exceeded the crushing limit state.

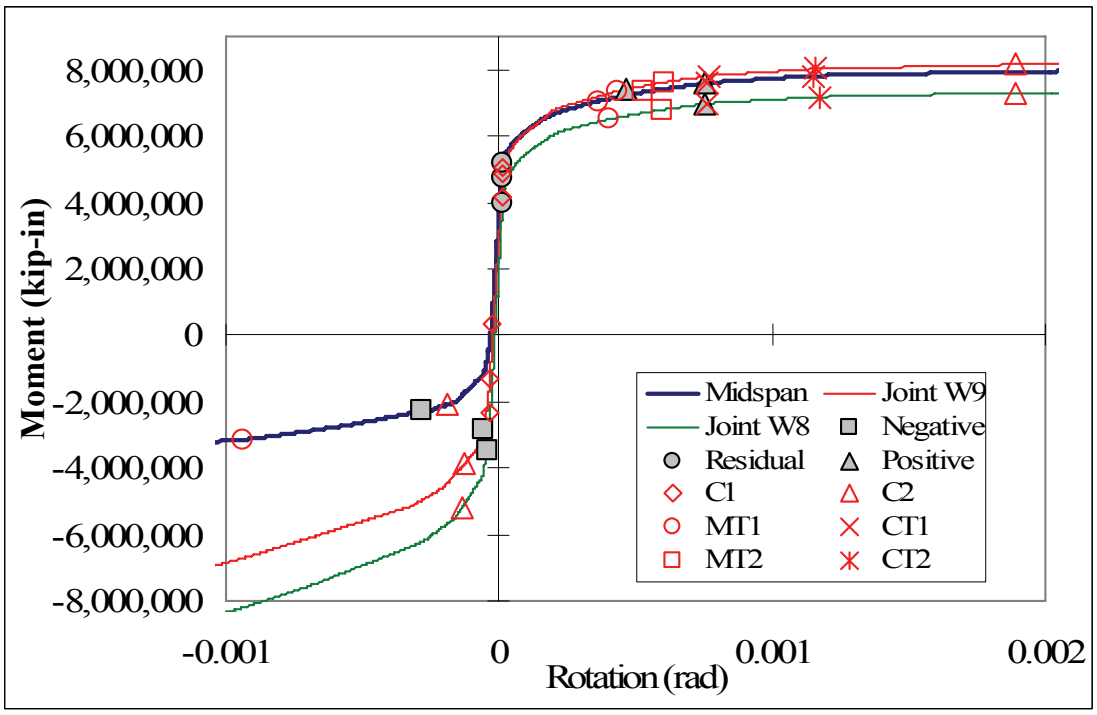

Figure 7-44 525 Foot Span - Summary of Worst-Case Joint Response Near Midspan

7.4. Longitudinal Response Study

The median scaled ground motions discussed in Sections 5.2 through 5.4 matched the horizontal design spectrum reasonably well up to a period of 2.0 seconds. The horizontal response at periods above 2.0 seconds, however, was significantly below the design spectrum. This was most evident in the displacement

response spectrum shown in Figure 5-9. The primary concern with this characteristic of the earthquake suite was that the structure would soften upon yielding of the piers and would be subjected to input energy that was less than that required by the design spectrum. This may result in displacement demands on the structure that were smaller than specified in the design criteria. Complicating the issue was the fact that impact with the abutment or between adjacent frames would stiffen the structural response and may negate any softening effects due to pier yielding. To study the impact of the response above 2.0 seconds, three spectrum compatible records were developed, as discussed in Section 5.5.

7.4.1. 300 Foot Span Model

Figure 7-45 compares the median peak drift ratio of the twenty range scaled records (i.e., "Range") with the median of the three spectrum compatible records (i.e., "SC"). On average the median peak pier drift ratio increased by 2% with the spectrum compatible ground motions, indicating that the input energy above a period of 2.0 seconds did not significantly influence the longitudinal response of the piers.

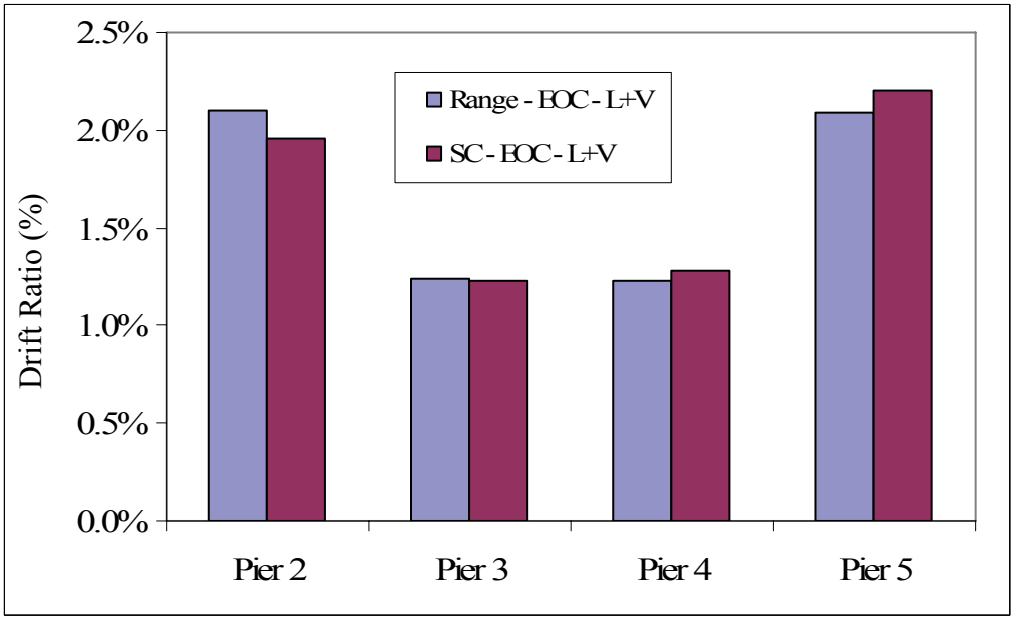

Figure 7-45 300 Foot Span – Longitudinal Study - Peak Drift Ratio Comparison

7.4.2. 525 Foot Span Model

Figure 7-46 compares the median peak drift ratio of the twenty range scaled records (i.e., "Range") with the median of the three spectrum compatible records (i.e., "SC"). On average the median peak pier drift ratio decreased by 2% with the spectrum compatible ground motions, indicating that the input energy above a period of 2.0 seconds did not significantly influence the longitudinal response of the piers.

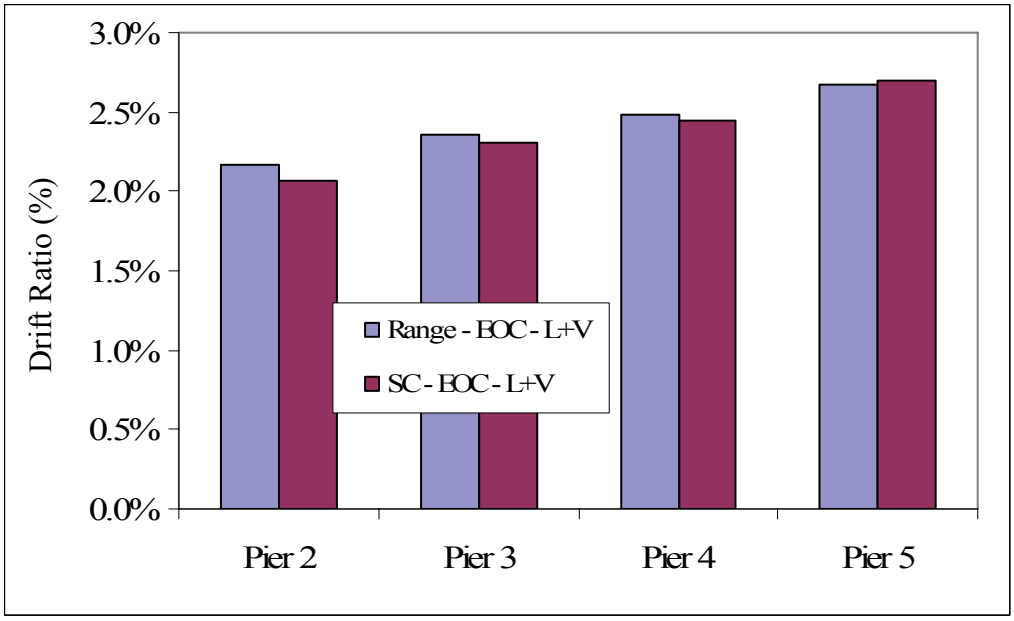

Figure 7-46 525 Foot Span – Longitudinal Study - Peak Drift Ratio Comparison

CHAPTER 8. LONGITUDINAL PT SENSITIVITY STUDY

The aim of the current seismic design philosophy for bridges is to prevent non-linear behavior in the superstructure by forcing in-elastic action to occur in the columns (see Section 2.4). Recent research, as discussed in Section 3.4, has shown that precast segmental superstructures can experience modest non-linear elastic behavior without effects to the service load carrying capabilities. Perhaps if the current design philosophy is changed such that the superstructure is designed to allow some non-linear elastic behavior, the longitudinal PT can be reduced. This chapter investigates the response of full scale precast segmental bridges with reduced longitudinal PT in the superstructure.

It is important to note that the design of the PT tendons for many segmental bridges is governed by either service or construction load cases and not earthquake load cases. Thus the results in this Chapter may not be an issue for many bridges. For other bridges, however, earthquake load cases may govern the tendon design and PT beyond that required for service conditions are required. For instance, the San

Francisco-Oakland Bay Bridge Skyway utilized low stressed auxiliary deck tendons in the superstructure to ensure that potential opening of segment joints remained small and closed completely following the earthquake. This deck continuity PT can be 10% of the total PT in the superstructure.

For simplicity and for ease of comparison between bridges of different span lengths, discrimination between various types of superstructure tendons (i.e. cantilever tendons, continuity tendons, deck tendons) was not done. Thus cantilever tendons were reduced in the same proportions as deck continuity tendons. From a practical construction point of view, it may be easier to simply eliminate all deck continuity PT rather than reducing all PT equally.

All ground motions for the PT sensitivity study were scaled using the method based on the primary natural period and the pre-earthquake joint stress-state was based on the best estimate of the stresses at both the end of construction and after creep and shrinkage losses. Some of the figures in this section remind the reader of this fact with the notation “T=2”, “EOC”, and “CS” in the legend.

8.1. Modeling Considerations

Section 7.3 showed that the pre-earthquake segment joint stress-state can impact the seismic response of segmental superstructures. Thus it was very important to accurately estimate the segment joint stress-state for the reduced PT condition. Difficulties in doing this arose from the fact that the structure was changing during construction and different tendons were installed and stresses at different stages during construction. For example, the cantilever tendons were installed and stressed when the structure was a simple cantilever. However, continuity tendons are stressed when the structure was a continuous frame. Thus, obtaining the pre-earthquake stress-state for the reduced PT condition using the model alone, that is based on the full PT pre-earthquake stress-state and then removing PT in the model, was insufficient. This would be effectively removing the tendons from a fully completed structure and not constructing a bridge with a smaller amount of PT. The approach used to obtain the pre-earthquake stress-state for the different span lengths is discussed below.

8.1.1. 300 Foot Span

Recall from Section 6.2, that the 300 foot span bridge was based on select details from the Otay River Bridge and to accurately consider construction staging effects on the pre-earthquake stress-state, the results of a full longitudinal construction staging analysis were obtained. These results were broken down into the contributions of various load cases, including dead load, superimposed dead load, PT, creep and shrinkage, and PT losses, to name a few. The pre-earthquake stress-state for the reduced PT models was obtained simply by multiplying the PT load cases by a scale factor. All other load cases were kept unchanged. The LCA considered the state of the bridge when the PT was stressed, thus a simple scale factor on the components of the LCA was reasonable. While this approach does not consider interactions between PT and creep and shrinkage, it was considered to be an acceptable approximation.

The PT was reduced in 10% increments until a tension stress-state was observed. It is important to reiterate that service load cases were not checked. In effect it was assumed that seismic governed the design of the PT. Tension was

observed near the piers when 70% of the full PT was used. Thus 80% of the full PT was investigated further.

Two different pre-earthquake stress-states were studied. These were at the end of construction and after creep and shrinkage losses occurred. These two stress-states were investigated because they were considered the most realistic, given the assumptions on determining the effects of reduced PT on the superstructure. The procedure for determining these pre-earthquake stress-states is described below.

1. Reduce PT axial force and PT bending moments from LCA by 20% (see Figure 8-1 and Figure 8-2)
2. Reduce PT area and pre-tension force in the model
3. Iterate on joint stresses until convergence with target EOC stresses based on reduced PT (see Figure 8-3 and Figure 8-4) For a description of the iteration process see Section 6.2.5.1.
4. Run earthquakes and vertical monotonic push-over analyses.
5. Repeat steps 1 to 4 using CS stresses.

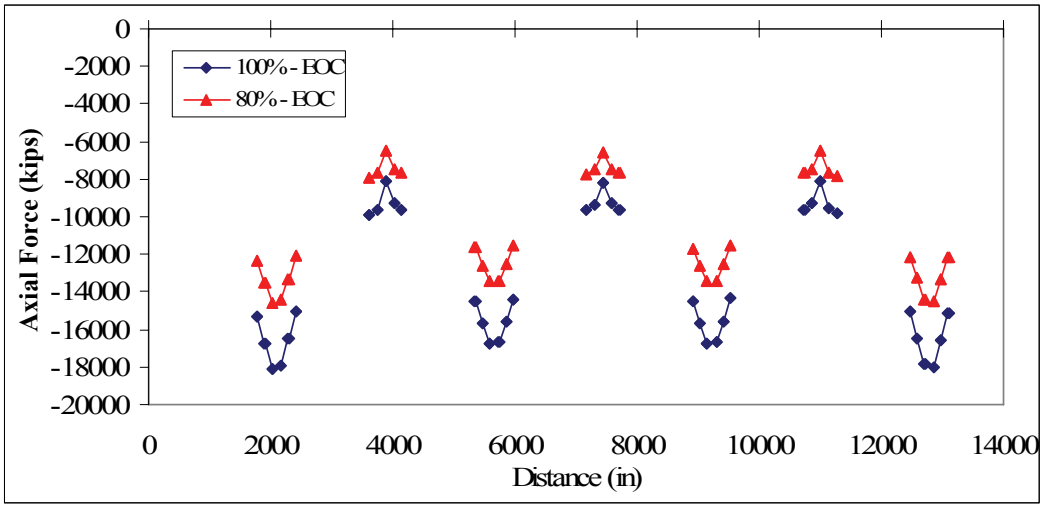

Figure 8-1 300 Foot Span - Reduced PT Axial Force Comparison

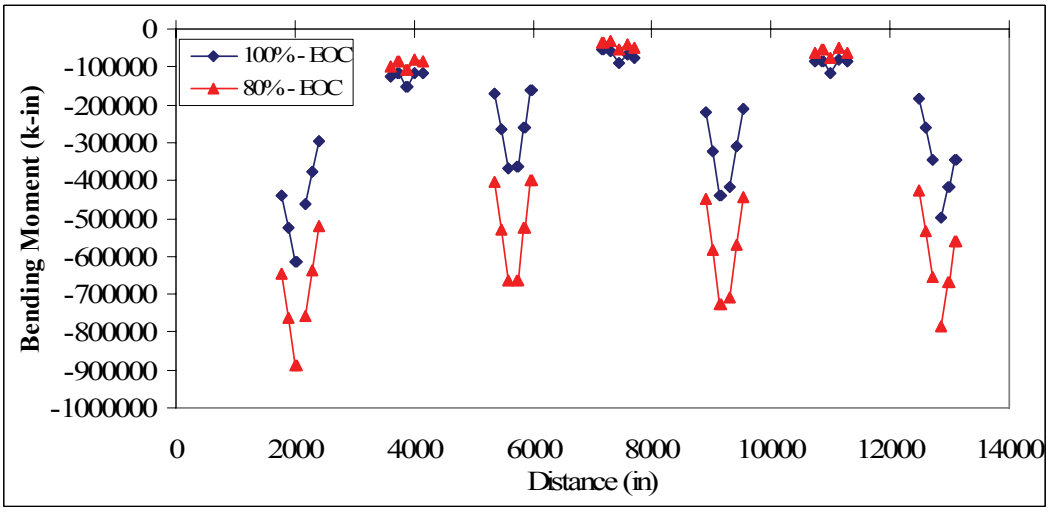

Figure 8-2 300 Foot Span - Reduced PT Bending Moment Diagram Comparison

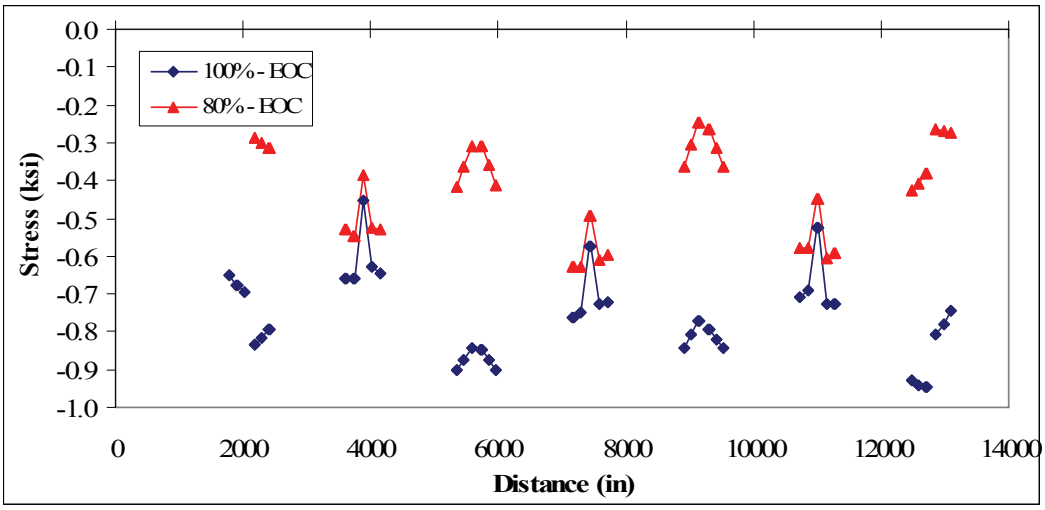

Figure 8-3 300 Foot Span - Reduced PT Top Fiber Stress Comparison

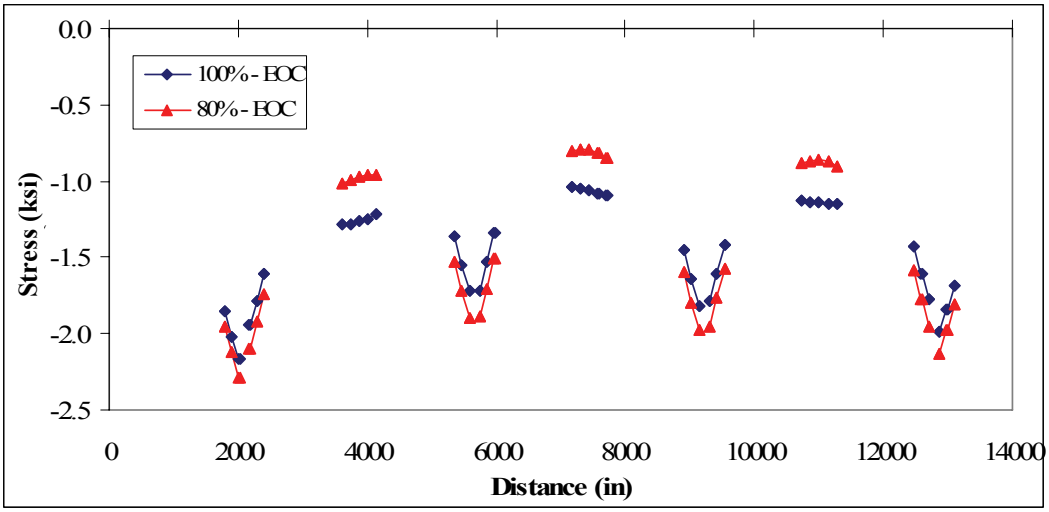

Figure 8-4 300 Foot Span - Reduced PT Bottom Fiber Stress Comparison

The average effect of the reduced PT on the extreme fiber stresses is shown in Figure 8-5. Reducing the PT reduced compression at all locations except at the bottom fibers near the piers, with the top fibers near the pier showing the largest compression reduction. It is interesting to recall that the effects of creep and shrinkage exhibited similar stress changes (see Figure 6-21). However, the behavior

was different. Creep and shrinkage impacted the stress near midspan most while the stresses adjacent to the piers were most sensitive to reduction in the PT.

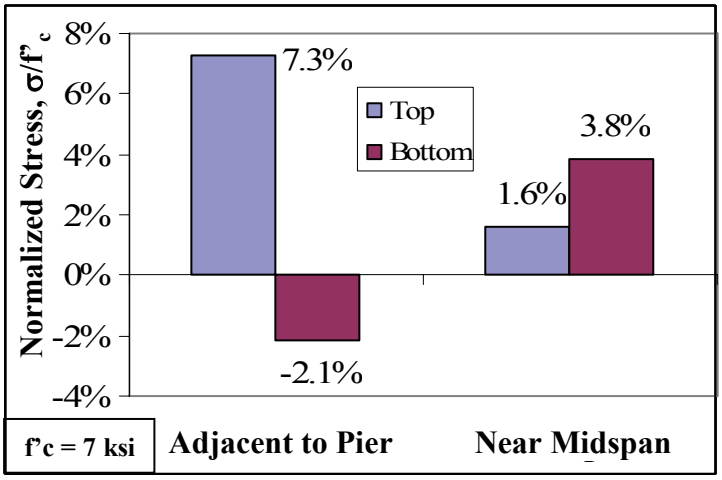

Figure 8-5 300 Foot Span - Average Normalized Stress Change due to Reduced PT

8.1.2. 525 Foot Span

The LCA results obtained from the contractor for the 525' span bridge were not broken down into components, thus estimation for the reduced stress-state, was not as straight forward as the 300 foot span model. The main difficulty arose from the fact that the structural state of the bridge changed during construction. The model developed for this study was able to accurately estimate the effect of the reduced PT tendons that were stressed when the bridge was a continuous frame, however, it could not accurately estimate the effects of the reduced cantilever tendons. Thus, effects of reducing the cantilever tendons were determined based on

hand calculations and the calibration process described in Section 6.2.5.1. The procedure is described below.

1. Calculate axial force and bending moments due to cantilevers PT only, as all other PT was stressed on the completed bridge structure.
2. Determine the difference in axial force and bending moment due to reduced PT.
3. Subtract out the difference calculated in step 2 from EOC axial forces and bending moment diagrams (See Figure 8-6 and Figure 8-7).
4. Calculate reduced PT EOC stresses.
5. Iterate until convergence. In the model use reduced cantilever PT (i.e. cross section area and pre-tension force) but 100% of non-cantilever PT.
6. After convergence with the extreme fiber stresses, reduce the non-cantilever PT (i.e. cross section area and pre-tension force) in the model to obtain the stress-state based on the reduced PT (See Figure 8-8 and Figure 8-9).
7. Run earthquakes and vertical monotonic push-over analyses.
8. Repeat steps 1 to 7 for the CS stress-state.

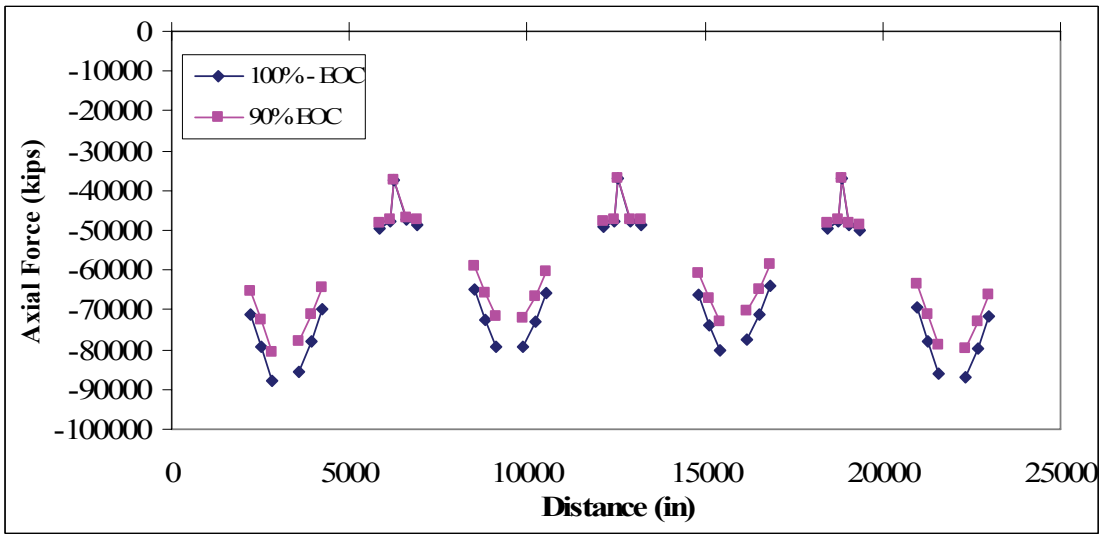

Figure 8-6 525 Foot Span Reduced PT - Axial Force Comparison

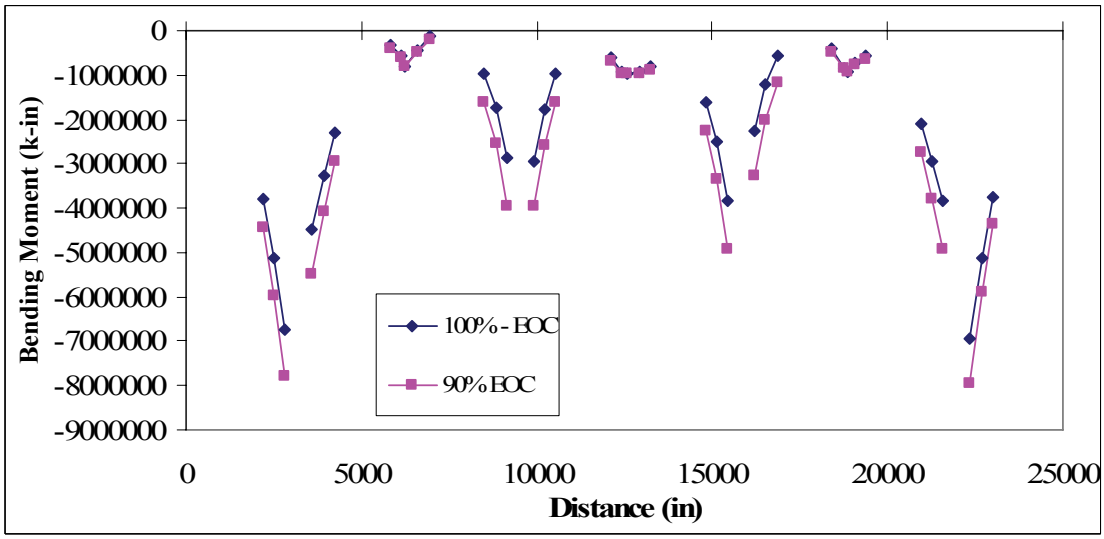

Figure 8-7 525 Foot Span Reduced PT - Bending Moment Comparison

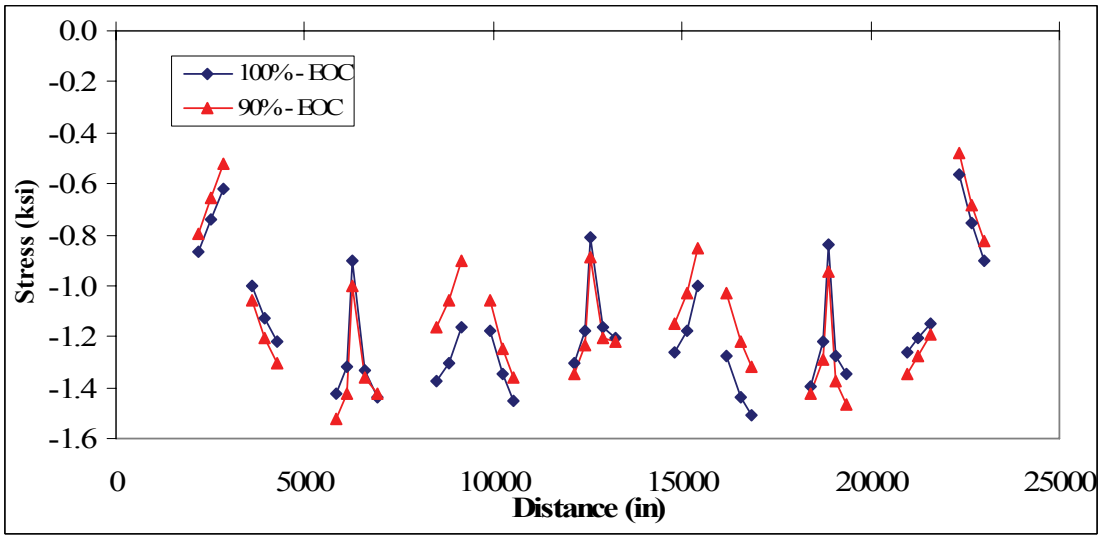

Figure 8-8 525 Foot Span Reduced PT – Top Stress Comparison

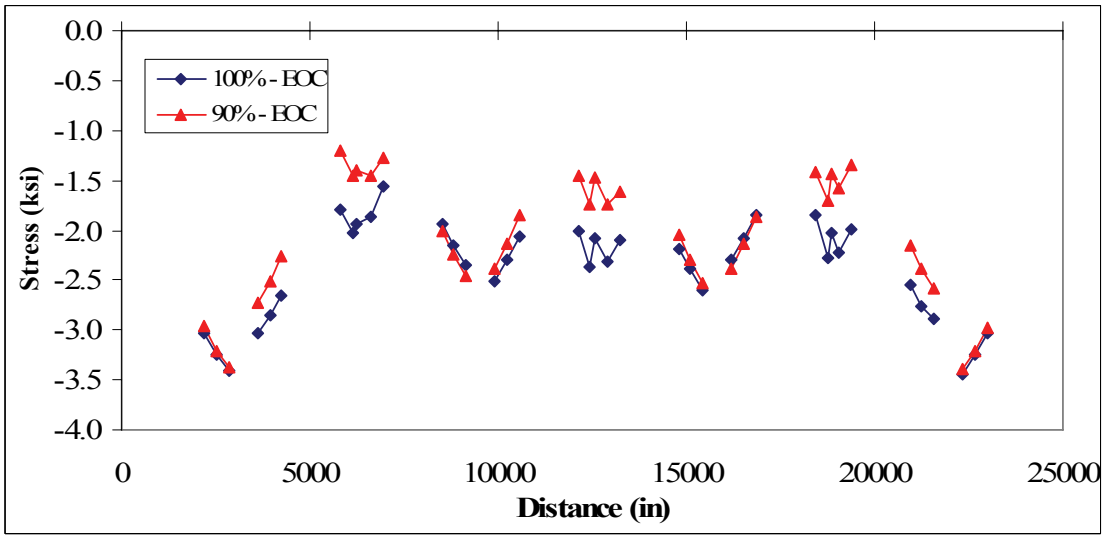

Figure 8-9 525 Foot Span Reduced PT – Bottom Stress Comparison

Figure 8-10 indicates the average effect of the reduced PT on the extreme fiber stresses. Reducing the PT reduced compression at all locations except at the top fibers near midspan, with the bottom fibers near midspan showing the largest compression reduction. It is interesting to recall that the effects of creep and

shrinkage exhibited a similar behavior (see Figure 6-49). This behavior is not the same as the 300 foot span model, likely due to the influence of the continuity PT on the response of the structure.

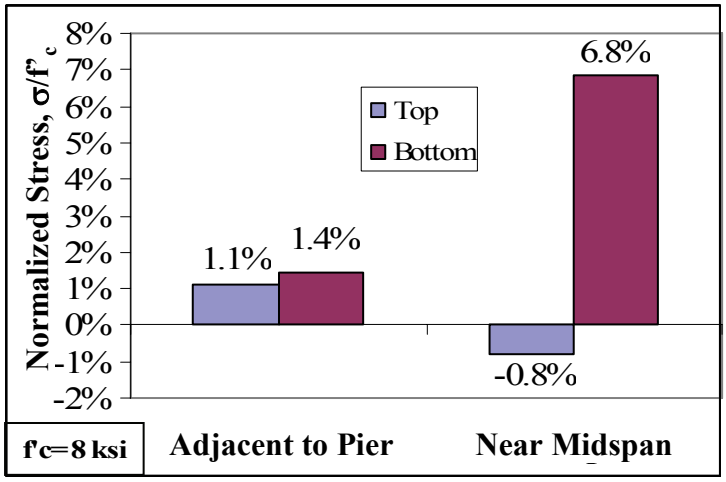

Figure 8-10 525 Foot Span - Average Normalized Stress Change due to Reduced PT

8.2. Longitudinal PT Sensitivity Study Results

The results of a longitudinal PT sensitivity study are presented below. The models were subjected to a suite of 20 earthquake records with both longitudinal and vertical components of ground motion. The records were scaled to match the design spectrum at the natural period of the structure. Two different pre-earthquake stress-

states and two different PT configurations were considered for both the 300 foot and the 525 foot span models.

8.2.1. 300 Foot Span

8.2.1.1. Vertical Monotonic Pushover Analysis

Vertical monotonic pushover analyses were performed to obtain the backbone curve for the moment-rotation behavior of each segment joint, and to identify the rotation where various performance limit states occurred. The limits states were defined per Table 6-3. The results of these vertical monotonic pushover analyses for Joint D1/U1 and midspan are shown in Figure 8-11 and Figure 8-12, respectively. The results from only these two joints are presented as they were considered to be representative of the response adjacent to the piers and near midspan as shown in Section 7.3.1.4. In general, the rotations at which the limits states occurred reduced slightly with the reduced PT, except for the crushing limit state, C2, which increased slightly.

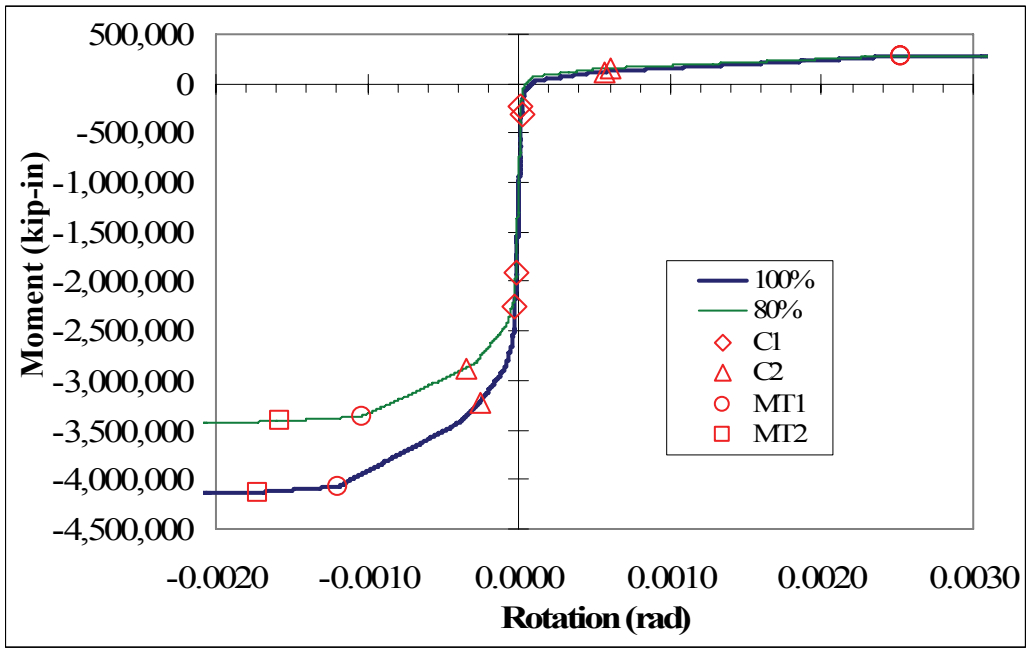

Figure 8-11 300 Foot Span - Reduced PT – Joint D1/U1

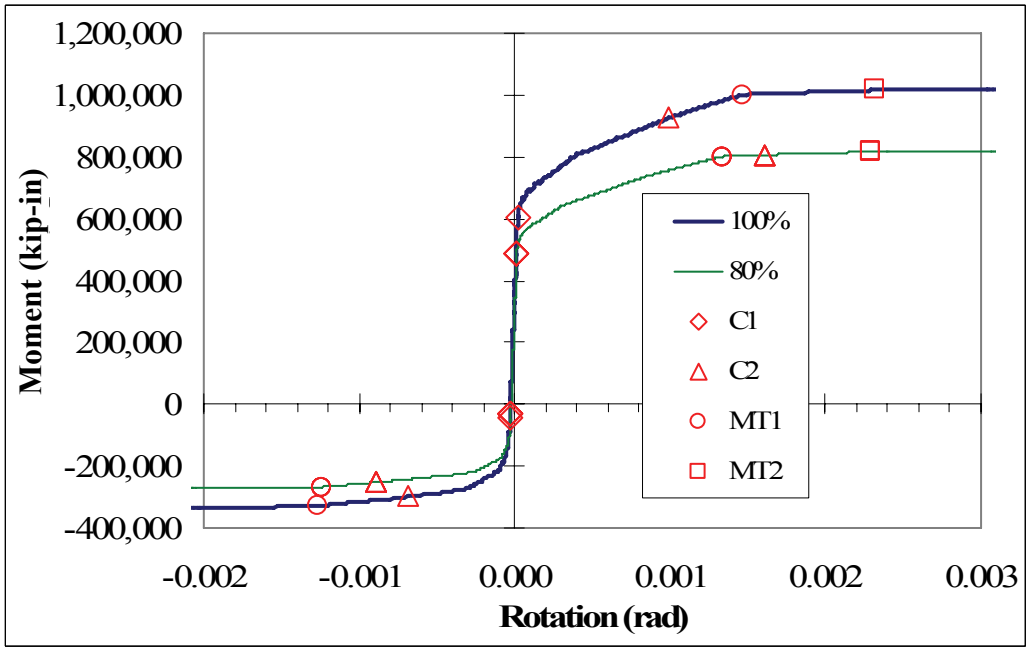

Figure 8-12 300 Foot Span - Reduced PT – Midspan Joint

8.2.1.2. Pier and Abutment Response

Figure 8-13 shows the median value of the peak longitudinal drift ratio from the twenty earthquake records. It is clear from this figure that neither the superstructure PT nor the superstructure pre-earthquake stress-state affected the longitudinal response of the bridge. Thus, the pier and abutment damage presented in Sections 7.3.1.1 and 7.3.1.2 apply here as well. Piers 2 and 5 developed full plastic hinges and experienced spalling, while a gap of 9 to 10 inches may be generated at the abutment due to yielding of the soil behind the abutment back wall.

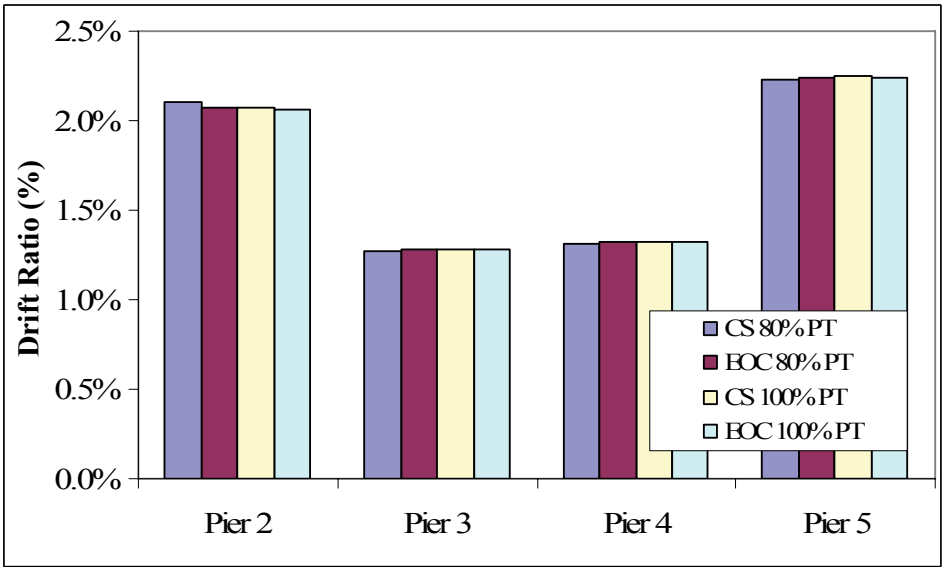

Figure 8-13 300 Foot Span - Reduced PT - Longitudinal Pier Drift Ratio

8.2.1.3. Superstructure Segment Joint Response

Figure 8-14 to Figure 8-19 compare the rotations from the 100% and 80% PT models with their respective limit states for the first joint adjacent to the piers, i.e. Joint D1/U1, and the midspan joint. The response of the reduced PT models at both the end of construction and after creep and shrinkage has occurred are compared with the 100% models. Each gray dot represents the peak rotation from one earthquake. The square marks represent the median rotation.

Figure 8-14 shows the positive bending joint response for Joint D1/U1. This figure indicates that the median response of the reduced PT models remained below the crushing limit state and was similar to the 100% PT response.

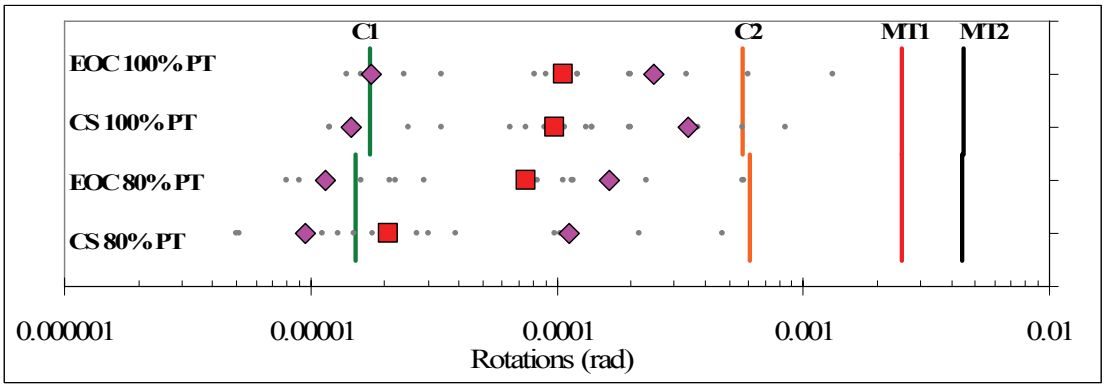

Figure 8-14 300 Foot Span - Reduced PT - Joint D1/U1 Positive Rotations

Figure 8-15 shows the negative bending joint response for Joint D1/U1. This figure indicates that the median response of the reduced PT models exceeded the

crushing limit state, yet remained below limit of proportionality of the main tendons. This was different from the 100% PT response where the median did not exceed crushing.

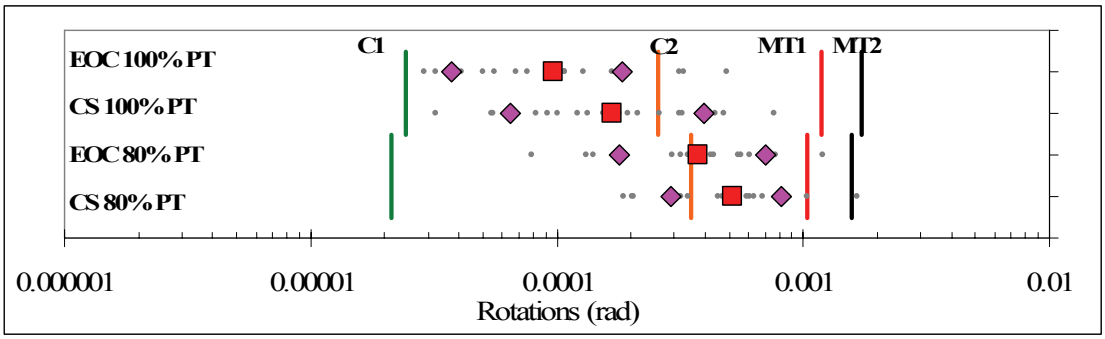

Figure 8-15 300 Foot Span - Reduced PT - Joint D1/U1 Negative Rotations

Figure 8-16 shows the residual joint response for Joint D1/U1. This figure indicates that the median response of the reduced PT models exceeded the cracking limit state, C1, after creep and shrinkage occurred. However the rotations were very small and residual cracks widths will be on the order of 0.003 inches (see Figure 6-36). This response was different from the 100% PT response where the median did not exceed C1.

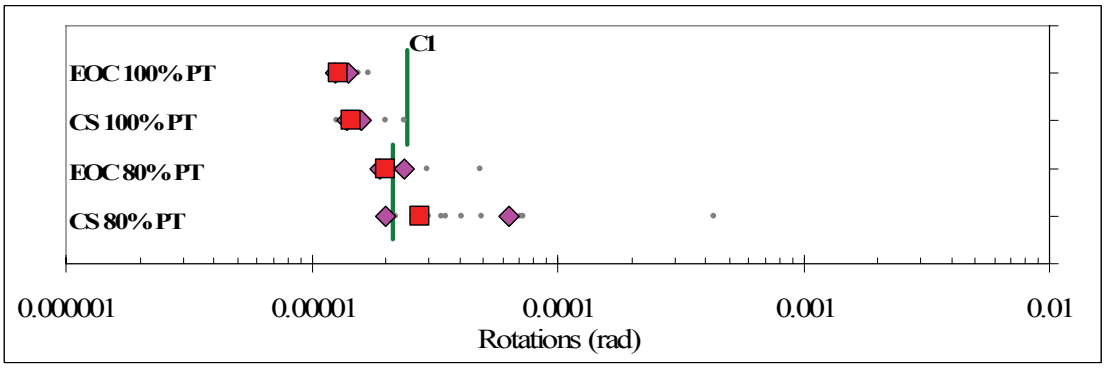

Figure 8-16 300 Foot Span - Reduced PT – Joint D1/U1 Residual Rotations

Figure 8-17 shows the positive bending moment response for the midspan joint. This figure indicates that the median response of the reduced PT models remained below the MT1 and C2 limit state and was similar to the 100% PT response.

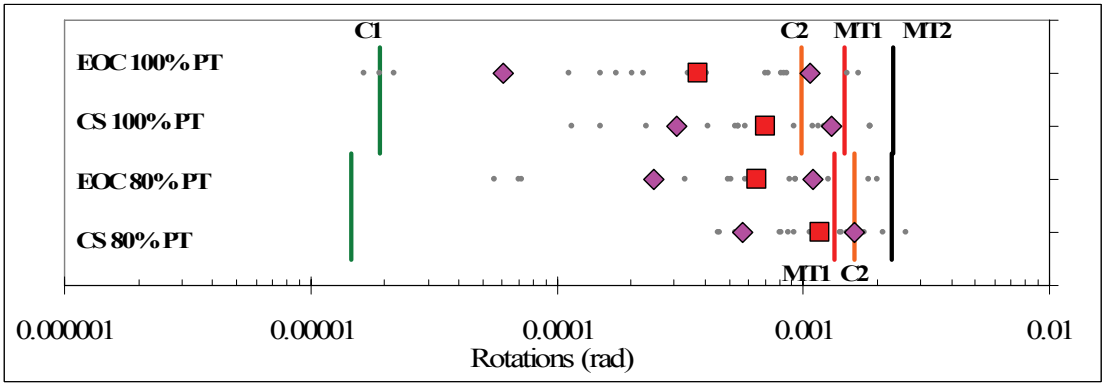

Figure 8-17 300 Foot Span - Reduced PT - Midspan Positive Rotations

Figure 8-18 shows the negative bending joint response for the midspan joint. This figure indicates that the median response of the reduced PT models exceeded the crushing limit state, yet remained below the limit of proportionality of the main

tendons when EOC stresses were considered. This response was similar to the response of the 100% PT response.

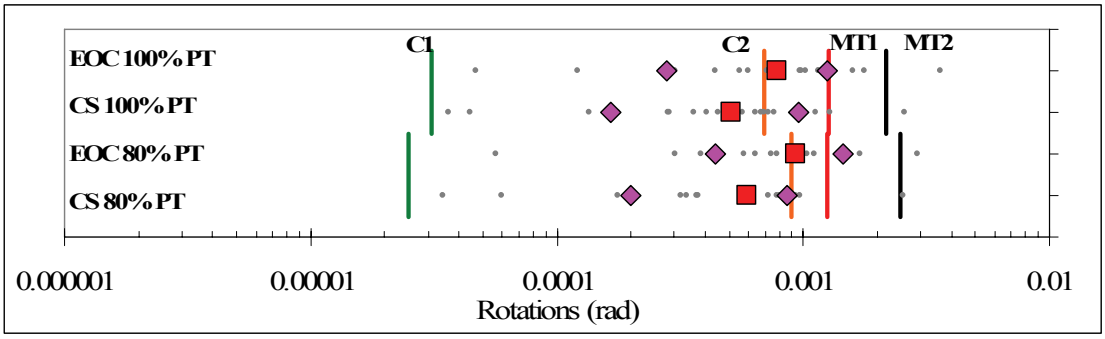

Figure 8-18 300 Foot Span - Reduced PT - Midspan Negative Rotations

Figure 8-19 shows the residual joint response for the midspan joint. This figure indicates that the median response of the reduced PT models remained below the C1 limit state and was similar to the 100% PT response.

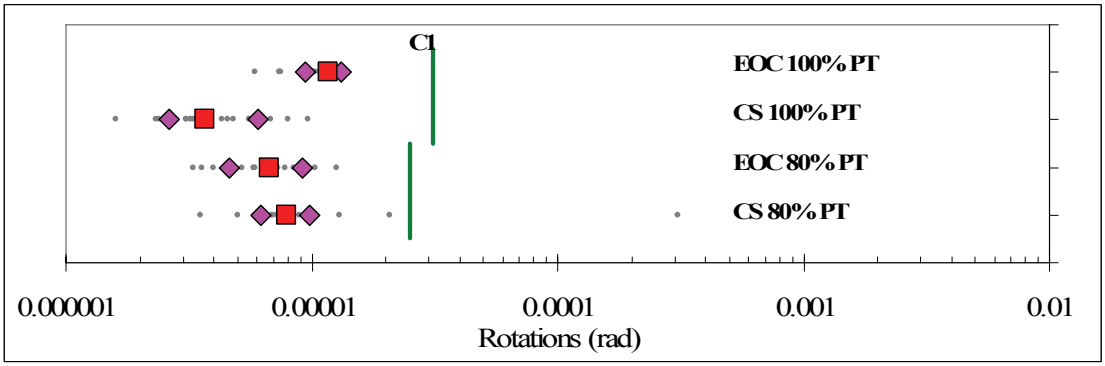

Figure 8-19 300 Foot Span - Reduced PT - Midspan Residual Rotations

In summary, the reduced PT joint median response of the 300 foot span model was similar to the 100% PT response except due to negative bending near the piers, where crushing of the bottom flange was observed. This crushing of the

bottom flange generated residual rotations that were slightly larger than the cracking limit state, indicating that the extreme top fibers exhibited a very small residual crack. This crack width was on the order of 0.003 inches (0.08mm).

It is important to consider that while the results indicated that crushing (i.e. $\varepsilon_c < -0.0016$) of the extreme superstructure fibers may occur, the damage in the short piers exceeded the spalling limit state (i.e. $\varepsilon_c = -0.004$) and required more repair than the superstructure.

8.2.2. 525 Foot Span

8.2.2.1. Vertical Monotonic Pushover Analyses

As discussed in Section 8.2.1 above, vertical monotonic pushover analyses were performed to obtain the backbone curve for the moment-rotation behavior of each segment joint, and to identify the rotation where various performance limit states occurred. The limit states were defined per Table 6-7. The results of these vertical monotonic pushover analyses for Joint W1 and midspan are shown in Figure 8-20 and Figure 8-21, respectively. The results from only these two joints are presented as they were considered representative of the response adjacent to the piers and near midspan as shown in Section 7.3.2.4. In general the rotations at which the

limits states occurred reduced slightly with the reduced PT, except for the crushing limit state, C2, which increased slightly.

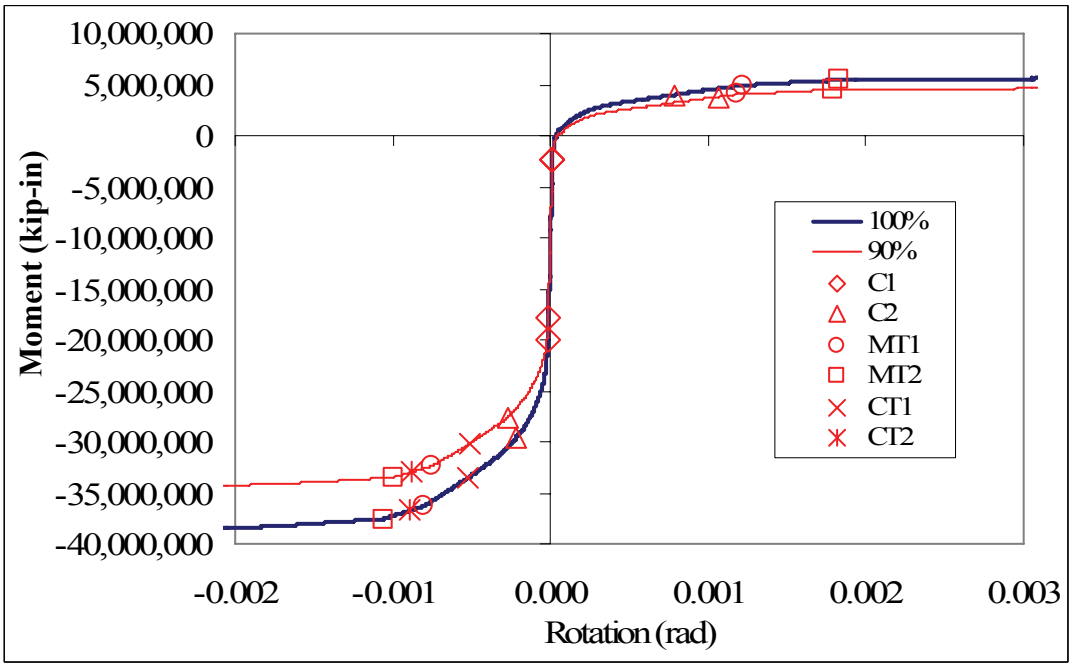

Figure 8-20 525 Foot Span - Reduced PT – Joint W1

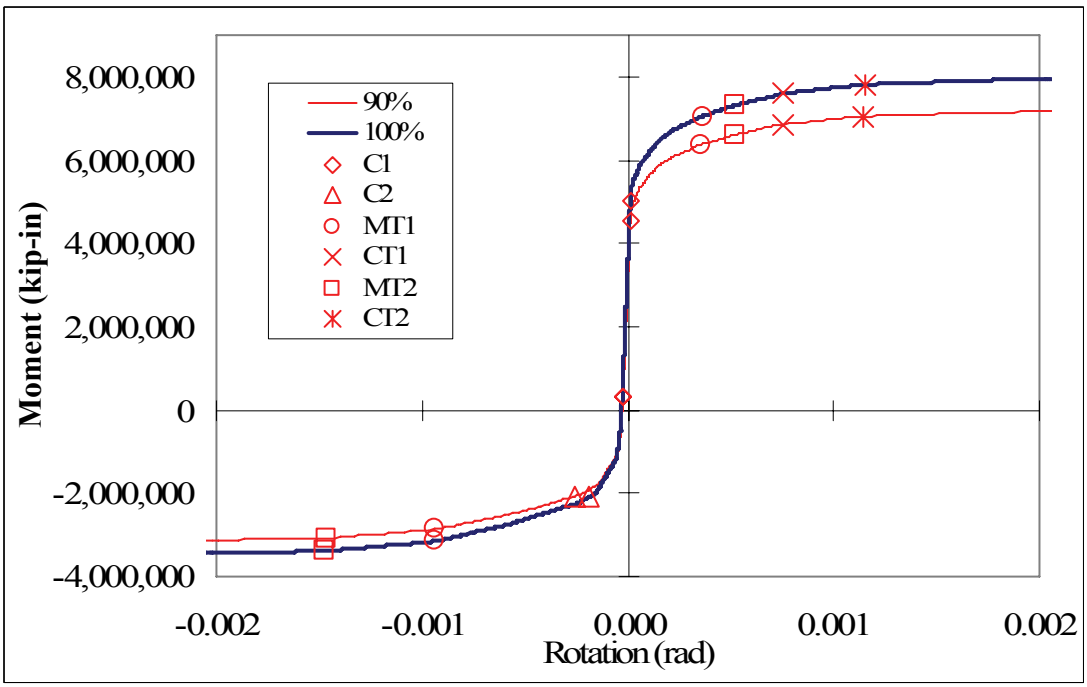

Figure 8-21 525 Foot Span - Reduced PT – Midspan Joint

8.2.2.2. Pier and Abutment Response

Figure 8-22 shows the median value of the peak longitudinal drift ratio from the twenty earthquake records. It is clear from this figure that neither the superstructure PT nor the superstructure pre-earthquake stress-state affected the longitudinal response of the bridge. Thus, the pier and abutment damage presented in Sections 7.3.2.1 and 7.3.2.2 apply here as well. Pier 5 developed a full plastic hinge near the superstructure and exceeded the spalling limit state, while a gap of 1 to 3 inches may be generated at the abutment due to yielding of the soil behind the abutment back wall.

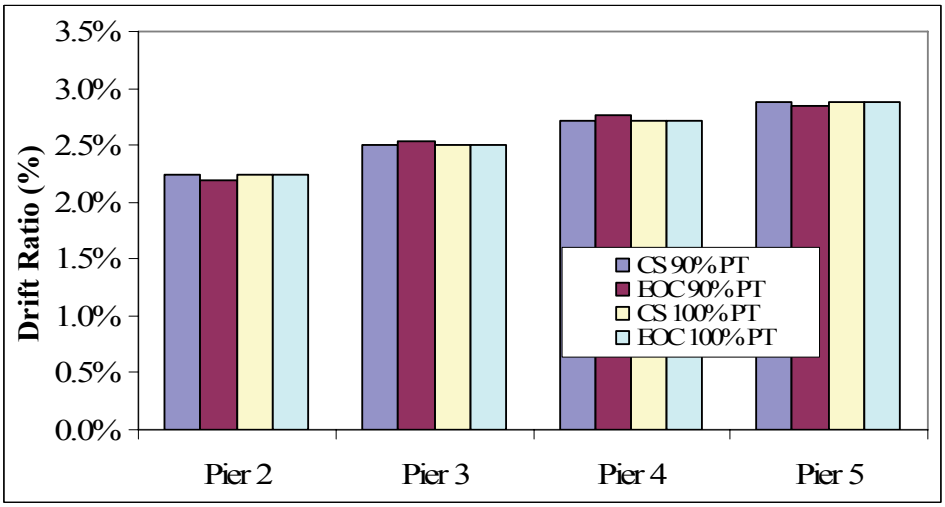

Figure 8-22 300 Foot Span - Reduced PT - Longitudinal Pier Drift Ratio

8.2.2.3. Superstructure Segment Joint Response

Figure 8-23 to Figure 8-24 compare the rotations from the 100% and 90% PT models with their respective limit states for the first joint adjacent to the piers, Joint W1 and the midspan joint. The response of the reduced PT models at both the end of construction and after creep and shrinkage has occurred are compared with the 100% models.

Figure 8-23 shows the positive bending joint response for Joint W1. This figure indicates that the median response of the reduced PT models slightly exceeded the cracking limit state yet remained well below the crushing limit state. This behavior was the same as that observed in the 100% PT models.

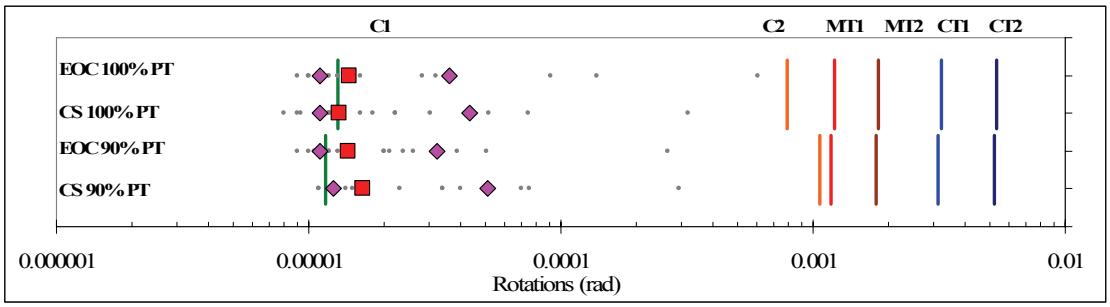

Figure 8-23 525 Foot Span - Reduced PT – Joint W1 Positive Rotations

Figure 8-24 shows the negative bending joint response for Joint W1. This figure indicates that the median response of the reduced PT models exceeded the cracking limit state, yet remained below the crushing limit. This behavior was the same as that observed in the 100% PT models.

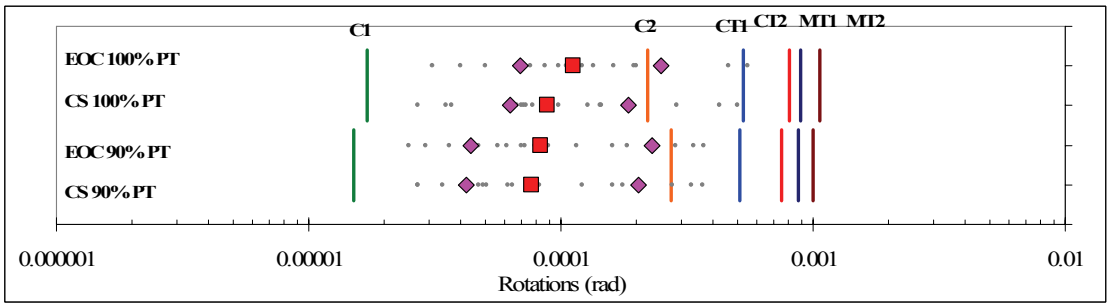

Figure 8-24 525 Foot Span - Reduced PT - Joint W1 Negative Rotations

Figure 8-25 shows the residual joint response for Joint W1. This figure indicates that the median response of the reduced PT models remained below the C1 limit state and was similar to the 100% PT response.

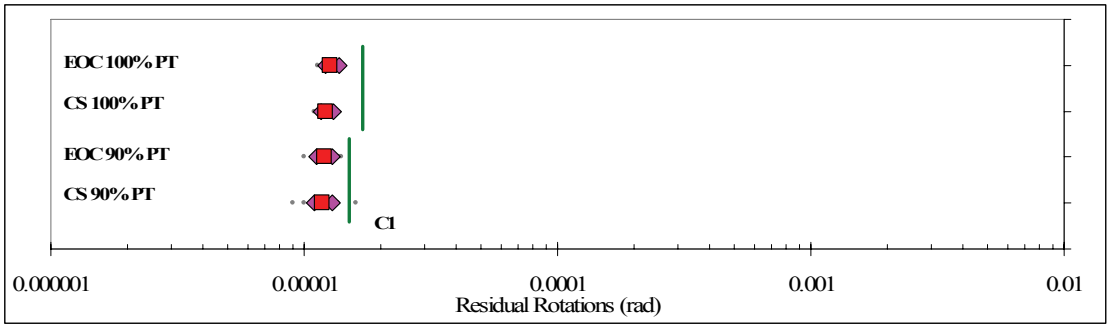

Figure 8-25 525 Foot Span - Reduced PT - Joint W1 Residual Rotations

Figure 8-26 shows the positive bending joint response for the midspan joint. This figure indicates that the median response of the reduced PT model based on the CS stress-state exceeded the both the MT1 and the CT1 limit state, and approached the MT2 limits state. This response was similar to the 100% PT models where the EOC stress-state remained below the MT1 limit sate and the CS stress state exceeded the MT1 limit state.

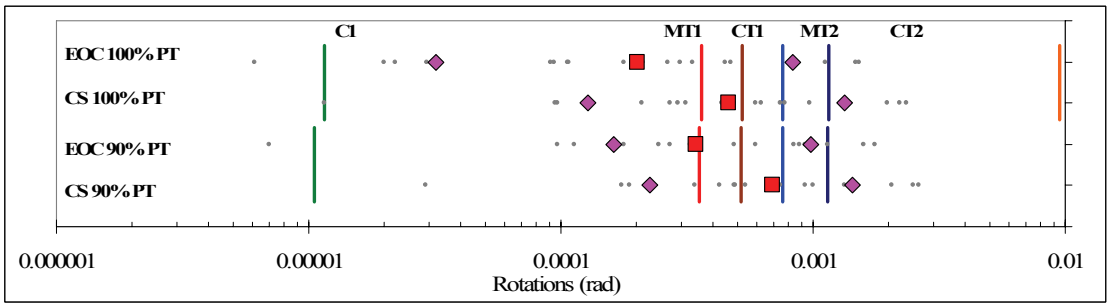

Figure 8-26 525 Foot Span - Reduced PT - Midspan Positive Rotations

Figure 8-27 shows the positive bending joint response for the midspan joint. This figure indicates that the median response of the reduced PT models exceeded the crushing limit state and was similar to the 100% PT response.

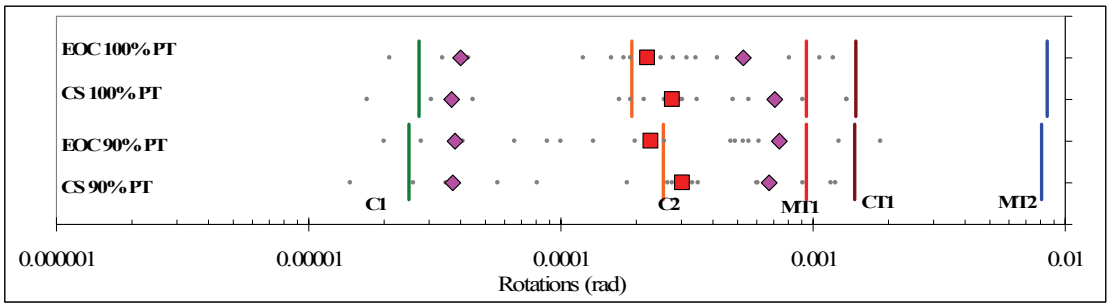

Figure 8-27 525 Foot Span - Reduced PT - Midspan Negative Rotations

Figure 8-28 shows the residual joint response for the midspan joint. This figure indicates that the median response of the reduced PT models remained below the C1 limit state. The median response was similar to the 100% PT response, however the reduced PT models exhibited significant variability of response.

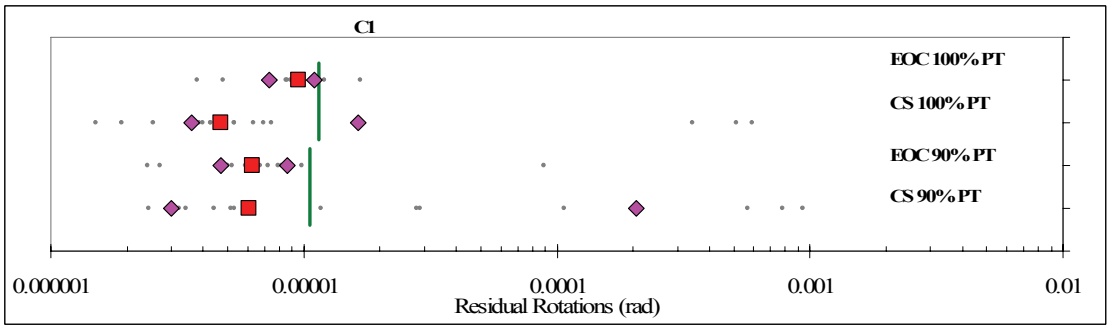

Figure 8-28 525 Foot Span - Reduced PT - Midspan Residual Rotations

In summary, the reduced PT joint median response of the 525 foot span model was similar to the 100% PT response except near midspan due to positive bending, where the limit of proportionality of both the main tendons and the continuity tendons was exceeded.

It is important to consider that while the results indicated that crushing of the extreme superstructure fibers (i.e. $\varepsilon_c < -0.0021$) and the limit of proportionality ($f_{pt} > 210$ ksi) of the main tendons and continuity tendons near midspan was exceeded, the damage at the top of Pier 5 developed a full plastic hinge and exceeded the spalling limit state (i.e. $\varepsilon_c < -0.004$) and required more repair than the superstructure.

CHAPTER 9. MODEL LIMITATIONS

The results presented in this dissertation are better understood when one fully comprehends the limitations of the model. The limitations are as follows.

- 3D effects were not considered at this time. It is important to first understand the 2D response before looking into the contributions of transverse earthquake motions on the segment joint response.
- The unbonded length of the PT tendons was based on large scale experiments with 16 – 0.6 inch strand tendons (Megally et al., 2002). This may be similar to the number of strands in bridges with 300 foot span, but is likely much smaller than tendons used in larger spans. Thus the unbonded length for larger tendons will likely be larger than that of the 16 strand tendons used in the model. This underestimate of the unbonded length will underestimate the yield rotation of the segment joints, thus the rotation capacity of the 525 foot spam bridge presented herein, are likely underestimated.
- Both the 300 foot span and 525 span bridges were modeled with longitudinal abutment soil springs. Most segmental bridges are very long, thus the

contribution of the abutment to the global response of the bridge will likely be very small. Instead there may be interaction between adjacent frames, in the form of pounding. In the end the response is expected to be similar, since the vertical component of the ground motion governed the segment joint response (see Section 7.1).

- The focus of this investigation was limited to segmental superstructures with bonded tendons. Megally et al. (2002) showed that the rotation capacity of unbonded tendons is larger than bonded tendons, thus their seismic response is expected to exhibit less damage than that presented in this study.
- The pier foundations for the 300 foot span model were assumed to be completely fixed, thereby neglecting soil-foundation structure interaction. The piers for this model were tall and flexible relative to the span length, thus adding additional flexibility in the foundation will likely not significantly alter the response of the superstructure. In addition, the vertical earthquake motion dominated the bridge response and soil structure interaction will predominately affect the longitudinal bridge response, thus the general conclusions presented in this will likely remain unchanged.

- The models were subjected to coherent earthquake excitation. Given the long spans of the bridges investigated herein, and the possibility for varying soil conditions at a given site, the seismic waves may not enter the base of the piers in a synchronized manner. Thus the assumption of coherent earthquake motion may not be correct. Incoherent ground motions may increase the demands on the segment joint.

CHAPTER 10. CONCLUSIONS

This dissertation studied the seismic response of precast segmental bridges with an emphasis on the behavior of superstructure segment joints constructed using the balanced cantilever method. The primary research tool used in this investigation was detailed 2D non-linear time history analyses. The approach to modeling the segment joints was calibrated with experimental results on large scale sub-assemblages. Analytical models of two full scale precast segmental bridges were developed based on select details from the Otay River Bridge and the San Francisco-Oakland Bay Bridge Skyway, in California. The span-to-depth ratios of the two bridge models were similar, with the 525 foot span bridge being slightly more slender and the superstructure axial load ratio, due to longitudinal PT, of the 525 foot span model was greater than the 300 foot span model by 23% adjacent to the piers and 69% near midspan.

The full bridge models were subjected to a suite of twenty near field earthquake records. These records were scaled to the design spectrum using two different methods and the effect on the bridge response was quantified. The

influence of the vertical earthquake motion was studied as well as the impact of the pre-earthquake stress-state on the seismic response of segment joints. In addition, a sensitivity study into the effect of reduced longitudinal PT on the segment joint response was performed.

10.1. Contribution of Vertical Earthquake Motions

The full bridge models were subjected to longitudinal ground motion only, as well as simultaneous longitudinal and vertical ground motions, to quantify the contribution of the vertical ground motion on the segment joint response. The models for this study were based on end of construction joint stress-states and utilized earthquake motions that were scaled to match the natural period of the bridge.

The results presented in Section 7.1 indicated that vertical earthquake motions significantly contributed to the joint response, and increased the peak negative moment joint rotations by over 500%, the peak positive moment rotations by at least 140%, yet did not affect the residual rotations. Segment joints in positive bending near midspan experienced the largest rotation increases due to vertical ground motions. These large increases were generated because the vertical ground

motion pushed the joints beyond the cracking limit state and into the non-linear range.

In general, the influence of vertical motion on the joint response decreased as span length increased. This is due to the fact that the superstructure of the 300 foot span model was stiffer than the 500 foot span model and consequently was subjected to larger vertical excitation due to the large amount of energy at low periods in near field vertical records. The effect of the vertical ground motions on the segment joint response will likely reduce significantly if the bridge site is not in close proximity to the fault, because the vertical accelerations attenuate rapidly with distance.

10.2. Joint opening

The median results presented in Section 7.3 showed that the segment joints exceeded the cracking limit state and opened gaps at the extreme fibers of the superstructure during a significant seismic event. In general, the first joint adjacent to the pier and the joint at midspan exhibited the largest rotation demands. The 300 foot span model indicated that peak gap widths adjacent to the piers and near midspan may be up to 0.05 inches and 0.15 inches, respectively. The gap widths of

the 525 foot span model were slightly smaller and were up to 0.02 inches adjacent to the piers and 0.1 inches near midspan.

10.3. Performance Limit States

Vertical pushover analyses were performed to identify the rotations where various performance limit states occurred (see Sections 6.3.4 and 6.5.4). The limits states of interest were cracking of the section (C1), crushing of the extreme concrete fibers (C2), the limit of proportionality of the main/continuity PT tendons (MT1, CT1), defined as a stress of 210 ksi, and full yielding of the main/continuity PT tendons (MT2, CT2), defined as a strain of 1.2%.

The time history results presented in Section 7.3 showed that the response of the segment joints relative to the performance limits states varied depending on the pre-earthquake stress-state. The performance limits states that were exceeded are summarized in Table 10-1. This table was generated based on the worst case pre-earthquake stress-state. In general, the first joint adjacent to the pier and the joint at midspan exhibited the largest rotational response and the most damage.

Table 10-1 Summary of Exceeded Performance Limit State

	Bridge Model	
	300 Foot Span	**525 Foot Span**
Pier Positive Rotations	C1	C1
Pier Negative Rotations	C2	C1
Pier Residual Rotations	Below C1	Below C1
Midspan Positive Rotations	C2	MT1
Midspan Negative Rotations	C2	C2
Midspan Residual Rotations	Above C1	Below C1

In the 300 foot span model, crushing of extreme concrete fibers occurred, which generated residual rotations at midspan that were larger than the cracking limit state, however these residual rotations remained very small creating crack widths of less than 0.01 inches.

The 525 foot model exceeded the cracking limit state near the piers, but did not crush the extreme concrete fibers. At midspan, however, the main tendons exceeded the limit of proportionality. All residual rotation, however remained below the cracking limit state, thus all joints closed completely after the earthquake. This was due to the fact that the majority of tendons near midspan were continuity tendons, thus serviceability was unaffected by exceeding the MT1 limit state.

The expected superstructure damage of both full bridge models was considered repairable. It is important to note that while the damage observed in the superstructure was relatively light and repairable, the damage at the piers was significantly more severe, exceeding the full plastic hinge limit state, and the concrete spalling limit state ($\varepsilon_c = 0.004$).

10.4. Pre-Earthquake Stress-State

The stress-state of concrete bridges fluctuates on a daily basis due to temperature and over the service life of the bridge due to creep, shrinkage, and relaxation. The full bridge models were calibrated with four different pre-earthquake stress-states to investigate the influence of the pre-earthquake stress-state on the seismic response of superstructure segment joints. These stress-states represented the possible range of stresses that may occur during the service life of a segmental bridge and are defined and discussed in detail in Sections 6.2.5 and 6.4.5.

The results presented in Section 7.3 indicated that the pre-earthquake stress-state can influence the seismic response of segment joints. This finding is contrary to common knowledge that volumetric changes have negligible effects on a structure's response to earthquakes. The extreme stress-states (i.e. -CS and +2CS)

generated the most damage as summarized in Table 10-1. In fact the central stress-states (i.e. CS and EOC) remained elastic except at midspan of 300 foot model, due to positive bending where crushing of the extreme fibers occured. This was because the extreme stress-state required the smallest seismic rotation demand to exceed a performance limit state.

10.5. Record Scaling

The influence of two different record scaling methods on the response of precast segmental bridge structures was studied. One method scaled the horizontal ground motion to match the design spectrum at the natural period of the structure. The other method scaled the horizontal motions for a least squares fit over a period range.

The results presented in Section 7.2 indicated that, while the impact varied from joint to joint and for positive and negative bending, on the whole, the two methods produced a similar median result. In addition, scaling to a range reduced variation in response. Thus, if only the median response is desirable, either method is acceptable.

10.6. Superstructure PT Sensitivity

The response of the full bridge models with reduced longitudinal PT in the superstructure was investigated to study the sensitivity of the segment joint response due to variations in the longitudinal superstructure PT and to see if it is possible to achieve the same level of seismic performance with less longitudinal PT. The reduced PT 300 foot span bridge utilized 80% of the full PT, while the 525 foot span model utilized 90% of the full PT. The reduced PT models were subjected to a suite of twenty near field earthquake with two different pre-earthquake stress-states. It is important to note that the conclusions presented here assumed that service load cases did not govern the design of the longitudinal superstructure PT.

The results presented in Chapter 8 showed that reducing the longitudinal PT reduced the rotation at which all the limit states occurred, except for crushing of the concrete. The performance limit states that were exceeded are summarized in Table 10-2. In general, the response of the 300 foot span model with reduced PT was similar to the 100% PT models except at the bottom fibers near the pier, where crushing generated residual rotations that were above the C1 limit state. The residual rotations were very small and created residual cracks that were less than 0.002

inches. The response of the 525 foot span model with reduced PT was similar to the 100% PT models except near midspan where both the main and continuity tendons exceeded the limit of proportionality. The results also indicated that reducing the superstructure PT did not alter the response of the abutment or piers. The piers will likely develop full plastic hinges and exceeded the spalling limit state.

Table 10-2 Summary of Peak Performance Limit State for Reduced PT Models

	Bridge Model	
	300 Foot Span	**525 Foot Span**
Pier Positive Rotations	C1	C1
Pier Negative Rotations	C2	C1
Pier Residual Rotations	Above C1	Below C1
Midspan Positive Rotations	C2	MT1, CT1
Midspan Negative Rotations	C2	C1
Midspan Residual Rotations	Below C1	Below C1

In conclusion, the response near midspan was more vulnerable to reduced PT than regions adjacent to the piers. Given the concurrent damage in the piers, and assuming service load cases do not govern the PT design, it may be possible to reduce the longitudinal PT in segmental bridge superstructures. This is particularly true for bridges at far field sites where the contribution of vertical earthquake motion

is significantly reduced. One way to reduce the PT is to eliminate the low-stressed auxiliary deck tendons which do not alter the pre-earthquake stress-state.

CHAPTER 11. DESIGN CONSIDERATIONS

Chapter 7 showed that the jointed nature of precast segmental bridges makes them susceptible to the effects of vertical earthquake motion. In addition, Chapter 7 indicated that the pre-earthquake segment joint stress-state can alter the response of segmental bridges. Thus the near field effects on vertical ground motion and the superstructure pre-earthquake stress state should be considered during the design process. This chapter investigates various methods in which these effects can be considered during the design process.

11.1. Pre-Earthquake Stress-State Design Considerations

The stress-state of pre-stressed concrete bridges changes on a daily basis due to temperature effects, particularly temperature gradients, and over the bridge service live due to creep, shrinkage and relaxation. The superstructure pre-earthquake stress-state can affect the response of segmental bridges as shown in Chapter 7. The extreme pre-earthquake stress-states (i.e. at end construction plus temperature gradient or after creep and shrinkage plus temperature gradient) typically exhibit the largest superstructure demands. However, the temperature gradient is caused by

solar radiation which heats the top of the bridge superstructure while the shaded webs and bottom soffit remain cool. This effect is increased when the bridge crosses low over water which can further cool the bridge soffit. In addition, this temperature gradient is typically largest during the hottest part of summer days, i.e. for about six hours per day during 3 months of the year. Thus combining the full temperature gradient with earthquake will result in a design combination with a return period significantly larger than the design earthquake alone is likely over conservative. However, neglecting pre-earthquake stress-states may result in undesirable superstructure damage during a design level earthquake scenario. Therefore, some consideration of these load cases is required and is discussed further in Section 11.3.

11.2. Vertical Earthquake Demand Considerations

The vertical earthquake demands can be estimated a number of ways. The demand can be approximated using an equivalent static load based on the dominant vertical modes, or using a vertical modal analysis along with a vertical design spectrum, or from a time history analysis using ground motions that are consistent with a vertical design spectrum. These different linear elastic methods are discussed and compared in greater detail below.

11.2.1. Equivalent Static Analysis

One method of approximating the vertical earthquake demands is through the use of equivalent static loads. The static loads considered here were developed based on a simple modal combination of the two dominant vertical modes of the 300 foot span model, shown in Figure 11-1. This span length is expected to be representative of future segmental bridge spans in California. Modes with less than 10% mass participation were neglected as they will not contribute significantly to bending of the superstructure. A sinusoidal equivalent static load, q, was generated based on a simple modal combination shown in Equation 11-1.

$$q_{tot}(x) = \sum_{i=1}^{2} q_i(x) = \sum_{i=1}^{2} \Phi_i(x) \Gamma_i m(x) S_{av_i} \qquad \textbf{11-1}$$

where, Φ_i is the ith mode shape, Γ_i is the participation factor of the ith mode, $m(x)$ is the unit mass at location x, and S_{av_i} is the vertical spectral acceleration of the ith mode. It should be noted that the mass distribution along the 300 foot span model and used in this calculation was such that the unit mass at midspan was 81% of the unit mass at the piers. For simplicity and to ensure a general approach that is applicable to bridges of various lengths, stiffnesses and mass distributions, the vertical spectral acceleration for all modes was assumed to be equal to the peak

vertical ground acceleration. This approach is justified because the dominant modes of future bridges are likely to be above 0.3 seconds where the vertical spectral acceleration is on the order of the peak ground acceleration. The relative sign of the modes was selected to produce the largest distributed load for the end spans (see Figure 11-2) and the interior spans (see Figure 11-3).

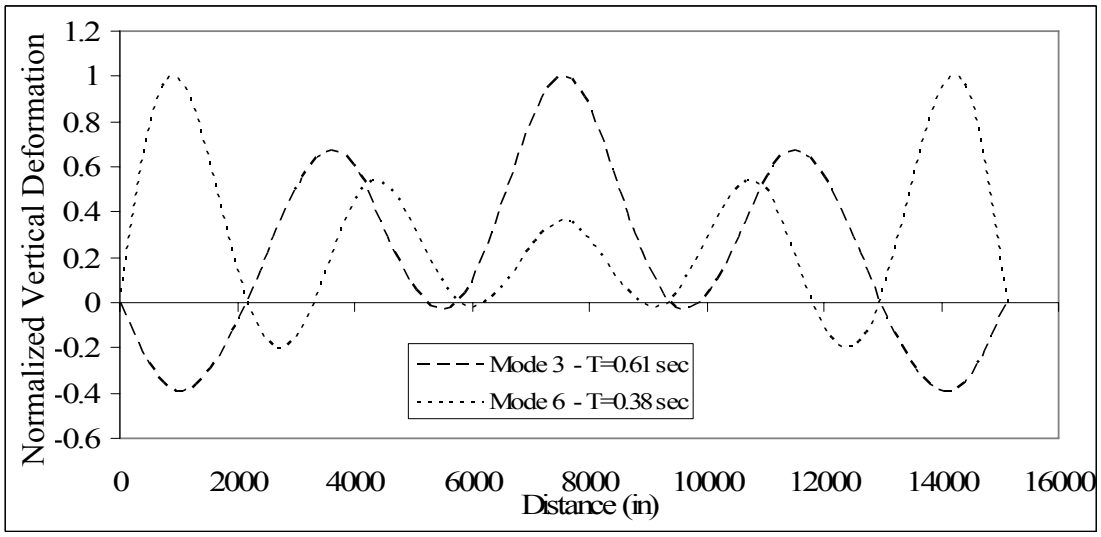

Figure 11-1 Dominant Vertical Mode Shapes

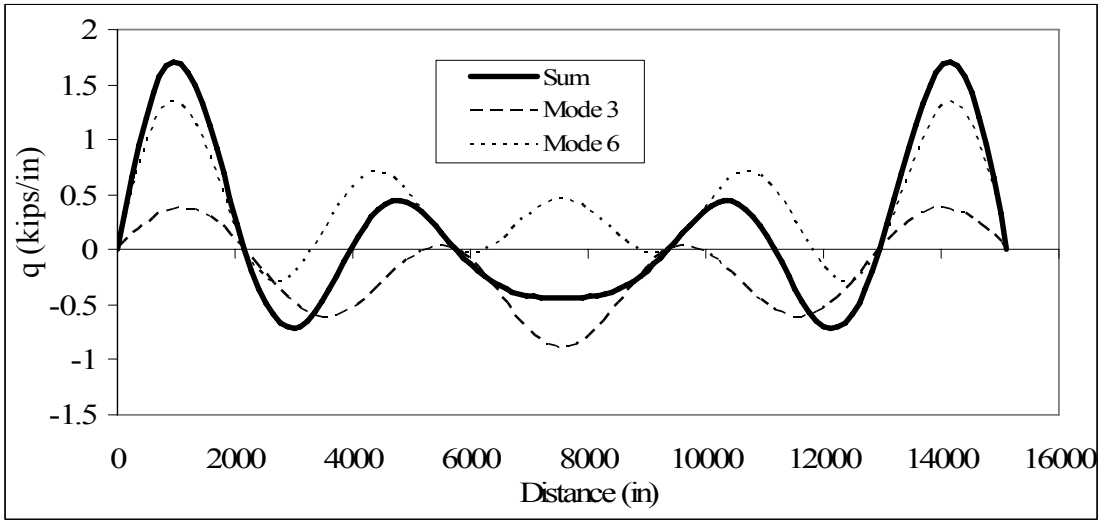

Figure 11-2 Equivalent Static Sinusoidal Loads for End Spans

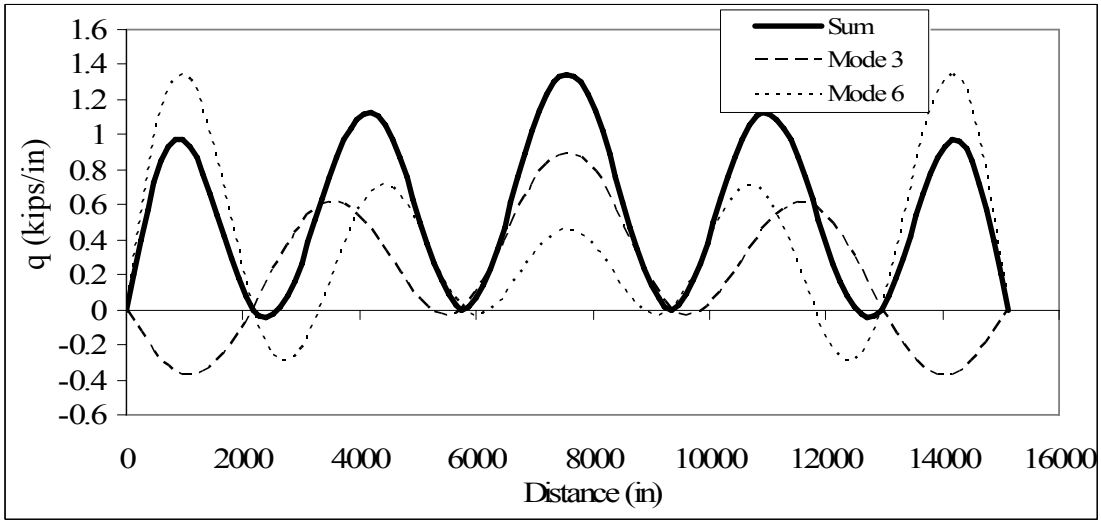

Figure 11-3 Equivalent Static Sinusoidal Loads for Interior Spans

A uniformly distributed load (UDL) is more desirable than a sinusoidal distributed load because a UDL is easier to implement in a model. A UDL that produced equivalent midspan and end moments was generated by multiplying the

sinusoidal load by 0.81 and is shown in Figure 11-4 and Figure 11-5 for the end and interior spans, respectively.

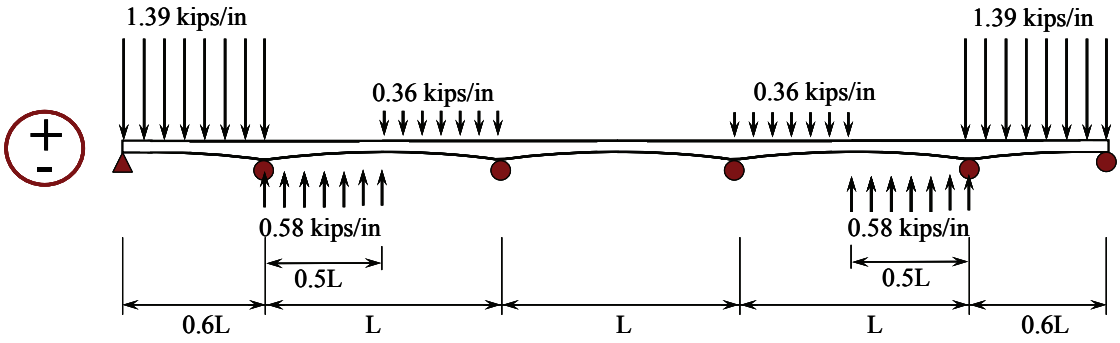

Figure 11-4 Equivalent Static Uniform Distributed Loads for End Spans

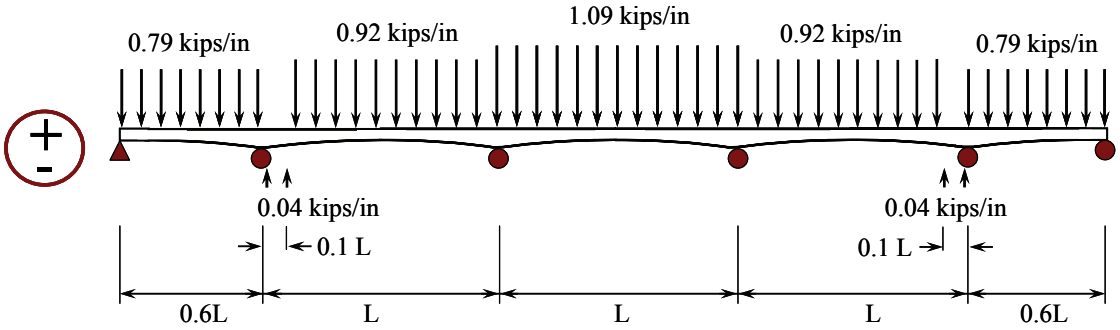

Figure 11-5 Equivalent Static Uniform Distributed Loads for Interior Spans

This equivalent static approach was intended for use with 'Ordinary' segmental bridge designs of various span lengths that will have different mass and stiffness distributions along the span. The equivalent static loads from Figure 11-4 and Figure 11-5 were generalized for use on future bridges as shown in Figure 11-6 and 11-7, where W_{end} is the weight of the end span, W_{int} is the weight of interior spans and PGA_v is the vertical peak ground acceleration. PGA_v should be less than

the peak spectral acceleration as illustrated in Figure 11-8. It may be the case that PGA_v is not indicated in this manner on the design spectrum. If this occurs, designers can determine PGA_v based on V/H spectral ratios per Bozorgnia and Campbell (2004) and shown in Figure 3-1. Multiple frame continuous bridges with midspan expansion joints that are designed to carry moment and shear across the expansion joint, similar to the detail shown in Figure 2-4 should be treated as interior spans. It should be noted that this equivalent static approach is similar to the current recommendations in the Caltrans Seismic Design Criteria (Caltrans, 2004) for 'Ordinary' bridges with horizontal peak ground accelerations greater than 0.6g (see Section 3.2), although the loading outlined above is approximately three times more severe.

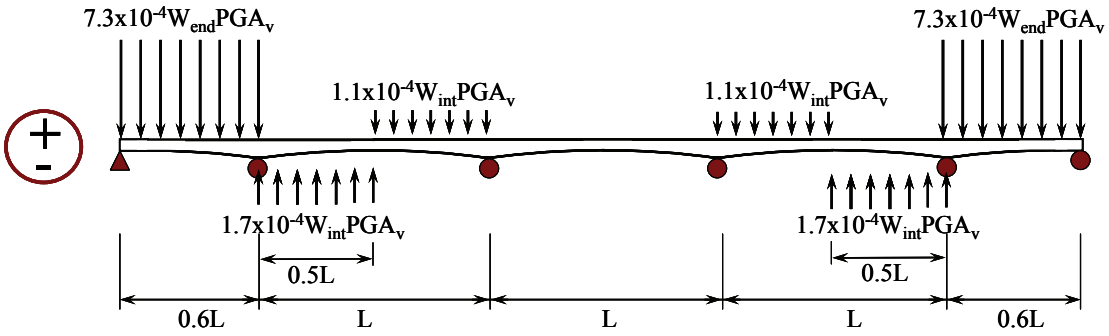

Figure 11-6 Generalized Equivalent Static Loads for End Spans

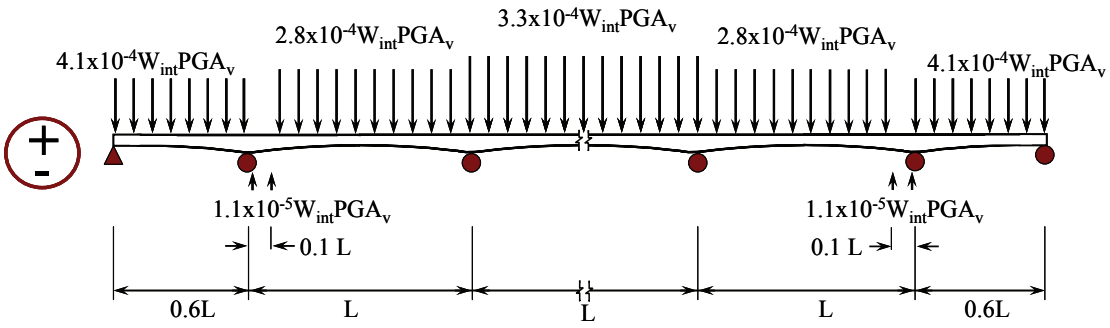

Figure 11-7 Generalized Equivalent Static Loads for Interior Spans

11.2.2. Vertical Modal Analysis

Vertical earthquake demands can be approximated based on a vertical modal analysis using the complete quadratic combination (CQC) modal combination method. Modal analysis is generally considered an acceptable tool for linear elastic structures only and thus will likely not be appropriate if non-linear response in the superstructure is anticipated. A vertical design spectrum based on recommendations by Bozorgnia and Campbell (2004), was developed, as shown in Figure 11-8. Figure 11-8 also shows the median vertical spectral acceleration of the twenty earthquake ground motions that were scaled to a period range (see Section 5.3) for comparative purposes. It is important to note that these spectra were calculated based on 5% damping.

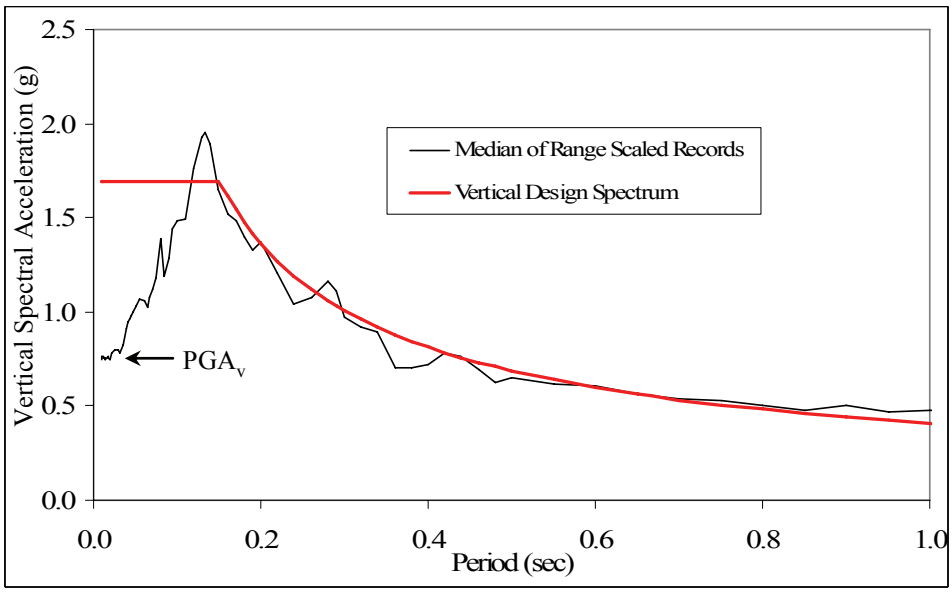

Figure 11-8 Vertical Design Spectrum

This approach is very simple to implement as modal analysis is a common option in bridge finite element software packages and the finite element model of the bridge is typically required to estimate lateral earthquake demands. All that is required is an appropriate vertical design spectrum which can be easily determined based on the horizontal spectral acceleration at a period of 0.1 seconds and an estimate of the vertical-to-horizontal spectral ratio per Bozorgnia and Campbell (2004).

11.2.3. Time History Analysis

A time history analysis is generally considered the most accurate way to estimate earthquake demands. Common practice is to use three sets of spectrum

compatible ground motions and to design the bridge for the envelope of these three motions. To this end, three vertical spectrum compatible ground motions were generated using the program WAVGEN (Mukherjee and Gupta, 2002b) and are shown in Figure 11-9 along with the target vertical design spectrum. The target spectrum was the same as the design spectrum for the vertical modal analysis shown in Figure 11-8. Time history analysis can be used for both linear and non-linear superstructure response if the superstructure segments are modeled appropriately.

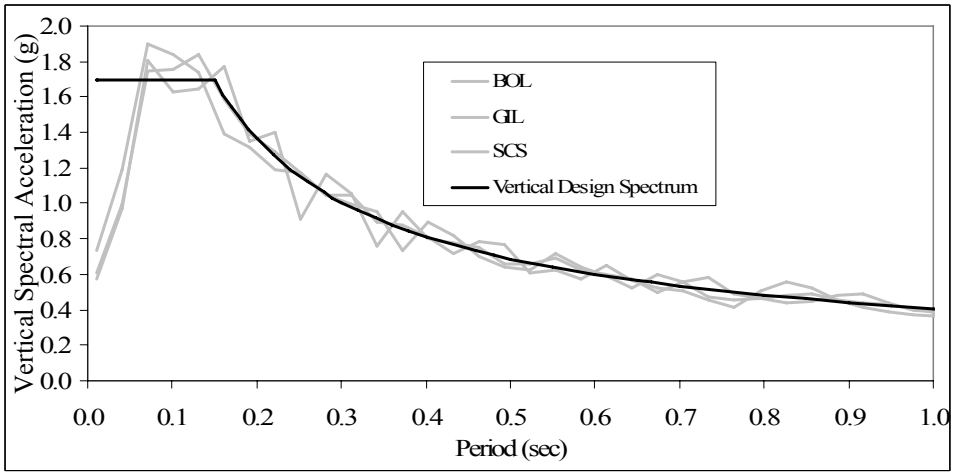

Figure 11-9 Response Spectrum of Spectrum Compatible Vertical Ground Motions

11.2.4. Comparison of Vertical Earthquake Demand Methods

The three different vertical earthquake demands methods, outlined above, were applied to a linear elastic 300 foot span superstructure model. The envelope

superstructure bending moment demands from each method are compared in Figure 11-10. The envelope of the three spectrum compatible elastic time history analyses are identified as “TH” and are considered to be the most accurate estimate of the vertical earthquake demands. These demands were determined using a Rayleigh damping model with 2% damping at the period of the two dominant vertical modes (see Figure 11-1). The envelopes of the static and modal results were amplified by 33% because they were based on a design spectrum with 5% damping. This 33% increase was based on recommendations by Kawashima and Aizawa (1986) for enstimating the spectral response for damping ratios other than the standard 5% of critical damping. The negative bending envelope for the modal analysis, identified as “Modal” in the diagram, was developed by simply multiplying the positive envelope by -1.0. The equivalent static analysis, identified as “Static” in the diagram, typically overestimated the vertical earthquake demands, while the modal analysis slightly underestimated the demands

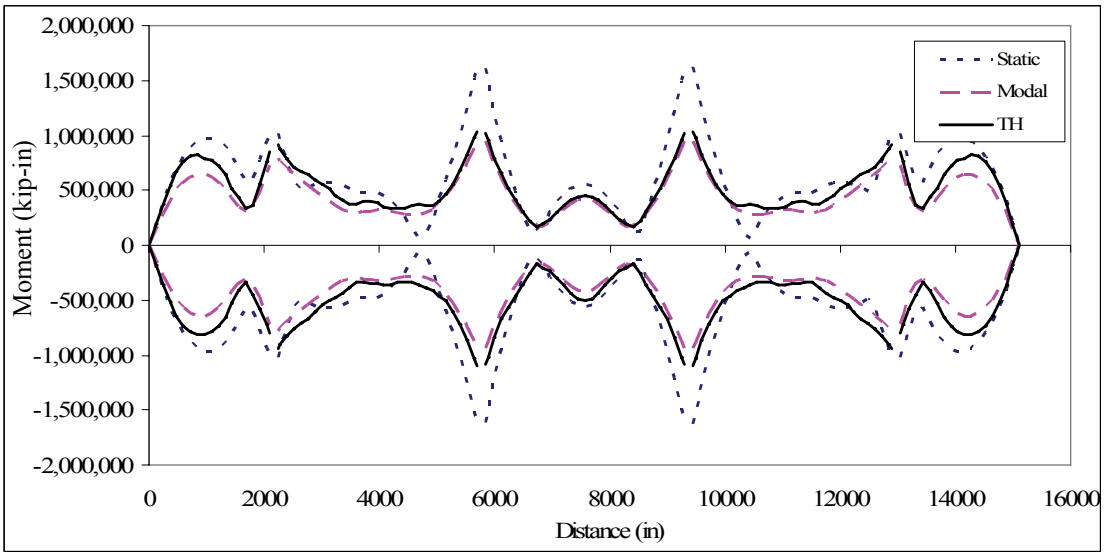

Figure 11-10 Comparison of Vertical Elastic Demand Options

The ratio of the bending moment diagrams between the equivalent static loads and the time history records as well as between the modal analysis and the time history records are shown in Figure 11-11. The modal analysis typically generated moment demands that were on average 84% of the time history demands with small variations along the span. This difference was likely due to inaccuracies in the modal CQC combinations and the fact that modal analysis is intended to estimate the average response while Figure 11-10 shows the envelope of the three spectrum compatible ground motions. The equivalent static approach overestimated the superstructure moment demands by 20% on average, with peak differences of up to 70%. These discrepancies were likely due to the assumptions that the two dominant

modes were in phase and that the spectral accelerations of these modes were equal to the peak ground acceleration.

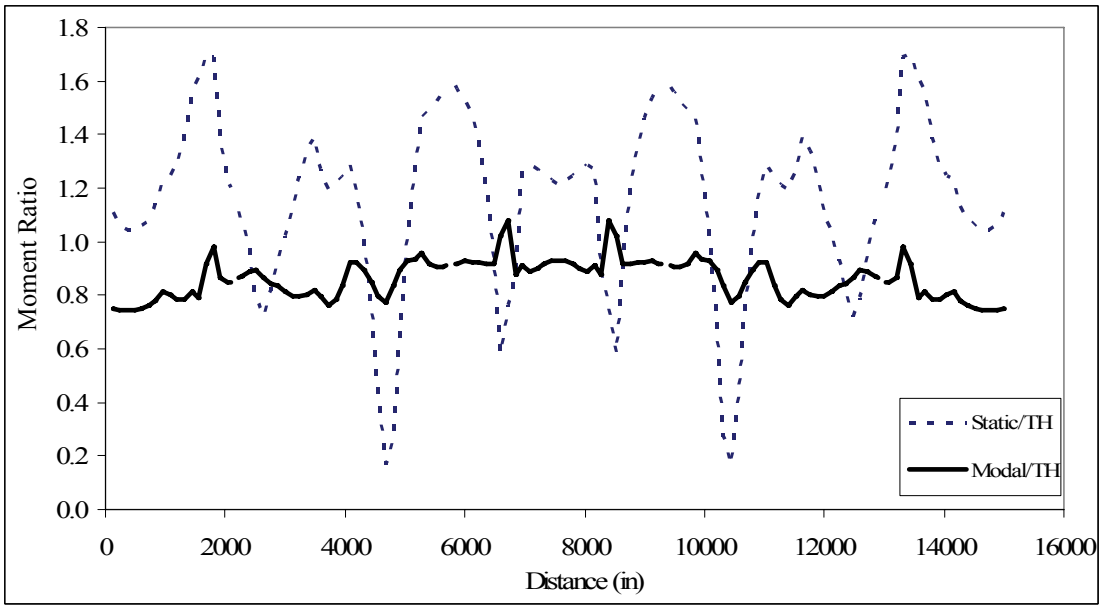

Figure 11-11 Comparison of Vertical Elastic Demand Options

Figure 11-12 shows the Fourier amplitude spectrum of the superstructure bending moment time histores at select nodes of the interior and end spans. It is clear from this diagram that two modes dominate the superstructure moment response. The period of these two modes match the primary vertical mode shapes shown in Figure 11-1. This result validates the assumption that only two modes are required for the equivalent static approach outlined in Section 11.2.1.

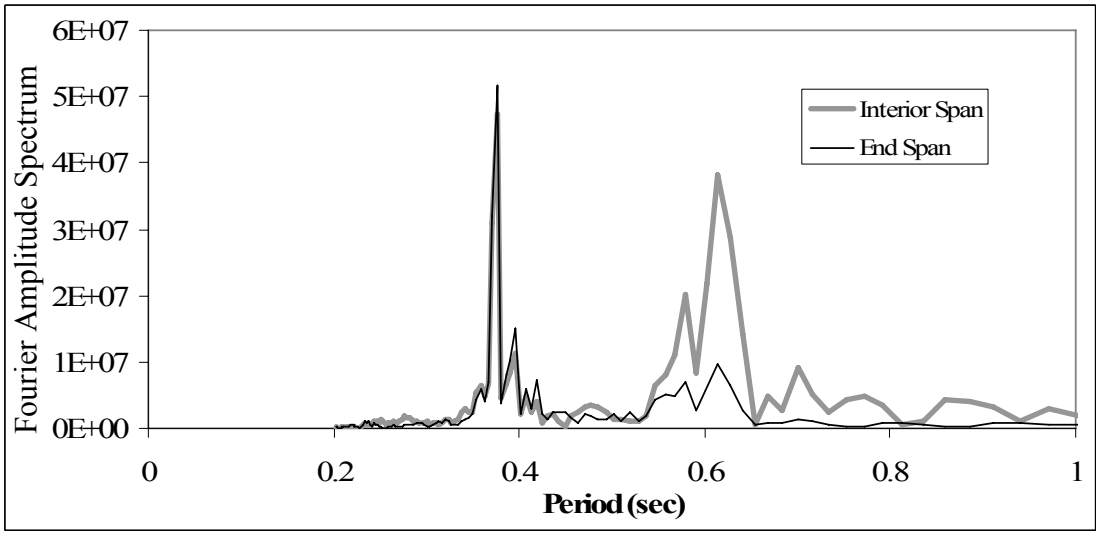

Figure 11-12 Fourier Amplitudes Spectrum of Superstructure Bending Moment Time Histories

11.3. Earthquake Load Combinations

The peak vertical and horizontal earthquake demands are not likely to occur simultaneously due to the differences between the periods of the dominant modes and between the characteristics (i.e. frequency content) of the vertical and horizontal input motions. Thus, it is reasonable to consider the two effects independently. The horizontal earthquake combinations are addressed adequately in the Caltrans Seismic Design Criteria (Caltrans, 2004) and will not be discussed herein. However, vertical earthquake combinations are not sufficiently addressed and should include considerations for the pre-earthquake stress-state of the superstructure. The vertical earthquake demands should be combined with dead load demands as obtained from a

longitudinal construction staging analysis at end of construction and after creep and shrinkage has occurred, as well as a fraction of the temperature gradient load case.

11.4. Superstructure Capacity

The capacity of superstructure segment joints can be determined by a number of different methods, such as simple hand calculations, moment-curvature analyses or detailed local non-linear finite element models. These different methods are discussed below.

Simple hand calculations can generate very good moment capacity estimates and should always be used as a check of other methods. Detailed hand calculations can also account for the unbonded length of PT tendons and can be used to approximate the rotation capacity, although the calculations can become cumbersome when multiple tendons, with different jacking loads, are used.

Moment-curvature analyses are advantageous because there are many readily available and easy to use programs with excellent graphical interfaces that can generate accurate moment capacities. The disadvantage of this tool is that it cannot consider the unbonded length of the PT tendons. Thus, the rotation capacities will be incorrect.

Local non-linear finite element models of the superstructure segment joints are advantageous because they can simulate the unbonded length of the PT tendons and will produce the most accurate joint rotation capacities. The disadvantage is that they require significant effort to develop and should be calibrated with experimental data.

In summary, all methods should generate similar moment capacities at cracking, yield and ultimate. However hand calculations and moment-curvature analyses will not accurately estimate the rotation capacity because they cannot account for the unbonded length of the PT tendons.

11.5. Vertical Collapse Mechanisms

The default seismic design requirement in California is a no collapse criteria. Vertical superstructure collapse mechanisms can be used as a means of satisfying the no collapse criteria. The most likely vertical collapse mechanisms for end and interior spans are shown in Figure 11-13 and Figure 11-14, respectively. The uniform distributed load, w_{end} and w_{int}, that will develop these collapse mechanisms are shown in Equation 11-2 for both end and interior spans.

End Spans $$w_{end} = \frac{8}{L_{end}^2}\left(\left|\frac{M_{Pier}^-}{2}\right| + M_{Mid-end}^+\right) \quad \textbf{11-2a}$$

Interior Spans $$w_{\text{int}} = \frac{8}{L_{\text{int}}^2}\left(\left|M_{Pier}^-\right| + M_{Midspan}^+\right) \quad \textbf{11-2b}$$

where M_{Pier}^- is the ultimate negative bending capacity of the segment joint adjacent to the pier, $M_{Midspan}^+$ is the ultimate positive bending capacity of the midspan segment joint of interior spans, $M_{Mid-end}^+$ is the ultimate positive bending capacity of the middle segment joint of end spans, L_{end} is the clear end span length and L_{int} is the clear interior span length.

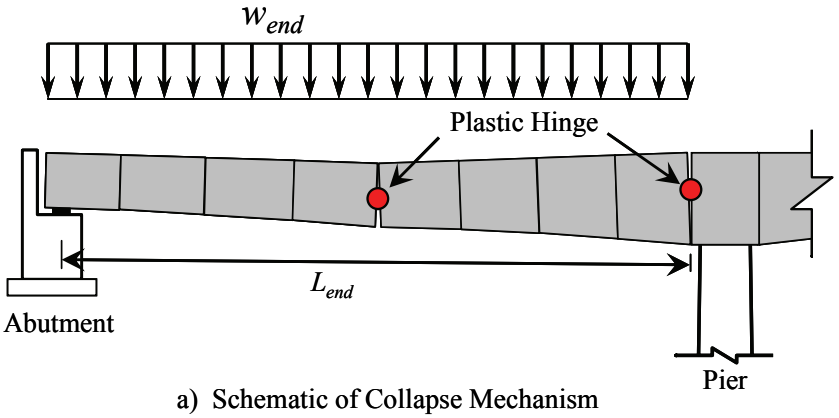

a) Schematic of Collapse Mechanism

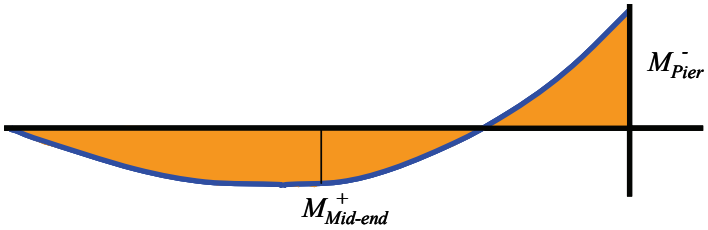

b) Bending Moment Diagram

Figure 11-13 End Span Collapse Mechanism

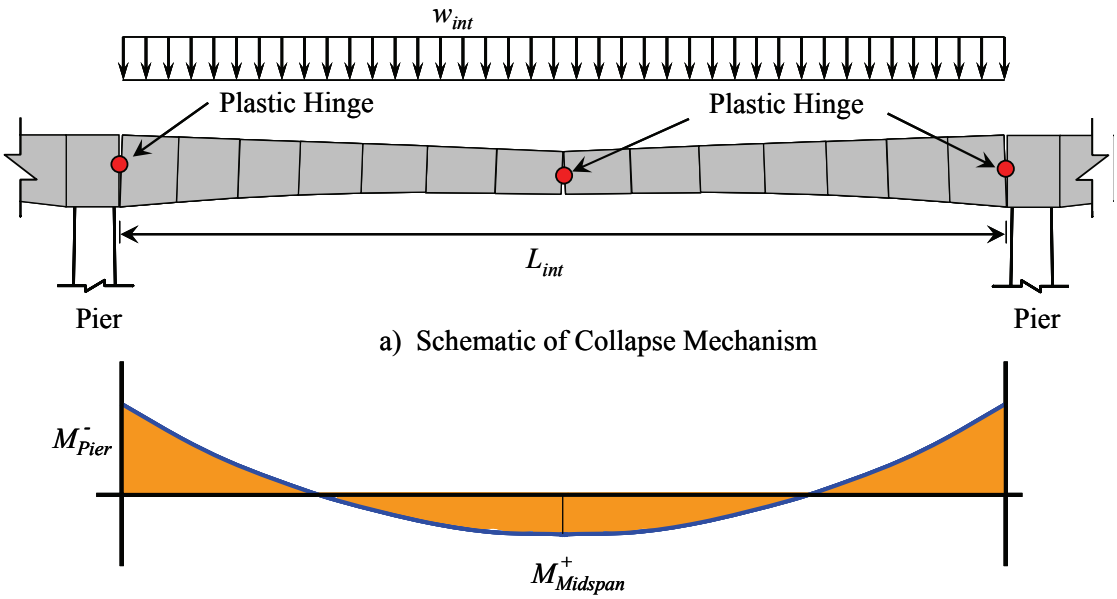

Figure 11-14 Interior Span Collapse Mechanism

These uniform distributed loads can be divided by the average unit weight of the superstructure for the span of interest to determine the capacity of the collapse mechanism in terms of multiples of the bridge self weight. Subtract unity from this ratio to obtain the capacity, S_c, of the collapse mechanism in terms of vertical earthquake accelerations as shown in Equation 11-3.

Interior Spans $$S_{c_{\text{int}}} = \frac{w_{\text{int}}}{W_{\text{int}} / L_{\text{int}}} - 1$$ **11-3a**

End Spans $$S_{c_{end}} = \frac{w_{end}}{W_{end} / L_{end}} - 1$$ **11-3a**

where, W_{int} and W_{end} are the total weights of the interior and end span segments, respectively. This value can be compared with the peak vertical ground acceleration,

PGA_v, as defined in Section 11.2.1, to determine if the superstructure is likely to collapse during a significant seismic event.

CHAPTER 12. DESIGN RECOMMENDATIONS

Based on the results, limitations and conclusions presented in the previous chapters of this dissertation, the following design recommendations are proposed.

12.1. Flange Thickness

The top and bottom flange thickness must be large enough to ensure that the neutral axis of the superstructure does not migrate into the webs upon joint opening and crushing of the extreme concrete fibers. In other words, the top flange at the piers must be able to take the jacking force of the top and continuity tendons plus the yield force of the bottom tendons. Similarly, the bottom flange at the piers must be able to take the jacking force of the bottom tendons plus the yield force of the top and continuity tendons. Likewise for the midspan joints. This may be especially relevant under 3D loading and confinement of the corners should be considered, see Figure 12-1.

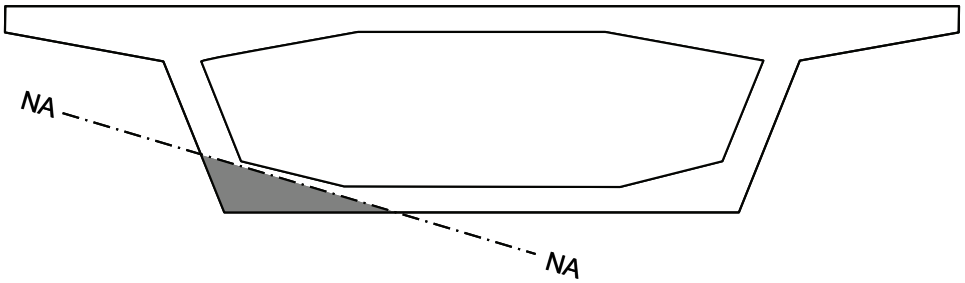

Figure 12-1 Schematic of Neutral Axis Depth due to 3D loading

12.2. Future Post-Tensioning Tendons

While the results indicated that critical PT tendons were unlikely to exceed the full yield limit state, the possibility of loss of prestressing due to yielding of tendons warrant the recommendation that new segmental bridges allow for the possibility of future tendons in the design. The AASHTO Guide Specifications for Design and Construction of Segmental Concrete Bridges (AASHTO, 1999) requires provision for access and anchorage attachment of future tendons with a PT force not less than 10% of the positive and negative moment primary PT forces. While this provision was intended to be an allowance for the addition of future dead load or to adjust for cracking or deflection of the bridge, it will likely be acceptable for seismic concerns as well.

12.3. Capacity Design

Continue using capacity design principles to design precast segmental superstructures as this approach appears to prevent permanent joint opening and yielding of the PT tendons adjacent to the piers. Capacity design principles are essential to control the seismic performance of the column-superstructure connection. The current capacity design approach considers over-strength of the column in the design of the superstructure but does not consider the column axial force increase due to vertical excitation and the corresponding increase in the column moment capacity. This approach is thus not a truly rigorous capacity design approach, but it appears to be acceptable and considerations for the effects of vertical earthquake motion on the column moment capacity are not recommended for the capacity design of the superstructure. It is important to note that capacity design principles will have no effect near midspan, thus additional design requirements are required and outlined in Section 12.4.

12.4. Seismic Design Framework

A two level design approach is recommended in which different performance limits are required for different levels of earthquakes as shown in Table 12-1. The

recommended return period of these earthquake events varies depending on the bridge classification. This approach is compatible with current seismic design practice for 'Important' bridges.

Table 12-1 Recommended Seismic Design Framework

Bridge Classification	Functional Evaluation Earthquake (FEE)	Safety Evaluation Earthquake (SEE)
'Ordinary'	No joint opening (100 year return period)	No collapse (1000 year return period)
'Important'	No joint opening (500 year return period)	Non-linear elastic joint response (2500 year return period)

For the lower level functional evaluation earthquake (FEE), it is recommended that the superstructure be designed such that the segment joints remained closed.

For the safety evaluation earthquake (SEE), the recommended design approach varies depending on the classification of the bridge. It is recommended that 'Ordinary' bridges be designed for a no collapse criteria and 'Important' bridge structures be designed to remain undamaged. The superstructure of 'Important' bridges should be designed to allow joint opening but ensure that the PT tendons remain elastic, i.e., $f_{pt} < 0.78f_u = 210$ ksi, and that the concrete does not crush, i.e., $\varepsilon_c < 0.002$.

Recommendations for the appropriate method to determine the vertical earthquake demands, segment joint capacity and load combinations that consider the pre-earthquake stress state are discussed below

12.4.1. Pre-Earthquake Stress-State and Load Combinations

Chapter 7 indicated that the superstructure pre-earthquake stress-state can affect the response of segmental bridge superstructures and should be considered during the design process. It is recommended that the superstructure dead load demands at end of construction and after the majority of creep and shrinkage has occurred, as determined from a full longitudinal construction staging analysis, be combined with a fraction of the temperature gradient and the vertical earthquake demands per Section 12.4.2. 25% of the temperature gradient is considered appropriate at this time given the likelihood of the extreme temperature gradient occurring simultaneously with a design level earthquake. The recommended load combinations are as follows.

$$DL_{EOC} \ \& \ 0.25T \ \& \ EQK_{Vert} \qquad \textbf{12-1a}$$

$$DL_{CS} \ \& \ 0.25T \ \& \ EQK_{Vert} \qquad \textbf{12-1b}$$

The peak vertical and horizontal earthquake demands are not likely to occur simultaneously, thus horizontal earthquake demands are not included in these load combinations.

12.4.2. Vertical Earthquake Demands

Chapter 7 showed that vertical earthquake ground motion can significantly increase the demands on segmental superstructures and should be considered in the design process. The recommended method to estimate the vertical earthquake demands depends on the design level (i.e., FEE or SEE) and the importance classification of the bridge as summarized in Table 12-2.

Table 12-2 Recommended Modeling Approach for Vertical Earthquake Demands

Bridge Classification	Functional Evaluation Earthquake (FEE)	Safety Evaluation Earthquake (SEE)
'Ordinary'	Elastic Modal Analysis	Check Collapse Mechanism
'Important'	Elastic Modal Analysis	Non-Linear Time History Analysis

12.4.2.1. FEE Design Level of 'Ordinary' Bridges

It is recommended that the vertical earthquake demands for the FEE design level of 'Ordinary' bridges be determined from a vertical modal analysis based on a

design spectrum per Bozorgnia and Campbell (2004). Sufficient number of modes should be considered in the modal analysis to capture at least 90% of the total bridge mass in the vertical direction. Preliminary results indicated that modal analyses generated lower elastic demands than elastic time history analysis. Thus, it is recommended that the demands from a modal analysis be increased by a factor of 1.15 (~1/0.84).

It is recommended that these vertical earthquake demands be combined with dead load and temperature gradient demands per Equation 12-1.

12.4.2.2. SEE Design Level of 'Ordinary' Bridges

It is recommended that designers satisfy the no collapse criteria for 'Ordinary' bridges by checking the capacity of all vertical collapse mechanisms relative to the vertical design spectrum. Designers should determine the capacity of the collapse mechanism for both interior and end spans based on Equation 11-3. This capacity, S_c, must be greater than the vertical peak ground acceleration, PGA_v, in the vertical design spectrum. PGA_v should be less than the peak spectral acceleration as illustrated in Figure 11-8. It may be the case that PGA_v is not indicated in this manner on the design spectrum. If this occurs, designers can

determine PGA_v based on V/H spectral ratios per Bozorgnia and Campbell (2004) as shown in Figure 3-1.

Pre-earthquake stress-states do not need to be considered in the capacity of the collapse mechanisms as they will not significantly affect the ultimate capacity of the superstructure.

12.4.2.3. FEE Design Level of 'Important' Bridges

It is recommended that the vertical earthquake demands for the FEE design level of 'Important' bridges be determined from a vertical modal analysis as outlined in Section 12.4.2.1. Since a full 3D non-linear time history analysis is recommended for the SEE design level of 'Important' bridges (see 12.4.2.4), in practice, it may be easier to use 3D time history analysis for the FEE runs as well. Time history analysis is considered to be more realistic than modal analysis and is considered appropriate for the FEE design level as well.

12.4.2.4. SEE Design Level of 'Important' Bridges

It is recommended that the vertical earthquake demands for the SEE design level of 'Important' bridges be determined from 3D non-linear time history analysis, based on appropriate horizontal and vertical ground motions. Appropriate vertical

ground motions are considered to be ground motions that exhibit V/H ratios per Bozorgnia and Campbell (2004). It is recommended that the superstructure be modeled with non-linear elastic moment-rotation hinging elements at select segment joints. At a minimum two segment joints adjacent to the piers and three segment joints near midspan should be modeled. The moment-rotation characteristics of each joint should be determined from local finite element models as outlined in Section 12.4.3.2. Extreme pre-earthquake stress-states of the segment joints must be considered based on the end of construction stresses with 25% of the temperature gradient and the stresses after creep and shrinkage losses with 25% of the temperature gradient. Thus, it is recommended that forces be applied across the non-linear segment joints members to calibrate the model to these extreme pre-earthquake stress-states. See Section 6.2.5.1 for additions details of this model calibration process.

12.4.3. Segment Joint Capacity

12.4.3.1. 'Ordinary' Bridges

Moment-curvature analysis is recommended to determine the vertical capacity of the segment joints of 'Ordinary' bridges at cracking (i.e., joint opening)

for the FEE design level, and at ultimate for the SEE design level. Expected concrete and pre-stressing material properties should be used in these calculations as outlined in the Caltrans Seismic Design Criteria (Caltrans, 2004). The preload in the tendons should be based on the average tendon force expected over the life of the bridge (i.e., the average of the tendon forces at EOC and CS).

12.4.3.2. 'Important' Bridges

It is recommended that the vertical capacity of segment joints of 'Important' bridges be determined using detailed local non-linear finite element models based on the expected concrete and prestressing material properties. These models must capture the non-linear characteristics of the extreme concrete fibers in both tension and compression. In addition, the model must capture the non-linear characteristics of the PT tendons with accurate estimates of the pretension forces. It is recommended that these models be subjected to monotonic rotational push analyses to determine the moment-rotation characteristics of the segment joints. Cyclic push analyses are not required, thus the hysteretic rules used for the concrete and PT members are unimportant. The unbonded length of the PT tendons should be determined based on 50% of the length obtained from Equation 3-1, because the

unbonded length will be approximately half of the debond length based on a strain energy comparison. Since Equation 3-1 was determined based on tests of single strand tendons, this approach will likely be a lower bound for multi-strand tendons, thus ensuring lower bound rotation capacities.

CHAPTER 13. FUTURE RESEARCH

Possible avenues for further study are briefly outlined in this chapter.

1. The research presented herein focused solely on the two dimensional response of segmental superstructures. It is possible that the transverse earthquake response may increase the demands on the segment joint and the PT tendons. Since yielding of the PT and the subsequent loss of prestressing force can have a significant influence on the serviceability of bridges, the 3D response of precast segmental superstructure warrants further study.
2. The detailed analysis presented herein utilized a joint model that was based on an unbonded length from a 16 strand tendon. Most segmental bridges utilize larger tendons. The debond length of multi-strand tendons has never been investigated, and warrants further study, in the form of large scale testing, to more accurately assess the response of segmental bridge joints.
3. Long span bridges are susceptible to increased seismic demands caused by incoherent ground motion. It has been shown that segment joints of precast segmental bridges are sensitive to coherent vertical ground motion.

Incoherent ground motion may excite anti-symmetric modes that may increase segment joint demands and influence the serviceability of the bridge after a significant seismic event. Thus further research into this effect is warranted.

4. This dissertation focused on the response of segmental bridges with bonded tendons. The use of external unbonded PT tendons may increase the possibility of reducing the amount of PT required in the superstructure as unbonded tendons have significantly larger rotation capacity. Thus further studies into the response of unbonded tendons are warranted.
5. The vertical earthquake load combinations recommended herein were determined based on engineering intuition and comfort level and not from a thorough probabilistic analysis. In addition, the load combinations assumed that the peak vertical and horizontal earthquake motions did not occur simultaneously. Therefore, a thorough study of vertical earthquake load combinations from a probabilistic point of view is warranted.
6. The scaling of the vertical ground motions utilized the same scale factor for both the horizontal and vertical components of motion. While this approach

was used based on recommendations from experts in the engineering seismologist field, it may not be the most appropriate for structures that are susceptible to vertical accelerations. The dominant horizontal period for the segmental bridges considered was very different from the dominant vertical periods. Scaling records to match the horizontal design spectrum at or near the dominant horizontal period and using the same vertical and horizontal scale factors will result in ground motions that represent the vertical design spectrum only near the period of the dominant horizontal mode. The vertical response at the period of the vertical modes will likely exhibit significant scatter and may not accurately match the vertical design spectrum. Therefore, scaling methods that minimize the scatter in the vertical ground motions should be developed.

APPENDIX A - SAMPLE ITERATION PROCEDURE FOR CONVERGENCE WITH LCA

Initial Condition

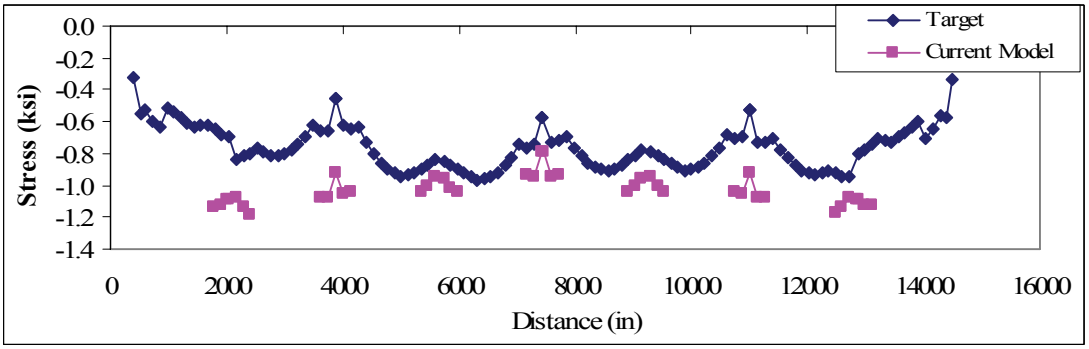

Figure A-13-1 Initial Top Stresses

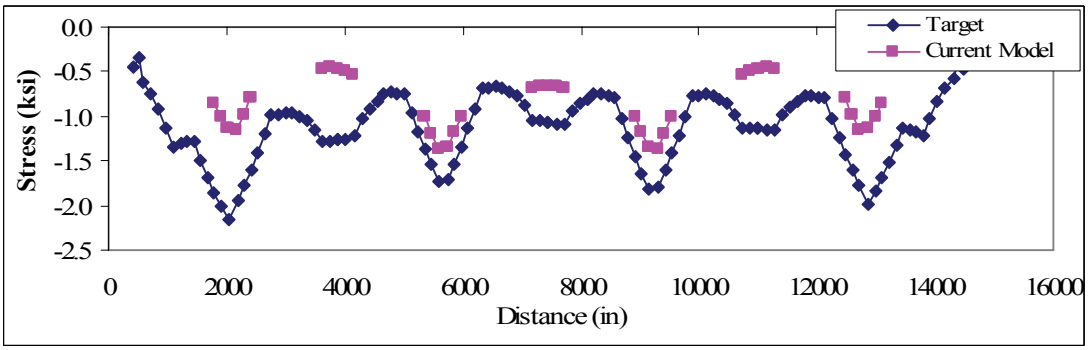

Figure A-13-2 Initial Bottom Stresses

Based on the top and bottom stresses and section properties of the superstructure, segment joints differential axial forces and bending moment are calculated.

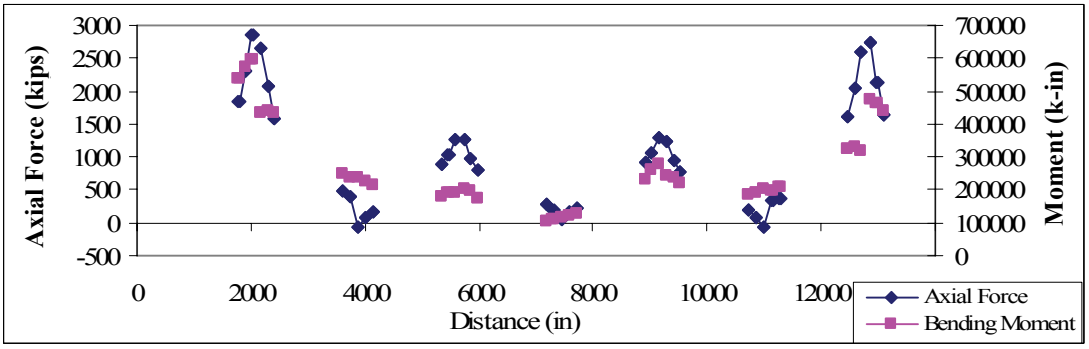

Figure A-13-3 Initial Differential Axial Forces and Bending Moments

Iteration #1

Apply differential forces to segment joints. New stresses are obtained.

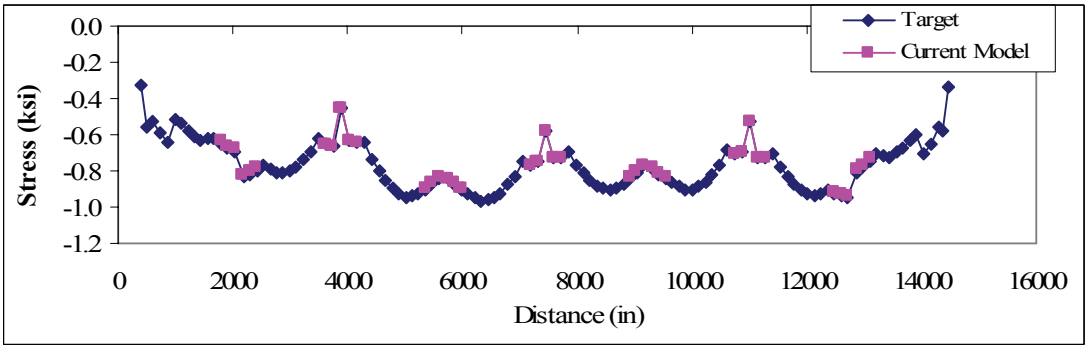

Figure A-13-4 Iteration #1 Top Stresses

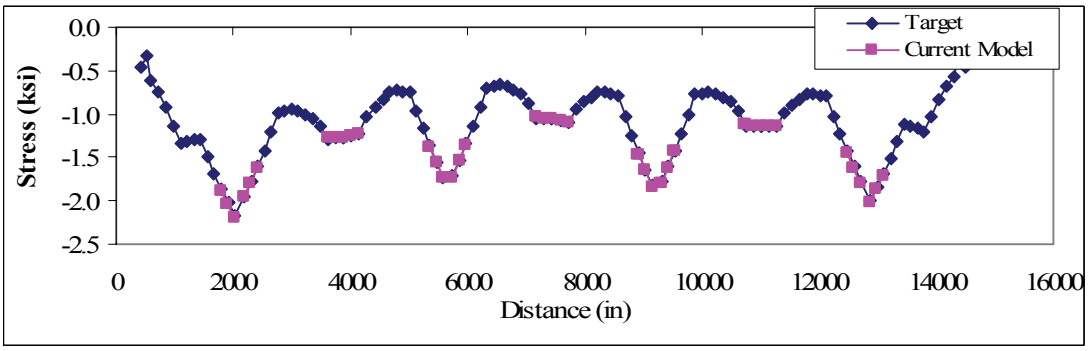

Figure A-13-5 Iteration #1 Bottom Stresses

Updated joints differential forces are calculated by adding the differential forces obtained from the new stresses to the previous differential forces.

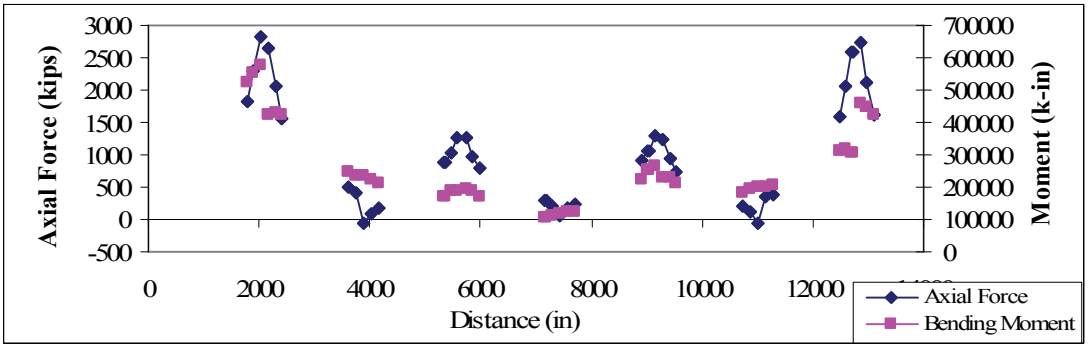

Figure A-13-6 Iteration #1 Differential Axial Forces and Bending Moments

The median change in the force differential is -0.66% ➔ try again.

Iteration #2

Apply differential forces to segment joints. New stresses are obtained.

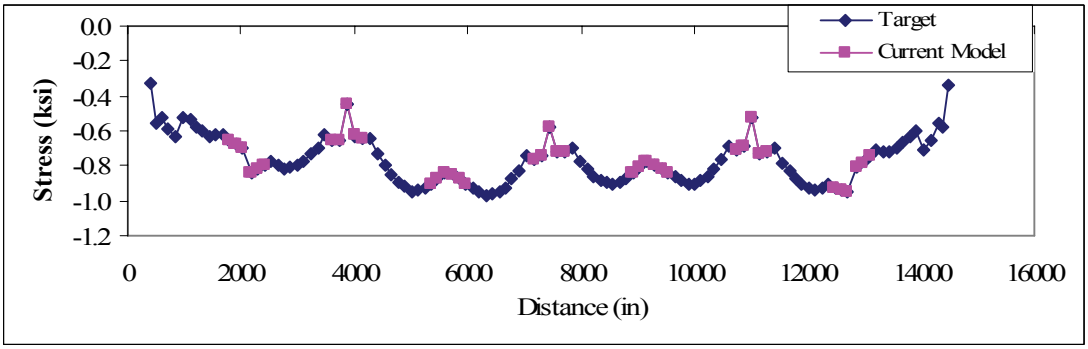

Figure A-13-7 Iteration #2 Top Stresses

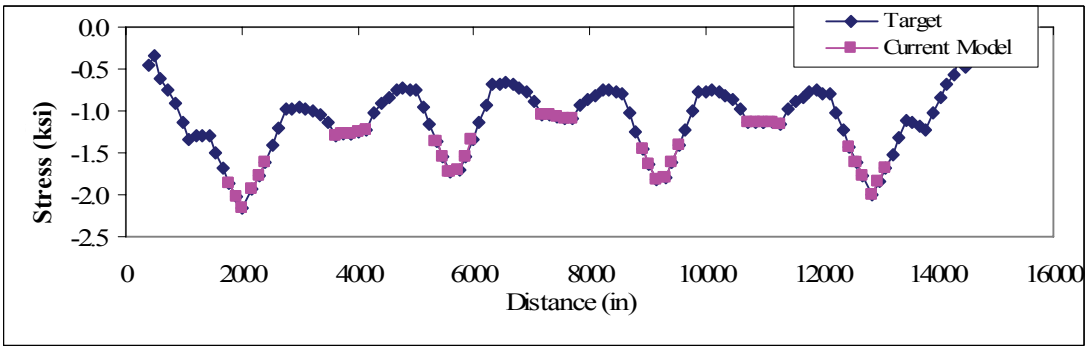

Figure A-13-8 Iteration #2 Bottom Stresses

Updated joints differential forces are calculated by adding the differential forces obtained from the new stresses to the previous differential forces.

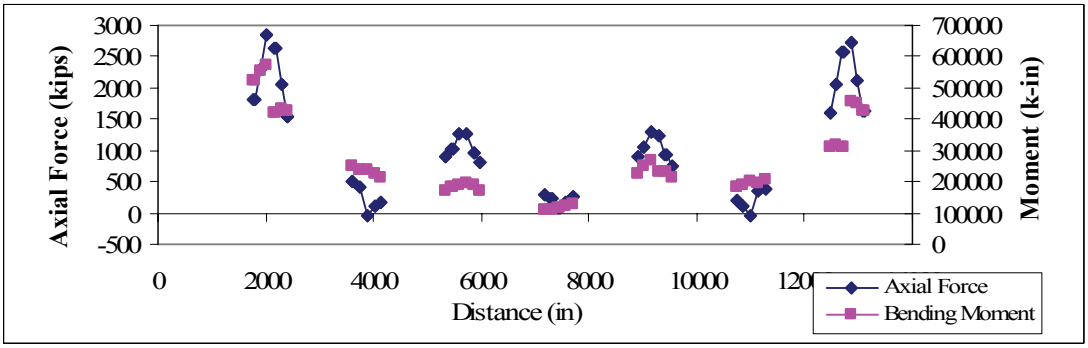

Figure A-13-9 Iteration #2 Differential Axial Forces and Bending Moments

The median change in the force differential is 0.08% ➔ Convergence!

APPENDIX B - EFFECT OF PRE-EARTHQUAKE STRESS-STATE ON LIMIT STATE

Table A-13-1 300 Foot Span – Comparison of Limit State for Joint D1/U1 based on EOC and CS

	C1		C2		MT1		MT2	
	Negative	**Positive**	**Negative**	**Positive**	**Negative**	**Positive**	**Negative**	**Positive**
EOC	-0.000024	0.000017	-0.00026	0.00056	-0.00119	0.00252	-0.00172	0.00450
CS	-0.000023	0.000016	-0.00028	0.00059	-0.00127	0.00252	-0.00188	0.00450
CS/EOC	0.94	0.93	1.10	1.05	1.07	1.00	1.09	1.00

All limit states above are in units of Radians

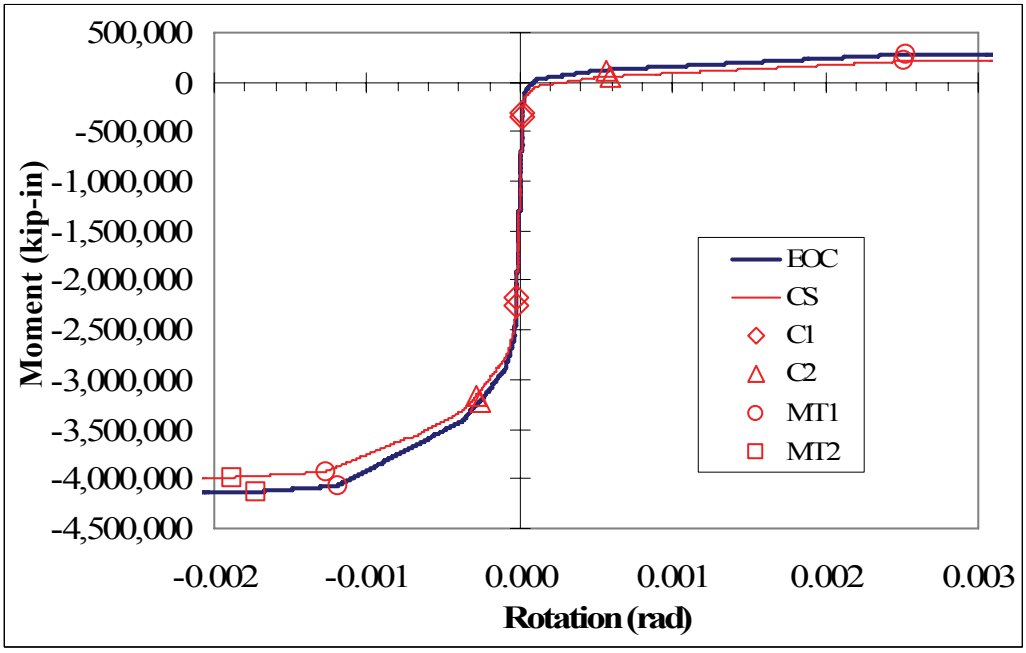

Figure A-13-10 300 Foot Span –Joint D1/U1

Table A-13-2 300 Foot Span – Comparison of Limit State for Midspan based on EOC and CS

	C1		C2		MT1		MT2	
	Negative	**Positive**	**Negative**	**Positive**	**Negative**	**Positive**	**Negative**	**Positive**
EOC	-0.000031	0.000019	-0.00069	0.00098	-0.00127	0.00147	-0.00216	0.00231
CS	-0.000027	0.000016	-0.00080	0.00110	-0.00125	0.00145	-0.00214	0.00228
CS/EOC	0.87	0.82	1.16	1.11	0.99	0.99	0.99	0.99

All limit states above are in units of Radians

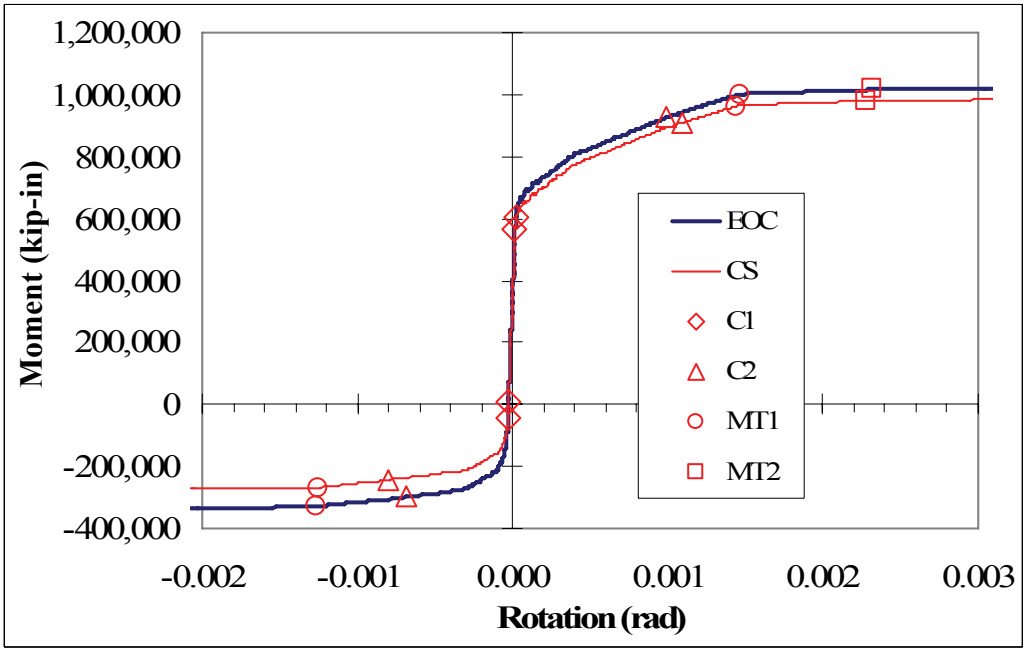

Figure A-13-11 300 Foot Span – Midspan Joint

Table A-13-3 525 Foot Span – Comparison of Limit State for Joint W1 based on EOC and CS

	C1		C2		MT1		MT2		CT1		CT2	
	Negative	Positive	Negative	Positive	Negative	Positive	Negative	Positive	Negative	Positive	Negative	Positive
EOC	-0.000020	0.000017	-0.00028	0.00077	-0.00096	0.00133	-0.00123	0.00194	-0.00056	0.00346	-0.00092	0.00553
CS	-0.000019	0.000015	-0.00030	0.00107	-0.00091	0.00130	-0.00118	0.00190	-0.00055	0.00332	-0.00091	0.00541
CS/EOC	0.93	0.89	1.07	1.39	0.95	0.97	0.96	0.98	0.98	0.96	1.00	0.98

All limit states above are in units of Radians

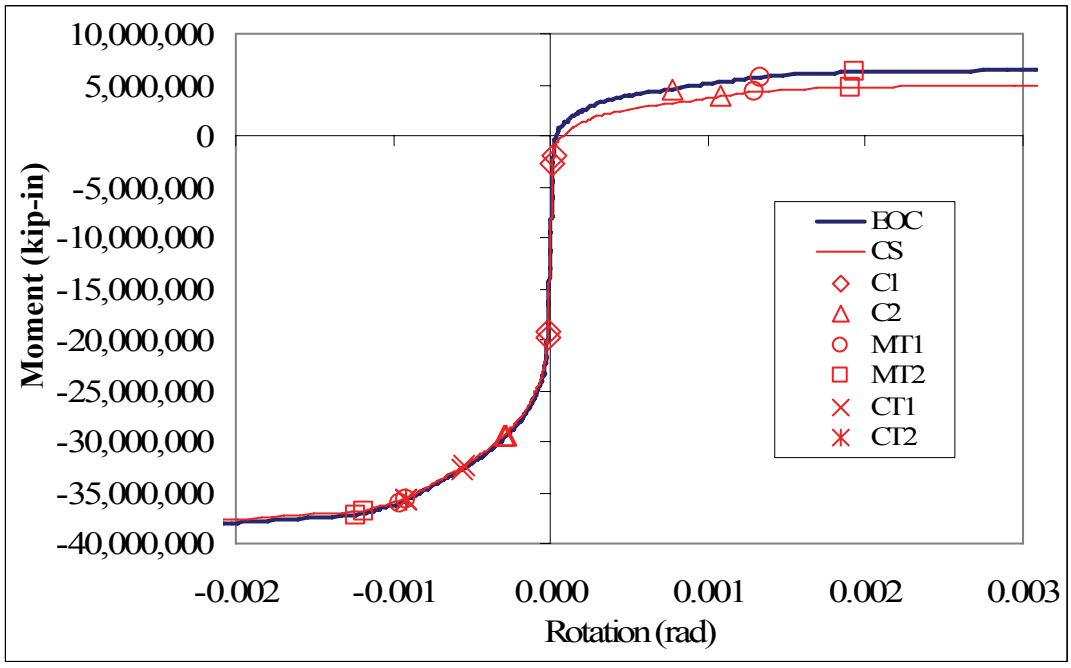

Figure A-13-12 525 Foot Span –Joint W1

Table A-13-4 525 Foot Span – Comparison of Limit State for Midspan based on EOC and CS

	C1		C2		MT1		MT2		CT1		CT2	
	Negative	Positive	Negative	Positive	Negative	Positive	Negative	Positive	Negative	Positive	Negative	Positive
EOC	-0.000034	0.000014	-0.00022	0.00856	-0.00100	0.00040	-0.00154	0.00060	-0.00924	0.00084	-0.01253	0.00118
CS	-0.000029	0.000013	-0.00032	0.01495	-0.00097	0.00041	-0.00147	0.00055	-0.00883	0.00083	-0.01210	0.00116
CS/EOC	0.86	0.93	1.43	1.75	0.97	1.03	0.96	0.92	0.96	0.99	0.97	0.99

All limit states above are in units of Radians

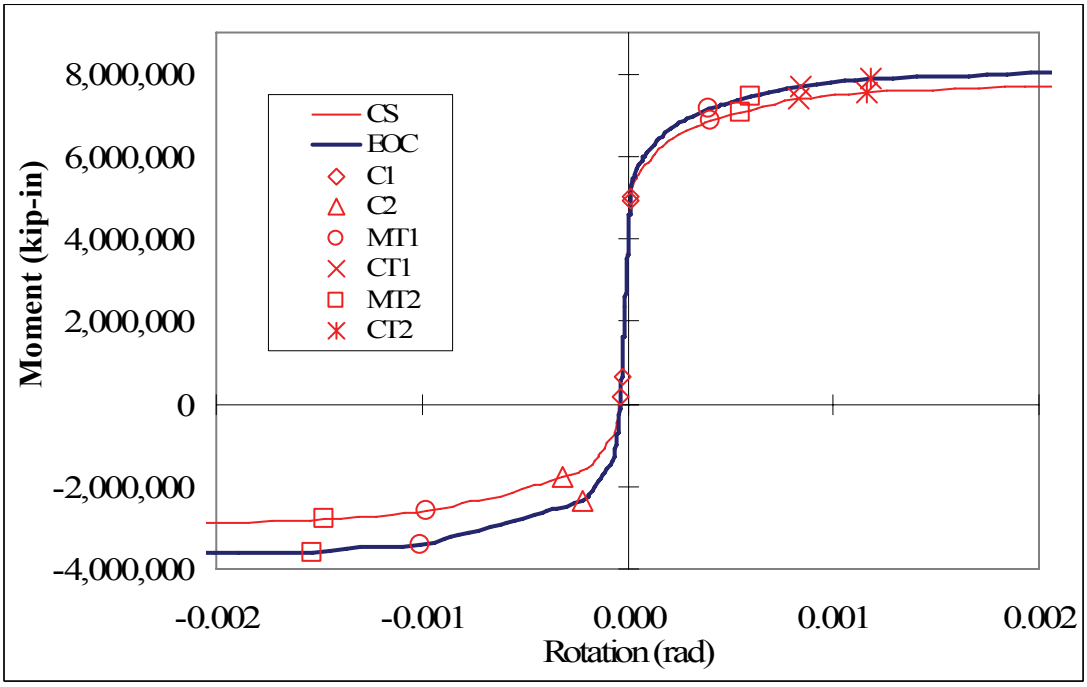

Figure A-13-13 525 Foot Span – Midspan Joint

APPENDIX C - RECORD SCALING DATA

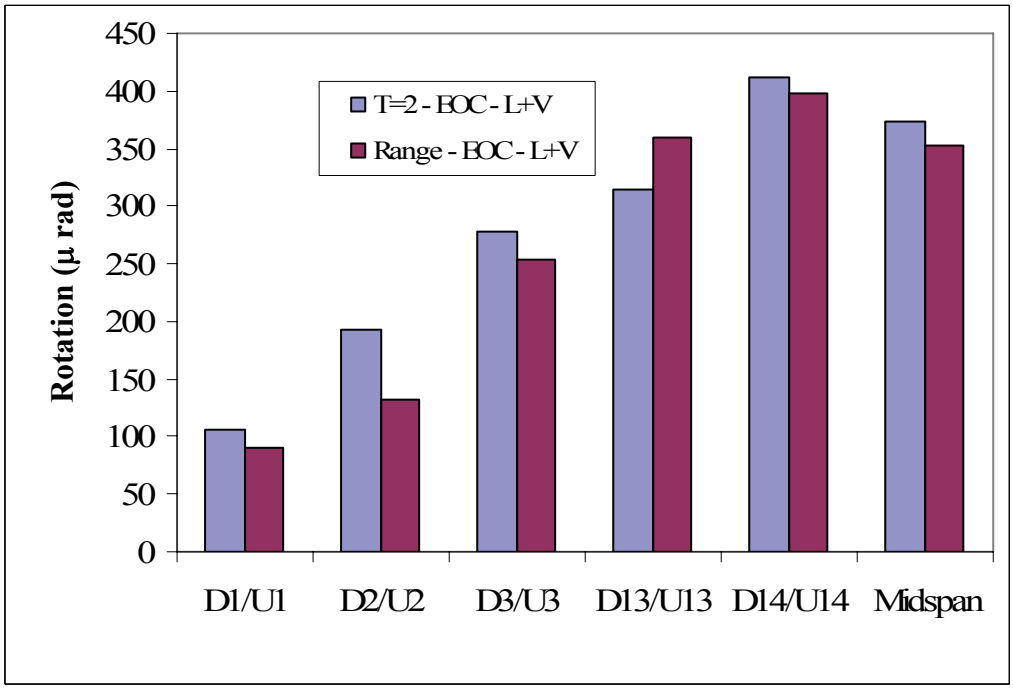

a) Median Rotations

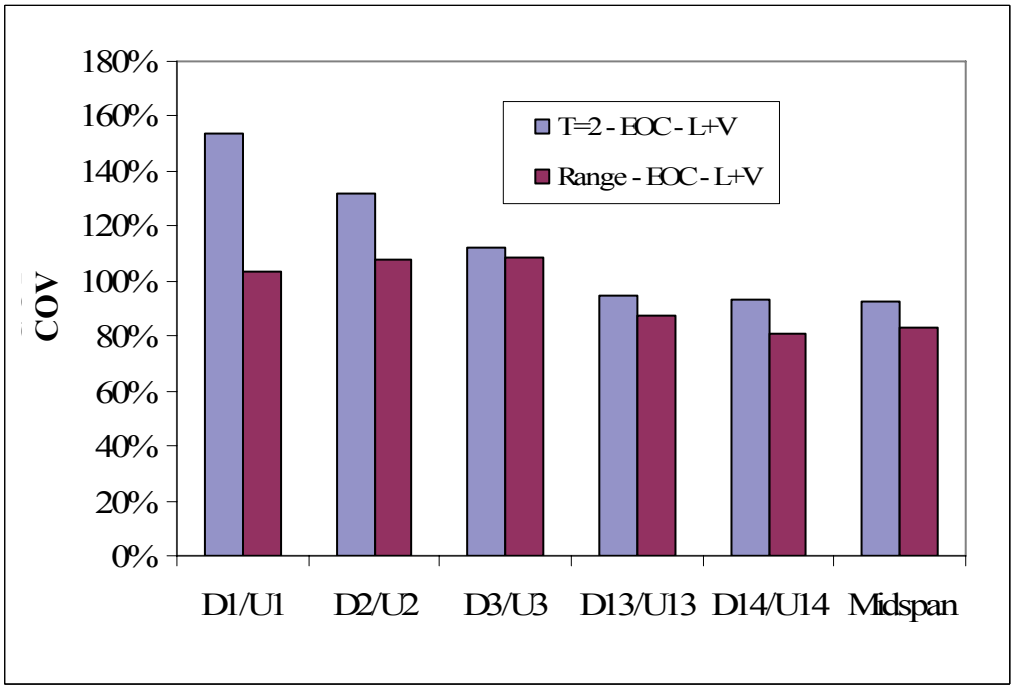

b) Coefficient of Variation

Figure A-13-14 300 Foot Span – Influence of Record Scaling on Positive Joint Rotations

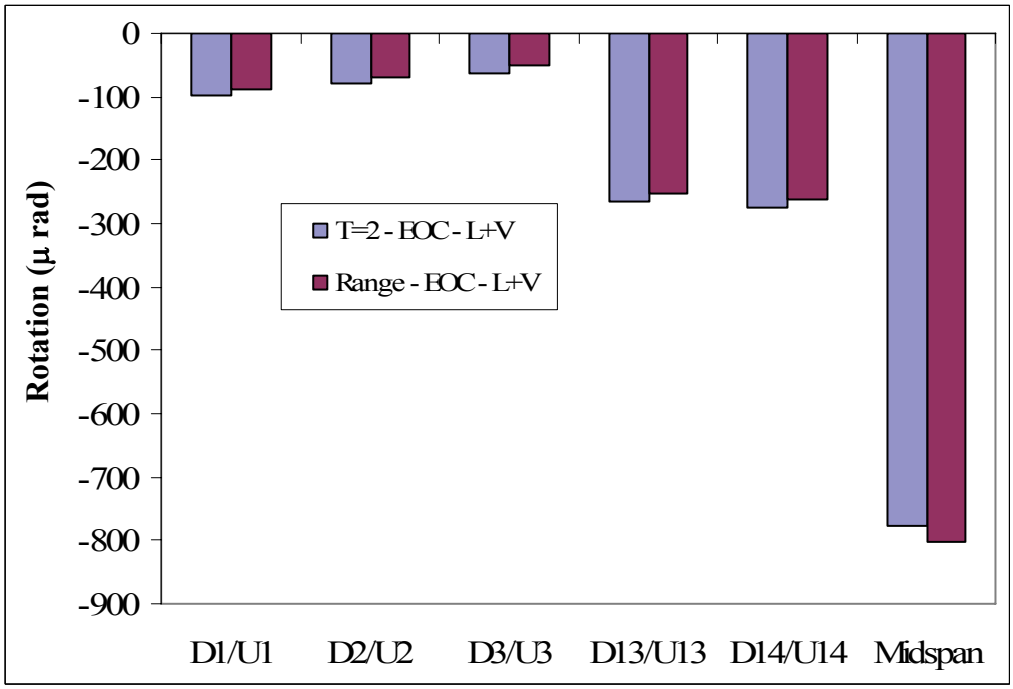

a) Median Rotations

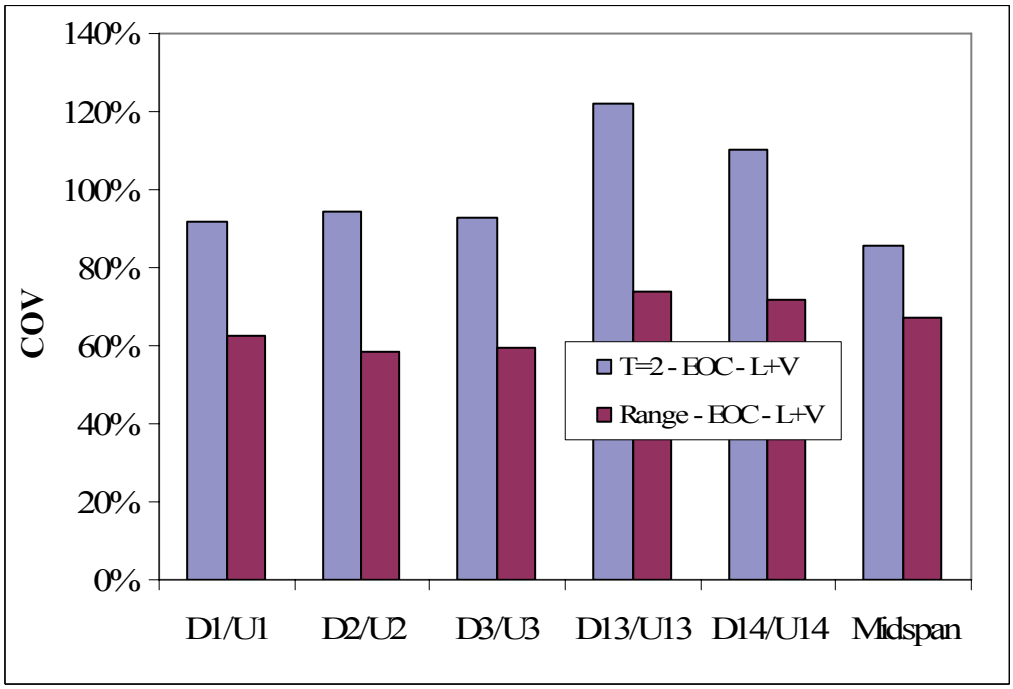

b) Coefficient of Variation

Figure A-13-15 300 Foot Span – Influence of Record Scaling on Negative Joint Rotations

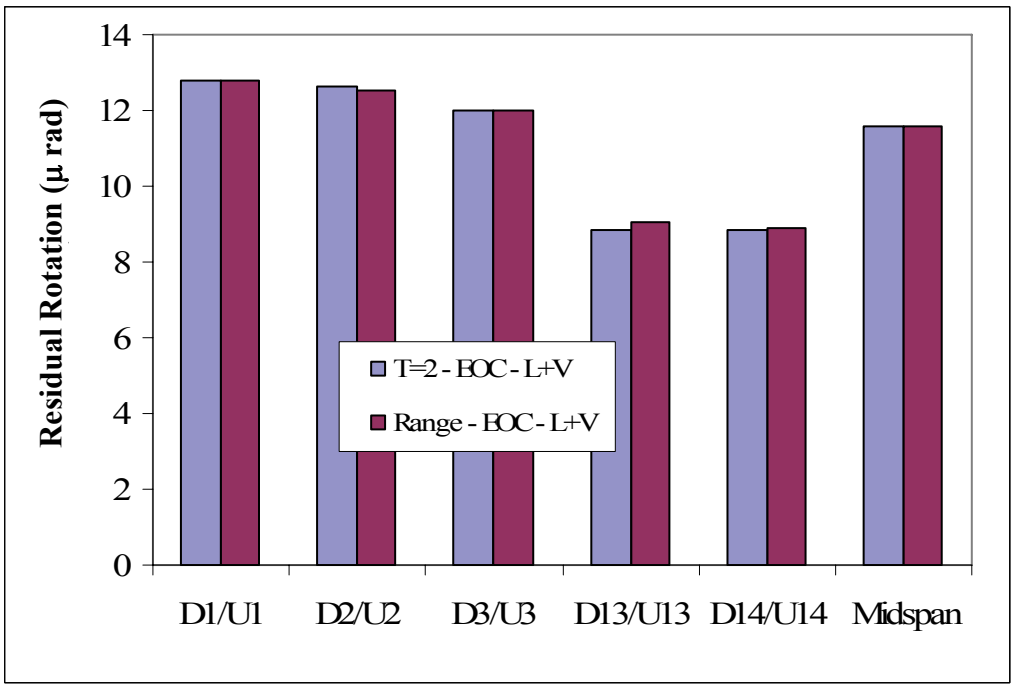

a) Median Rotations

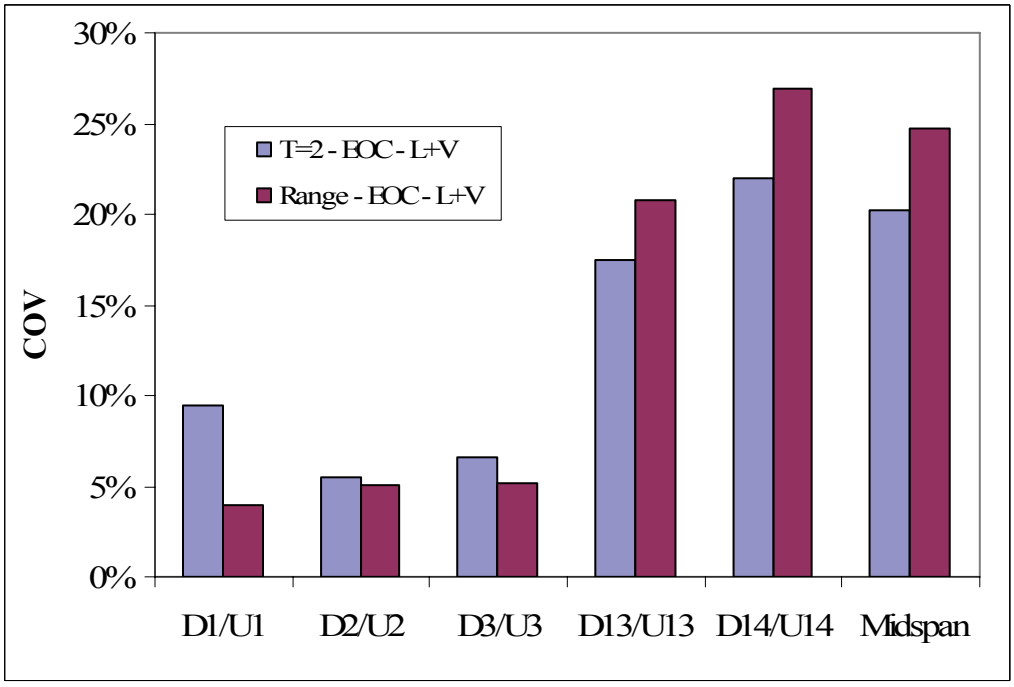

b) Coefficient of Variation

Figure A-13-16 300 Foot Span – Influence of Record Scaling on Residual Joint Rotations

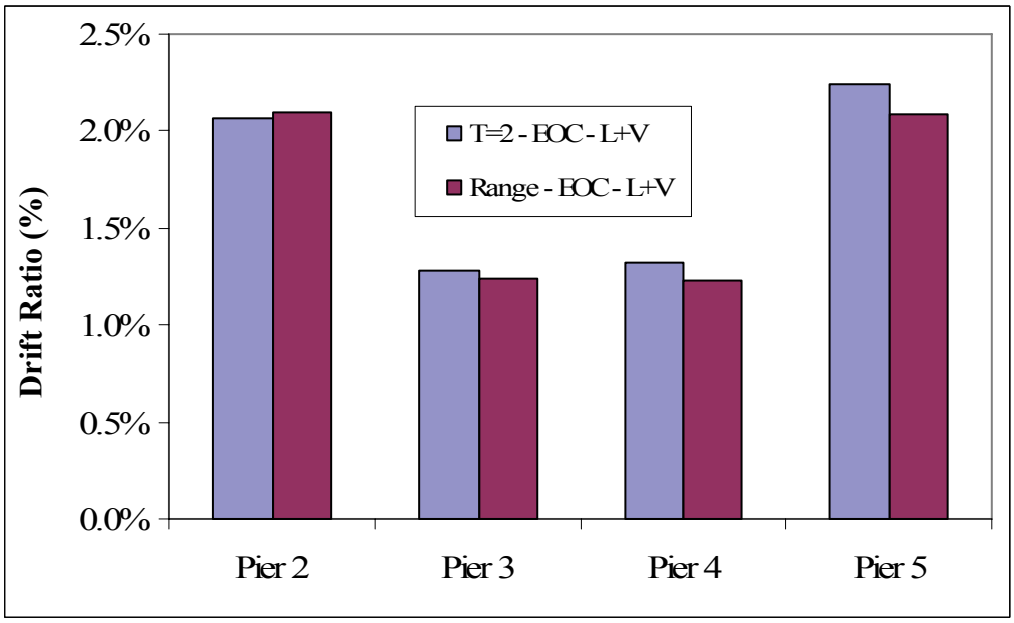

a) Median Drift Ratio

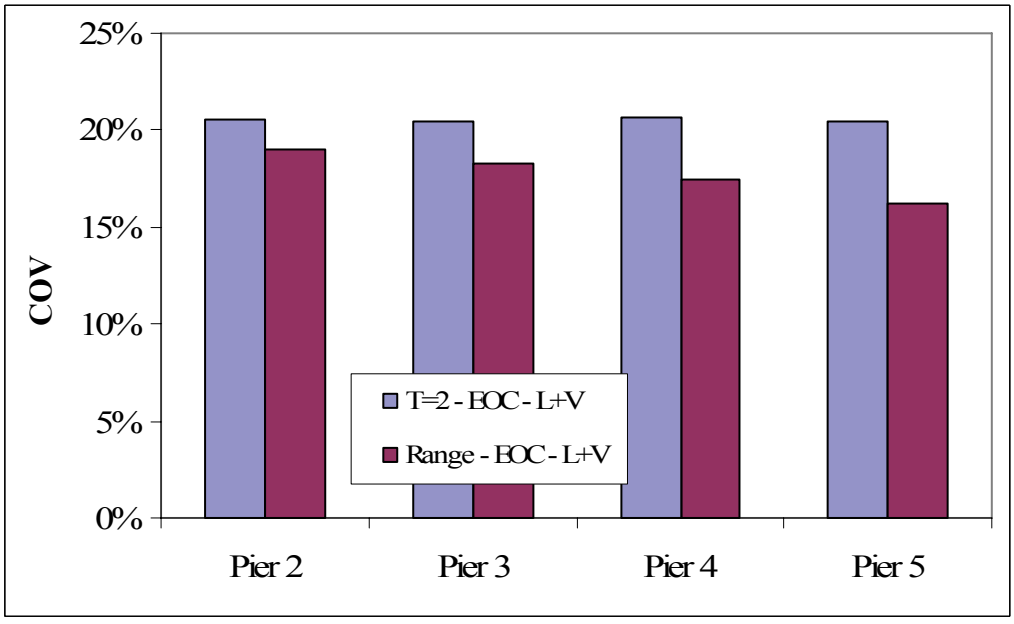

b) Coefficient of Variation

Figure A-13-17 300 Foot Span – Influence of Record Scaling on Pier Longitudinal Drift Ratios

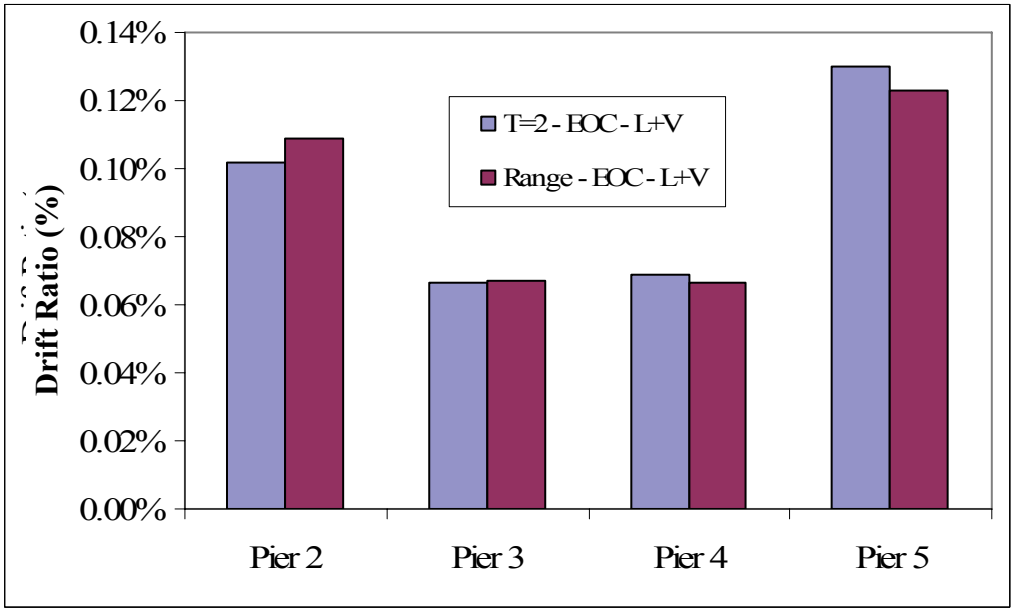

a) Median Drift Ratio

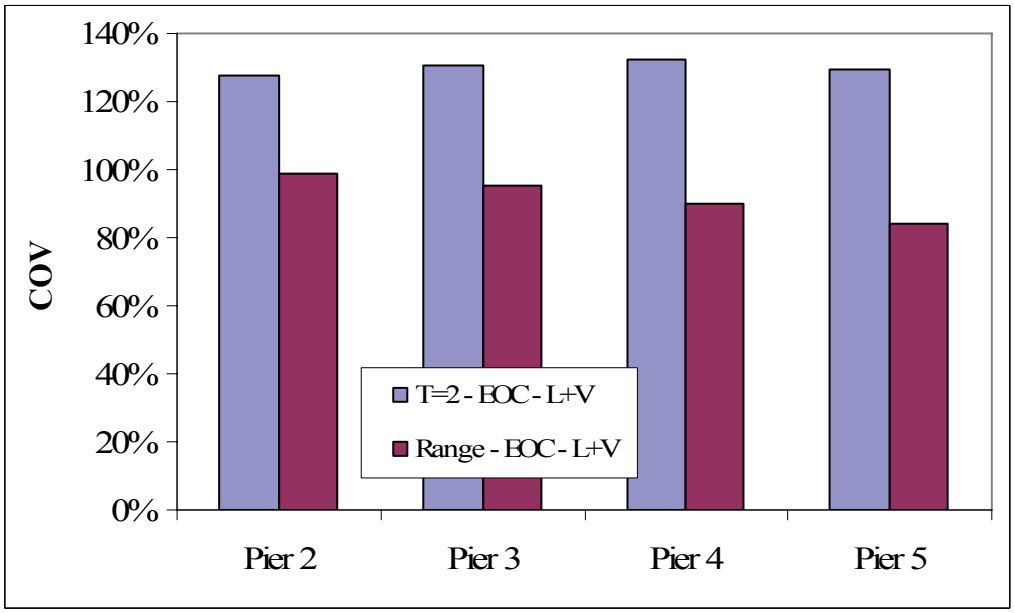

b) Coefficient of Variation

Figure A-13-18 300 Foot Span – Influence of Record Scaling on Pier Residual Drift Ratios

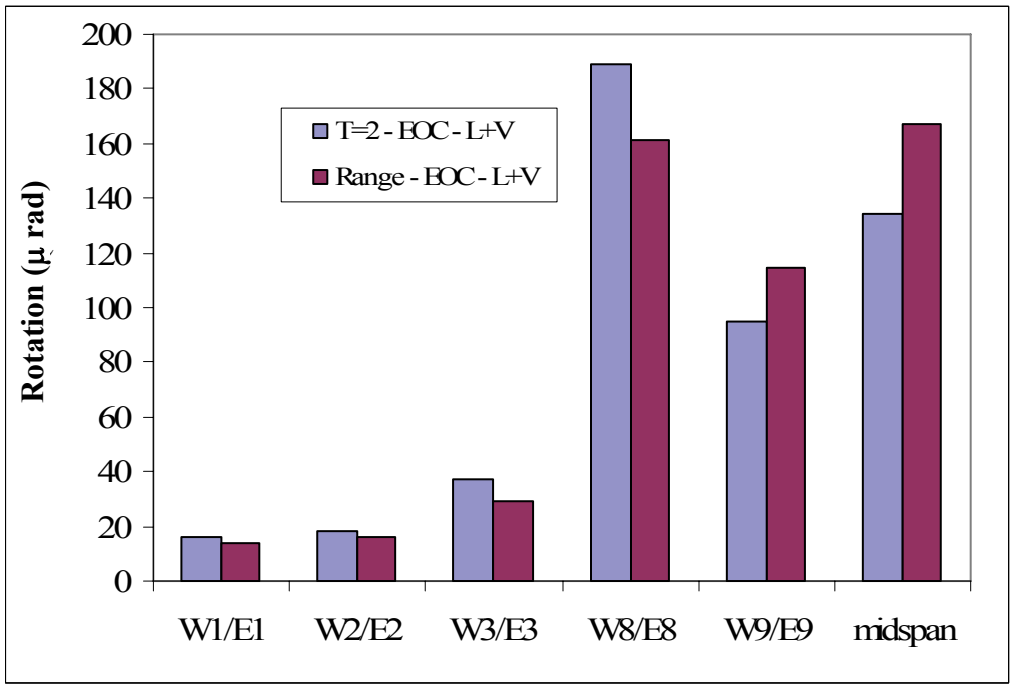

a) Median Rotations

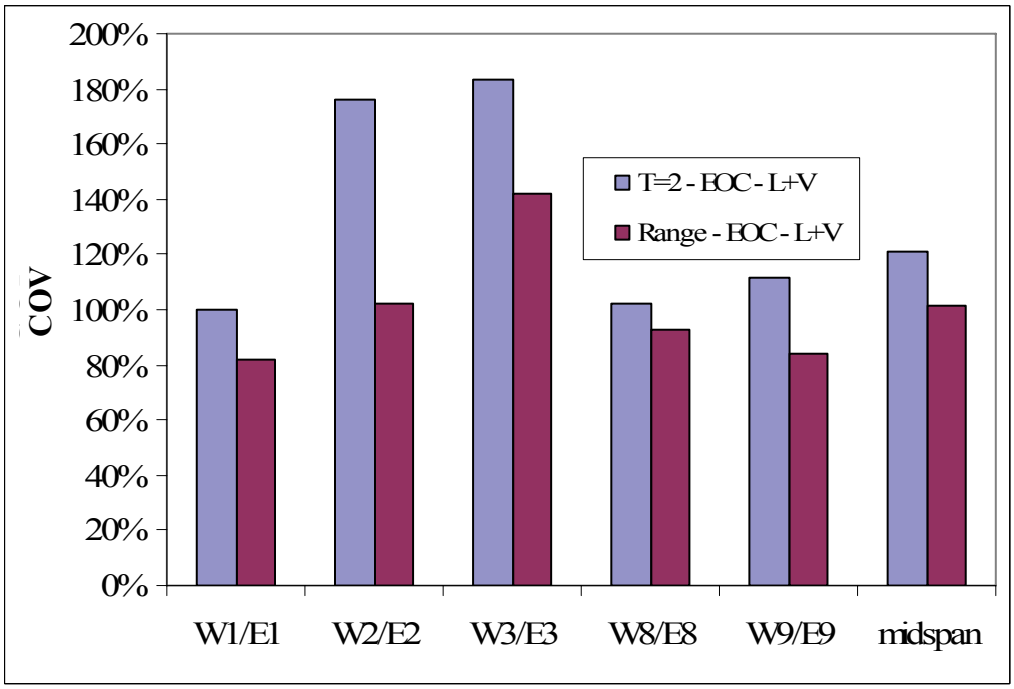

b) Coefficient of Variation

Figure A-13-19 525 Foot Span – Influence of Record Scaling on Positive Joint Rotations

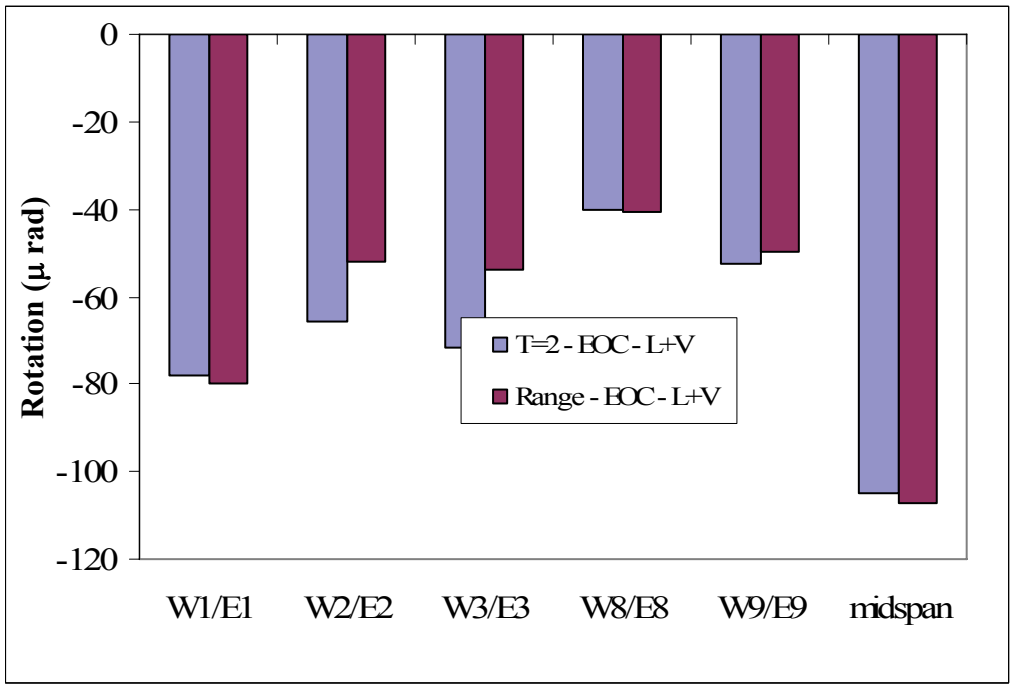

a) Median Rotations

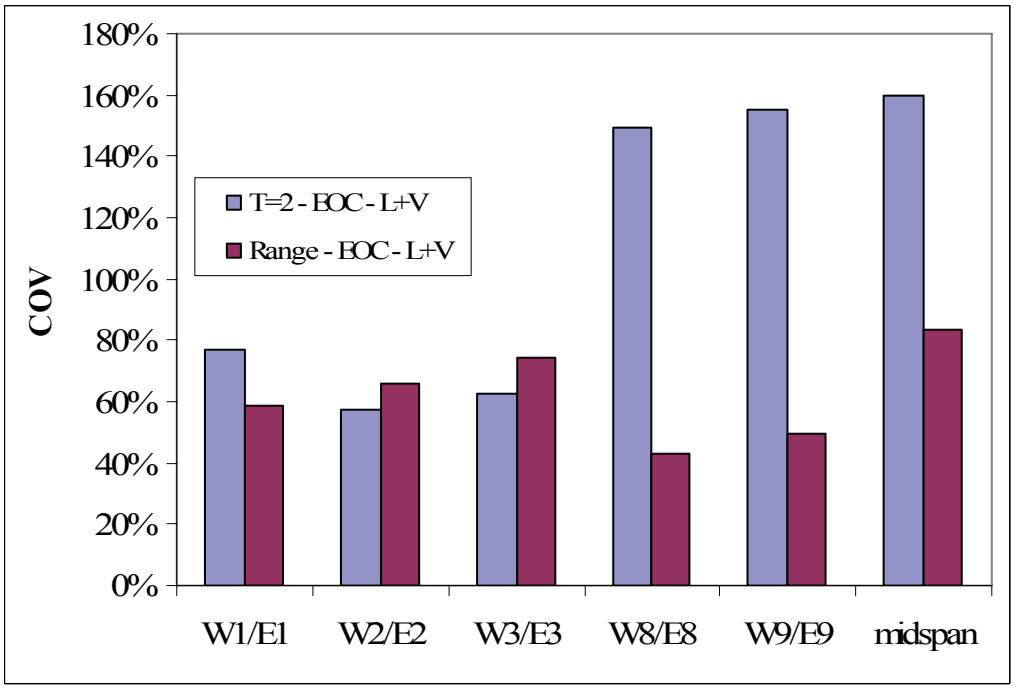

b) Coefficient of Variation

Figure A-13-20 525Foot Span – Influence of Record Scaling on Negative Joint Rotations

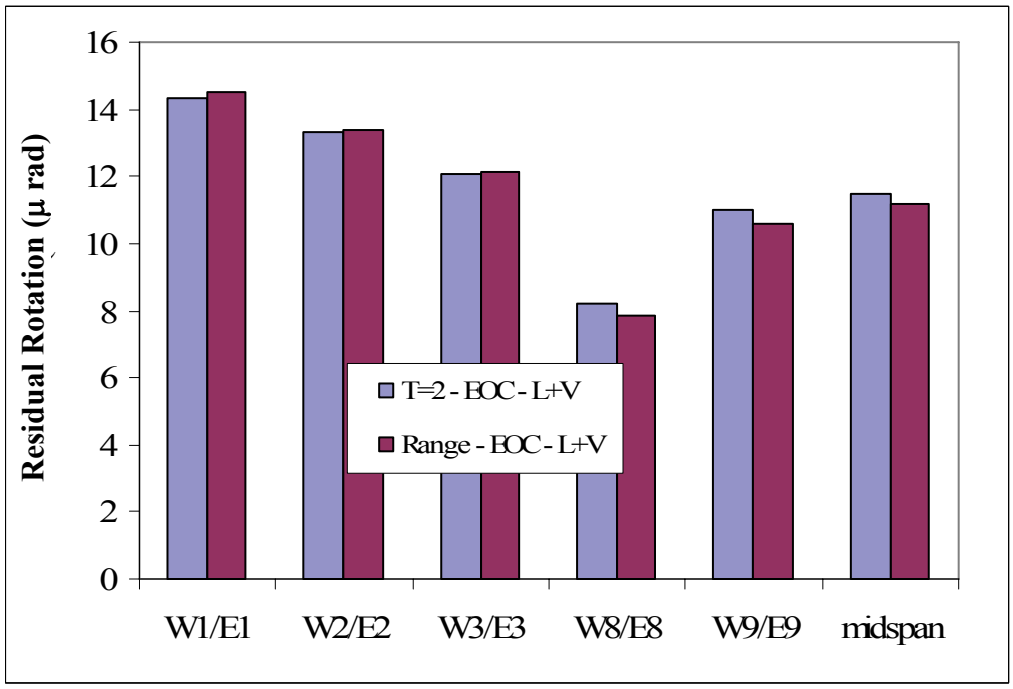

a) Median Rotations

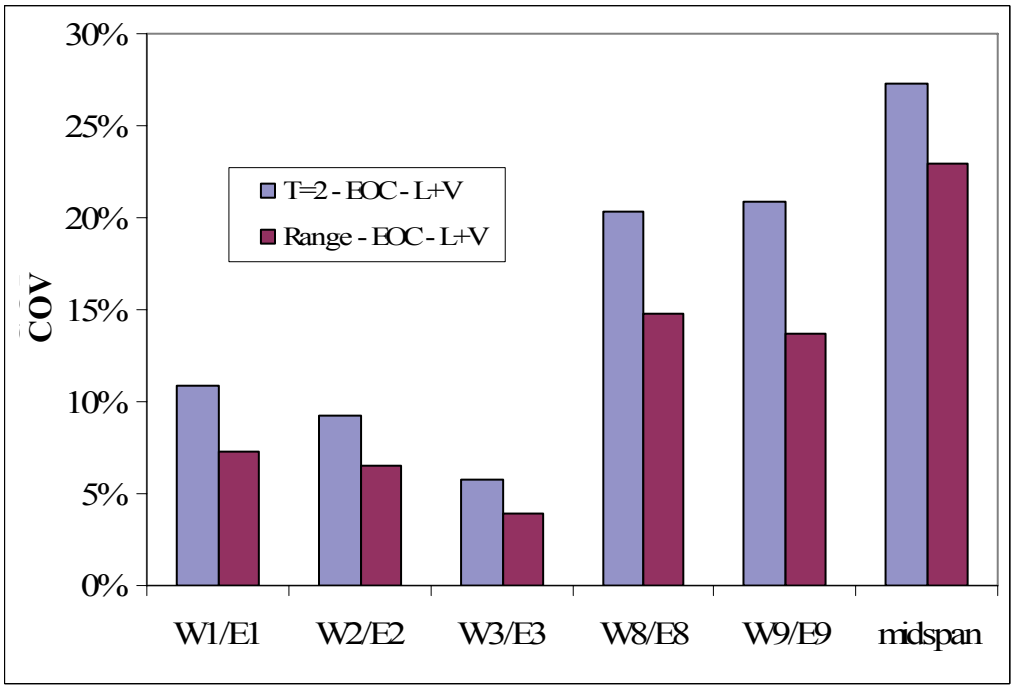

b) Coefficient of Variation

Figure A-13-21 525Foot Span – Influence of Record Scaling on Residual Joint Rotations

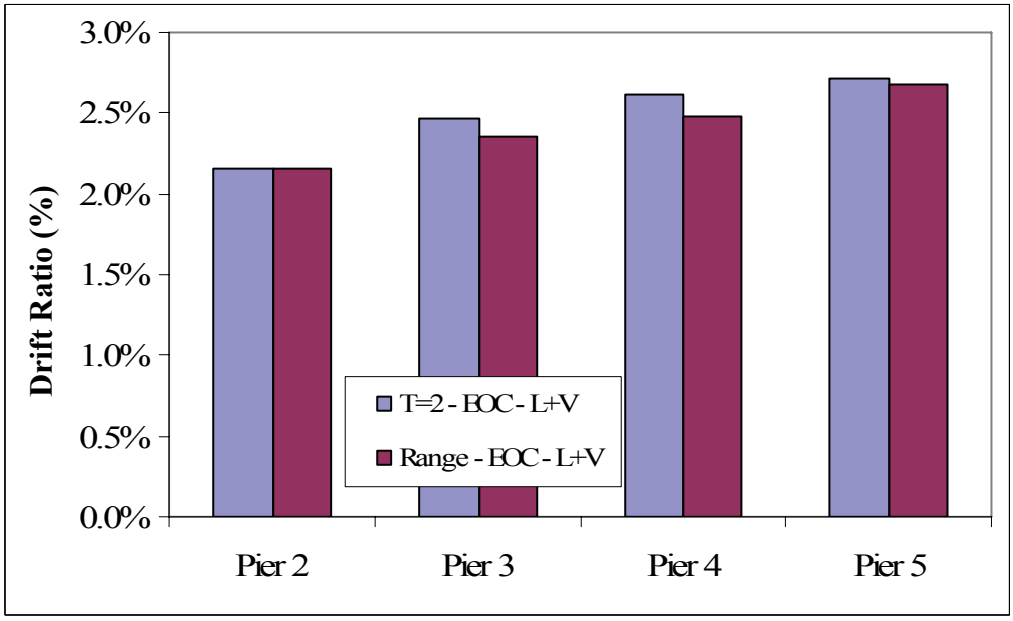

a) Median Drift Ratio

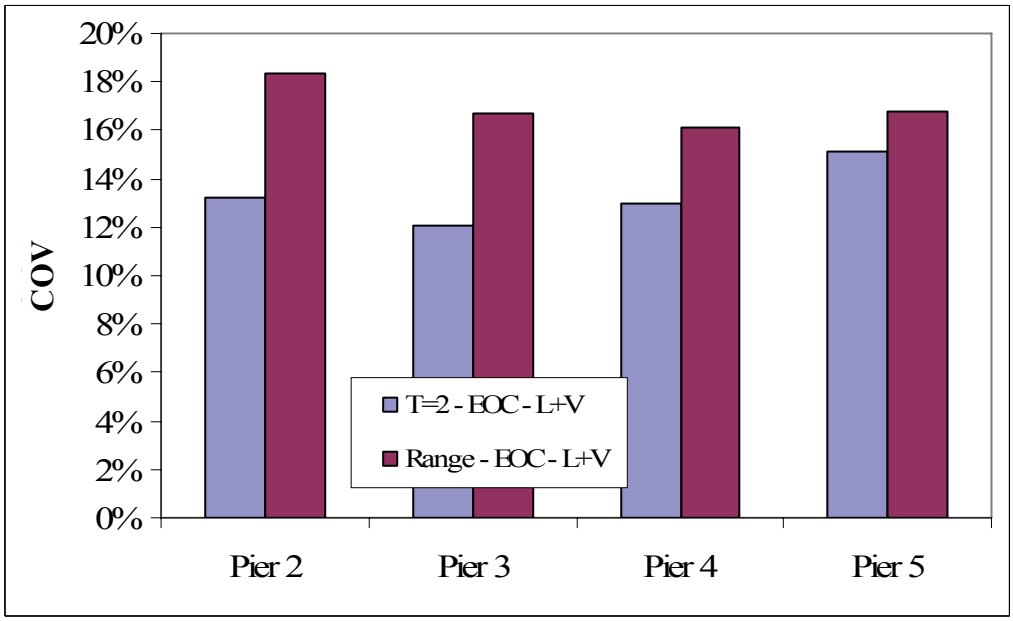

b) Coefficient of Variation

Figure A-13-22 525Foot Span – Influence of Record Scaling on Pier Longitudinal Drift Ratios

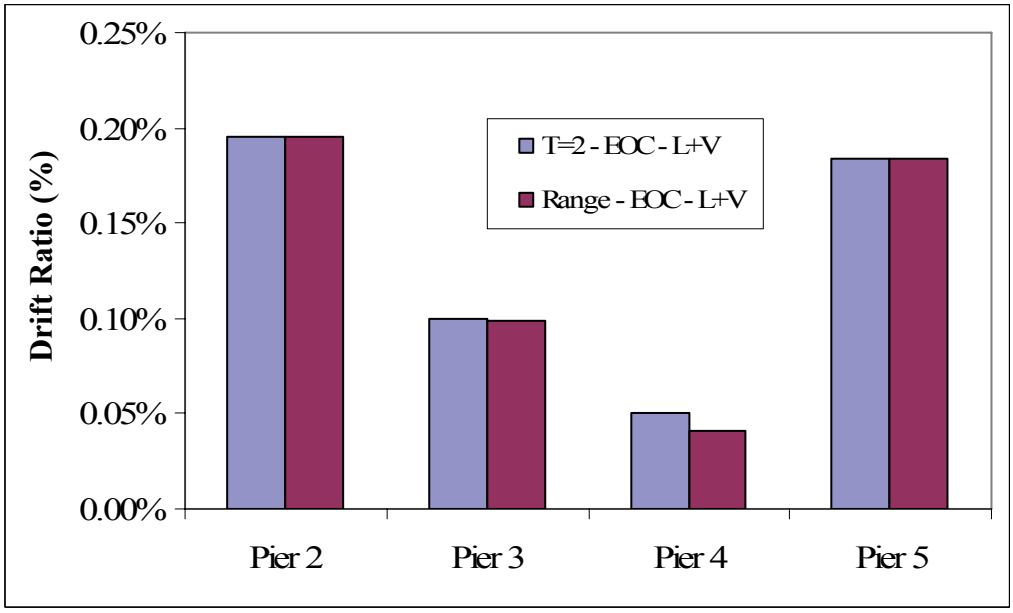

a) Median Drift Ratio

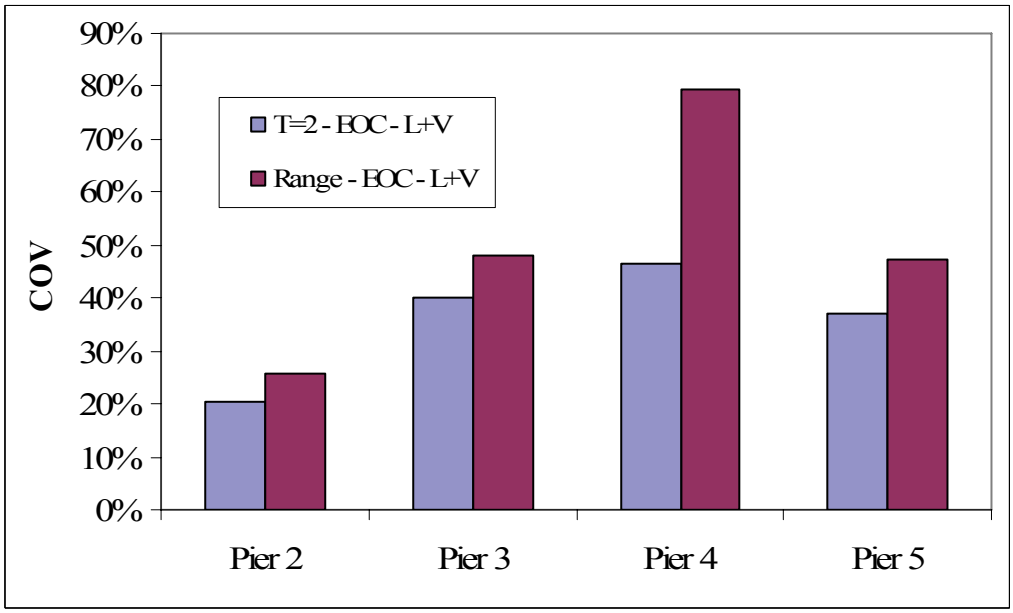

b) Coefficient of Variation

Figure A-13-23 525Foot Span – Influence of Record Scaling on Pier Residual Drift Ratios

APPENDIX D - JOINT ROTATION DATA

Legend

Red Square ➔ Median
Pink Diamond ➔ $16^{th}/84^{Th}$ percentile
Gray Dots ➔ Rotation from one earthquake

T=2 ➔ Ground motions scaled to natural period of 2 seconds
Range ➔ Ground motions scaled to period range

L_only ➔ Longitudinal ground motion only
L+V ➔ Longitudinal and vertical ground motions

-CS ➔ see Section 6.2.5.2
CS ➔ see Section 6.2.5.2
2CS ➔ see Section 6.2.5.2
EOC ➔ see Section 6.2.5.2

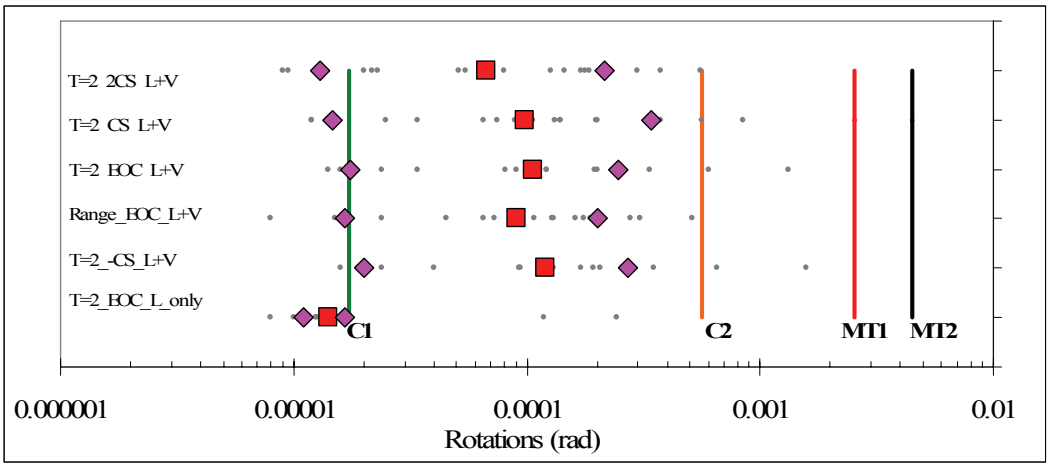

a.) Peak Positive Bending Rotation

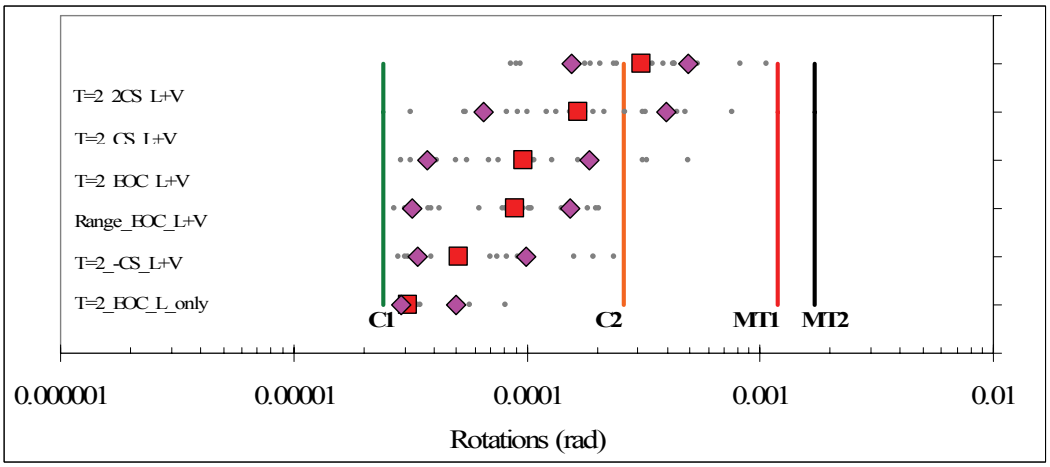

b) Peak Negative Bending Rotation

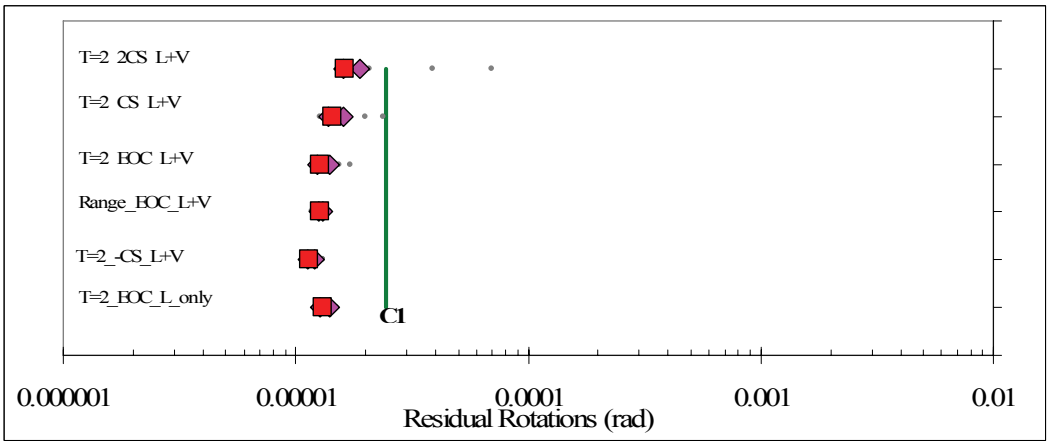

c) Residual Rotations

Figure A-13-24 300 Foot Span - Joint D1/U1 Rotations

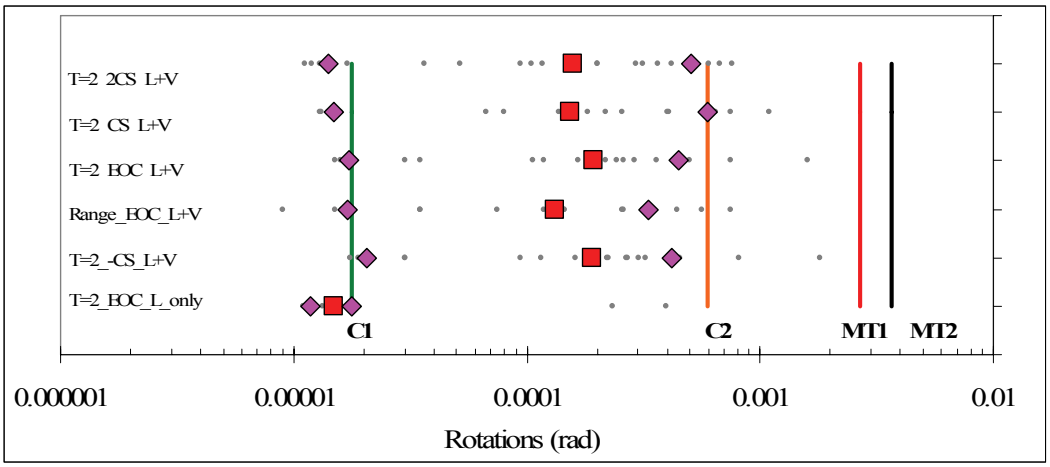

a.) Peak Positive Bending Rotation

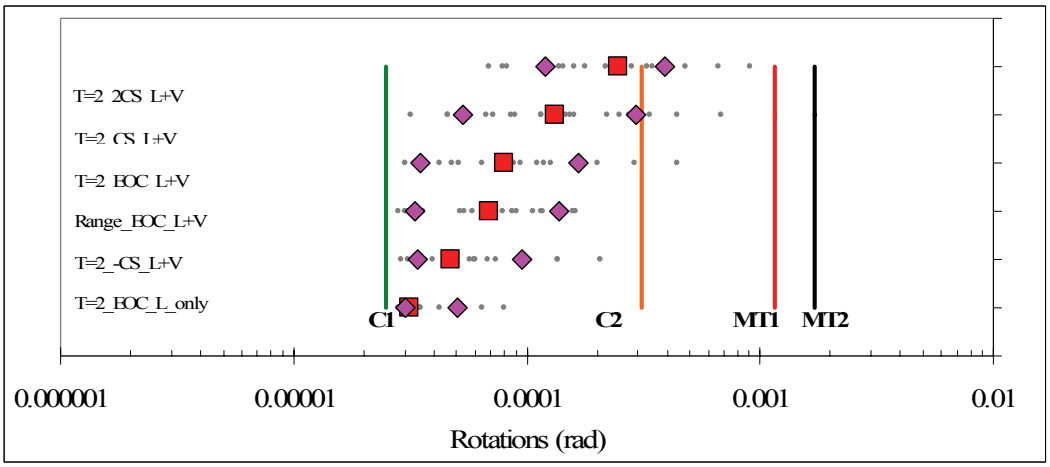

b) Peak Negative Bending Rotation

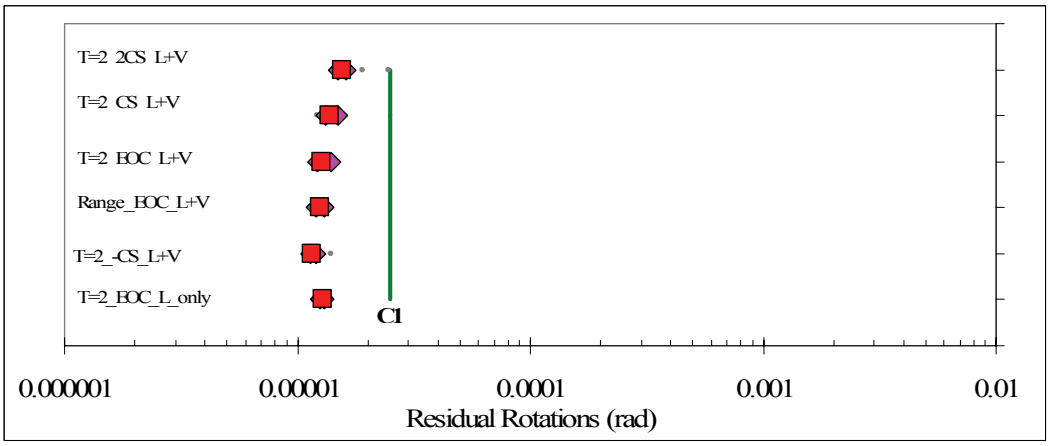

c) Residual Rotations

Figure A-13-25 300 Foot Span - Joint D2/U2 Rotations

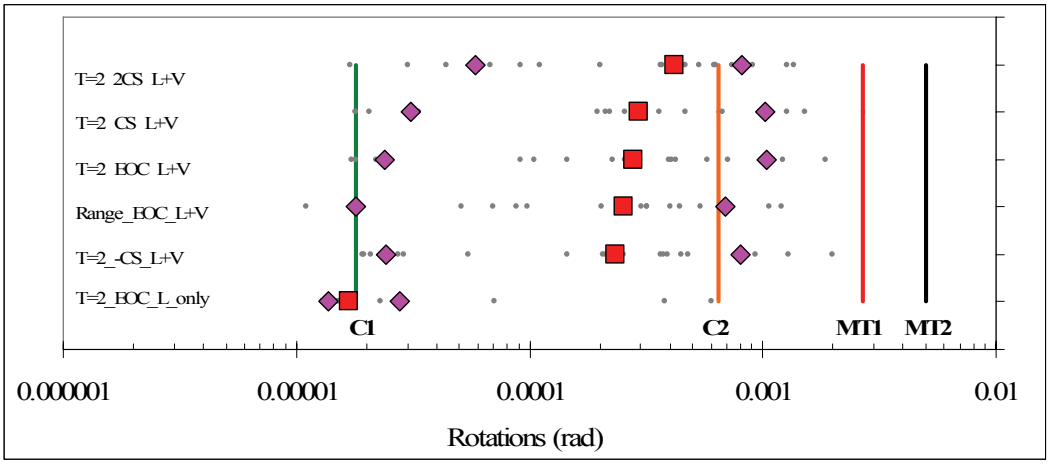

a.) Peak Positive Bending Rotation

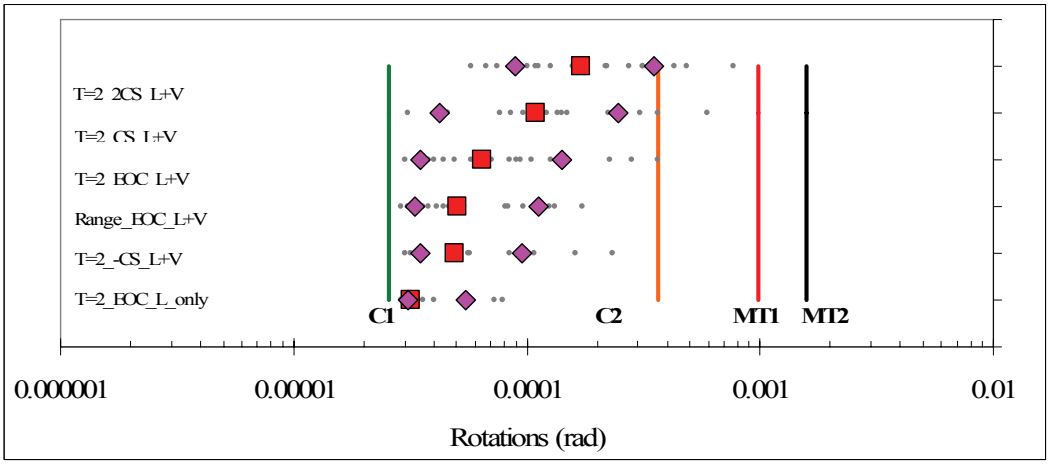

b) Peak Negative Bending Rotation

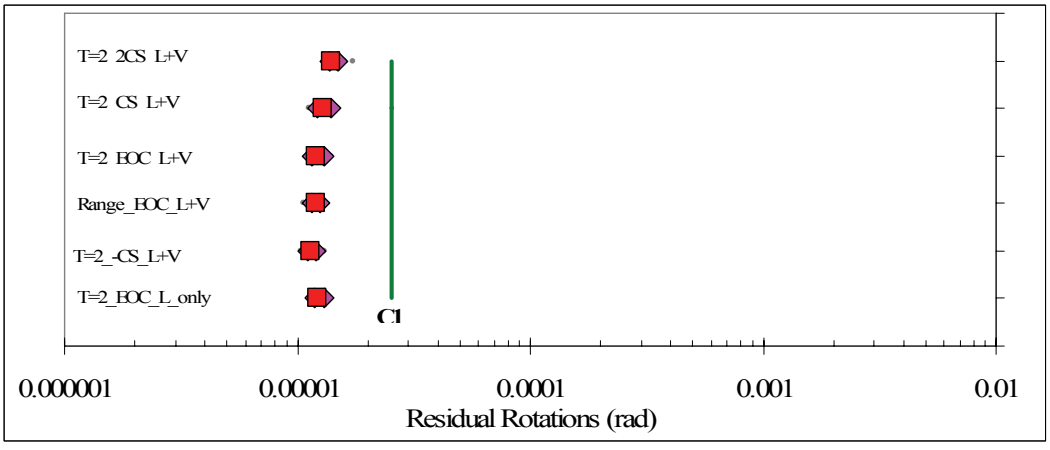

c) Residual Rotations

Figure A-13-26 300 Foot Span - Joint D3/U3 Rotations

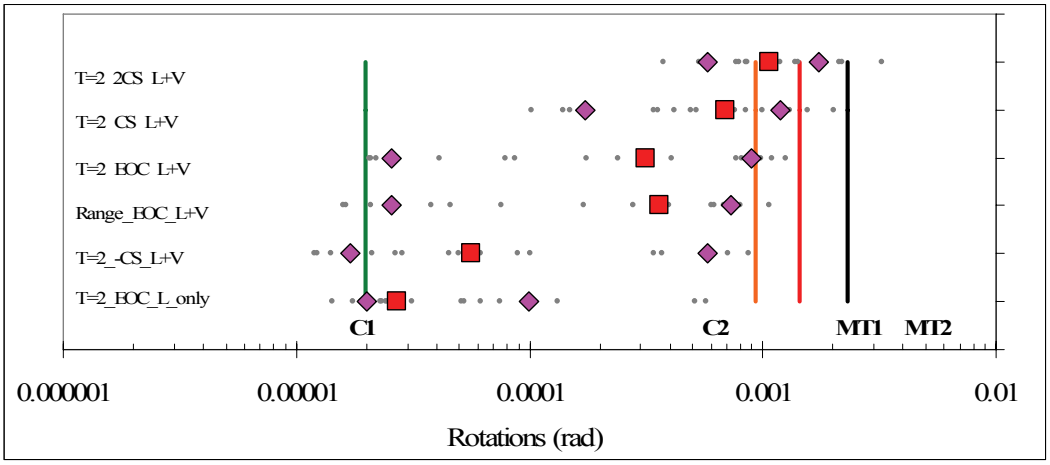

a.) Peak Positive Bending Rotation

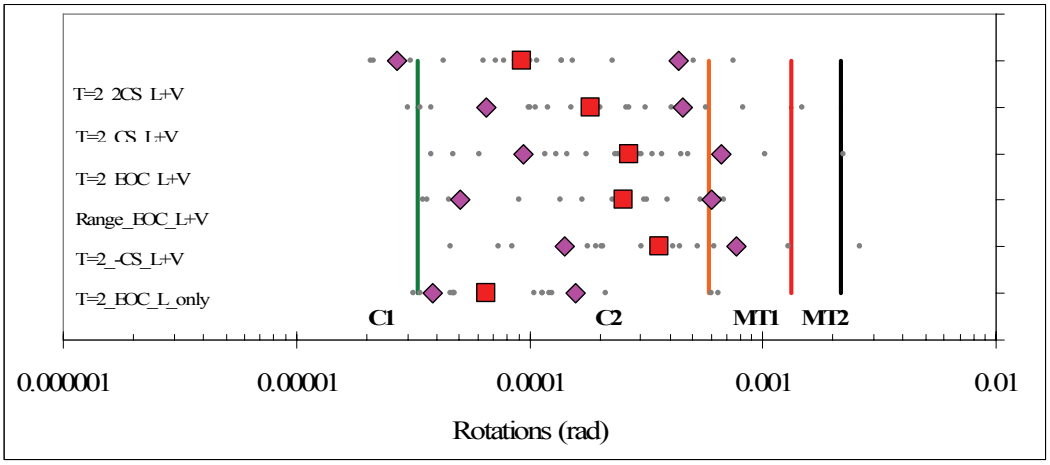

b) Peak Negative Bending Rotation

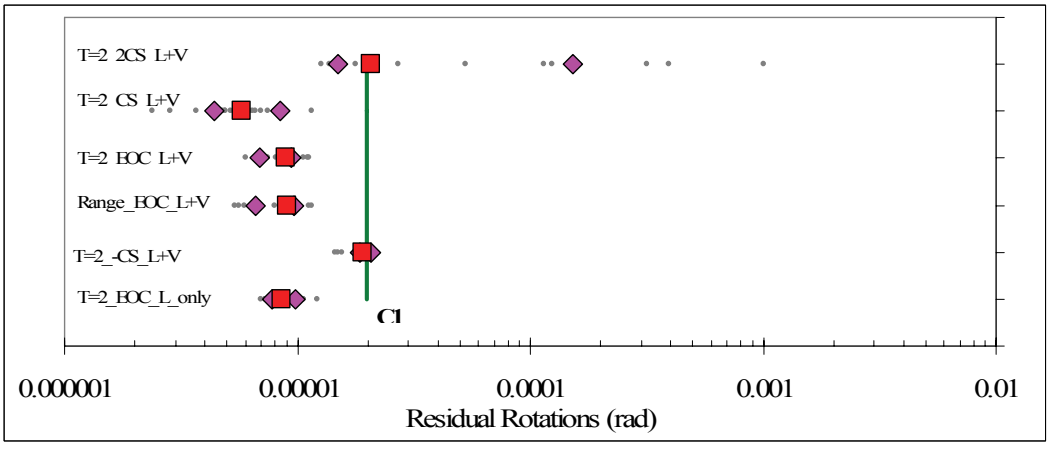

c) Residual Rotations

Figure A-13-27 300 Foot Span - Joint D13/U13 Rotations

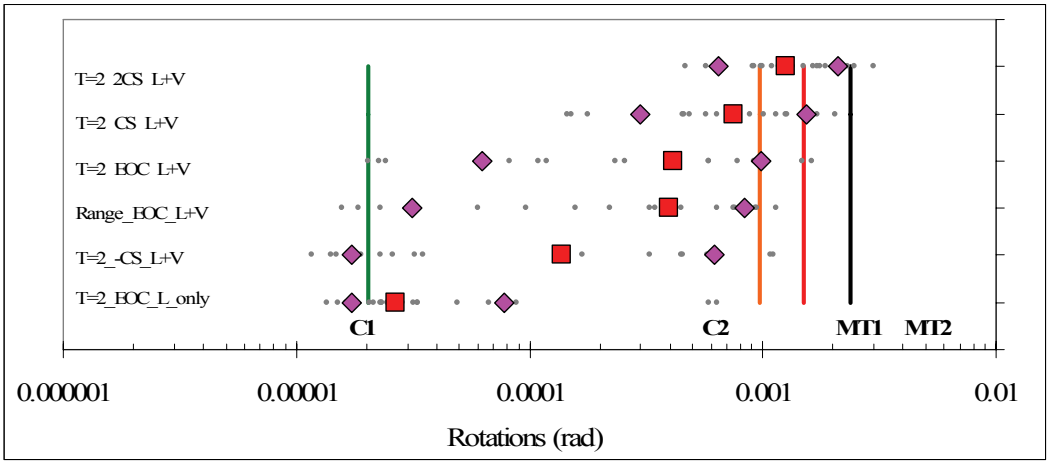

a.) Peak Positive Bending Rotation

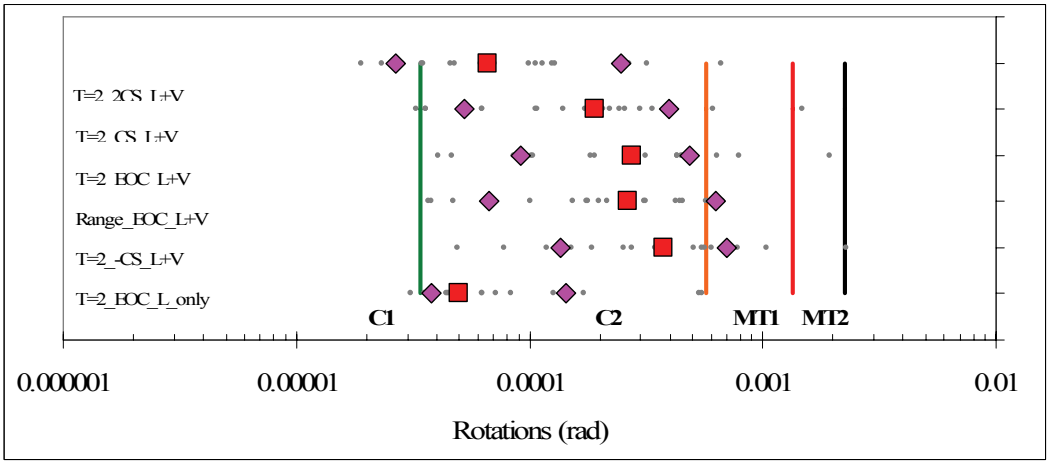

b) Peak Negative Bending Rotation

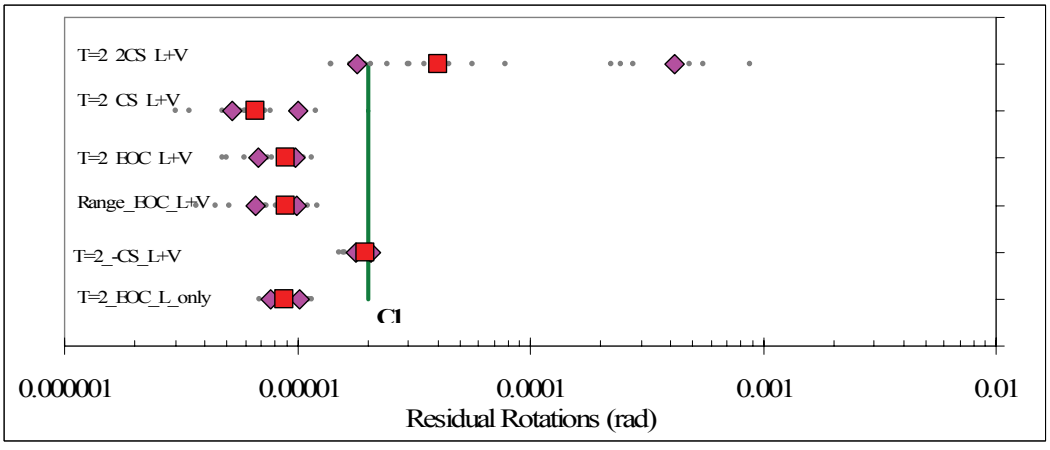

c) Residual Rotations

Figure A-13-28 300 Foot Span - Joint D14/U14 Rotations

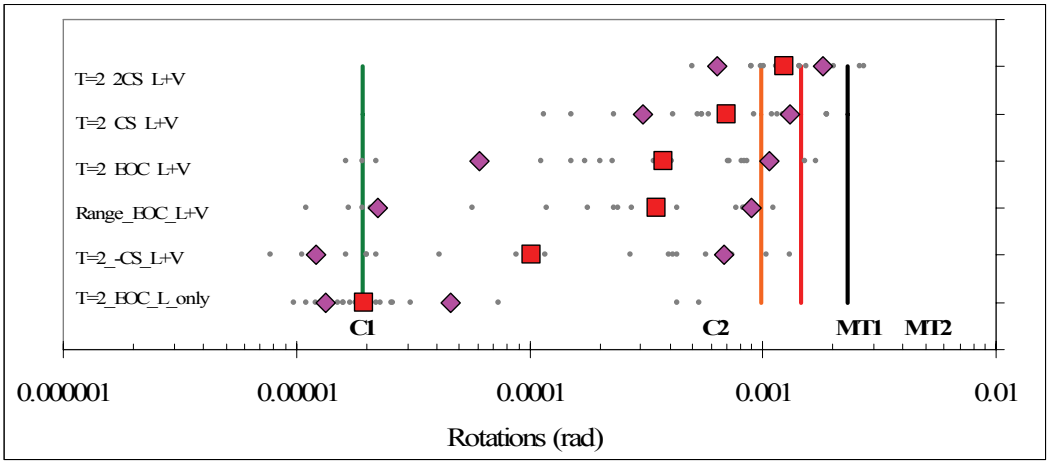

a.) Peak Positive Bending Rotation

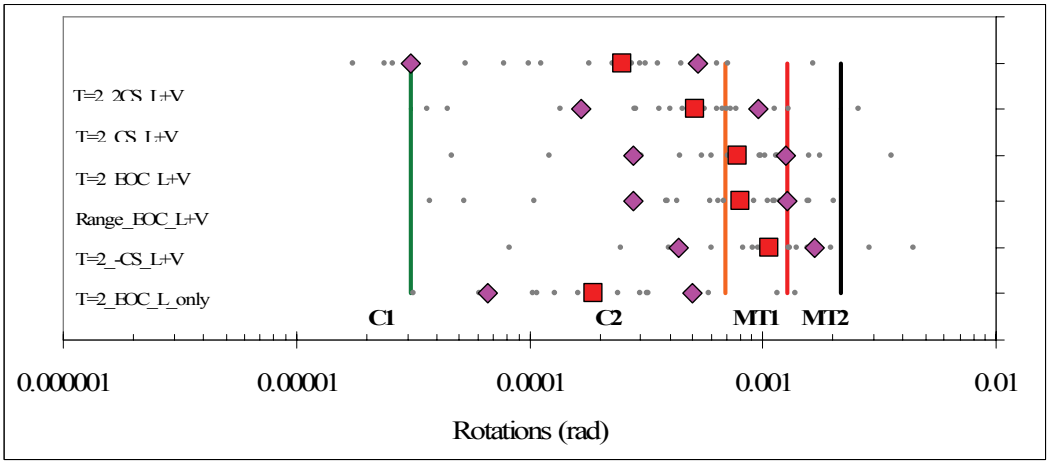

b) Peak Negative Bending Rotation

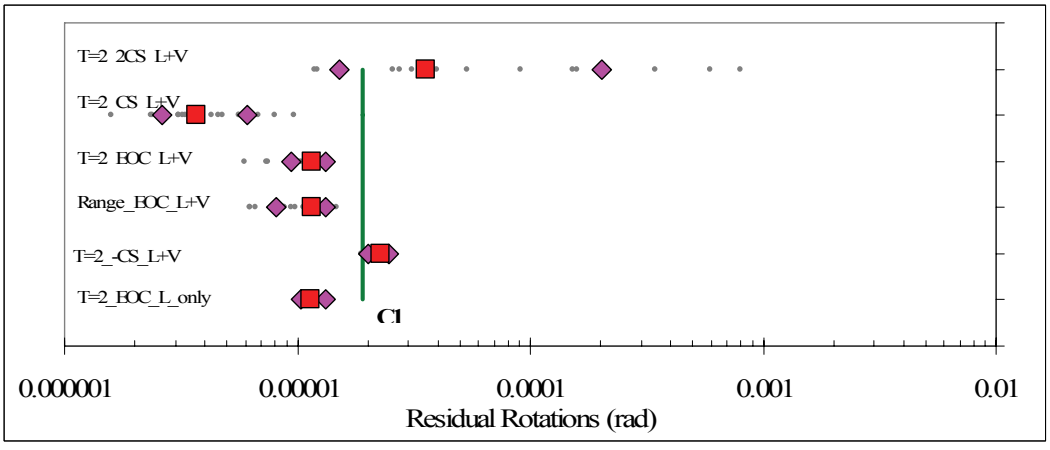

c) Residual Rotations

Figure A-13-29 300 Foot Span - Midspan Rotations

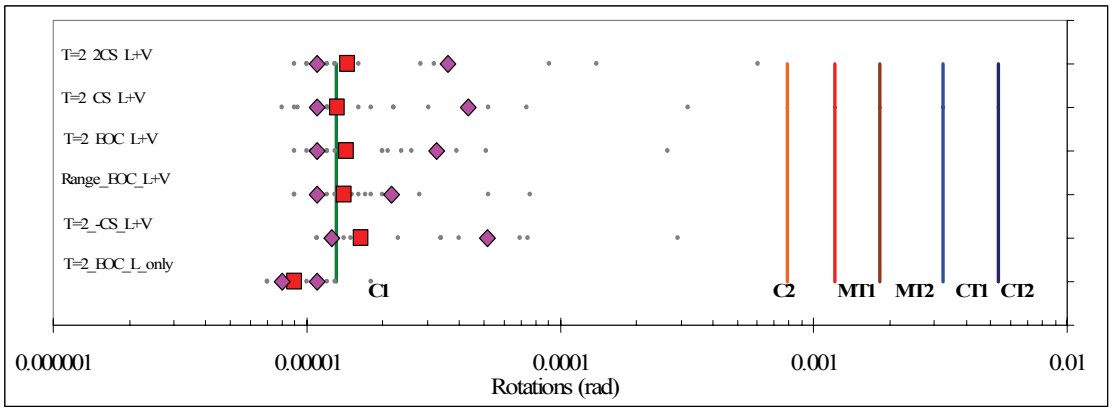

a.) Peak Positive Bending Rotation

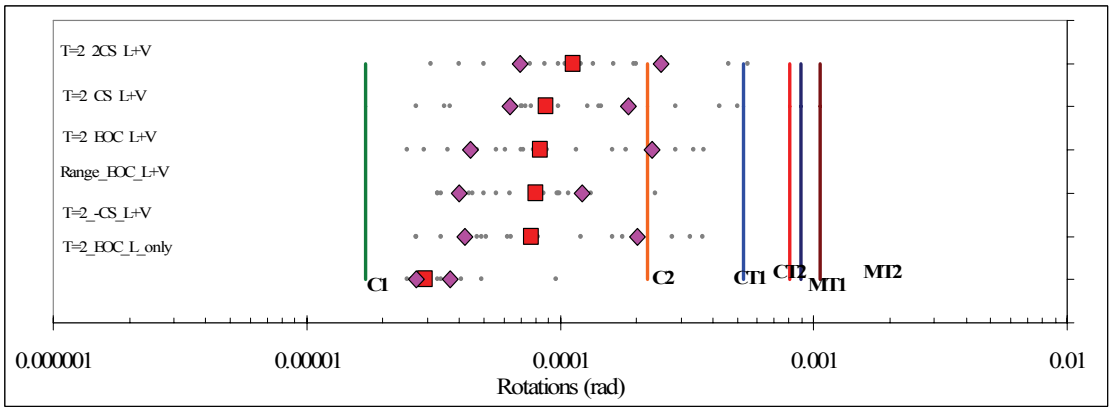

b) Peak Negative Bending Rotation

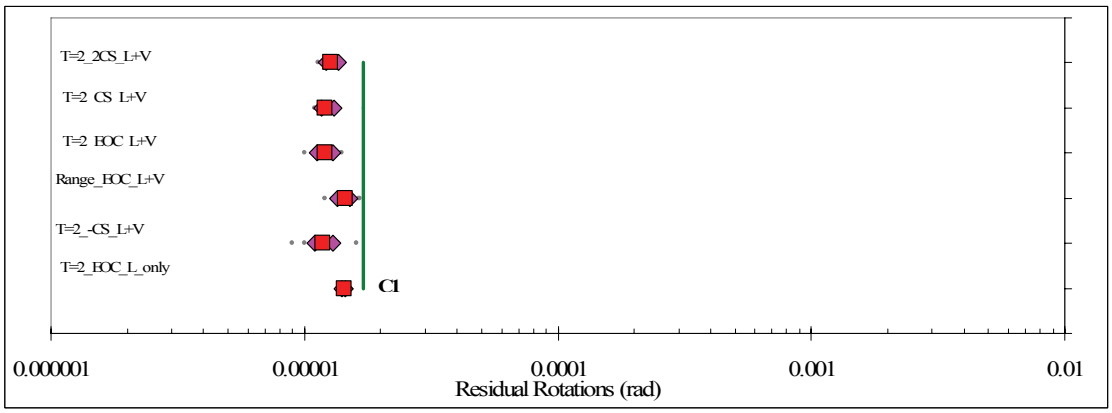

c) Residual Rotations

Figure A-13-30 525 Foot Span – Joint W1 Rotations

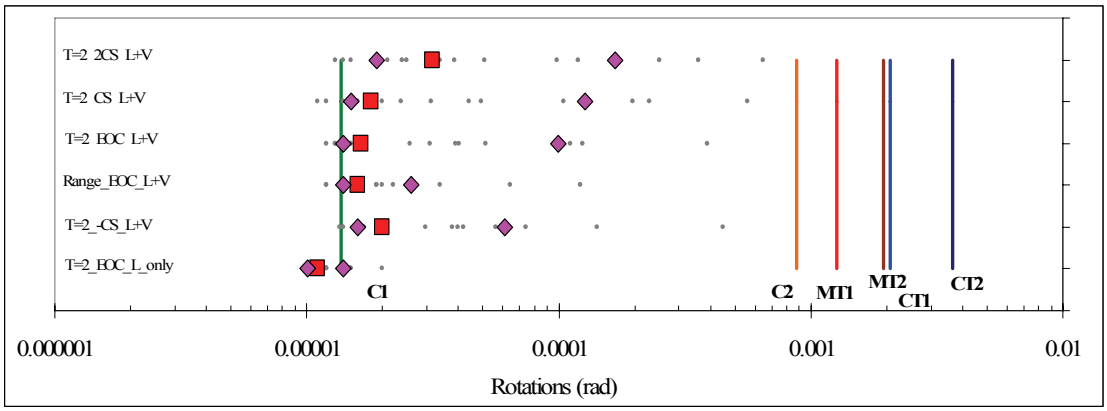

a.) Peak Positive Bending Rotation

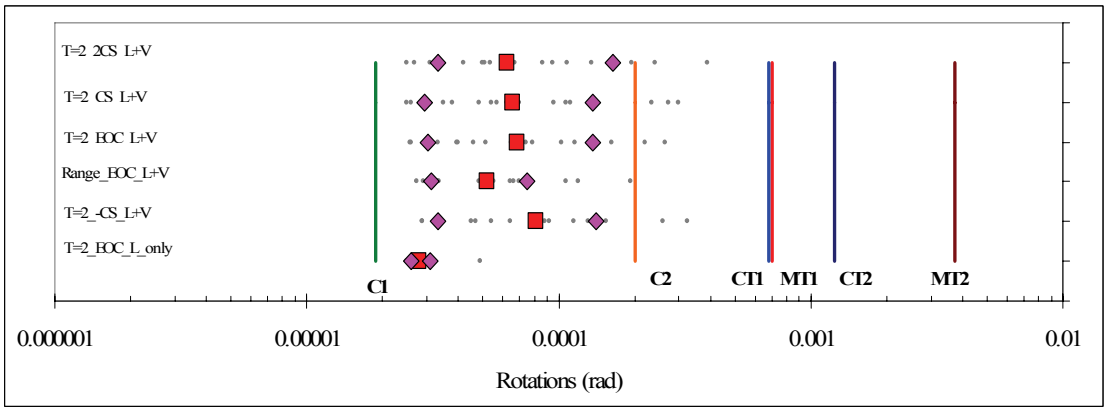

b) Peak Negative Bending Rotation

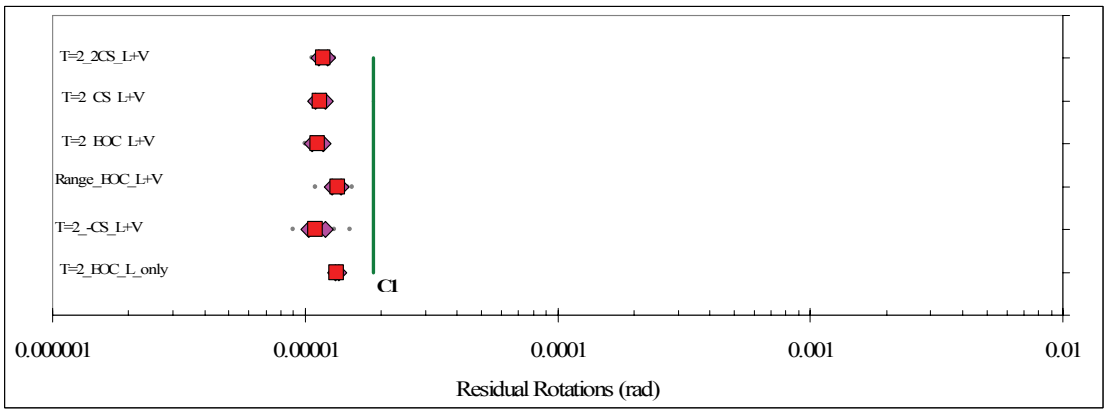

c) Residual Rotations

Figure A-13-31 525 Foot Span – Joint W2 Rotations

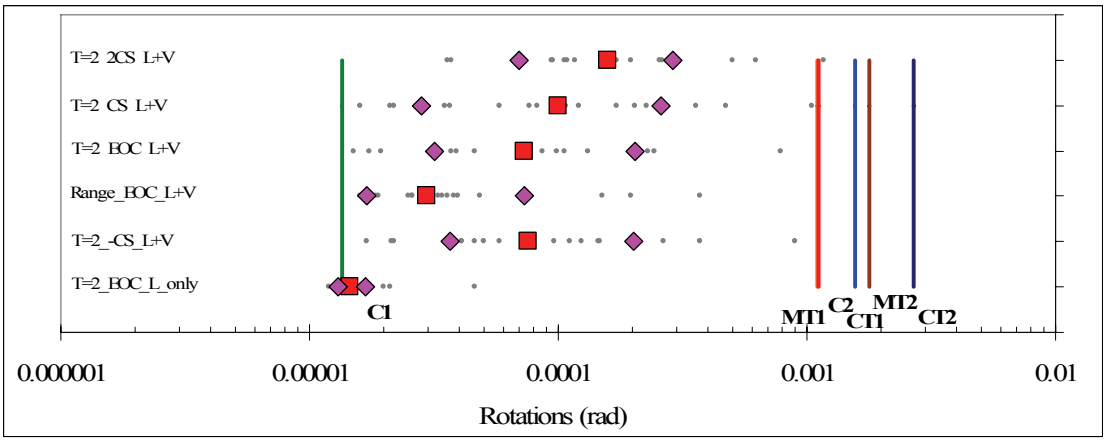

a.) Peak Positive Bending Rotation

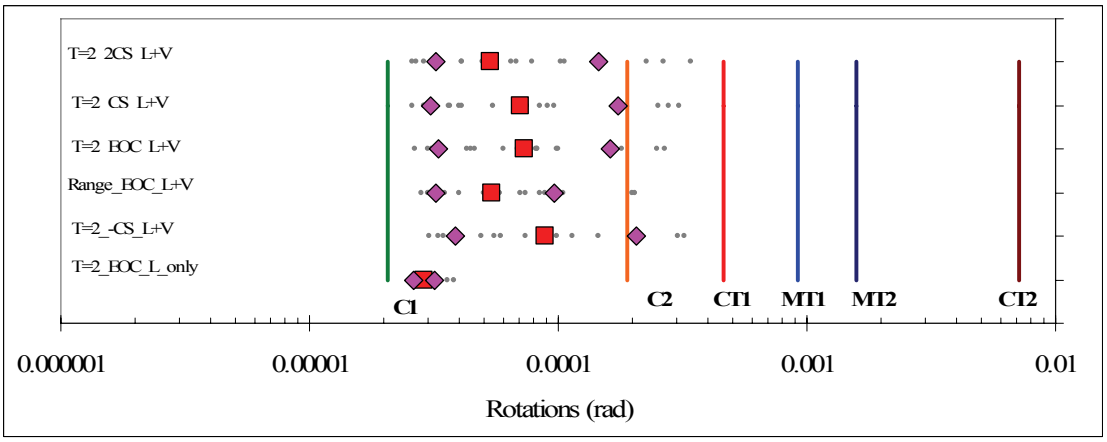

b) Peak Negative Bending Rotation

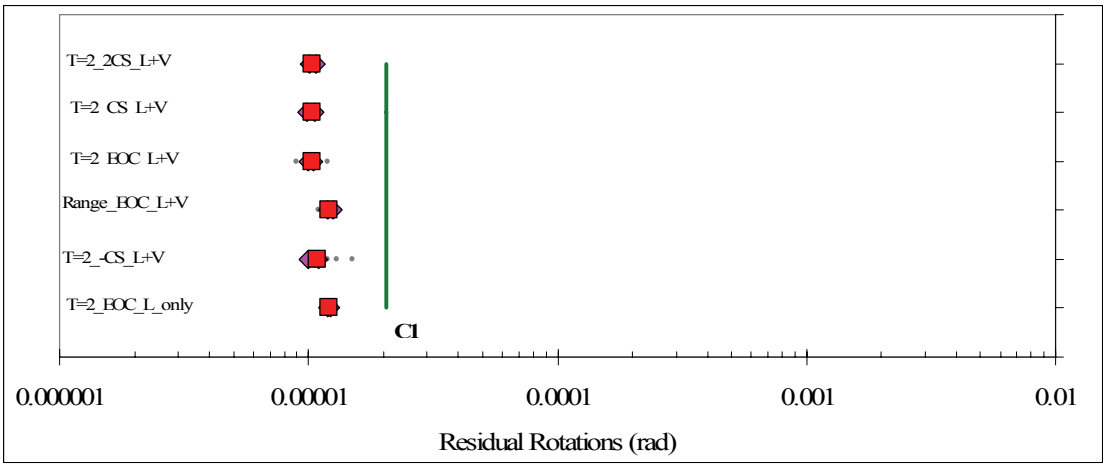

c) Residual Rotations

Figure A-13-32 525 Foot Span – Joint W3 Rotations

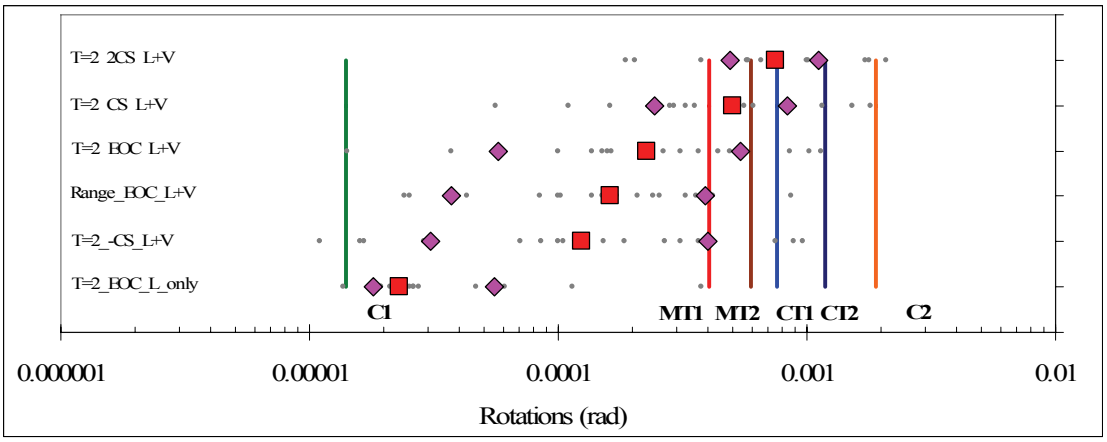

a.) Peak Positive Bending Rotation

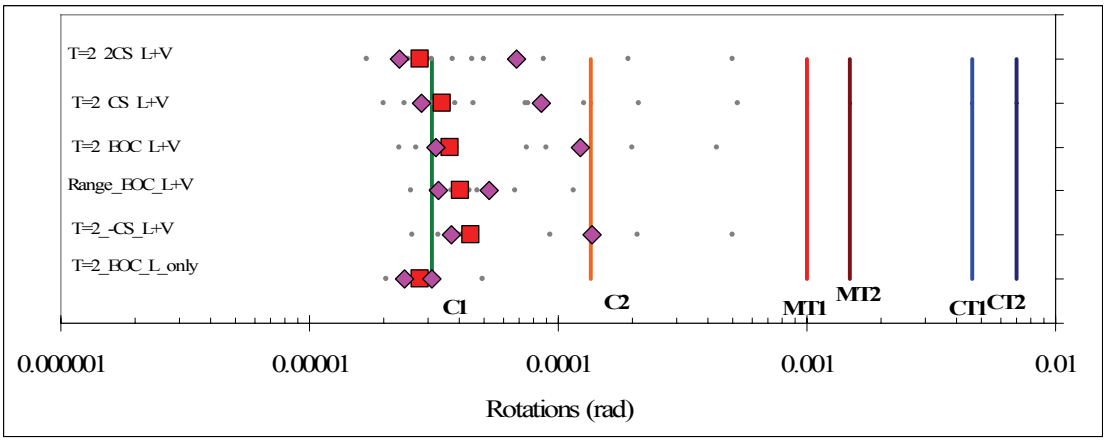

b) Peak Negative Bending Rotation

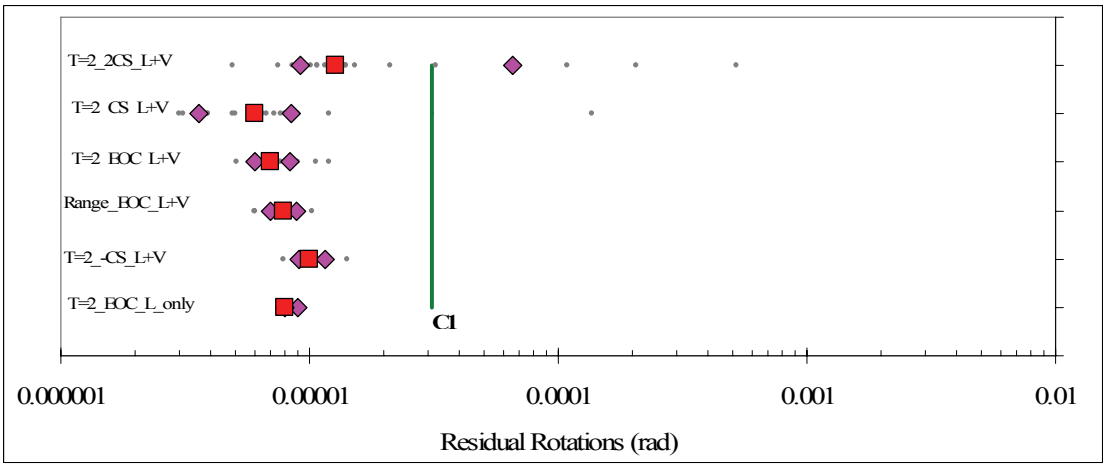

c) Residual Rotations

Figure A-13-33 525 Foot Span – Joint W8 Rotations

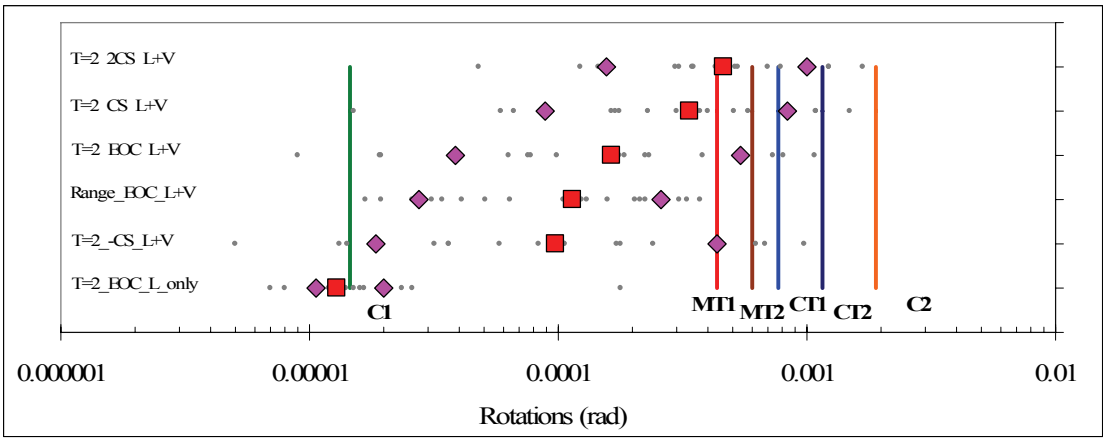

a.) Peak Positive Bending Rotation

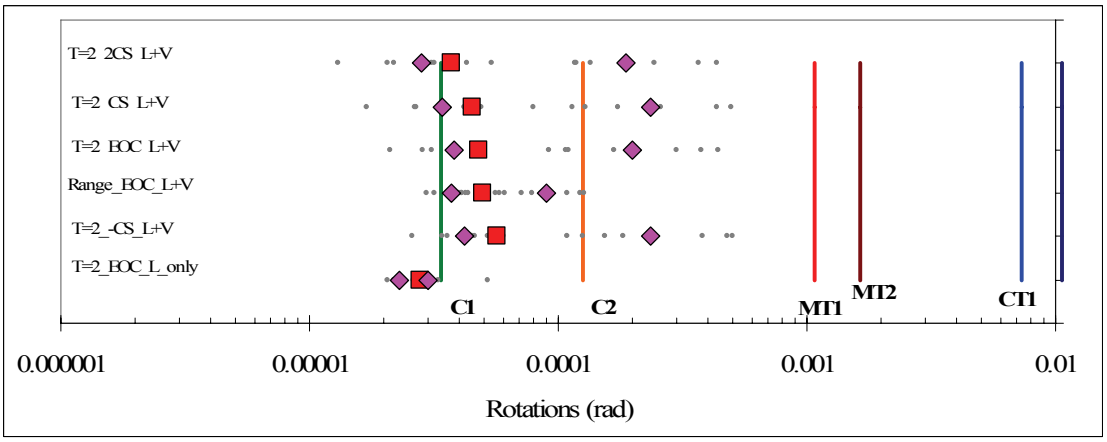

b) Peak Negative Bending Rotation

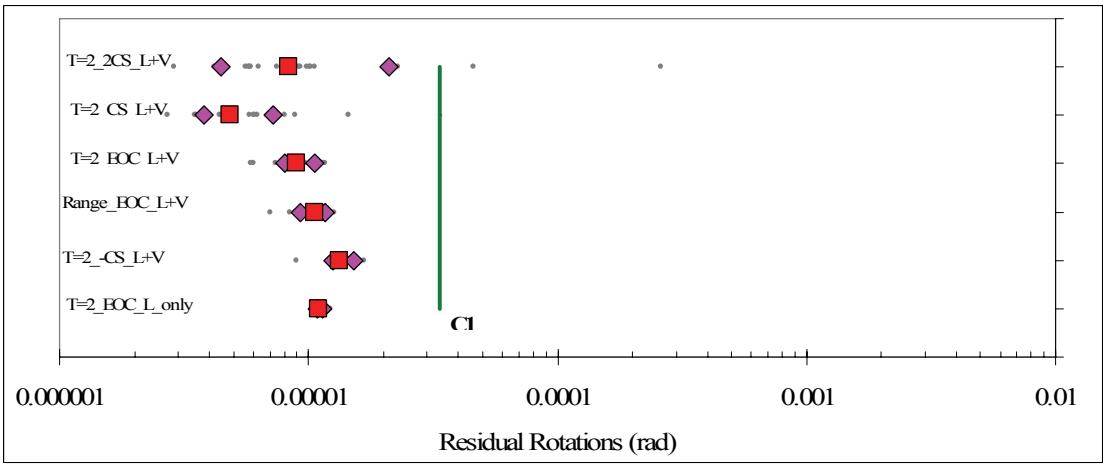

c) Residual Rotations

Figure A-13-34 525 Foot Span – Joint W9 Rotations

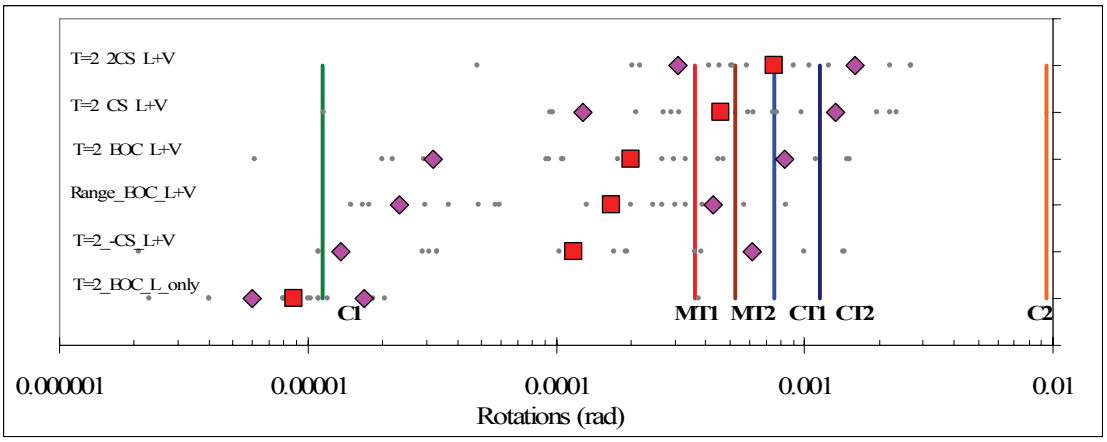

a.) Peak Positive Bending Rotation

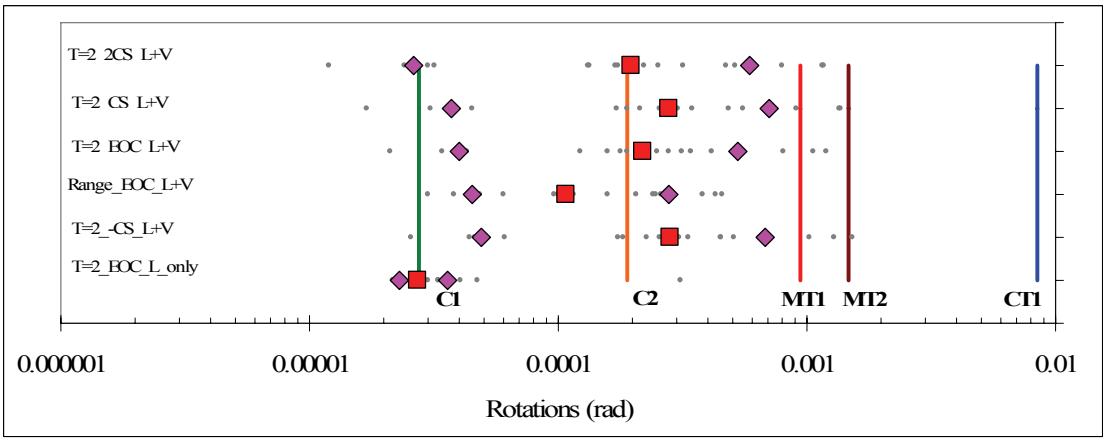

b) Peak Negative Bending Rotation

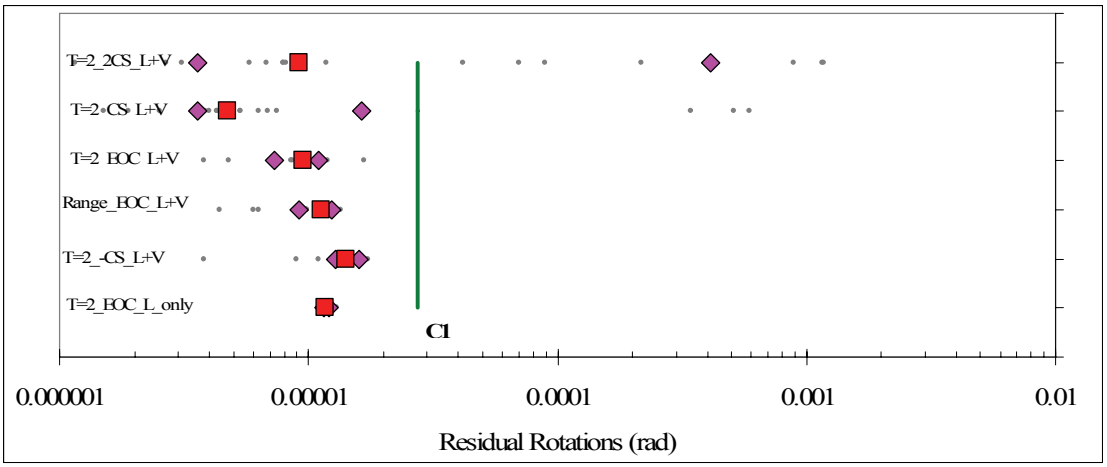

c) Residual Rotations

Figure A-13-35 525 Foot Span - Midspan Rotations

APPENDIX E - MISCELLANEOUS PHOTOS

Figure A-13-36 SFOBB Deck Reinforcement and PT

Figure A-13-37 SFOBB - Casting of Segments

Figure A-13-38 SFOBB - Segment Storage

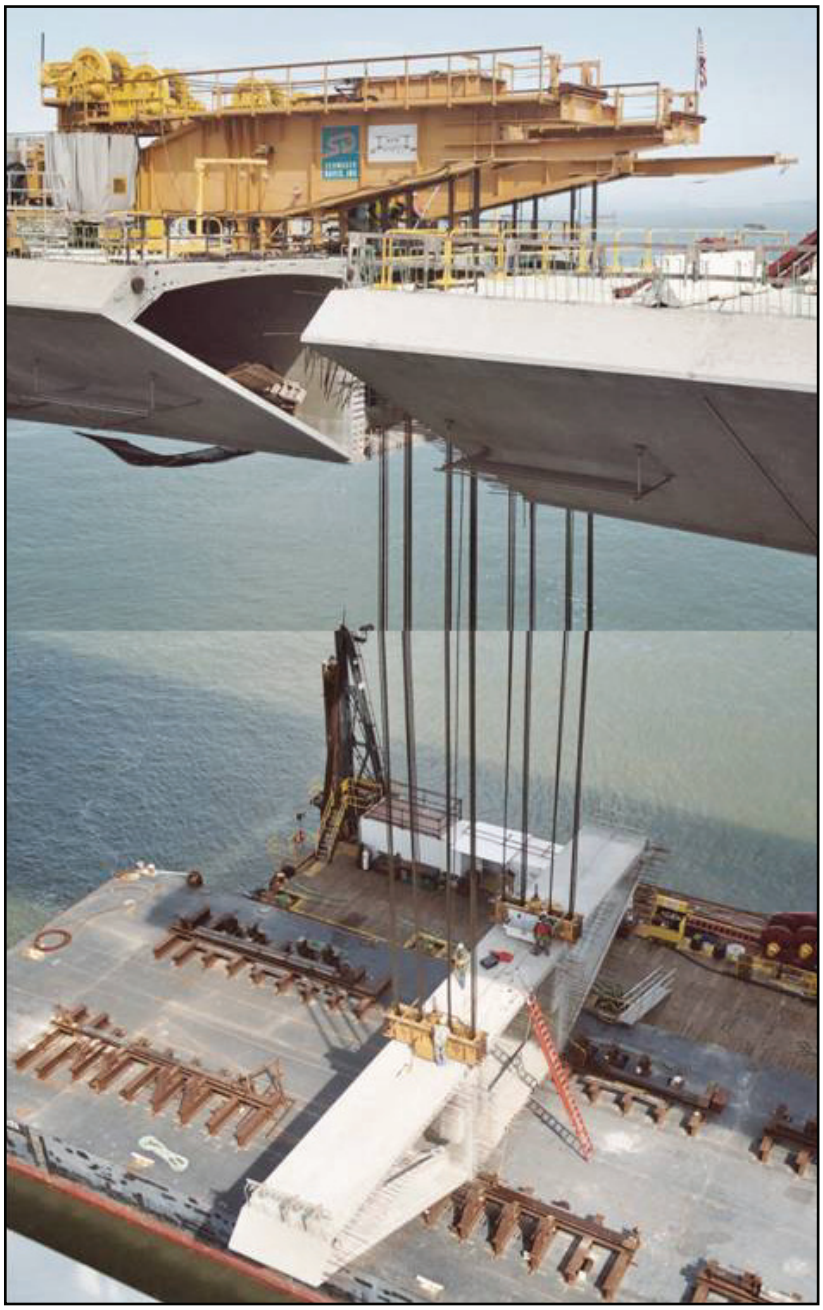

Figure A-13-39 SFOBB - Segment Lifting Operation

Figure A-13-40 SFOBB - Pier Table

Figure A-13-41 SFOBB - Looking West

Figure A-13-42 SFOBB - Typical Pier

Figure A-13-43 Otay River Bridge - Segment Forms (Courtesy of International Bridge Technologies)

Figure A-13-44 Otay River Bridge - Deck Rebar and PT (Courtesy of International Bridge Technologies)

Figure A-13-45 Otay River Bridge - Transport of Segment (Courtesy of International Bridge Technologies)

Figure A-13-46 Otay River Bridge - CIP Pier Table (Courtesy of International Bridge Technologies)

Figure A-13-47 Otay River Bridge – Overhead Erection Gantry (Courtesy of Parsons)

Figure A-13-48 Otay River Bridge - Segment Installation (Courtesy of Parsons)

Figure A-13-49 Otay River Bridge - Segment Installation (Courtesy of International Bridge Technologies)

Figure A-13-50 Otay River Bridge - Application of Epoxy to the Segment Joints (Courtesy of International Bridge Technologies)

Figure A-13-51 Segment Stressing Operation (Courtesy of International Bridge Technologies)

Figure A-13-52 Otay River Bridge (Courtesy of International Bridge Technologies)

Figure A-13-53 Otay River Bridge (Courtesy of International Bridge Technologies)

Figure A-13-54 Personal Advisory Committee

Figure A-13-55 The Family Consigliore

REFERENCES

1. AASHTO, "AASHTO LRFD Bridge Design Specifications – Customary U.S Units - 2006 Interim Revisions", Third Edition, American Association of State Highway and Transportation Officials, Washington, D.C., 2006.

2. AASHTO, "Guide Specifications for Design and Construction of Segmental Concrete Bridges", Second Edition, American Association of State Highway and Transportation Officials, Washington, D.C., 1999.

3. AASHTO, "Proposed AASHTO Guide Specifications for LRFD Seismic Bridge Design", American Association of State Highway and Transportation Officials, Subcommittee for Seismic Effects on Bridges, Washington, D.C., March 2007.

4. AASHTO, "Standard Specifications for Highway Bridges". 17th Edition, American Association of State Highway and Transportation Officials, Washington, D.C., 2002.

5. Abrahamson, N.A., "Non-Stationary Spectral Matching", Seismological Research Letters, Vol. 30, No. 1, 1992.

6. ACI, "Building Code Requirements for Structural Concrete (ACI 318-02) and Commentary (ACI 318R-02)"American Concrete Institute, Farmington Hills, Michigan, 2002.

7. Ang B.G., Priestley, M.J.N., and Paulay, T., "Seismic Shear Strength of Circular Bridge Piers", Research Report 85-5, Department of Civil Engineering, University of Canterbury, Christchurch, New Zealand, 1985.

8. Aparicio, A.C., Ramos, G., and, Casas J.R., "Testing of Externally Prestressed Concrete Beams", Engineering Structures, Vol. 24, pp 73-84, 2002.

9. Barnes R.W., Grove, J.W., Burns N.H., "Experimental Assessment of Factors Affecting Transfer Length", ACI Structural Journal, Vol. 100, No. 6, Nov-Dec 2003

10. Bazzurro P. and Luco N., "Parameterization of Non-Stationary Acceleration Time Histories", Final Report Task 1G00, Pacific Earthquake Engineering Research Center, December 2003

11. Bazzurro, P., Luco, N., "Do scaled and Spectrum-Matched Near-Source Records Produce Biased Nonlinear Spectral Response?", Proceedings of the 8th U.S. National Conference on Earthquake Engineering, San Francisco, CA, April 2006.

12. Bozorgnia, Y., Campbell, K.W., "The Vertical-to-Horizontal Response Spectral Ratio and Tentative Procedures for Developing Simplified V/H Vertical Design Spectra", Journal of Earthquake Engineering, Vol. 8, No 2, pp 175-207, 2004.

13. Broekhuizen, D.S., "Effects of Vertical Acceleration on Prestressed Concrete Bridges", MS Thesis, University of Texas at Austin, Austin, TX, 1996.

14. Burnell, K.P., Megally, S.H., Restrepo, J.I., and Seible, F., "Seismic Testing of Precast Segmental Systems Bridges: Phase III, Bridge Systems Test", Structural Systems Research Project SSRP 2005/01, University of California at San Diego, La Jolla, CA, June 2005.

15. Caltrans, "Seismic Design Criteria", Version 1.3, California Department of Transportation, Sacramento, CA, February 2004.

16. Campbell, K.W. and Bozorgnia, Y., "Updated Near-Source Ground Motion (Attenuation) Relations for the Horizontal and Vertical Components of Peak Ground Acceleration and Acceleration Response Spectra", Bulletin of the Seismological Society of America, Vol. 93, No 1, pp 314-331, 2004.

17. Carr, A.J., "RUAUMOKO – Users Manual". University of Canterbury, Christchurch, New Zealand, February 2004.

18. Chadwell, C.B., and Imbsen, R.A., "XTRACT: A Tool for Axial Force – Ultimate Curvature Interaction", http://www.imbsen.com/xtract.htm, 2002

19. Clough, R.W., Penzein, J., "Dynamics of Structures", Second Edition, McGraw-Hill, Inc., New York, N.Y., 1993.

20. Collins, M.P., and Mitchell, D., "Prestressed Concrete Structures", Prentice Hall, Englewood Cliffs, NJ, 1991.

21. Densley, D., Megally, S.H., and Seible, F., "Seismic Performance of Precast Segmental Bridge Superstructures with Lightly Stressed Continuity Tendons", Structural Systems Research Project SSRP-2003/10, University of California at San Diego, La Jolla, California, September 2003.

22. FEMA, "Prestandard and Commentary for the Seismic Rehabilitation of Buildings", Federal Emergency Management Agency, Washington, D.C., November, 2000.

23. Ghosh, S.K. and Fintel, M., "Development of Prestressing Strands, Including Debonded Strands, and Allowable Concrete Stress in Prestensioned Members". PCI Journal, Vol. 31, No. 5, Sept.-Oct. 1986.

24. Giberson, M.F., "Two Non-linear Beams with Definitions of Ductility", Journal of the Structural Division, ASCE, Vol. 95, pp 137-157, 1969.

25. Gloyd, S., "Design of Ordinary Bridges for Vertical Seismic Acceleration", Proceedings of the FHWA/NCEER Workshop on the National Representation of Seismic Ground Motions for New and Existing Highway Facilities, Technical Report No. NCEER-97-0010, National Center for Earthquake Engineering Research, State University of New York at Buffalo, Buffalo, NY, 1997.

26. Hancock, J., Watson-Lamprey, J., Abrahamson, N.A., Bommer, J.J., Markatis, A., McCoy, E. and Mendis, R., "An Improved Method of Matching Response Spectra of Recorded Earthquake Ground Motions Using Wavelets", Journal of Earthquake Engineering. Vol. 10, No. 4, pp. 67-89. 2006.

27. Hindi, A.I, Macgregor, R., Kreger, M.E. and Breen, J.E., "Enhancing Strength and Ductility of Post-Tensioned Segmental Box Girder Bridges", ACI Structural Journal, Vol. 92, Issue 1, pp 73-94, 1995.

28. Hines, E.M., Seible, F.S., and Priestley, M.J.N., "Cyclic Tests of Structural Walls with Highly-Confined Boundary Elements", Structural Systems Research Project SSRP 1999/15, University of California at San Diego, La Jolla, CA, August 1999.

29. http://www.peertestbeds.net/ Accessed April, 2007

30. Kawashima, K., and Aizawa, K., "Modification of Earthquake Response Spectra with Respect to Damping Ratio", Proceedings of the 3rd U.S. National Conference on Earthquake Engineering, Vol. 2, pp 1107-1116, 1986.

31. Lilhanand, K., and Tseng, W.S. "Generation of Synthetic Time Histories Compatible with Multiple-Damping Design Response Spectra", Transactions of the 9th International Conference on Structural Mechanics in Reactor Technology, Lausanne, 1987.

32. Lilhanand, K., and Tseng, W.S. "Development and Application of Realistic Earthquake Time Histories Compatible with Multiple-Damping Design Spectra", Proceedings of the 9th World Conference on Earthquake Engineering, Tokyo, Japan, 1988.

33. Madani, M., "General Guidelines for the Preliminary Design for Segmental Concrete Box Girder Superstructure", Article 6.0, Federal Highway Administration, http://www.fhwa.dot.gov/BRIDGE/segmental/task60.htm. Accessed July, 2006.

34. Megally, S.H., Garg, M., Seible, F, and Dowell, R.K., "Seismic Performance of Precast Segmental Bridge Superstructures", Structural Systems Research Project SSRP 2001/24, University of California at San Diego, La Jolla, CA, May 2002.

35. Megally, S.H., Silva, P.F., and Seible, F., "Seismic Response of Sacrificial Shear Keys in Bridge Abutments." Structural Systems Research Project SSRP-2001/23, University of California San Diego, La Jolla, CA, May 2001.

36. Mukherjee, S., and Gupta, V.K. "Wavelet-Based Characterization of Design Ground Motions", Earthquake Engineering and Structural Dynamics, Vol. 31, pp. 1173-1190, 2002a.

37. Mukherjee, S., and Gupta, V.K. "Wavelet-Based Generation of Spectrum-Compatible Time-Histories", Soil Dynamics and Earthquake Engineering, Vol. 22, No. 9, pp. 799-804, 2002b.

38. Murillo, J.A. and Showers, J.I., "Brief History of Segmental Concrete Bridge Construction", PB Network, Issue No. 57, Vol. XIX, No. 1, February 2004.4

39. Naaman, A.E. "Prestressed Concrete Analysis and Design: Fundamentals", Second Edition, Techno Press 3000, Ann Arbor, Michigan, 2004.

40. Naeim, F., and Lew, M., "On the Use of Design Spectrum Compatible Time Histories", Earthquake Spectra, Vol. 11, No. 1, pp. 111-127, 1995.

41. Niazi, M. and Bozorgnia, Y., "Behavior of Vertical Ground Motion Parameters in the Near-Field", Seismological Research Letters, Volume 60, pp 4, 1989.

42. Niazi, M. and Bozorgnia, Y., "Observed Ratios for PGV/PGA and PGD/ PGA for Deep Soil Sites across SMART-1 Array, Taiwan", Proceeding of the Fourth US National Conference on Earthquake Engineering, Palm Springs, CA, 1990.

43. Niazi, M. and Bozorgnia, Y., “Behavior of Near-Source Peak Vertical and Horizontal Ground Motions over SMART-1 Array, Taiwan”, Bulletin of the Seismological Society of America, Vol. 81, pp 715-732, 1991.

44. Niazi, M. and Bozorgnia, Y., “Behavior of Near-Source Peak Vertical and Horizontal Response Spectra at SMART-1 Array, Taiwan”, Earthquake Engineering and Structural Dynamics, Vol. 21, pp 37-50, 1992.

45. Presland, R.A., “Seismic Performance of Retrofitted Reinforced Concrete Bridge Piers”, Ph.D. Dissertation, University of Canterbury, Christchurch, New Zealand, 1999.

46. Ramirez, G., MacGregor, R., Breen, J.E., et al., "Shear Strength of Segmental Structures", Proceedings of the AFPC Workshop on External Prestressing in Structures, Saint_Remy-les-Chevreuse, France, 1993.

47. Rizzo, P.C., Shaw, D.E., and Jarecki, S.J., “Development of Real/Synthetic Time Histories to Match Smooth Design Spectra”, Nuclear Engineering and Design, Vol., 32, pp148-155, 1975.

48. Russell, B.W., and Burns, N.H., “Measured Transfer Lengths of 0.5 and 0.6 in. Stands in Concrete”, PCI Journal, Vol. 41, No. 5, Sept.-Oct. 1996.

49. Saadeghvaziri, M.A. and Foutch, D.A., “Dynamic Behavior of R/C Highway Bridges under the Combined Effect of Vertical and Horizontal Earthquake Motions”, Earthquake Engineering and Structural Dynamics, Volume 20, pp. 535-549, 1991.

50. Silva, W.J., and Lee, K., “WES RASCAL code for Synthesizing Earthquake Ground Motions”, State-of-the-Art for Assessing Earthquake Hazards in the United States, Report 24, Miscellaneous Paper S-73-1, US Army Corps of Engineers, Vicksburg, Mississippi, 1987.

51. Somerville, P., and Collins, N., “Ground Motions Time Histories for the Humboldt Bay Bridge”, Report prepared for the Pacific Earthquake Engineering Research Center Methodology Testbeds Project, March 2002.

52. T.Y. Lin International and Moffatt & Nichol Engineers, "Design Criteria – Skyway Structures", San Francisco-Oakland Bay Bridge Seismic Safety Project, March 2001.

53. Tabatabai, H., and Dickson, T.J., "The History of the Prestressing Strand Development Length Equation". PCI Journal, Vol. 38, No. 6, 1993.

54. Takebayashi, T., Deeprasertwong, L., and Leung, Y.W., "A full-Scale Destructive Test of a Precast Segmental Box Girder Bridge with Dry Joints and External Tendons", Proceedings of the Institution of Civil Engineering: Structures and Buildings, Vol. 104, No. 3, pp 297-315, 1994.

55. Tassin, D., Dodson, B., and Takebayashi, T., "Analyzing the Ultimate Capacity of a Precast Segmental Box Girder Bridge", Structural Engineering International, Vol. 44, Issue 3, pp 255-258, 1996.

56. Tse, J.K., "Considering Segmental Concrete Bridges", PB Network, Vol. XIX, No. 57-1, February 2004.

57. Turmo, J., Ramos, G., and Aparicio, A.C., "FEM Modelling of Unbonded Post-Tensioned Segmental Beams with Dry Joints", Engineering Structures, Vol. 28, pp. 1852-1863, 2006b.

58. Turmo, J., Ramos, G., and Aparicio, A.C., "Shear Behavior of Unbonded Post-Tensioned Segmental Beams with Dry Joints", ACI Structural Journal, Vol. 103, No. 3, pp. 409-417, 2006a.

59. Uniform Building Code, International Conference of Building Officials, Vol. 2, 1997.

60. Watson-Lamprey, J, and Abrahamson, N, "Biased Caused by Use of Spectrum Compatible Motions", Proceedings of the 8th U.S. National Conference on Earthquake Engineering, San Francisco, CA, April 2006a.

61. Watson-Lamprey, J; and Abrahamson, N, "Selection of Ground Motion Time Series and Limits on Scaling", Soil Dynamics and Earthquake Engineering. Vol. 26, no. 5, pp. 477-482. May 2006b.

62. Yu, C.P., Broekhuizen, D.S., Roesset, J.M., Breen, J.E., and Kreger, M.E., "Effect of Vertical Ground Motion on Bridge Dech Response", Proceedings of the Workshop on Earthquake Engineering Frontiers in Transportation Facilities,. Technical Report No. NCEER-97-0005, National Center for Earthquake Engineering Research, State University of New York at Buffalo, Buffalo, NY, 1997.

63. Zhou, X., Mickleborough, N., and Li, Z., "Shear Strength of Joint in Precast Concrete Segmental Bridges", ACI Structural Journal, Vol. 102, Issue 1, pp. 3-11, 2005.

64. Zia, P., and Mostafa, T., "Development Length of Prestressing Strands", PCI Journal, Vol. 22, No. 5, 1977.